Cosmic evolution of black holes and the $M_\bullet - \sigma$ relation

A thesis

submitted for the degree of

Doctor of Philosophy

in

The Department of Physics,
Pondicherry University,
Puducherry - 605 014, India

by

Dipanweeta Bhattacharyya
Indian Institute of Astrophysics,
Bangalore - 560 034, India

January 2020

Cosmic evolution of black holes and the $M_\bullet - \sigma$ relation

Dipanweeta Bhattacharyya
Indian Institute of Astrophysics

Indian Institute of Astrophysics
Bangalore - 560 034, India

Title of the thesis	:	**Cosmic evolution of black holes and the $M_\bullet - \sigma$ relation**
Name of the author	:	**Dipanweeta Bhattacharyya**
Address	:	Indian Institute of Astrophysics II Block, Koramangala Bangalore - 560 034, India
Email	:	dipanweeta@iiap.res.in
Name of the supervisor	:	**Prof. Arun Mangalam**
Address	:	Indian Institute of Astrophysics II Block, Koramangala Bangalore - 560 034, India
Email	:	mangalam@iiap.res.in

Declaration of Authorship

I hereby declare that the matter contained in this thesis is the result of the investigations carried out by me at the Indian Institute of Astrophysics, Bangalore, under the supervision of Prof. Arun Mangalam. This work has not been submitted for the award of any other degree, diploma, associateship, fellowship, etc. of any other university or institute.

Signed: Dipanweeta Bhattacharyya

Date: 10/01/20

Certificate

This is to certify that the thesis entitled **'Cosmic evolution of black holes and the $M_\bullet - \sigma$ relation'** submitted to the Pondicherry University by Ms. Dipanweeta Bhattacharyya for the award of the degree of Doctor of Philosophy, is based on the results of the investigations carried out by her under my supervision and guidance, at the Indian Institute of Astrophysics. This thesis has not been submitted for the award of any other degree, diploma, associateship, fellowship, etc. of any other university or institute.

Signed: Ann Mangalam

Date: 10/01/20

List of Publications

Refereed Publications

1. *$M_\bullet - \sigma$ relation in spherical systems,*

   Bhattacharyya, D. & Mangalam, A. 2018, JAA, Issue 39, article id 4, pp 9.

   Chapter 4

2. *Cosmic spin and mass evolution of black holes and its impact,*

   Bhattacharyya, D. & Mangalam, A. 2020, The Astrophysical Journal (ApJ), Volume 895:130 (35pp), Number 2.

   Chapters 5 and 6

3. *Evolution of the $M_\bullet - \sigma$ relation,*

   Bhattacharyya, D.; Mangalam, A. 2018, Proceedings of the International Astronomical Union, 14(S342), 254-256, DOI: 10.1017/S1743921318007251.

   Chapter 6

Under Preparation

4. *$M_\bullet - \sigma$ relation in axisymmetric systems,*

   Bhattacharyya, D.; Mangalam, A. 2020, in preparation.

   Chapter 7

5. *Models of black hole demographics*

   Bhattacharyya, D.; Mangalam, A. 2020, in preparation.

   Chapter 7

Presentations

1. Oral presentation titled "Spin and mass evolution of the black hole" in REcent Trends in the study of Compact Objects - IV, 17 - 20 June, 2019, IUCAA, Pune, India.

2. Poster presentation titled "Evolution of the $M_\bullet - \sigma$ relation" in IAU Symposium 342, 13 - 18 May, 2018, Noto, Sicily, Italy.

3. Oral presentation titled "Black hole Evolution and the $M_\bullet - \sigma$ Relation" in REcent Trends in the study of Compact Objects - III, 5 - 7 June, 2017, IIST, Trivandrum, India.

4. Poster presentation titled "Evolution of black hole nuclei in ellipticals" in Astronomical Society of India meeting, 6 - 10 March, 2017, Jaipur, MP Birla Auditorium, India.

5. Poster presentation titled "$M_\bullet - \sigma$ relation and Galactic Structure" in Astronomical Society of India meeting, 10- 13 May, 2016, University of Kashmir, Srinagar, India.

Acknowledgements

First of all, I would like to express my sincere gratitude and deep regards to my supervisor Prof. Arun Mangalam for his invaluable guidance, encouragement and constant involvement throughout my work. His perspectives, expertise in the subject and immense knowledge helped me lot during my PhD. It is a pleasure working with him.

My sincere thanks to my doctoral committee members Prof. S. Sivaprakasam and Prof. C. S. Stalin and the staff at the Pondicherry University for their timely help and relevant suggestions.

I would thank all the staff members of the Vainu Bappu Observatory, Kavalur (Indian Institute of Astrophysics), for the hospitality provided during my visits there.

I am thankful to IIA for providing me an excellent academic environment and the necessary facilities for my research work during my tenure.

I also thank all my friends and fellow students at the IIA for their constant support and encouragement.

I will also thank my family members and my teachers for always supporting and encouraging me. Last, but not the least, I acknowledge with pleasure the unconditional love and support of my parents for making me what I am today. No words will be enough to honour their sacrifices in my whole journey, till date. I would like to thank them from the bottom of my heart for everything.

Dedicated to

my

parents

Abstract

The connection of the SMBHs to their host galaxies is evidenced by the strong correlation between the mass of SMBH and velocity dispersion, σ, of the stars in rest of the galaxy. This is somewhat surprising because the velocity dispersion is measured for the stars which are too far from the SMBH to be affected by its gravitational field. Its origin is still a topic of debate. This relation is important since the mass of SMBH which is very difficult to measure directly can be calculated with relatively better precision using a quantity σ (the velocity dispersion of stars far from the SMBH) which is easier to measure for nearby systems. The cosmological $M_\bullet - \sigma$ relation is given by the equation

$$M_\bullet(z) = k_0(z)\sigma^{p(z)}, \tag{1}$$

We worked on the static as well as the dynamical aspects of this relation. For the static aspect, we deduce the $M_\bullet - \sigma$ relation for elliptical (spherical) galaxies by calculating σ from their observed intensity profiles and for the dynamical aspect, we compute the evolution of this relation as an application of our model of the evolution of mass and spin of the black hole.

To investigate the $M_\bullet - \sigma$ relation, we consider realistic elliptical (spherical) galaxy profiles that are taken to follow a single power law density profile given by $\rho(r) = \rho_0(r/r_0)^{-\gamma}$ or the Nuker intensity profile. We calculate the density using Abel's formula in the latter case by employing the derived stellar potential in both cases, we derive the distribution function $f(E)$ of the stars in presence of the supermassive black hole (SMBH) at the center and hence compute the line of sight (LOS) velocity dispersion as a function of radius. For the typical range of values for masses of SMBH, we obtain $M_\bullet \propto \sigma^p$ for different profiles. An analytical relation $p = (2\gamma + 6)/(2 + \gamma)$ is found which is in reasonable agreement with observations (for γ = 0.75 - 1.4, p = 3.6 - 5.3). Assuming that a proportionality relation holds between the black hole mass and bulge

mass, $M_\bullet = f_b M_b$, and applying this to several galaxies we find the individual best fit values of p as a function of f; also by minimizing χ^2, we find the best fit global p and f_b. For Nuker profiles we find that $p = 3.81 \pm 0.004$ and $f_b = (1.23 \pm 0.09) \times 10^{-3}$ which are consistent with the observed ranges.

We build an evolution model of the central black hole that is mainly dependent on the processes of gas accretion, the capture of stars, mergers as well as electromagnetic torque. In the case of gas accretion in the presence of cooling sources, the flow is momentum-driven, after which the black hole reaches a saturated mass and subsequently, it grows only by stellar capture and mergers. We model the evolution of the black hole mass and spin with the initial seed mass and spin as a function of redshift in a ΛCDM cosmology. For the stellar capture, we have assumed a power-law density profile for the stellar cusp in a framework of relativistic loss cone theory that includes the effect of the black hole spin, Carter's constant, loss cone angular momentum, and capture radius. The predicted capture rates of $10^{-5} - 10^{-6}$ yr^{-1} are closer to the observed range. We have considered the merger activity to be effective for $z \lesssim 4$, and we self-consistently include the Blandford-Znajek torque for spin evolution. We predict the impact of the evolution on the $M_\bullet - \sigma$ relation and show that our results are consistent with available observations. We model the specific cases of the quasars ULASJ134208.10+092838.61 (z=7.54), ULASJ112001.48+064124.3 (z=7.08) and DELSJ003836.10-152723.6 (z=7.02) and retrodict their formation parameters at $z = \{10, 15, 20\}$ to find that heavy seeds of $10^7 M_\odot$ are required. Our model is useful for building demographics of the black holes, in constraining formation scenarios and in providing inputs for future simulations.

We present some preliminary results of the derivation of the $M_\bullet - \sigma$ relation in axisymmetric systems and a formulation of initial seed mass and spin functions of black holes. We also discuss future work stemming from the ideas in this Thesis.

Contents

List of Figures

List of Tables

Glossary of symbols

$M_\bullet$	Mass of the black hole
j	Spin parameter of the black hole
M_s	Seed black hole mass
t_0	Unit of time (1 Gyr)
j_0	Seed black hole spin parameter
p	Index of the $M_\bullet - \sigma$ relation
M_b	Bulge mass
σ	Velocity dispersion of stars
f_b	$M_\bullet/M_b$
$M_\odot$	Solar mass
M_x	$M_\bullet$ / $10^x M_\odot$
σ_x	$\sigma/(x$ km sec$^{-1})$
G, c	Gravitational constant, Speed of light
r_g	$GM_\bullet/c^2$
t, z	Look back time and redshift
z_f	Formation redshift
Ω_m, a	Cosmological parameter, scale factor
H_0	Hubble constant
$\mu_\bullet$	$M_\bullet/M_s$
t_0	1 Gyr
$\dot{M}_{\bullet g}$	Rate of mass growth by accretion
η	efficiency factor of Eddington accretion = $\dot{M}_\bullet/\dot{M}_E$
x_c, x_ℓ	Capture and loss cone radius in units of r_g
l_ℓ	Angular momentum in units of $\frac{GM}{c}$ at x_l
$l_{\ell p}$, $l_{\ell r}$	Angular momentum in units of $\frac{GM}{c}$ at x_c
x_t	Tidal radius in units of r_g
x_H	Horizon in units of r_g
V_{eff}	Effective potential in Kerr metric

γ	Power law index of mass density
$\dot{N}_f$, $\dot{N}_s$	Rate of capture of stars in full and steady loss cone
$\dot{M}_{\bullet *}$	Rate of mass growth by stellar capture
q	Merger mass ratio
$\dot{M}_{\bullet m}$	Rate of growth of mass by mergers
B_4	Magnetic field in units of 10^4 Gauss
f_h	Ratio of black hole mass to the halo mass
z_s	Saturation redshift
$M_{\bullet t}$	Saturation mass
t_s	Saturation time

Chapter 1

Introduction

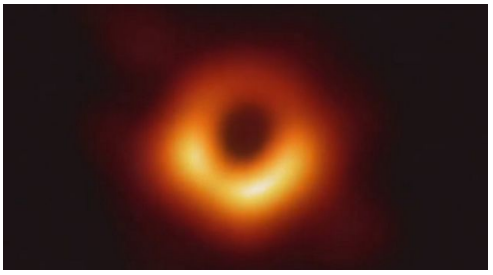

Image: jpl.nasa.gov

1.1 Introduction to Schwarzschild and Kerr black holes

A black hole in the Universe is formed when due to the self-gravity a massive object collapses into a very high-density object, where the escape velocity is of the order of the speed of light, c. This is thought to be a possible origin of the supermassive black holes (SMBH) $\geq 10^6 M_\odot$, at the centers of galaxies. Using Newtonian mechanics, the escape velocity, v_{esc}, for an object of mass M with radius R, is calculated as

$$v_{esc} = \left(\frac{2GM}{R}\right)^{1/2}. \tag{1.1}$$

For a very dense object $v_{esc} \sim c$, general relativistic treatment is required. Schwarzschild gave the solution for non-spinning black holes, from Einstein's field equations in

general relativity (Kolb 2010). It is a lucky coincidence that the exact general relativistic solutions for Schwarzschild black holes match with eqn. (1.1) for $v_{esc} = c$ (Kolb 2010). This type of black holes form when, object of mass M, collapses into a radius of R_s given as

$$R_s = \frac{GM}{c^2}, \tag{1.2}$$

which is termed as the Schwarzschild radius. At the boundary of this radius $v_{esc} \sim c$. Inside this region resides another region, which is completely unknown to the rest of the universe, because no information can come out of it, not even light. This is termed as the event horizon of the black holes [see Fig. 1.1]. Accretion is

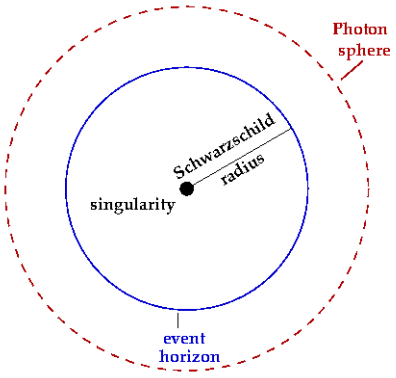

FIGURE 1.1: Schematic of a Schwarzschild black hole. Image: galileospendulum.org

one of the main sources of black hole growth, which is the inflow of matter towards the black hole from its surroundings due to its high gravity. Before the matter falls into the black hole, it orbits the hole. For the case of Schwarzschild black holes, there is an innermost stable circular orbit, near to the black hole, after which there are no stable orbits. The radius of this orbit is $3R_s$.

Stars usually acquire angular momentum during their formation and that will exist during the evolution phase, unless some braking mechanism removes the angular momentum. Therefore, the black holes formed from the collapse of these rotating stars will be rotating too. The Kerr solution to the field equations of Einstein give

more general results for rotating black holes than the Schwarzschild solution [see Fig. 1.2].

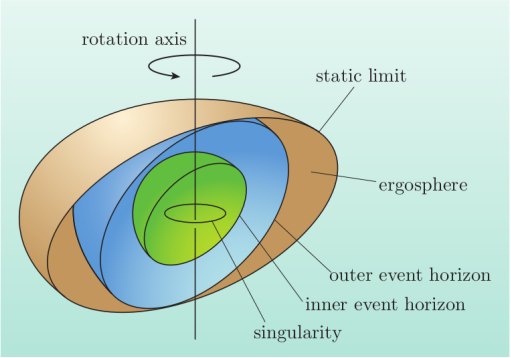

FIGURE 1.2: Schematic of a Kerr black hole. Image: Kolb (2010).

When the space-time is infinite, both types of black holes will have gravitational singularities. For the Schwarzschild case, this will be a point, while for the Kerr black holes, this will be ring lying in a plane that is exactly perpendicular to the axis of rotation. Outside the outer event horizon of Kerr black holes, there is another surface called the static limit in the shape of an oblate spheroid which touches the polar points of the event horizon. The middle region is termed as the ergosphere, where, the spacetime is dragged in the direction of rotation with speed $\geq c$ (rest of the Universe is assumed to be at rest). In the static limit, this speed is c. This implies that matter can not stay at rest inside the ergosphere. There can be one possibility that the matter even leaves the ergosphere and the energy required for that is gained from the black hole, which in turn reduces the spin of the black hole (Kolb 2010). In this process, the Kerr black hole can become a Schwarzschild black hole, when the spin value reaches zero.

1.2 Important parameters in the study of black hole physics

One remarkable thing is that, the properties of a black hole can completely be described by two parameters, mass, $M_\bullet$ and the angular momentum, J. The third parameter can come into play when the black hole has an electric charge $\mathcal{Q}$. Now, the existence of a black hole for a given set of these three parameters, $\{M_\bullet, J, \mathcal{Q}\}$, is determined by a inequality given as (Frolov and Novikov 1998)

$$M_\bullet^2 - (J/M_\bullet)^2 - \mathcal{Q}^2 \geq 0, \tag{1.3}$$

where, $G = c = 1$. The solutions of the Einstein-Maxwell equations for black holes, for which the parameters, $\{M_\bullet, J, \mathcal{Q}\}$, obey this relation given by eqn. (1.3), will be unique solutions.

For neutral black holes, when, the angular momentum is zero, the geometry will be spherical and for rotating cases, in presence of the angular momentum, the structure is axially symmetric. Therefore, at distances far from the black hole, it can be treated as an extended system, and the potential is assumed for a generally extended body (Frolov and Novikov 1998). Therefore, following simple multipole decomposition, mass (μ_ℓ), current (j_ℓ), multipole coefficients ($\ell > 0$) can be defined. The lowest order of these parameters are (Frolov and Novikov 1998)

$$\mu_0 = M_\bullet, \quad j_1 = J = jM_\bullet^2. \tag{1.4}$$

Therefore, black holes having the same mass and angular momentum will have the same gravitational properties. Thus, the mass, $M_\bullet$ and the spin parameter, j of the black hole are two very important parameters for studying the physics of the black holes and their evolution as a function of redshift. This motivates us to study the mass and spin evolution of the black holes to throw some light on

the evolutionary history of the black holes which may have a connection to the evolution of the galaxy within which they reside.

1.3 Growth of the mass and the spin of black holes

This black hole mass and spin grow via mainly four processes - accretion, stellar capture, mergers, and electromagnetic torque.

1.3.1 Accretion

Accretion means the inflow of matter towards the central gravitating object or the center of mass of an extended system. Accretion onto super-massive or near solar mass black holes is suggested to be the power source from black holes. All accreting matter is in the gaseous form. Therefore, the free electrons and ions interact only by collisions. For gas to accrete some of it must lose angular momentum and move inward. For the sake of conservation of angular momentum, other gas must gain angular momentum and move outward. Accretion of gas on the black holes can be in spherical shape as well as in disc-like shape (Frank *et al.* 2002). It depends on the angular momentum of the accreting gas. When the radial motion is significant the flow is spherical. In this case, the angular momentum is very small. In spherical accretion, the gas mostly carries much entropy into the hole without releasing it by radiation, because the flow is almost free falling with velocity $c\left(\frac{r}{R_s}\right)^{\frac{1}{2}}$. When the angular momentum of the accreting matter is too large to hit the surface of the compact star directly, it forms accretion disc [see Fig. 1.3]. While the accreting matter spirals down towards the gravity center of the compact star, its gravitational energy is released. One part of this energy increases the kinetic energy of rotation and the other part turns into thermal energy. A fraction of the

heat gets converted into radiation which partially escapes taking some amount of internal energy along with it. Radiation emitted from a black hole, depends on the state of the inflowing gas, because, it does not have any outer hard surface. The amount of radiation emitted is more in case of high-temperature flow than the low-temperature one because, the higher the temperature, higher the work done by the gravity resulting in more radiation. The feedback caused by the outflow, causes the black hole to reach a saturated mass, after which the accretion process stops or contributes very little to the flow [Silk and Rees (1998), King (2003)]. We discuss these processes in detail later in Chapter 3.

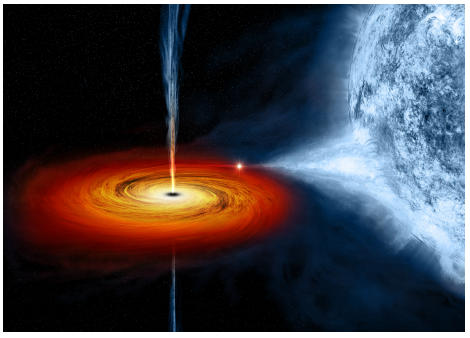

FIGURE 1.3: An artistic image of accretion onto a black hole (Cygnus X-1), Image courtesy: sun.org.

1.3.2 Stellar capture

Another process that helps the black holes to grow their mass is stellar capture. This capture can occur in two ways: tidal disruption and direct capture. Beyond a certain critical mass ($M_c = 3 \times 10^8 M_\odot$), the stars get directly captured instead of getting tidally disrupted. This critical mass depends also on the black hole spin (we discuss this in detail in Chapter 5). Though the contribution of stellar capture in mass growth of black hole is small, it plays an important role after the saturation time, when the accretion stops. We calculate the tidal radius, r_t, the capture radius, r_c and the loss cone radius, $r_\ell = \mathrm{Max}[r_t, r_c]$, in a relativistic

framework and using steady loss cone theory, to determine the rate of capture which in turn gives the mass growth rate by stellar capture process (discussed in Chapter 6). The loss cone is a region in velocity space, where, if a star is within that region, it is captured by the black hole [see Fig. 1.4]. Alexander and

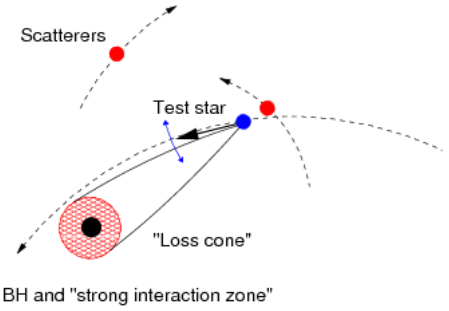

FIGURE 1.4: A schematic of the loss cone. Image courtesy: Alexander (2015).

Bar-Or (2017b) have studied the evolution of the mass of the black hole by star capture as well as accretion with and without merger activity. Non-relativistic loss cone theory is used for their analysis but the spin evolution of the black hole has not been considered. The rates of tidal disruption events for a single black hole in steady-state have been derived by different authors. Syer and Ulmer (1999) found the rate of capture to be $10^{-6} - 10^{-4}$ yr^{-1} gal^{-1} for main-sequence stars in the galaxies following the Nuker profile. Magorrian and Tremaine (1999), found that the rate is $10^{-9} - 10^{-4}$ yr^{-1} gal^{-1}, using a two integral model for non-spherical galaxies (triaxial) assuming that all the stars have centrophobic loop orbits and where the refilling of loss cone occurs by the two-body relaxation process. Rauch and Tremaine (1996) found an enhancement in the rate of tidal disruption due to resonant relaxation processes for stars bound to the black hole, but Rauch and Ingalls (1998) find that in the presence of relativistic precession of black hole masses $\geq 10^8 M_\odot$, this effect is quenched. By assuming a single mass star distribution and solving the steady-state Fokker - Planck equation for 51 galaxies following the Nuker profile, Wang and Merritt (2004), derived the rate of disruption to be $10^{-9} - 10^{-4}$ yr^{-1} with revised $M_\bullet - \sigma$ relation. Brockamp *et al.* (2011), using Aarseth's NBODY 6 code found the rate to be $10^{-6} - 10^{-4}$ yr^{-1} gal^{-1} assuming the Sersic profile with $n = 4$ for initial stellar distribution around black

hole. Kesden (2012) derived the capture rate in presence of the spin of the back hole to be $\sim 10^{-5} - 10^{-6}$ yr^{-1}. Mageshwaran and Mangalam (2015) derived the rate of $10^{4} - 10^{-5}$ yr^{-1} for $M_8 = 10^{-2} - 10^{2}$ in a non-relativistic steady-state loss cone regime. Komossa (2015), Donley *et al.* (2002) (ROSAT surveys), and Gezari *et al.* (2009) (in UV band) have provided observed values of TDEs for different wavelength bands to be about 10^{-5}yr^{-1}. We predicted capture rates of $10^{-5} - 10^{-6}$ yr^{-1} (discussed in Chapter 6), which are closer to the observed range.

1.3.3 Mergers

The merger of galaxies is a very important phenomenon in the field of Astrophysics, because, it can give implications about the galaxy evolution. During the merger process, the dark matter halos of two interacting galaxies get affected. Due to the violent relaxation process during mergers, the stars completely change their orbits losing any trace of the previous orbits (Binney and Tremaine 2008). In the new galaxy formed, stars are found mainly following random orbits, which is common in elliptical galaxies. In this course of galaxy mergers, the black holes residing at the centers of these galaxies also merge forming a single black hole at the center of the final galaxy. This can be an important fuel in the growth of supermassive black holes. This merger process is studied by simulations [see Fig. 1.5]. For this, one has to take care of the gravity along with hydrodynamics, dissipation and also energy and mass released due to supernovae. The galaxy can be formed due to several mergers causing the dark matter halos of the galaxies to merge together. This is called the merger tree (Binney and Tremaine 2008) and can be studied by the N- body simulations [Sheth and Lemson (1999), Somerville and Kolatt (1999)]. These mergers cause changes in the black hole spin also along with an increase in the mass of SMBH. Mergers can be classified, depending on the sizes of the galaxies involved, as major and minor mergers.

Major mergers

Major mergers are those, where, the merging galaxies are of almost the same size (Binney and Tremaine 2008). Active galactic nuclei (AGN) can be formed because of a major merger if the colliding angle and the colliding speed are appropriate. The final galaxy formed are elliptical galaxies. Many quasars are believed to be driven by this mechanism. This type of merger causes the spin of the black hole typically to increase.

Minor mergers

Minor mergers are those, where one galaxy is of sufficiently less size than the other one (Binney and Tremaine 2008). In this process, the larger galaxy does not get affected much, but it eats up the smaller one. In this type of merger, the black hole typically spins down.

FIGURE 1.5: A simulated image showing a major merger of two galaxies. Image courtesy: arstechnica.com.

Stewart *et al.* (2009) uses high-resolution ΛCDM N-body simulations for predicting merger rates in dark matter halos and investigate the scaling of common merger-related observables with luminosity, stellar mass, merger mass ratio, and redshift $z = 4 \rightarrow 0$. They derive the expression for merger rate (infall) valid for $0 \leq z \lesssim 4$ considering the peak of merger activity while the dependence on different parameters has been determined using simple fitting functions. The developed simulations which contained 512 particles of mass $3.16 \times 10^8 h^{-1} M_{\odot}$ which was

evolved within a comoving volume of $80h^{-1}$ Mpc on a side by the Adaptive Refinement Tree (ART) N - body code developed by Kravtsov *et al.* (1997, 2004). Using this, we derive the mass growth rate of SMBH by mergers considering a connection between the black hole and the dark matter halo mass. The detailed derivation has been given in Chapter 6. Gammie *et al.* (2004), Hughes and Blandford (2003) provide theories for the spin evolution of the black holes. Gammie *et al.* (2004) show that the major mergers cause the black hole to spin up while the minor merger causes spin down. We discuss the details of spin evolution by these authors in Chapter 5 and we use these factors to derive the complete evolution model of black holes in Chapter 6.

1.3.4 Blandford-Znajek effect

The Blandford-Znajek effect is the process of energy extraction from a rotating black hole by a strong magnetic field. Blandford and Znajek (1977) derive the process by which the magnetic field drives the powerful jet from the black hole from its rotational energy [see Fig. 1.6]. When magnetic field lines thread a rotating black hole which is supported by external currents that are flowing in an equatorial disc, there will be induced electrical potential difference. For large field strengths, the vacuum will be unstable to the cascade production of electron-positron pair creating a force-free magnetosphere leading to an electromagnetic extraction of energy and angular momentum. Blandford and Znajek (1977) have derived approximate solutions for the black holes rotating slowly to provide a model of the central engine of the AGN. The advantage of this model is that the relativistic electrons can be accelerated efficiently compared to other models. This causes the spin-down of the black hole due to the extraction of energy. We discuss the Blandford-Znajek model (Frank *et al.* 2002) in detail in Chapter 5.

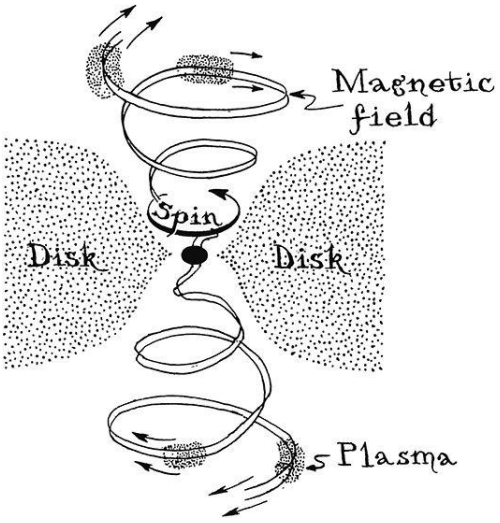

FIGURE 1.6: Blandford Znajek effect for producing jets. Image courtesy: Drawing by Matt Zimet based on a sketch by Kip Thorne from the book- Black Holes & Time Warps: Einstein's Outrageous Legacy.

1.4 Evolution of black holes

Mangalam (2015) used a theoretical model for mass and spin evolution of the accreting black hole taking into account the spin-down torque caused by the electrodynamical jet. The evolution in the presence and absence of accretion was studied for different cases such as the thin disk, Bondi accretion, and the MHD disk. Dubois *et al.* (2014) has derived the mass evolution through simulations caused by accretion and mergers and used semi-analytic methods for spin evolution for the same. Our calculations, for deriving the joint black hole mass and spin evolution, consider all the possible factors contributing to the growth of black holes like accretion, stellar capture, mergers, and BZ torque simultaneously; previously, there were models for determination of the evolution for these different factors separately. We have built a model for the evolution of measured spin of black holes and estimated its impact on the $M_\bullet - \sigma$ relation (which we discuss next) in ΛCDM cosmology that is predicated on the physics of gas accretion and star capture, electromagnetic torque, and mergers (discussed in Chapter 6). We have self-consistently solved coupled equations to get a more complete picture of

the evolution of the spin and mass of the SMBH. Our results seem to agree well with a preliminary analysis of observational data of different galaxies (discussed in Chapter 6).

1.5 Galaxy scaling relations

For studying the nuclear activity in galaxies, in the standard models, it is assumed that, black holes exist at their centers with masses $10^6 - 10^9\ M_\odot$ and they emit in radio wavelengths (Frolov and Novikov 1998). For many galaxies, having active nuclei, there is evidence for the existence of these black holes. The mass of the black hole is $\sim 10^{-3}$ times of that of the galactic bulge [Merritt and Ferrarese (2001), Marconi and Hunt (2003), Häring and Rix (2004), Bhattacharyya and Mangalam (2018)], though, for higher masses, the relation is said to be nonlinear and given by $M_\bullet \propto M_b^{1.12}$ (Häring and Rix 2004). Kormendy and Ho (2013) have also found the following relation:

$$\left(\frac{M_\bullet}{10^9 M_\odot}\right) = 0.49^{+0.06}_{-0.05}\left(\frac{M_b}{10^{11} M_\odot}\right)^{1.17\pm0.08}. \tag{1.5}$$

King and Pounds (2015) also derive $M_\bullet - M_b$ relation to be a linear one, where they use momentum driven flow (discussed in detail in chapter 3), to determine the bulge mass and the saturated black hole mass and they conclude that the ratio is $\sim 10^{-3}$. For simplicity, a proportionality relation is not a very bad approximation. This relation between the bulge mass and the black hole mass encourages us to consider the co-evolution of the galaxy and the black hole at its center.

The relation of the SMBHs to the host galaxies can be found by the strong correlation of the mass of SMBH and velocity dispersion, σ, of the stars in the galaxy. This is quite surprising because the stars are far from the black hole for σ to be

affected by the gravitational field of the hole. The origin of this correlation is still a topic of debate.

The general form of the $M_\bullet - \sigma$ relation is given by

$$M_\bullet = k\sigma^p, \tag{1.6}$$

which was first reported by Ferrarese and Merritt (2000) with $p = 4.8 \pm 0.5$, whereas, Gebhardt *et al.* (2000) reported the index, $p = 3.75 \pm 0.3$. But this relation was published some five years later after the first attempt to derive the relation between $M_\bullet$ and the luminosity, L. The relationship between σ and luminosity of elliptical galaxy, L_{ell}, is given by the Faber - Jackson relation which states that

$$L_{ell} \propto \sigma^\alpha,$$

where, $\alpha \approx 4$. Faber - Jackson relation is considered as a projection of the fundamental plane of elliptical galaxies. If the elliptical galaxies are plotted in a three dimensional plane described by the effective radius, R_e, average surface brightness, μ_e and central velocity dispersion σ_0, all the galaxies lie in one plane called the fundamental plane. Any of these three parameters can be determined if one knows the other two. This plane is described by

$$\log(R_e) = a\log(\sigma_0) + b\log < \mu >_e + \text{constant}.$$

From literature values of a and b are within $1.17 - 1.61$ and $(-0.84) - (-0.74)$. The fundamental plane of elliptical galaxies is shown in Fig. 1.7. For the disk galaxies, a connection between luminosity, L_{disk} and the rotation curve amplitude, ΔV, is provided by the Tully - Fisher relation, which is

$$l_{disk} = (\Delta v)^\beta,$$

with $\beta = 4$. With these relations and by the dynamically measured $M_\bullet$, one can

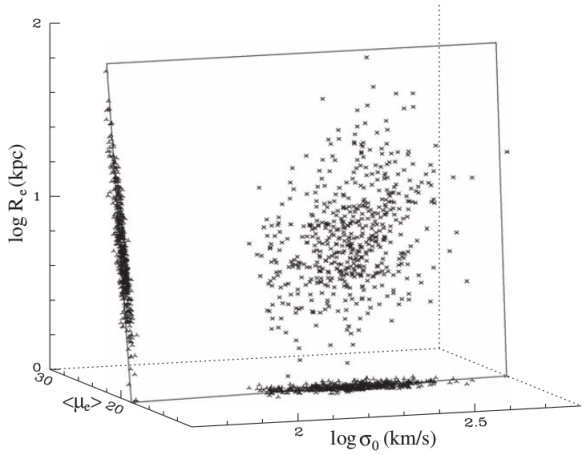

FIGURE 1.7: The fundamental plane of the elliptical galaxies is shown. Image courtesy: Saglia *et al.* (1997), Wegner *et al.* (1999).

derive the $M_\bullet - \sigma$ relation. But, this was not done prior to 2000, because, the scatter in the plot of $M_\bullet - \sigma$ was larger compared to the infrared $M_\bullet - L$ plot and almost comparable to the visual $M_\bullet - L$ plot. After it was realized that, the scatter depends largely on the selection of the sample (Ferrarese and Merritt 2000), progress was made in this field. When the $M_\bullet$ - σ relation was derived for a restricted sample showing central velocity rise, the scatter found was almost consistent with the zero intensity scatter (shown in Fig. 1.8) and Ferrarese and Merritt (2000), deduced $p = 4.8 \pm 0.5$, as mentioned earlier. A list of values of p determined by different authors is given in Chapter 3 [see Table 3.1]. There are some theoretical derivations of these relations given by Silk and Rees (1998), King (2003) and Zhao *et al.* (2002). In the first two arguments this relation automatically comes from the concept of feedback in accretion process during the growth of the black hole, while, the last work finds the $M_\bullet - \sigma$ relation through stellar capture (shown for an isothermal sphere case). Natarajan and Treister (2009) found that the upper limit of the mass of black hole can be set by these arguments provided by King (2003), King (2005), (Silk and Rees 1998), (Haehnelt *et al.* 1998), all of which finally lead to the observed $M_\bullet - \sigma$ naturally. We discuss these models in detail in Chapter 3.

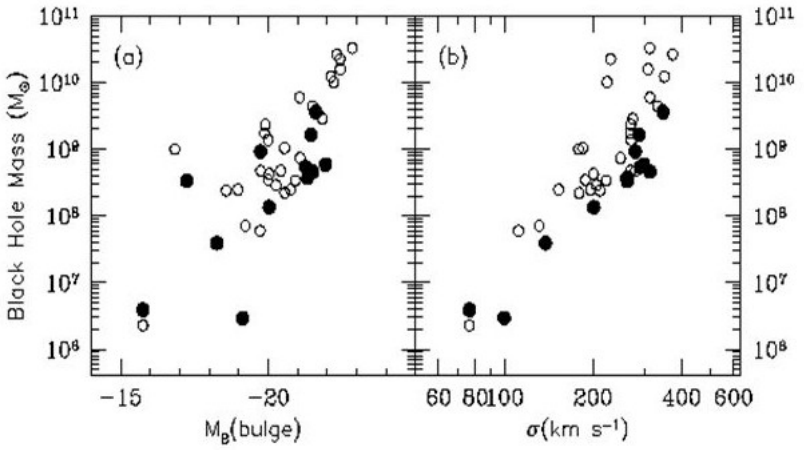

FIGURE 1.8: (a) Plot of $M_\bullet$ vs bulge visual luminosity, M_B, (b) $M_\bullet - \sigma$ plot, where, open circles correspond to the masses derived from mostly stellar dynamical measurements and the filled circles are for the restricted sample with high central velocity. Image courtesy: Ferrarese and Merritt (2000).

The evolution of the $M_\bullet - \sigma$ relation has received a lot of attention. Shen *et al.* (2015) and Salviander and Shields (2013) have analyzed the evolution of this relation from SDSS data for quasars and they report no evolution of the relation up to $z \simeq 1$. Robertson *et al.* (2006) studied the evolution of this relation till $z = 6$, for merging disk galaxies through hydrodynamic simulations and they have taken into account the effects of accretion and supernovae. They also found almost no change in $p(z)$ and a very small change of the constant, $k_0(z)$, similarly to Shankar *et al.* (2009a). From their analysis, $k_0(z) \propto (1+z)^\alpha$, with $\alpha = 0.33$. Sijacki *et al.* (2015) and Taylor and Kobayashi (2016), from the Numerical simulations, of the large-scale structure of the Universe, found almost up to $z \simeq 4$ that, this relation holds without much variation. We also study the evolution of $p(z)$ and k as an application of our theoretical model (details are given in Chapter 6). We consider the Faber - Jackson relation to be the initial condition, which provides that $p = 5$ at formation redshift and due to saturation of the black hole mass, we see that it reaches near 4 at $z \simeq 0$. But, this value of p remains well within 4 - 5, as found observationally [details are given in Chapter 6].

1.6 Black hole archaeology and the black hole initial seed mass and spin function

The model, we construct to study the evolution of black hole mass and spin, has an application to black hole archaeology (discussed in Chapter 6). We run our model backwards in time taking the observed mass and spin value to be the initial condition and retrieve the initial seed mass and spin values at the formation redshift. We derive the the seed spin and mass of the black holes by retrodicting our model from the known parameters of the quasars ULASJ134208.10+092838.61 (z=7.54), ULASJ112001.48+064124.3 (z=7.08) and DELSJ003836.10-152723.6 (z=7.02) (Campitiello *et al.* 2019) (details are in Chapter 6). Black hole initial seed mass and spin functions are another unsolved problem in Astrophysics. The probability distribution of the spin parameter of the halo λ can be obtained by cosmological N - body simulations and Lodato and Natarajan (2007), Warren *et al.* (1992) use log normal distributions. Using that probability and the Schechter mass function for black holes we derive some preliminary results for the initial seed mass and spin function of black holes which we present in chapter 7.

1.7 Goals of the Thesis

1. Studying the static as well as the dynamical aspect of the $M_\bullet - \sigma$ relation.

2. Building a complete evolution model of black holes and to throw some light on the black hole-galaxy co-evolution as an application of our model.

3. As a part of the static aspect, to provide a detailed model of determining the $M_\bullet - \sigma$ relation and $M_\bullet - M_b$ relation simultaneously from observed intensity profiles or the mass density profiles of the galaxies (assuming spherical geometry).

4. To compute the stellar capture rate in the relativistic framework by deriving the tidal radius, capture radius and the loss cone radius in the relativistic case and applying them to the capture rate calculation in steady loss cone theory.

5. To build a complete model of the evolution of the black hole starting from an initial seed mass and spin, taking into account all the effects that can contribute to the spin and mass evolution of black holes - accretion, stellar capture, mergers and Blandford-Znajek torque.

6. As an application of our evolution model, we study the evolution of the $M_\bullet - \sigma$ relation and compare that with observations. This forms the dynamical study of the $M_\bullet - \sigma$ relation.

7. Black hole archaeology is another application of our evolution model, where we run our model backward to guess the seed mass and spin of the black hole at formation redshift considering the present values as the initial conditions.

8. Sketch the $M_\bullet - \sigma$ relation in the axisymmetric system theoretically and also derive the initial seed mass and spin functions of the black holes.

9. To provide a context for future work.

1.8 The plan of the Thesis

The chapter-wise plan of the thesis is given below and the concept flow chart is shown in Fig 1.9.

- In chapter 2, we discuss the basics of stellar dynamics, derive the formulae that connects the observables to the distribution function in both spherical and axisymmetric system, which we use later on in Chapter 4 and 7, to

build our model of deriving the $M_\bullet - \sigma$ relation in spherical systems and in axisymmetric systems respectively. Then, we also derive the distribution function for some known potential-density models. Also, we discuss the Jeans equations in spherical as well as axisymmetric systems which we will be using in our future work for building some models.

- In chapter 3, we present an introduction to the $M_\bullet - \sigma$ relation followed by the literature survey of this relation. Then, we discuss some well known theoretical models to explain this relation and lastly we present a literature survey of the evolution of the $M_\bullet - \sigma$ relation.

- In chapter 4, we present our model of deriving $M_\bullet - \sigma$ relation and the $M_\bullet - M_b$ relation simultaneously, from the mass density profile of the power-law galaxies and the observed Nuker intensity profiles of some elliptical galaxies assuming a spherical structure. This is published in Bhattacharyya and Mangalam (2018).

- In chapter 5, we sketch the basic physics of the growth of the black hole via accretion, stellar capture, mergers, electromagnetic torque and we present a literature study of the mass and spin evolution of the black holes through these processes.

- In chapter 6, we present our relativistic treatment of the tidal, capture and loss cone radius, thereby deriving the relativistic stellar capture rate followed by our complete model of black hole evolution including all the effects mentioned in Chapter 5. We also discuss two applications of our model: evolution of the $M_\bullet - \sigma$ relation and the black hole archaeology and its use in some recently observed quasars. This is under review in ApJ.

- In chapter 7, we discuss two of our ongoing projects: $M_\bullet - \sigma$ relation in axisymmetric systems and the initial seed mass and spin function. We formulate the problems and present the preliminary results found, and discuss our future work.

- In chapter 8, we summarize our work, discuss the the novel aspects, and its implications for future studies. We also present the caveats and future theoretical approaches.

1.9 Resource summary

In this chapter, we presented basic introduction to black holes, its evolution, the $M_\bullet - \sigma$ evolution, their literature survey along with the motivation of the Thesis. We also presented a schematic of the Thesis and its goals in Fig. 1.9. The main resources we used for discussion are - Kolb (2010), Binney and Tremaine (2008), Frolov and Novikov (1998), and Frank *et al.* (2002).

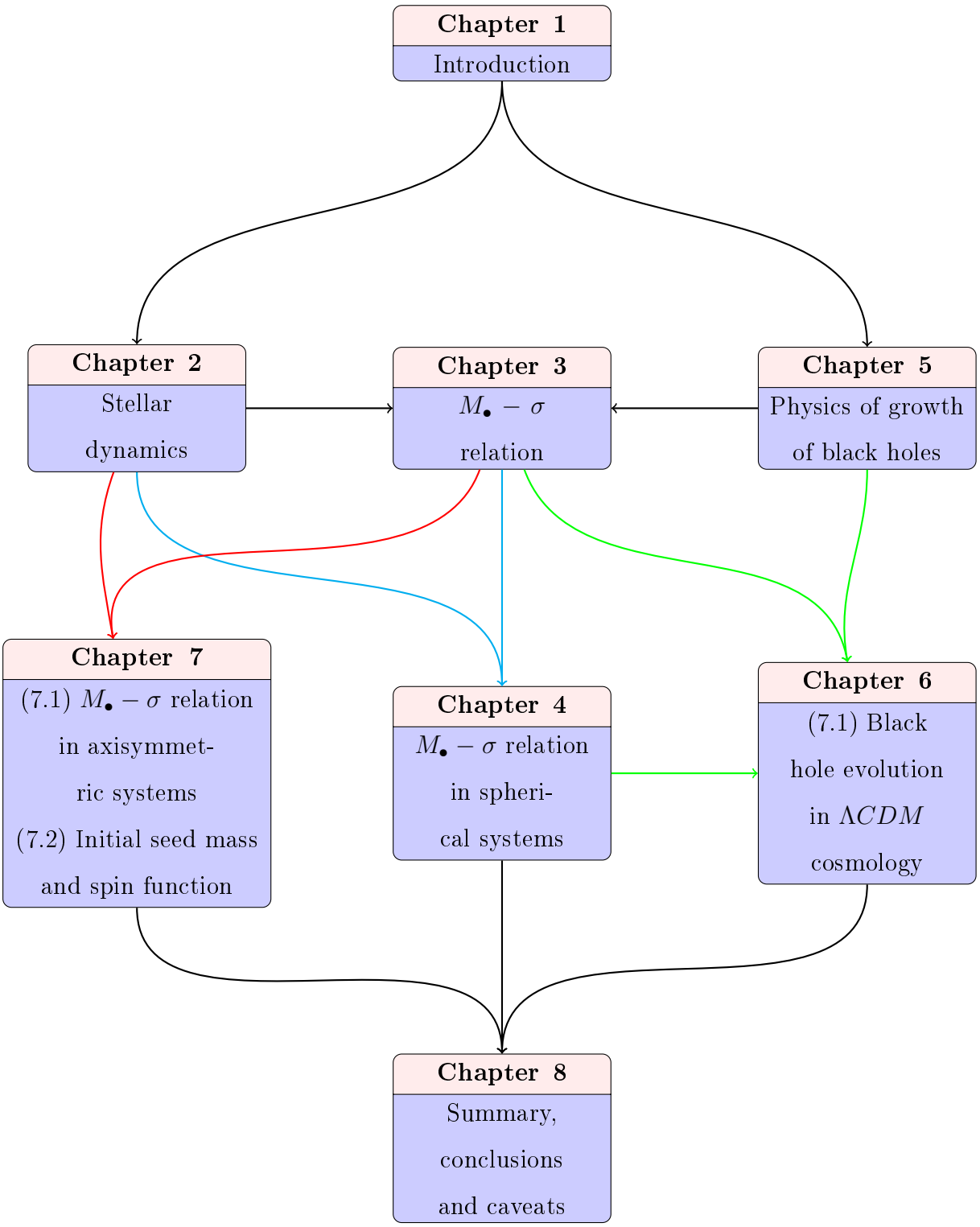

FIGURE 1.9: The plan of the thesis is shown.

Chapter 2

Image: astro.yale.edu

Stellar Dynamics

2.1 Introduction

The fundamental and basic building blocks of our universe are the galaxies and to understand them, one of the main tools is studying stellar dynamics. A stellar system is an assembly of point masses or stars which are gravitationally bound to each other and stellar dynamics is a subject where, their motions are studied under their self- gravitational field. In this chapter, we discuss the relationship of the observable quantities in stellar dynamics, with the distribution function (DF) of the stars followed by the discussion of the DF of spherical systems in isotropic as well as anisotropic cases with examples of some known potential-density pairs. Then, we discuss the Jeans equations in spherical systems. The next section provides the DF of the axisymmetric systems along with some special cases followed by the Jeans equations in axisymmetric systems and their importance.

2.2 Relationship between the observables and the DF

The probability of finding a star irrespective of its velocity, $\mathbf{v}$, at a fixed position $\mathbf{x}$, per unit volume is given by (Binney and Tremaine 2008)

$$\nu(\mathbf{x}) = \int \mathrm{d}^3\mathbf{v} f(\mathbf{x}, \mathbf{v}), \tag{2.1}$$

where $f(\mathbf{x}, \mathbf{v})$ is the phase space DF of the stars. Integration of $f(\mathbf{x}, \mathbf{v})$ over the phase space provides the probability of finding a particular star in the phase space volume. The probability distribution of the velocities of stars at $\mathbf{x}$ is given by the ratio of $f(\mathbf{x}, \mathbf{v})$ and $\nu(\mathbf{x})$ as

$$P_x(\mathbf{v}) = \frac{\mathbf{f}(\mathbf{x}, \mathbf{v})}{\nu(\mathbf{x})}, \tag{2.2}$$

which is measurable near the Sun [Binney and Merrifield (1998), §10.3]. For the external galaxies, P_x can be measured via the line of sight (LOS) velocity distribution [Binney and Merrifield (1998), §11.1], for a fraction of stars $F(v_{||})dv_{||}$, whose LOS velocities lie within $v_{||} + \mathrm{d}v_{||}$. Since, the stars are quite far from us, any point $\mathbf{x}$ in the galaxy can be considered to lie in parallel with unit vector $\hat{s}$, connecting the galaxy center and the observer. Therefore, the components of $\mathbf{x}$ and $\mathbf{v}$, in the parallel and perpendicular direction of the LOS is written as

$$x_{||} = \mathbf{x} \cdot \hat{s}, \quad v_{||} = \mathbf{v} \cdot \hat{s}, \quad \mathbf{x}_\perp = \mathbf{x} - x_{||}\hat{s}, \quad \mathbf{v}_\perp = \mathbf{v} - v_{||}\hat{s}. \tag{2.3}$$

$F(v_{||}, x_\perp)$ can be expressed as

$$\begin{aligned} F(v_{||}, \mathbf{x}_\perp) &= \frac{\int \mathrm{d}x_{||} \nu(\mathbf{x}) \int \mathrm{d}^2\mathbf{v}_\perp P_x(\mathbf{v}_\perp + v_{||}\hat{s})}{\int \mathrm{d}x_{||} \nu(\mathbf{x})} \\ &= \frac{\int \mathrm{d}x_{||} \int \mathrm{d}^2\mathbf{v}_\perp f(\mathbf{x}, \mathbf{v})}{\int \mathrm{d}x_{||} \int \mathrm{d}^2\mathbf{v} f(\mathbf{x}, \mathbf{v})} \end{aligned} \tag{2.4}$$

The LOS velocity distribution is quantified the mean velocity in the direction of LOS, $\bar{v}_{||}$, and the dispersion about this mean value, $\sigma_{||}$ given as

$$\begin{aligned} v_{||}(\mathbf{x}_\perp) &= \int \mathrm{d}v_{||} v_{||} F(v_{||}, \mathbf{x}_\perp) \\ &= \frac{\int \mathrm{d}x_{||} \nu(\mathbf{x}) \hat{s} \cdot \bar{\mathbf{v}}}{\int \mathrm{d}x_{||} \nu(\mathbf{x})}, \end{aligned} \tag{2.5}$$

where

$$\bar{\mathbf{v}}(\mathbf{x}) \equiv \int \mathrm{d}^3\mathbf{v}\mathbf{v}P_x(\mathbf{v}) = \frac{1}{\nu(\mathbf{x})} \int \mathrm{d}^3\mathbf{v} f(\mathbf{x}, \mathbf{v}), \tag{2.6}$$

and

$$\begin{aligned} \sigma_{||}^2 &\equiv \int \mathrm{d}v_{||} (v_{||} - \bar{v}_{||})^2 F(v_{||}, \mathbf{x}_\perp) \\ &= \frac{\int \mathrm{d}x_{||} \mathrm{d}^3\mathbf{v} v_{||}^2 f(x, v)}{\int \mathrm{d}x_{||} \mathrm{d}^3\mathbf{v} f(x, v)}. \end{aligned} \tag{2.7}$$

We use this eqn. (2.7) later on to derive the LOS velocity dispersion of galaxies and determine the $M_\bullet - \sigma$ relation.

2.3 DF for spherical systems

Spherical models are important to study in astrophysics, because, globular clusters, some elliptical galaxies, and galaxy clusters are almost in spherical shape and spherical models are simpler to study and understand. The systems have one stellar population, thus have a single f, where, the stellar potential is obtained by the Poisson's equation from mass density (which is proportional to $\int f \mathrm{d}^3\mathbf{v}$) and the f is obtained via the collisionless Boltzmann equation using the potential, are called the self - consistent systems. The relative potential, ψ, and energy, ε, of a star are defined as (Binney and Tremaine 2008)

$$\psi \equiv -\Phi + \Phi_0, \varepsilon \equiv -H + \Phi_0 = \psi - \frac{1}{2}v^2, \tag{2.8}$$

where the Hamiltonian, $H = \Phi(\mathbf{x}) + \frac{1}{2}v^2$, and Φ_0 is a constant, chosen such that the DF is always positive, i.e, $f > 0$ for $\varepsilon > 0$ and $f = 0$ for $\varepsilon \leq 0$. For an isolated system having its extent upto ∞, $\Phi_0 = 0$ and the relative energy, in this case, will be equal to that of gravitational binding energy. Therefore, the Poisson's equation with new parameters is written as

$$\nabla^2\psi = -4\pi G\rho, \tag{2.9}$$

where the boundary condition is that $\psi \to \Phi_0$ for $|x| \to \infty$.

2.3.1 Ergodic DF for spherical systems

For a spherical system with a known potential $\Phi(r)$, an ergodic DF can be obtained which will depend on the Hamiltonian $H(\mathbf{x}, \mathbf{v})$, thus on the phase space coordinate. The DF can be expressed as a function of ε while f, depends only on the magnitude of the velocity vector $\mathbf{v}$ and not its direction. Therefore, $\nu(r)$, the probability density is written as (Binney and Tremaine 2008)

$$\nu(r) = 4\pi \int \mathrm{d}v v^2 f(\psi - \frac{1}{2}v^2) = 4\pi \int_0^\psi \mathrm{d}\varepsilon f(\varepsilon)\sqrt{2(\psi - \varepsilon).} \tag{2.10}$$

Since, ψ is a monotonic function of r, $\nu(r)$ can be written as $\nu(\psi)$. Therefore

$$\frac{1}{\sqrt{8}\pi}\nu(\psi) = 2\int_0^\psi \mathrm{d}\varepsilon f(\varepsilon)\sqrt{(\psi - \varepsilon).} \tag{2.11}$$

Differentiation of both sides with respect to ψ gives

$$\frac{1}{\sqrt{8}\pi}\frac{\mathrm{d}\nu}{d\psi} = \int_0^\psi \mathrm{d}\varepsilon \frac{f(\varepsilon)}{\sqrt{\psi - \varepsilon}}. \tag{2.12}$$

Using Abel's equation, the form of DF is obtained as

$$f(\varepsilon) = \frac{1}{\sqrt{8}\pi^2}\frac{\mathrm{d}}{\mathrm{d}\varepsilon}\int_0^{\varepsilon}\frac{\mathrm{d}\nu}{\mathrm{d}\psi}\frac{\mathrm{d}\psi}{\sqrt{\varepsilon-\psi}}. \tag{2.13}$$

This is called Eddington's formula (Binney and Tremaine 2008). We use this eqn. (2.13) later on in Chapter 5 to find the DF of the stars of the galaxy (assuming a spherical geometry), which in turn gives the velocity dispersion and we use that to compute the $M_\bullet - \sigma$ relation [the model is shown in Fig. 2.1].

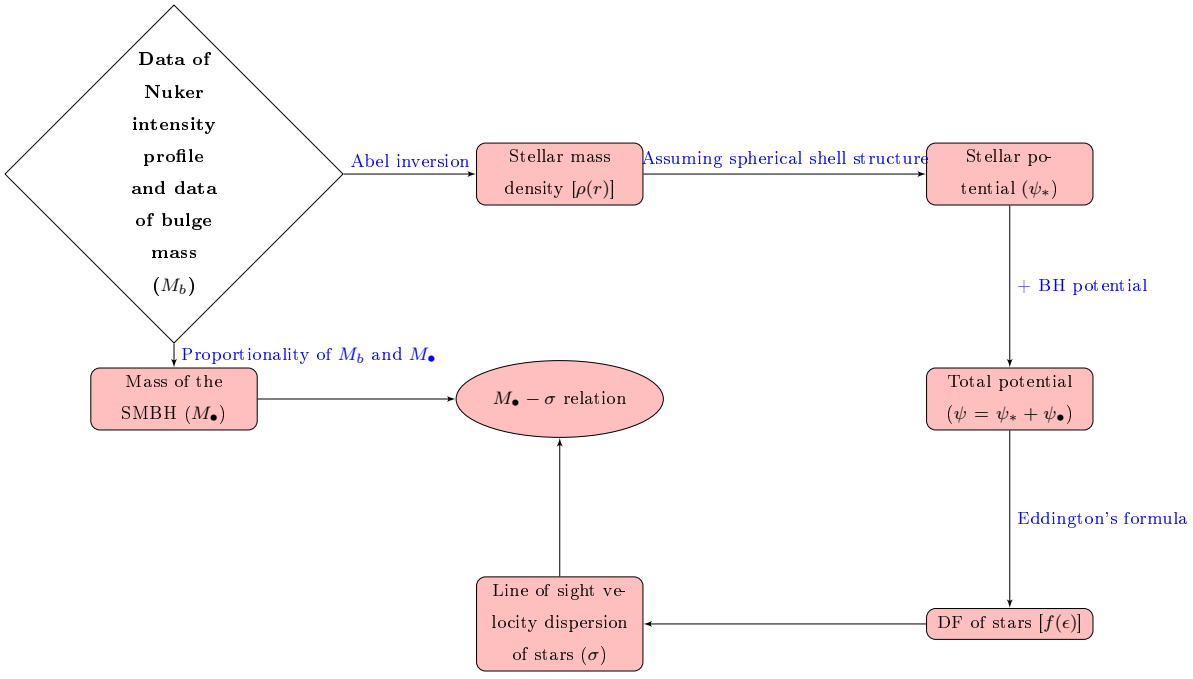

FIGURE 2.1: The model for deriving $M_\bullet - \sigma$ relation in presence of central black holes.

2.3.1.1 Ergodic DF for some known models

Double power law density models

Observationally, it has been seen that many elliptical galaxies show double power law luminosity profiles that can be fit by a power - law, then, whose index changes

after some intermediate point, but, the transition is smooth. These type of profiles are called double power law profiles [Binney and Merrifield (1998), §4.3.1]. It is also suggested from numerical simulations that, the mass density also follows similar type of profiles [Binney and Tremaine (2008), §9.3]. The general mass density for these models is given by

$$\rho(r) = \frac{\rho_0}{(r/a)^{\alpha}(1+r/a)^{\beta-\alpha}}, \tag{2.14}$$

where a is the length scale and α and β are the power law indices. From eqn. (2.14), the total mass within radius r is

$$M(r) = 4\pi\rho_0 a^3 \int_0^{r/a} \mathrm{d}s \frac{s^{2-\alpha}}{(1+s)^{\beta-\alpha}}. \tag{2.15}$$

The potential of these models is computed as

$$\Phi = -G \int_r^{\infty} \mathrm{d}r \frac{M(r)}{r^2}. \tag{2.16}$$

We discuss two such simple models here.

(a) Hernquist model

Substituting $\alpha = 1$ and $\beta = 4$, in the double power law profile (Hernquist 1990)

$$\rho(r) = \frac{\rho_0}{(r/a)(1+r/a)^3}, \tag{2.17}$$

$$M(r) = 4\pi\rho_0 a^3 \int_0^{r/a} \mathrm{d}s \frac{s}{(1+s)^3}, \tag{2.18}$$

$$\Phi = -4\pi G\rho_0 a^2 \frac{1}{2(1+r/a)}. \tag{2.19}$$

If $\tilde{\psi}$ is defined as

$$\tilde{\psi} \equiv \frac{\psi a}{GM} = -\frac{\Phi a}{GM},$$

then, from eqn. (2.19)

$$\frac{r}{a} = \frac{1}{\tilde{\psi}} - 1. \tag{2.20}$$

Using this eqn. (2.20), in eqn. (2.17), $\nu(\psi)$ for Hernquist model is obtained as

$$\nu(\psi) = \frac{\rho}{M} = \frac{1}{2\pi a^3}\frac{\tilde{\psi}^4}{1-\tilde{\psi}}. \tag{2.21}$$

By using Eddington's formula [eqn. (2.13)] with the eqns. (2.21, 2.19), the ergodic DF for the Hernquist model is

$$f_H(\varepsilon) = \frac{1}{\sqrt{2}(2\pi)^3(GMa)^{3/2}}\frac{\sqrt{\tilde{\varepsilon}}}{(1-\tilde{\varepsilon})^2}\times\left[(1-2\tilde{\varepsilon})(8\tilde{\varepsilon}^2-8\tilde{\varepsilon}-3)+\frac{3\sin^{-1}\sqrt{\tilde{\varepsilon}}}{\sqrt{\tilde{\varepsilon}(1-\tilde{\varepsilon})}}\right], \tag{2.22}$$

where $\tilde{\varepsilon} \equiv -Ea/GM$.

(b) Jaffe model

$\alpha = 2$ and $\beta = 4$, in the double power law profile gives the Jaffe model (Jaffe 1983). For this model

$$\rho(r) = \frac{\rho_0}{(r/a)^2(1+r/a)^2}, \tag{2.23}$$

$$M(r) = 4\pi\rho_0 a^3 \int_0^{r/a} \mathrm{d}s \frac{1}{(1+s)^2}, \tag{2.24}$$

$$\Phi = -4\pi G\rho_0 a^2 \frac{\ln(1+r/a)}{r/a}. \tag{2.25}$$

For Jaffe model, $\frac{r}{a} = \frac{1}{e^{\tilde{\psi}}-1}$, where $\tilde{\psi}$ is the same as defined above. Therefore, the resulting ν in this case is

$$\nu = \frac{1}{4\pi a^3} e^{-2\tilde{\psi}}(e^{\tilde{\psi}}-1)^4. \tag{2.26}$$

Now, using eqns. (2.26, 2.25) in Eddington's formula [eqn. (2.13)], the ergodic DF for Jaffe model is given by

$$f_J(\varepsilon) = \frac{1}{2\pi^3(GMa)^{3/2}}\left[F_-(\sqrt{2\tilde{\varepsilon}}) - \sqrt{2}F_-(\sqrt{\tilde{\varepsilon}}) - \sqrt{2}F_+(\sqrt{\tilde{\varepsilon}}) + F_+(\sqrt{2\tilde{\varepsilon}})\right], \tag{2.27}$$

where $F_{\pm}$ is Dawson's integral.

Isochrone models

Isochrone potential is given as (Binney and Tremaine 2008)

$$\Phi(r) = -\frac{GM}{b + \sqrt{b^2 + r^2}}, \tag{2.28}$$

where b is the scale length. Using Poisson's equation, for this potential [eqn. (2.28)] the corresponding mass density of the isochrone model is given by

$$\rho(r) = \frac{1}{4\pi G}\frac{1}{r^2}\frac{\mathrm{d}}{\mathrm{d}r}\left(r^2\frac{\mathrm{d}\Phi}{\mathrm{d}r}\right) = M\left[\frac{3(b+a)a^2 - r^2(b+3a)}{4\pi(b+a)^3a^3}\right]. \tag{2.29}$$

Therefore, the central density is obtained as

$$\rho(0) = \frac{3M}{16\pi b^3}. \tag{2.30}$$

Using eqns. (2.29, 2.28) in Eddington's formula [eqn. (2.13)], the ergodic DF for isochrone model is given by (Hénon 1960)

$$f_I(\tilde{\varepsilon}) = \frac{1}{\sqrt{2}(2\pi)^3(GMb)^{3/2}}\frac{\sqrt{\tilde{\varepsilon}}}{[2(1-\tilde{\varepsilon})]^4}$$
$$\left[27 - 66\tilde{\varepsilon} + 320\tilde{\varepsilon}^2 - 240\tilde{\varepsilon}^3 + 64\tilde{\varepsilon}^4 + 3(16\tilde{\varepsilon}^2 + 28\tilde{\varepsilon} - 9)\frac{\sin^{-1}\sqrt{\tilde{\varepsilon}}}{\sqrt{\tilde{\varepsilon}(1-\tilde{\varepsilon})}}\right]. \tag{2.31}$$

2.3.2 DF for anisotropic spherical systems

If we take the DF of the form $f(E)$, it is not always possible that $f \geq 0$. But if it is of the form $f(E, L)$ built by only using circular orbits, then we can always get non-negative DFs (Binney and Tremaine 2008).

Reason for getting non-negative DFs

The circular orbits of relative energy ε' are combined with their angular momentum vectors which are distributed over a sphere uniformly to generate a spherical shell with the radii of the circular orbits with relative energy ε'. Then, any density profile can be formed by weighing the spherical shells radially. The DF of the spherical shells is proportional to the product of the two delta functions as $f_s(\varepsilon, L) = \delta(\varepsilon - \varepsilon')\delta[L - L_c(\varepsilon')]$. Here, $L_c(\varepsilon')$ is the angular momentum of a circular orbit of relative energy ε'. Therefore, the DF generating required density distribution $\nu(r)$ is given by (Binney and Tremaine 2008)

$$f_c(\varepsilon, L) \equiv \int_0^{\varepsilon_{max}} \mathrm{d}\varepsilon' f_s(\varepsilon', L) F(\varepsilon') = F(\varepsilon)\delta[L - L_c(\varepsilon)]. \tag{2.32}$$

Here, $F(\varepsilon')$ is a suitably chosen non-negative function. If circular orbit DF along with the non-negative ergodic function exists together, then, the two DFs are joined by a continuum of DFs as

$$f_\alpha \equiv \alpha f_i + (1 - \alpha) f_c, (0 \leq \alpha \leq 1), \tag{2.33}$$

where f_c is for circular orbit (associated with vanishing radial dispersion σ_r) and f_i is for ergodic DF. Increase of α makes the orbits more eccentric and σ_r also increases and tends to σ_θ. If $\alpha > 1$, then $\sigma_r > \sigma_\theta$, but as the eccentricity increases, the constraints on $\nu(r)$ that $f_\alpha > 0$ becomes severe. If $\nu(r)$ is such that ergodic DF is negative somewhere, then also the circular orbit DF is non negative, making the total contribution to be non - negative.

Anisotropy parameter

The anisotropy parameter is defined as (Binney and Tremaine 2008)

$$\beta \equiv 1 - \frac{\sigma_\theta^2 + \sigma_\phi^2}{2\sigma_r^2} = 1 - \frac{v_\theta^2 + v_\phi^2}{2v_r^2,} \tag{2.34}$$

which defines the degree of anisotropy of the system. Some special cases are listed below :

- If all the orbits are circular, $\sigma_r = 0$ and $\beta = -\infty$.
- For ergodic DFs, $\beta = 0$.
- For all radial orbits, $\sigma_\theta = \sigma_\phi = 0$ and $\beta = 1$.
- For $\beta < 0$, the DFs are called tangentially biased.
- For $\beta > 0$, the DFs are called radially biased.

Models with constant anisotropy

Here, the anisotropy parameter β takes some fixed non - zero value at all radii when the DF can be written in the form (Binney and Tremaine 2008)

$$f(\varepsilon, L) = L^{-2\beta} f_1(\varepsilon), \tag{2.35}$$

where f_1 is an arbitrary non - negative function. Here, we will be using polar coordinates in velocity space as [see Fig. (2.2)]

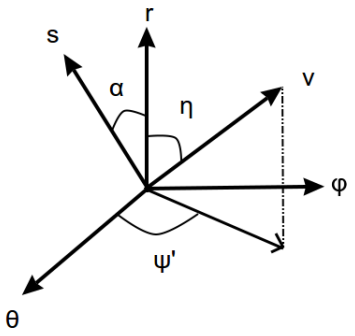

FIGURE 2.2: The velocity vector $\mathbf{v}$, LOS direction $\hat{s}$ and the definition of the angles α, η and ψ' are sketched.

$$v_r = v\cos\eta, v_\theta = v\sin\eta\cos\psi', v_\phi = v\sin\eta\sin\psi'. \tag{2.36}$$

The density profile can be written as

$$\nu(r) = \int \mathrm{d}^3\vec{v} f(\varepsilon, L) = 2\pi \int_0^\pi \mathrm{d}\eta \sin\eta \int_0^{\sqrt{2\psi}} dv v^2 f(\psi - \frac{1}{2}v^2, rv\sin\eta) \tag{2.37}$$

Since, $v_t = \sqrt{v_\theta^2 + v_\phi^2} = v\sin\eta$ and $L = rv_t$, $f(\varepsilon, L)$ can be expressed as

$$f(\varepsilon, L) = (rv_t)^{-2\beta} f_1(\psi - \frac{1}{2}v^2) = (rv\sin\eta)^{-2\beta} f_1(\psi(r) - \frac{1}{2}v^2). \tag{2.38}$$

Therefore

$$\begin{aligned}\nu(r) &= 2\pi \int_0^\pi \mathrm{d}\eta \sin^{1-2\beta}\eta \int_0^\infty \mathrm{d}v r^{-2\beta} v^{2-2\beta} f_1(\psi(r) - \frac{1}{2}v^2) \\ &= \frac{2\pi I_\beta}{r^{2\beta}} \int_0^\infty \mathrm{d}v v^{2-2\beta} f_1(\psi(r) - \frac{1}{2}v^2)\end{aligned} \tag{2.39}$$

where $I_\beta = \int_0^\pi \mathrm{d}\eta \sin^{1-2\beta}\eta = \sqrt{\pi}\frac{(-\beta!}{(\frac{1}{2}-\beta)!}(\beta < 1)$.
Now, $\varepsilon = \psi - \frac{1}{2}v^2$, which implies $\mathrm{d}\varepsilon = -v\mathrm{d}v$. Therefore, ν can be written as

$$\nu = \frac{2\pi I_\beta}{r^{2\beta}} \int_0^\psi \mathrm{d}\varepsilon (2(\psi - \varepsilon))^{\frac{1-2\beta}{2}} f_1(\varepsilon)$$

$$\Rightarrow \frac{2^{\beta-\frac{1}{2}}}{2\pi I_\beta} r^{2\beta}\nu = \int_0^\psi d\varepsilon \frac{f_1(\varepsilon)}{(\psi - \varepsilon)^{\beta-\frac{1}{2}}} \tag{2.40}$$

This equation resembles the Abel's integral equation as long as $\frac{1}{2} < \beta < \frac{3}{2}$. If value of β goes below or equal to $\frac{1}{2}$, then, by taking one or more derivatives of this equation it can be reduced again to Abel's equation, since, the term $r^{2\beta}\nu$ is a function of ψ.

If the LOS direction is considered to be an arbitrary direction, say $\hat{s}$, which lies in the $r - \theta$ plane (we have to orient our coordinate system in velocity space like

that), then

$$\hat{s} = \cos\alpha\hat{r} + \sin\alpha\hat{\theta}. \tag{2.41}$$

The projected velocity in this plane of LOS will be then

$$\vec{v}.\hat{s} = v_{||} = v\cos\eta\cos\alpha + v\sin\eta\cos\psi'\sin\alpha. \tag{2.42}$$

The direction of LOS is now $x_{||} = r\sin\alpha$. Therefore, $x_\perp = \omega = r\sin\alpha$.
Now, $x_{||} = \sqrt{r^2 - r^2\sin^2\alpha} = \sqrt{r^2 - \omega^2}$. This implies

$$\mathrm{d}x_{||} = \frac{1}{2}\frac{1}{\sqrt{r^2-\omega^2}}\mathrm{d}(r^2), \tag{2.43}$$

where r^2 can vary from ω^2 to ∞. The expression of velocity dispersion along the LOS is given as

$$\sigma_{||}^2 = \frac{\int \mathrm{d}x_{||}d^3\vec{v}v_{||}^2 f(x,v)}{\int \mathrm{d}x_{||}\mathrm{d}^3\vec{v}f(x,v)}. \tag{2.44}$$

The numerator, N, and the denominator, D, are calculated separately, where

$$D = \int \mathrm{d}x_{||}\mathrm{d}^3\vec{v}f(x,v)$$

$$= \frac{1}{2}\int_{r^2=\omega^2}^{\infty}\frac{\mathrm{d}(r^2)}{\sqrt{r^2-\omega^2}}\int_{v=0}^{\sqrt{2\psi}}\int_{\eta=0}^{\pi}\int_{\psi'=0}^{2\pi} v^2\mathrm{d}v\sin\eta\mathrm{d}\eta\mathrm{d}\psi'\frac{1}{(rv\sin\eta)^{2\beta}}f_1(\varepsilon)$$

After changing the variable of the first integral to $x = \dfrac{r^2}{\omega^2}$ and performing the integral over ψ', the expression becomes

$$\pi\int_1^{\infty}\frac{\omega^2\mathrm{d}x}{\omega\sqrt{x-1}}\frac{1}{x^\beta\omega^{2\beta}}\int_0^{\pi}\sin^{1-2\beta}\eta\mathrm{d}\eta\int_{v=0}^{\sqrt{2\psi}}v^2\mathrm{d}v v^{-2\beta}f_1(\varepsilon)$$

By changing the variable of the first integral by $u = \dfrac{1}{x}$, writing the second integral as J_β and changing the variable of the third integral to ε, by using the relation:

$v^2 = 2(\psi - \varepsilon)$, the final expression for the denominator becomes

$$D = \pi\omega^{1-2\beta} J_\beta \int_0^1 \frac{\mathrm{d}u}{u^{2-\beta}\sqrt{\frac{1}{u}-1}} \int_0^\psi \mathrm{d}\varepsilon (2(\psi-\varepsilon))^{\frac{1}{2}-\beta} f_1(\varepsilon). \tag{2.45}$$

Similarly the numerator is also calculated to be given by

$$N = \int \mathrm{d}x_{||} \mathrm{d}^3\vec{v} v_{||}^2 f(x,v)$$

$$= \frac{1}{2}\int_{r^2=\omega^2}^\infty \frac{\mathrm{d}(r^2)}{\sqrt{r^2-\omega^2}} \int_{v=0}^{\sqrt{2\psi}} \int_{\eta=0}^{\pi} \int_{\psi'=0}^{2\pi} v^2 \mathrm{d}v \sin\eta \mathrm{d}\eta \mathrm{d}\psi' v^2$$

$$\left(\cos\eta \frac{\sqrt{r^2-\omega^2}}{\sqrt{r^2}} + \sin\eta\cos\psi'\sqrt{\frac{\omega^2}{r^2}}\right)^2 \frac{1}{(rv\sin\eta)^{2\beta}} f_1(\varepsilon)$$

Using the variable x as before, the expression is obtained as

$$\frac{\omega^{1-2\beta}}{2}\int_1^\infty \frac{\mathrm{d}x}{x^\beta\sqrt{x-1}} \int_{v=0}^{\sqrt{2\psi}} \int_{\eta=0}^{\pi} \int_{\psi'=0}^{2\pi} v^{4-2\beta}\mathrm{d}v \left[\sin^{1-2\beta}\eta\cos^2\eta\frac{x-1}{x}\right.$$

$$\left. + \frac{2\sin^2\eta\cos\eta\cos\psi'}{\sin^{2\beta}\eta}\frac{\sqrt{x-1}}{x} + \sin^{3-2\beta}\eta\cos^2\psi'\frac{1}{x}\right] f_1(\varepsilon)\mathrm{d}\eta\mathrm{d}\psi'$$

Again, the variable x is changed to u and variable v to ε is defined above and the final expression derived is

$$N = \omega^{1-2\beta}2^{\frac{1}{2}-\beta}\left[2\pi J1_\beta \int_0^1 \frac{du\sqrt{\frac{1}{u}-1}}{u^{1-\beta}} \int_0^\psi \mathrm{d}\varepsilon(\psi-\varepsilon)^{\frac{3}{2}-\beta} f_1(\varepsilon)\right.$$
$$\left. + J2_\beta J3_\beta \int_0^1 \frac{\mathrm{d}u}{u^{1-\beta}\sqrt{\frac{1}{u}-1}} \int_0^\psi \mathrm{d}\varepsilon(\psi-\varepsilon)^{\frac{3}{2}-\beta} f_1(\varepsilon)\right], \tag{2.46}$$

where

$$J1_\beta = \int_0^\pi \sin^{1-2\beta}\eta\cos^2\eta\mathrm{d}\eta, \tag{2.47}$$

$$J2_\beta = \int_0^\pi \sin^{3-2\beta}\eta \mathrm{d}\eta, \tag{2.48}$$

$$J3_\beta = \int_0^{2\pi} \cos^2\psi' \mathrm{d}\psi'. \tag{2.49}$$

The ratio of these two has been calculated to find the LOS velocity dispersion ($\sigma_{||} = \frac{N}{D}$) for three different cases ($\beta = \frac{1}{2}$, $\beta = -\frac{1}{2}$, $\beta = 0$), for the Hernquist model. $f_1(\varepsilon)$ for the three cases are obtained separately and plugging that in the equation for $\sigma_{||}$, the LOS velocity dispersion is calculated.

(i) $\beta = \frac{1}{2}$

For this model if $\beta = \frac{1}{2}$, then, the denominator of RHS of eqn. (2.40) is a constant and the DF can be found to be

$$\begin{aligned} f_1(\psi) &= \frac{1}{2\pi^2}\frac{\mathrm{d}}{\mathrm{d}\psi}(r\nu) \\ &= \frac{3\tilde{\varepsilon}^2}{4\pi^3 GMa}, \end{aligned} \tag{2.50}$$

where $\tilde{\varepsilon} = \dfrac{\varepsilon a}{GM}$. The plot of $\sigma_{||}$ vs $\left(\dfrac{r}{a}\right)$ is shown in Fig. 2.3.

(ii) $\beta = -\frac{1}{2}$

Here, the form of the DF will be

$$f_1(\psi) = \frac{1}{2\pi^2}\frac{\mathrm{d}^2(\nu/r)}{\mathrm{d}\psi^2}. \tag{2.51}$$

Expressing as a function of ε in case of Hernquist model, this gives,

$$f_1(\varepsilon) = \frac{1}{4\pi^3(GMa)^2}\frac{\mathrm{d}^2}{\mathrm{d}\tilde{\varepsilon}^2}\left(\frac{\tilde{\varepsilon}^5}{(1-\tilde{\varepsilon})^2}\right). \tag{2.52}$$

(iii) $\beta = 0$

As mentioned earlier, in this case the DF is ergodic. Here, the DF is

$$f(\varepsilon, L) = f_1(\varepsilon) = \frac{1}{\sqrt{2}(2\pi)^3(GMa)^{\frac{3}{2}}}\frac{\sqrt{\tilde{\varepsilon}}}{(1-\tilde{\varepsilon})^2} \times \left[(1-2\tilde{\varepsilon})(8\tilde{\varepsilon}^2 - 8\tilde{\varepsilon} - 3) + \frac{3\sin^{-1}\sqrt{\tilde{\varepsilon}}}{\sqrt{\tilde{\varepsilon}(1-\tilde{\varepsilon}}}\right] \tag{2.53}$$

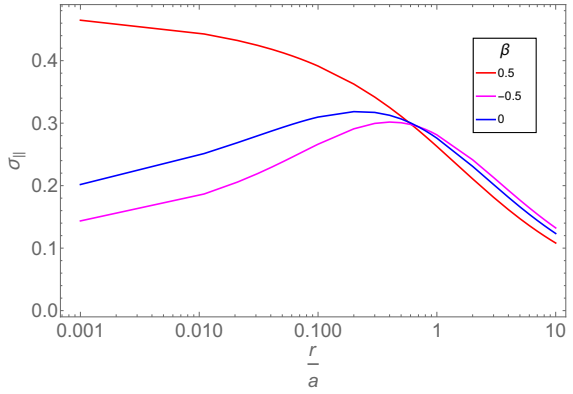

FIGURE 2.3: The LOS velocity dispersion (in units of $\sqrt{GM/a}$), is shown as a function of the projected radius for different values of the anisotropy parameter, β. For the isotropic case, $\beta = 0$, the dispersion falls of near the center [Binney and Tremaine (2008), Fig. 4.4].

2.4 Jeans equations in spherical systems

The collisionless Boltzmann equation in spherical polar coordinate system is (Binney and Tremaine 2008)

$$\frac{\partial f}{\partial t} + p_r \frac{\partial f}{\partial r} + \frac{p_\phi}{r^2}\frac{\partial f}{\partial \theta} + \frac{p_\phi}{r^2 \sin^2\theta}\frac{\partial f}{\partial \phi} - \left(\frac{\partial \Phi}{\partial r} - \frac{p_\theta^2}{r^3} - \frac{p_\phi^2}{r^3 \sin^2\theta}\right)\frac{\partial f}{\partial p_r} - \left(\frac{\partial \Phi}{\partial \theta} - \frac{p_\phi^2 \cos\theta}{r^2 \sin^3\theta}\right)\frac{\partial f}{\partial p_\theta} - \frac{\partial \Phi}{\partial \phi}\frac{\partial f}{\partial p_\phi} = 0, \tag{2.54}$$

where p_r, p_θ and p_ϕ are the canonical momenta in the r, θ and ϕ directions respectively, and are given as

$$p_r = \dot{r} = v_r; \quad p_\theta = r^2\dot{\theta} = r v_\theta; \quad p_\phi = r^2 \sin^2\theta \dot{\phi} = r \sin\theta v_\phi. \tag{2.55}$$

For a time independent and spherical system, $\frac{\partial f}{\partial t}$, $\frac{\partial \Phi}{\partial \theta}$, $\frac{\partial \Phi}{\partial \phi}$, and $\frac{\partial f}{\partial \phi}$ will be zero. $\frac{\partial f}{\partial \theta}$ may not be zero, because, through the p_ϕ term in eqn. (2.55), any dependence on v_ϕ may lead to dependence of f on θ. Therefore, for such a system, eqn. (2.54)

is written as

$$p_r\frac{\partial f}{\partial r}+\frac{p_\phi}{r^2}\frac{\partial f}{\partial \theta}-\left(\frac{\partial \Phi}{\partial r}-\frac{p_\theta^2}{r^3}-\frac{p_\phi^2}{r^3\sin^2\theta}\right)\frac{\partial f}{\partial p_r}+\frac{p_\phi^2\cos\theta}{r^2\sin^3\theta}\frac{\partial f}{\partial p_\theta}=0. \tag{2.56}$$

Again

$$\int \mathrm{d}p_r\mathrm{d}p_\theta\mathrm{d}p_\phi f = r^2\sin\theta\int \mathrm{d}v_r\mathrm{d}v_\phi\mathrm{d}v_\phi f = r^2\sin\theta\nu. \tag{2.57}$$

After multiplying eqn. (2.56) by $p_r\mathrm{d}p_r\mathrm{d}p_\theta\mathrm{d}p_\phi$, integrating over all momenta, then using eqn. (2.57) and the divergence theorem for elimination of the derivatives done with respect to the all the momenta, the final version becomes

$$\frac{\partial}{\partial r}(r^2\sin\theta\nu\overline{p_r^2})+\frac{\partial}{\partial\theta}(\sin\theta\nu\overline{p_rp_\theta})+r^2\sin\theta\nu\left(\frac{\partial\Phi}{\partial r}-\frac{\overline{p_\theta^2}}{r^3}-\frac{\overline{p_\phi^2}}{r^3\sin^2\theta}\right)=0. \tag{2.58}$$

For a spherical static system, the DF is an even function of v_r, leading to $\overline{p_rp_\theta}=r\overline{v_rv_\theta}=0$. Then, after using eqn. (2.57) and dividing by $r^2\sin\theta$, eqn. (2.58) finally takes the form

$$\frac{\mathrm{d}(\nu\overline{v_r^2})}{\mathrm{d}r}+\nu\left(\frac{\partial\Phi}{\partial r}-\frac{2\overline{v_r^2}-\overline{v_\theta^2}-\overline{v_\phi^2}}{r}\right)=0. \tag{2.59}$$

Finally, using eqn. (2.34), the eqn. (2.59) can be expressed in terms of β, the anisotropy parameter as (Binney and Tremaine 2008)

$$\frac{\mathrm{d}(\nu\overline{v_r^2})}{\mathrm{d}r}+2\frac{\beta}{r}\nu\overline{v_r^2}=-\nu\frac{\partial\Phi}{\partial r}. \tag{2.60}$$

This equation can be used to derive the velocity dispersion of the stars in the galaxy for known stellar potential or mass density as done by Häring and Rix (2004). This can be an useful tool to derive the $M_\bullet-\sigma$ relation analytically, for known black hole masses and stellar density profiles.

2.5 DFs for axisymmetric density distributions

Here, the DF is of the form $f(\varepsilon,\mathrm{L}_z)$. It can be written as a sum of two parts $f_+(\varepsilon, L_z)$ and $f_-(\varepsilon, L_z)$, where the probability density $\nu(R, z)$ is independent of f_- and the azimuthal flux νv_ϕ is independent of f_+. The first part is even in L_z and the second part is odd in L_z (Binney and Tremaine 2008).

Coordinates

Here, cylindrical coordinates are used for the velocity space (v_m, ψ, v_ϕ). Velocities in position coordinates can be written as (Binney and Tremaine 2008)

$$v_R = v_m \cos\psi, v_z = v_m \sin\psi. \tag{2.61}$$

Therefore, the volume in velocity coordinates can be written as $\mathrm{d}^3\mathbf{v} = v_m \mathrm{d}v_m \mathrm{d}\psi \mathrm{d}v_\phi$. The Jacobian of transformation from (v_ϕ, v_m) to (ε, L_z) is

$$\frac{\partial(\varepsilon, L_z)}{\partial(v_\phi, v_m)} = \begin{vmatrix} \frac{\partial\varepsilon}{\partial v_\phi} & \frac{\partial L_z}{\partial v_\phi} \\ \frac{\partial\varepsilon}{\partial v_m} & \frac{\partial L_z}{\partial v_m} \end{vmatrix} \tag{2.62}$$

Now ε and L_z is written as

$$\varepsilon = \psi - \frac{1}{2}(v_R^2 + v_\phi^2 + v_z^2), \quad L_z = R v_\phi. \tag{2.63}$$

Therefore,

$$\frac{\partial\varepsilon}{\partial v_\phi} = -v_\phi, \frac{\partial L_z}{\partial v_\phi} = R, \quad \frac{\partial\varepsilon}{\partial v_m} = -v_m, \quad \frac{\partial L_z}{\partial v_m} = 0, \tag{2.64}$$

which results in the Jacobian $\dfrac{\partial(\varepsilon, L_z)}{\partial(v_\phi, v_m)} = R v_m$. The volume element becomes $\mathrm{d}\varepsilon \mathrm{d}\psi \mathrm{d}L_z = R v_m \mathrm{d}\psi \mathrm{d}v_\phi$, and thus

$$\frac{1}{R}\mathrm{d}\varepsilon \mathrm{d}\psi \mathrm{d}L_z = v_m \mathrm{d}\psi \mathrm{d}v_\phi. \tag{2.65}$$

Therefore, the density van be calculated as

$$\rho(R,z) = \frac{2\pi}{R}\int_0^{\psi} \mathrm{d}\varepsilon \int_{-R\sqrt{2(\psi-\varepsilon)}}^{R\sqrt{2(\psi-\varepsilon)}} \mathrm{d}L_z f(\varepsilon, L_z)$$
$$= \frac{4\pi}{R}\int_0^{\psi} \mathrm{d}\varepsilon \int_0^{R\sqrt{2(\psi-\varepsilon)}} \mathrm{d}L_z f_+(\varepsilon, L_z) \tag{2.66}$$

The velocity dispersion tensor is isotropic, which leads to

$$\sigma_R^2 = \bar{v_R^2} = \frac{1}{\rho}\int \mathrm{d}v_R \mathrm{d}v_\phi \mathrm{d}v_z v_R^2 f(\varepsilon, L_z)$$
$$= \frac{1}{\rho}\int v_m \mathrm{d}v_m \mathrm{d}v_\phi \mathrm{d}\psi v_m^2 \cos^2\psi f(\varepsilon, L_z) \tag{2.67}$$
$$= \frac{4\pi}{\rho R}\int_0^{\psi} \mathrm{d}\varepsilon \int_0^{R\sqrt{2(\psi-\varepsilon)}} \mathrm{d}L_z f_+(\varepsilon, L_z)[\psi - \varepsilon - \frac{L_z^2}{2R^2}] \tag{2.68}$$

Now, the expression of σ_z^2 becomes

$$\sigma_z^2 = \frac{4\pi}{\rho R}\int_0^{\psi} \mathrm{d}\varepsilon \int_0^{R\sqrt{2(\psi-\varepsilon)}} \mathrm{d}L_z f_+(\varepsilon, L_z)[\psi - \varepsilon - \frac{L_z^2}{2R^2}] \tag{2.69}$$

Therefore, $\sigma_z^2 = \sigma_R^2$. Again $\sigma_\phi^2 = \bar{v_\phi^2} - (\bar{v_\phi})^2$, and v_ϕ is given by

$$v_\phi = \frac{1}{\rho}\int \mathrm{d}v_R \mathrm{d}v_\phi \mathrm{d}v_z v_\phi f(\varepsilon, L_z)$$
$$= \frac{4\pi}{\rho R^2}\int_0^{\psi} \mathrm{d}\varepsilon \int_0^{R\sqrt{2(\psi-\varepsilon)}} \mathrm{d}L_z L_z f_-(\varepsilon, L_z) \tag{2.70}$$

This equation is odd in L_z. Now

$$v_\phi^2 = \frac{4\pi}{\rho R^3}\int_0^{\psi} \mathrm{d}\varepsilon \int_0^{R\sqrt{2(\psi-\varepsilon)}} \mathrm{d}L_z L_z^2 f_+(\varepsilon, L_z), \tag{2.71}$$

which is even in L_z.

2.5.1 Evans model

Here, we have used Frickle component of DF, where the DF is written in the form $f = \varepsilon^{\zeta} L_z^{2\eta}$. For the DF to be positive always the value of L_z can be both positive or negative and η should take only integer values. But, the quantity ζ can take any value. The term 2η ensures that the component is even in L_z and has non vanishing density. Then the expression of density becomes (Binney and Tremaine 2008)

$$\begin{aligned}\rho(R,z) &= \frac{4\pi}{R}\int_0^{\psi} \mathrm{d}\varepsilon \varepsilon^{\zeta} \int_0^{R\sqrt{2(\psi-\varepsilon)}} \mathrm{d}L_z L_z^{2\eta} \\ &= \frac{R^{2\eta} 2^{\eta+\frac{5}{2}}\pi}{2\eta+1}\int_0^{\psi} \mathrm{d}\varepsilon \varepsilon^{\zeta}(\psi-\varepsilon)^{\eta+\frac{1}{2}} \end{aligned} \tag{2.72}$$

For solving this integral let us consider $\dfrac{\varepsilon}{\psi} = t$, which implies $\mathrm{d}\varepsilon = \psi \mathrm{d}t$. Therefore,

$$\begin{aligned}\rho(R,z) &= \frac{R^{2\eta} 2^{\eta+\frac{5}{2}}\pi\psi^{\zeta+\eta+\frac{3}{2}}}{2\eta+1}\int_0^{1} dt t^{\zeta}(1-t)^{\eta+\frac{1}{2}} \\ &= R^{2\eta} 2^{\eta+\frac{5}{2}}\pi\psi^{\zeta+\eta+\frac{3}{2}} \frac{\zeta!(\eta-\frac{1}{2})!}{(\zeta+\eta+\frac{3}{2})!} \end{aligned} \tag{2.73}$$

If $\rho = R^{2\eta}\psi^{\zeta}$, then, DF will be of the form $L_z^{2\eta}\varepsilon^{\zeta-\eta-\frac{3}{2}}$. The full expression of DF is given by

$$f = \frac{2^{-\eta+\frac{3}{2}}\zeta!}{\pi(\eta-\frac{1}{2})!(\zeta-\eta-\frac{3}{2})!} L_z^{2\eta}\varepsilon^{\zeta-\eta-\frac{3}{2}}. \tag{2.74}$$

For the Evans model, the potential is considered to be a function of m^2, where $m^2 = R_c^2 + R^2 + \dfrac{z^2}{q_\phi^2}$. Poisson's equation in cylindrical coordinates is written as

$$-4\pi G\rho = \frac{1}{R}\frac{\partial}{\partial R}\left[R\frac{\partial\psi}{\partial R}\right] + \frac{\partial^2\psi}{\partial z^2}. \tag{2.75}$$

After performing some algebric operations, we obtain

$$\frac{1}{R}\frac{\partial}{\partial R}(R\frac{\partial\psi}{\partial R}) = 4\psi' + 4R^2\psi'',$$

$$\frac{\partial^2\psi}{\partial z^2} = \frac{4(m^2 - R_c^2 - R^2)}{q_\phi^2}\psi'' + \frac{2\psi'}{q_\phi^2}$$

which implies that

$$-4\pi G\rho = \frac{4(m^2 - R_c^2)}{q_\phi^2}\psi'' + 4(1 - \frac{1}{q_\phi^2})R^2\psi'' + (4 + \frac{2}{q_\phi^2})\psi'. \tag{2.76}$$

where all the derivatives are performed with respect to m^2. Now, $\psi = \psi_a\left[\frac{R_c^2}{m^2}\right]^y, y > 0$, and $\psi_a = \text{const}$. Therefore, $m^2 = R_c^2(\frac{\psi}{\psi_a})^{-\frac{1}{y}}$, and

$$\begin{aligned}\psi' &= \psi_a R_c^{2y}(-y)(m^2)^{-(y+1)} \\ &= -\frac{\psi_a y}{R_c^2}(\frac{\psi}{\psi_a})^{1+\frac{1}{y}}\end{aligned} \tag{2.77}$$

and the double derivative is written as

$$\psi'' = y(y+1)\frac{\psi_a}{R_c^4}(\frac{\psi}{\psi_a})^{1+\frac{2}{y}}. \tag{2.78}$$

Thus, the expression for ρ becomes

$$\rho = \frac{y[2 - (2y+1)q_\phi^{-2}]\psi_a}{2\pi G R_c^2}(\frac{\psi}{\psi_a})^{1+\frac{1}{y}} + \frac{y(y+1)\psi_a}{\pi q_\phi^2 G R_c^2}(\frac{\psi}{\psi_a})^{1+\frac{2}{y}}\left(1 + (1-q_\phi^2)\frac{R^2}{R_c^2}\right). \tag{2.79}$$

The DF can be written as a sum of three Frickle components

$$f(\varepsilon, L_z) = A\varepsilon^{\frac{1}{y}-\frac{1}{2}} + B\left(1 + \frac{CL_z^2}{\varepsilon}\right)\varepsilon^{\frac{2}{y}-\frac{1}{2}}, \tag{2.80}$$

where

$$A = \frac{y[2 - (2y+1)q_\phi^{-2}](1+\frac{1}{y})!}{(2\pi)^{\frac{5}{2}}(\frac{1}{y} - \frac{1}{2})! G R_c^2 \psi_a^{\frac{1}{y}}}, \tag{2.81}$$

$$B = \frac{2y(y+1)(1+\frac{2}{y})!}{(2\pi)^{\frac{5}{2}}(\frac{2}{y} - \frac{1}{2})! q_\phi^2 G R_c^2 \psi_a^{\frac{2}{y}}}, \tag{2.82}$$

$$C = \frac{(1-q_\phi^2)}{R_c^2}\left(\frac{2}{y} - \frac{1}{2}\right). \tag{2.83}$$

The models of this type are called Evans model (Evans 1993).

2.5.2 Calculating observables for Evans model

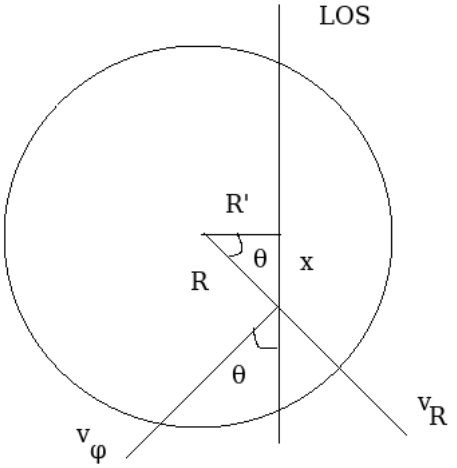

FIGURE 2.4: Geometry of the LOS direction in the axisymmetric system.

Calculation of $v_{||}$

From Fig. 2.4, we define $v_{||}$

$$v_{||} = v_R \sin\theta + v_\phi \cos\theta. \tag{2.84}$$

and $\bar{v_{||}}$ is calculated from

$$\bar{v_{||}} = \frac{\int \mathrm{d}x_{||} \mathrm{d}^3\vec{v} v_{||} f(\vec{x},\vec{v})}{\Sigma}$$

$$= \frac{1}{\Sigma}\left[\int \mathrm{d}x \sin\theta \int \mathrm{d}^3\vec{v} v_R f(\varepsilon, L_z) + \int \mathrm{d}x \cos\theta \int \mathrm{d}^3\vec{v} v_\phi f(\varepsilon, L_z)\right]$$

$$= \frac{1}{\Sigma}\left[\int_{-\infty}^{\infty} \mathrm{d}x \sin\theta \rho \bar{v_R} + \int_{-\infty}^{\infty} \mathrm{d}x \cos\theta \rho \bar{v_\phi}\right] \tag{2.85}$$

Since, $\bar{v_R} = 0$, the first term vanishes. Therefore,

$$\begin{aligned} \bar{v_{||}} &= \frac{2}{\Sigma}\int_0^\infty \mathrm{d}x \cos\theta \rho \bar{v_\phi} \\ &= \frac{2R'}{\Sigma}\int_{R'}^\infty \frac{\rho\bar{v_\phi}}{\sqrt{R^2 - R'^2}}\mathrm{d}R \end{aligned} \tag{2.86}$$

For solving this, it is assumed that $\dfrac{R}{R_c} = t$, and $\dfrac{R'}{R_c} = p$; therefore,

$$\bar{v_{||}} = \frac{2pR_c}{\Sigma}\int_p^\infty \frac{\rho\bar{v_\phi}}{\sqrt{t^2 - p^2}}\mathrm{d}t. \tag{2.87}$$

Next, $\bar{v_\phi}$ is calculated:

$$\bar{v_\phi} = \frac{4\pi\alpha_0}{\rho R^2}\int_0^\psi \mathrm{d}\varepsilon \int_0^{R\sqrt{2(\psi-\varepsilon)}} \mathrm{d}L_z L_z f_1(\varepsilon, L_z). \tag{2.88}$$

$$= \frac{4\pi\alpha_0}{\rho R^2}\int_0^\psi \mathrm{d}\varepsilon \int_0^{R\sqrt{2(\psi-\varepsilon)}} \mathrm{d}L_z L_z [A\varepsilon^{\frac{1}{y}-\frac{1}{2}} + B(1 + \frac{CL_z^2}{\varepsilon})\varepsilon^{\frac{2}{y}-\frac{1}{2}}]$$

$$= \frac{4\pi\alpha_0}{\rho}\left[\int_0^\psi \mathrm{d}\varepsilon A\varepsilon^{\frac{1}{y}-\frac{1}{2}}(\psi-\varepsilon) + \int_0^\psi \mathrm{d}\varepsilon B\varepsilon^{\frac{2}{y}-\frac{1}{2}}(\psi-\varepsilon) + \int_0^\psi \mathrm{d}\varepsilon BCR^2\varepsilon^{\frac{2}{y}-\frac{1}{2}}(\psi-\varepsilon)^2\right]$$

$$= \frac{4\pi\alpha_0}{\rho}\left[\frac{A\psi^{\frac{1}{y}+\frac{3}{2}}}{\left(\frac{1}{y}+\frac{1}{2}\right)\left(\frac{1}{y}+\frac{3}{2}\right)} + \frac{B\psi^{\frac{2}{y}+\frac{3}{2}}}{\left(\frac{2}{y}+\frac{1}{2}\right)\left(\frac{2}{y}+\frac{3}{2}\right)} + BCR^2\psi^{\frac{2}{y}+\frac{3}{2}}\left(\frac{1}{\frac{2}{y}-\frac{1}{2}} - \frac{2}{\frac{2}{y}+\frac{1}{2}} + \frac{1}{\frac{2}{y}+\frac{3}{2}}\right)\right]$$

$$= \frac{16\pi\alpha_0 y^2}{\rho}\psi^{\frac{1}{y}+\frac{3}{2}}\left[\frac{A}{(2+y)(2+3y)} + \frac{B\psi^{\frac{1}{y}}(4-y+4yCR^2)}{(4+3y)(16-y^2)}\right]$$

Now, inserting the values of A, B and C, it is found that

$$\rho\bar{v_\phi} = \frac{16\pi\alpha_0 y^2\psi_a^{\frac{3}{2}}}{(2\pi)^{\frac{5}{2}}GR_c^2}\left[\frac{1}{1+t^2}\right]^{1+\frac{3y}{2}}\left[P + Q\left(\frac{1}{1+t^2}\right)(4-y+4ySt^2)\right], \tag{2.89}$$

where $P = \frac{A(2\pi)^{\frac{5}{2}} G R_c^2 \psi_a^{\frac{1}{y}}}{(2+y)(2+3y)}$, $Q = \frac{B(2\pi)^{\frac{5}{2}} G R_c^2 \psi_a^{\frac{2}{y}}}{(4+3y)(16-y^2)}$ and $S = (1-q^2)\left(\frac{2}{y} - \frac{1}{2}\right)$. Therefore

$$\bar{v_{||}}(p) = \frac{32 R_c \pi \alpha_0 y^2 \psi_a^{\frac{3}{2}}}{(2\pi)^{\frac{5}{2}} G R_c^2 \Sigma} p \int_p^\infty \frac{\mathrm{d}t}{\sqrt{t^2 - p^2}} \left[\frac{1}{1+t^2}\right]^{1+\frac{3y}{2}} \left[P + Q\left(\frac{1}{1+t^2}\right)(4 - y + 4ySt^2)\right]. \tag{2.90}$$

where the integral is called as I_1. Next, Σ is calculated by the expression

$$\Sigma(R') = \int \mathrm{d}x \rho(R) = 2\int_{R'}^\infty \frac{R\mathrm{d}R}{\sqrt{R^2 - R'^2}} \rho(R). \tag{2.91}$$

It can be written as a function of p as

$$\Sigma(p) = 2R_C \int_p^\infty \frac{t\mathrm{d}t}{\sqrt{t^2 - p^2}} \rho(t). \tag{2.92}$$

From the definition of ψ as a function of m^2 (putting $z = 0$ in the expression), ρ can be simplified to be

$$\rho(t) = \frac{\psi_a}{2\pi G R_C^2}\left[y\left(2 - \frac{2y+1}{q^2}\right)\left(\frac{1}{1+t^2}\right)^{y+1} + \frac{2y(y+1)}{q^2}\left(\frac{1}{1+t^2}\right)^{y+2}(1 + (1-q^2)t^2)\right]. \tag{2.93}$$

Therefore, the expression for Σ is

$$\Sigma(p) = \frac{\psi_a}{\pi G R_C} \int_p^\infty \frac{t\mathrm{d}t}{\sqrt{t^2 - p^2}}\left[y\left(2 - \frac{2y+1}{q^2}\right)\left(\frac{1}{1+t^2}\right)^{y+1} + \frac{2y(y+1)}{q^2}\left(\frac{1}{1+t^2}\right)^{y+2}(1 + (1-q^2)t^2)\right] \tag{2.94}$$

where, the integral is written as I_2. The final expression of $\bar{v_{||}}$ can be written as

$$\begin{aligned} v_{||}(p) &= \frac{32 R_C \pi \alpha_0 y^2 \psi_a^{\frac{3}{2}} G R_C \pi p}{(2\pi)^{\frac{5}{2}} G R_C^2 \psi_a} \frac{I_1}{I_2} \\ &= \frac{16\pi \alpha_0 y^2 \sqrt{\psi_a} p}{(2\pi)^{\frac{3}{2}}} \frac{I_1}{I_2}. \end{aligned} \tag{2.95}$$

Similarly, the average of the square of the LOS velocity can be written as

$$\bar{v_{||}^2} = \frac{1}{\Sigma}\int \mathrm{d}x_{||}\int \mathrm{d}^3\vec{v}v_{||}^2 f$$
$$= \frac{1}{\Sigma}\left[\int \mathrm{d}x_{||}\sin^2\theta\int \mathrm{d}^3\vec{v}v_R^2 f + \int \mathrm{d}x_{||}\cos^2\theta\int \mathrm{d}^3\vec{v}v_\phi^2 f\right]. \tag{2.96}$$

The cross term $v_R v_\phi$ vanishes as the dispersion tensor is diagonal in (R, ϕ, z) coordinates. The expression finally becomes

$$\bar{v_{||}^2} = \frac{2}{\Sigma}\int_{R'}^{\infty}\mathrm{d}R\frac{\sqrt{R^2-R'^2}}{R}\rho\bar{v_R^2} + \frac{2R'^2}{\Sigma}\int_{R'}^{\infty}\mathrm{d}R\frac{1}{R\sqrt{R^2-R'^2}}\rho\bar{v_\phi^2}. \tag{2.97}$$

Now $\bar{v_R^2}$ and $\bar{v_\phi^2}$ are calculated:

$$\bar{v_R^2} = \frac{4\pi}{\rho R}\int_0^{\psi}\mathrm{d}\varepsilon\int_0^{R\sqrt{2(\psi-\varepsilon)}}\mathrm{d}L_z f_+(\varepsilon, L_z)\left(\psi-\varepsilon-\frac{L_z^2}{2R^2}\right) \tag{2.98}$$

$$= \frac{4\pi}{\rho R}\int_0^{\psi}\mathrm{d}\varepsilon\int_0^{R\sqrt{2(\psi-\varepsilon)}}\mathrm{d}L_z\left[A\varepsilon^{\frac{1}{y}-\frac{1}{2}} + B\left(1+\frac{CL_z^2}{\varepsilon}\right)\varepsilon^{\frac{2}{y}-\frac{1}{2}}\right]\left(\psi-\varepsilon-\frac{L_z^2}{2R^2}\right)$$

$$= \frac{4\pi}{\rho}\int_0^{\psi}\Bigg[(A\varepsilon^{\frac{1}{y}-\frac{1}{2}} + B\varepsilon^{\frac{2}{y}-\frac{1}{2}})\sqrt{2}(\psi-\varepsilon)^{\frac{3}{2}} + \frac{BC}{3}R^2 2\sqrt{2}\varepsilon^{\frac{2}{y}-\frac{3}{2}}(\psi-\varepsilon)^{\frac{5}{2}} -$$

$$\frac{2\sqrt{2}}{6}(A\varepsilon^{\frac{1}{y}-\frac{1}{2}} + B\varepsilon^{\frac{2}{y}-\frac{1}{2}})(\psi-\varepsilon)^{\frac{3}{2}} - \frac{2\sqrt{2}}{5}BCR^2\varepsilon^{\frac{2}{y}-\frac{3}{2}}(\psi-\varepsilon)^{\frac{5}{2}}\Bigg]\mathrm{d}\varepsilon$$

Next, the variable of the integral is changed to x, which is defined as $\mathrm{d}x = \frac{\varepsilon}{\psi}$. The expression becomes

$$\bar{v_R^2} = \frac{4\pi}{\rho}\Bigg[A\frac{2\sqrt{2}}{3}\psi^{\frac{1}{y}-\frac{1}{2}}\psi^{\frac{3}{2}}\psi\int_0^1\left(\frac{3}{2}-\frac{1}{2}\right)x^{\frac{1}{y}-\frac{1}{2}}(1-x)^{\frac{3}{2}}\mathrm{d}x$$

$$+B\frac{2\sqrt{2}}{3}\psi^{\frac{2}{y}-\frac{1}{2}}\psi^{\frac{3}{2}}\psi\int_0^1\left(\frac{3}{2}-\frac{1}{2}\right)x^{\frac{2}{y}-\frac{1}{2}}(1-x)^{\frac{3}{2}}\mathrm{d}x$$

$$+BC\frac{2^{\frac{3}{2}}}{15}\psi^{\frac{2}{y}-\frac{1}{2}}\psi^{\frac{5}{2}}\psi R^2\int_0^1\Big(5-3\Big)x^{\frac{2}{y}-\frac{3}{2}}(1-x)^{\frac{5}{2}}\mathrm{d}x\Bigg]$$

The final expression is

$$\bar{v_R^2}=\frac{4\pi}{\rho}\Bigg[A\frac{2\sqrt{2}}{3}\psi^{\frac{1}{y}+2}\int_0^1 x^{\frac{1}{y}-\frac{1}{2}}(1-x)^{\frac{3}{2}}\mathrm{d}x+B\frac{2\sqrt{2}}{3}\psi^{\frac{2}{y}+2}\int_0^1 x^{\frac{2}{y}-\frac{1}{2}}(1-x)^{\frac{3}{2}}\mathrm{d}x$$

$$+BC\frac{2^{\frac{5}{2}}}{15}\psi^{\frac{2}{y}+2}R^2\int_0^1 x^{\frac{2}{y}-\frac{3}{2}}(1-x)^{\frac{5}{2}}\mathrm{d}x\Bigg] \tag{2.99}$$

The RHS of the equation is written as $\frac{\psi_a^2}{2\pi GR_C^2\rho}I_4$. Similarly, $\bar{v_\phi^2}$ is also calculated:

$$\bar{v_\phi^2}=\frac{4\pi}{\rho R^3}\int_0^\psi \mathrm{d}\varepsilon\int_0^{R\sqrt{2(\psi-\varepsilon)}}\mathrm{d}L_z f_+(\varepsilon,L_z)L_z^2. \tag{2.100}$$

$$=\frac{4\pi}{\rho R^3}\int_0^\psi \mathrm{d}\varepsilon\int_0^{R\sqrt{2(\psi-\varepsilon)}}\mathrm{d}L_z[A\varepsilon^{\frac{1}{y}-\frac{1}{2}}+B\Big(1+\frac{CL_z^2}{\varepsilon}\Big)\varepsilon^{\frac{2}{y}-\frac{1}{2}}\Bigg]L_z^2$$

$$=\frac{4\pi}{\rho}\int_0^\psi \mathrm{d}\varepsilon\Bigg[\frac{A\varepsilon^{\frac{1}{y}-\frac{1}{2}}}{3}2^{\frac{3}{2}}(\psi-\varepsilon)^{\frac{3}{2}}+\frac{B\varepsilon^{\frac{2}{y}-\frac{1}{2}}}{3}2^{\frac{3}{2}}(\psi-\varepsilon)^{\frac{3}{2}}+\frac{BC}{5}\varepsilon^{\frac{2}{y}-\frac{3}{2}}R^2 2^{\frac{5}{2}}(\psi-\varepsilon)^{\frac{5}{2}}\Bigg]$$

Therefore,

$$\bar{v_\phi^2}=\frac{4\pi}{\rho}\Bigg[A\frac{2\sqrt{2}}{3}\psi^{\frac{1}{y}+2}\int_0^1 x^{\frac{1}{y}-\frac{1}{2}}(1-x)^{\frac{3}{2}}dx+B\frac{2\sqrt{2}}{3}\psi^{\frac{2}{y}+2}\int_0^1 x^{\frac{2}{y}-\frac{1}{2}}(1-x)^{\frac{3}{2}}\mathrm{d}x$$

$$+BC\frac{2^{\frac{5}{2}}}{5}\psi^{\frac{2}{y}+2}R^2\int_0^1 x^{\frac{2}{y}-\frac{3}{2}}(1-x)^{\frac{5}{2}}\mathrm{d}x\Bigg] \tag{2.101}$$

The RHS of this equation is written in the form $\frac{\psi_a^2}{2\pi G R_C^2 \rho} I_3$. Now, the expression of $\bar{v_{||}^2}$ as a function of p is given by

$$\bar{v_{||}^2} = \frac{\psi_a^2}{\pi G \Sigma}\left(\int_p^\infty \frac{\sqrt{t^2 - p^2}}{t} I_4 dt + p^2 \int_p^\infty \frac{I_3}{t\sqrt{t^2 - p^2}} \mathrm{d}t \right). \tag{2.102}$$

The velocity dispersion along the LOS is calculated as

$$\sigma_{||} = \sqrt{\bar{v_{||}^2} - (\bar{v_{||}}^2)}. \tag{2.103}$$

Another observable for the Evans model (Evans 1993), the eccentricity, is defined as, $e = 1 - \frac{b}{a}$, where b and a are the intercepts of the isophotes along the minor and major axes respectively. To calculate this observable, the expression $\rho(R, z)$ is used and $R^2 = x^2 + y^2$ is considered. Now, to get the ellipse in the sky plane for isophotes, this expression is integrated over all x (x ranges from $-\infty$ to $+\infty$). Thus, the isophotes in Y -Z plane are obtained. Next, the intercepts along the two axes are calculated and here, the projected distance is along the Y - axis. All calculated observables are shown in a single figure [Fig. 2.5] with the projected distance along the LOS in units of R_C.

2.6 Jeans equations in axisymmetric systems

The collisionless Boltzmann equation in cylindrical coordinates is

$$\frac{\partial f}{\partial t} + p_R \frac{\partial f}{\partial R} + \frac{p_\phi}{R^2}\frac{\partial f}{\partial \phi} + p_z \frac{\partial f}{\partial z} - \left(\frac{\partial \Phi}{\partial R} - \frac{p_\phi^2}{R^3} \right) \frac{\partial f}{\partial p_R} - \frac{\partial \Phi}{\partial \phi}\frac{\partial f}{\partial p_\phi} - \frac{\partial \Phi}{\partial z}\frac{\partial f}{\partial p_z} = 0, \tag{2.104}$$

where p_R, p_ϕ, p_z are the momentum in the direction of r, ϕ and z. For steady state axisymmetric systems, all the derivatives of t and ϕ vanish. Under these

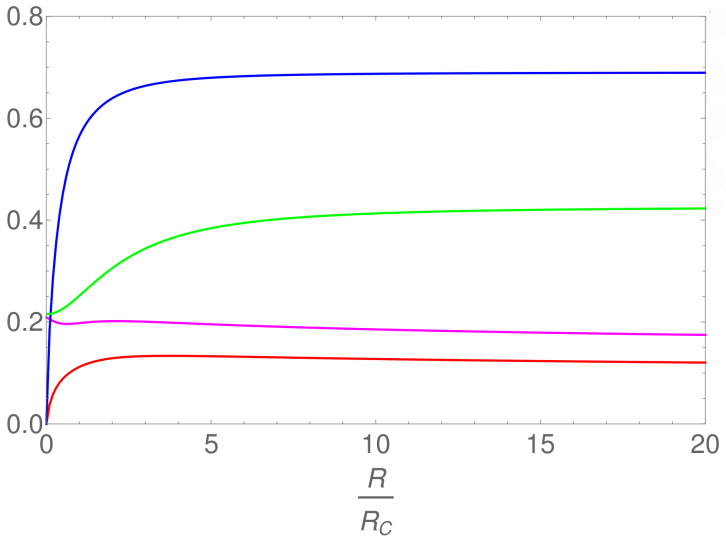

FIGURE 2.5: All the projected quantities are plotted against the major axis (red shows $v_{||}$ (in units of $\sqrt{\psi_a}$), purple represents $\sigma_{||}$ (in units of $\sqrt{\psi_a}$), blue is for $\frac{v_{||}}{\sigma_{||}}$ and green represents e), seen edge - on. The parameters used are $\alpha = 0.813$, $y = 0.09$ and $q_\phi = 0.85$ [Binney and Tremaine (2008), Fig. 4.12].

conditions, eqn. (2.104), takes the form

$$p_R \frac{\partial f}{\partial R} + p_z \frac{\partial f}{\partial z} - \left(\frac{\partial \Phi}{\partial R} - \frac{p_\phi^2}{R^3} \right) \frac{\partial f}{\partial p_R} - \frac{\partial \Phi}{\partial z} \frac{\partial f}{\partial p_z} = 0. \tag{2.105}$$

After multiplying eqn. (2.105) by p_R, and integrating it over all momenta and finally replacing the momenta with their form in terms of velocities, the eqn. (2.105) takes the following form

$$\frac{\partial(\nu \overline{v_R^2})}{\partial R} + \frac{\partial(\nu \overline{v_R v_z})}{\partial z} + \nu \left(\frac{\overline{v_R^2} - \overline{v_\phi^2}}{R} \right) + \frac{\partial \Phi}{\partial R} = 0. \tag{2.106}$$

The other Jeans equations are obtained by multiplying eqn. (2.105) by p_ϕ and p_z, and integrating over all momenta:

$$\frac{1}{R^2} \frac{\partial(R^2 \nu \overline{v_R v_\phi})}{\partial R} + \frac{\partial(\nu \overline{v_R v_\phi})}{\partial z} = 0, \tag{2.107}$$

$$\frac{1}{R} \frac{\partial(R \nu \overline{v_R v_\phi})}{\partial R} + \frac{\partial(\nu \overline{v_z^2})}{\partial z} + \nu \frac{\partial \Phi}{\partial z} = 0. \tag{2.108}$$

For known ν and Φ, the three Jeans equations [eqns. (2.106,2.107,2.108)] generate three constraints on six equations which are second order in velocity moments. But, unlike the spherical case, these equations are not closed in these systems. Higher order Jeans equations (nth order) can be related to nth order moments of $\nu(R,z)$ or $\nu\overline{v_\phi}(R,z)$ respectively for even and odd values of n (Magorrian and Binney 1994) and these moments are similar to what can be derived from the Hunter - Qian algorithm (Hunter and Qian 1993), for calculation of the DF in axisymmetric systems, $f(E,L_z)$.

2.7 Resource summary

1. In this chapter, we discussed the basics of the stellar dynamics [Binney and Tremaine (2008), Binney and Merrifield (1998)], which we use later on to build our model to derive the $M_\bullet - \sigma$ relation in spherical as well as in axisymmetric systems (Chapters 4 & 7).

2. We show derivations of the DFs followed by the LOS velocity dispersion, which is an observable quantity, for the spherical systems for both the isotropic and anisotropic cases (Binney and Tremaine 2008), with their application to some known potential-density models [Hernquist (1990), Jaffe (1983), Hénon (1960)].

3. We also derived the DF and the LOS velocity dispersion in axisymmetric systems for the Evans model (Evans 1993). We use the same geometry later, to derive the σ in an axisymmetric system (Chapter 7), for a particular type of mass density, $\rho(m^2)$, given in [Qian *et al.* (1995), Hunter and Qian (1993)].

4. Jeans equations in both spherical and axisymmetric systems are derived (Binney and Tremaine 2008). These equations are very useful to derive σ, for known potential-density pairs. We plan to use Jeans equation in spherical and axisymmetric systems (Häring and Rix 2004), with the total potential

(including that of the black hole), and a known mass density model, to derive σ; this can be used to give a better model for the $M_\bullet - \sigma$ relation from theoretical considerations.

Chapter 3

Image: ned.ipac.caltech.edu

$M_\bullet - \sigma$ relation

3.1 Introduction

It is now widely accepted that all massive galaxies have supermassive black holes at their centers. At distances close to the centers of these galaxies, stellar or gas motions are completely dominated by the gravity of the SMBH than that of the nearby stars. The relation of the SMBHs to their host galaxies can be seen by the strong correlation between the mass of SMBH and the velocity dispersion, σ, of the stars in the galaxy. This is somewhat surprising because the stars are too far from the SMBH for the velocity dispersion to be affected by its gravitational field. Its origin is still a topic of debate. But this relation is important since the mass of SMBH which is very difficult to measure directly can be calculated with relatively better precision using a quantity σ (evaluated far from the SMBH) which is easier to measure.

The $M_\bullet - \sigma$ relation is given by the equation

$$M_\bullet = k\sigma^p, \tag{3.1}$$

where, $p = 4 - 5$. $M_\bullet$ - σ relation was first reported by Ferrarese and Merritt (2000) with the index $p = 4.8 \pm 0.5$, whereas, Gebhardt *et al.* (2000) reported $p = 3.75 \pm 0.3$. Later on, many more studies came up with some other values which we list in Table 3.1.

3.2 Significance of the $M_\bullet$ - σ relation

- Even after setting up a perfect correlation between SMBH mass and spheroid mass in the early universe also, it is difficult to see how it could survive galaxy mergers that convert disks into bulges and can also channel the gas into the nucleus which produce uncorrelated changes in $M_\bullet$ and M_b. In order to maintain a correlation between these two quantities, some sort of "negative feedback" processes may be going on which helps the SMBH regulate its growth.

- The $M_\bullet$ - σ relation has provided the motivation to study the correlation of the SMBH with the components of its host galaxies.

- These relations suggest that the formation of the SMBH is tightly correlated with its host spheroid (galaxy or the bulge).

- Study of these relations can provide clues to the formation and growth of the SMBHs.

3.3 Literature survey of the $M_\bullet$ - σ relation

Ferrarese and Merritt (2000) used symmetric linear regression method for their analysis and in this process, both the variables $M_\bullet$ and σ had a unique error in measurements, as well as intrinsic scatter, while Gebhardt *et al.* (2000) used non-symmetrical least square regression, where it was assumed that σ had no uncertainty in measurement and $M_\bullet$ had same uncertainty for all. This relation is observed in ellipticals and evolved bulges. Debattista *et al.* (2013) claim that their latest measurements indicate that there is no evidence of offset for this relation between ellipticals and classical bulges. Table 3.1 shows the values of the indices determined by different authors using different techniques.

#	References	p	Comments
1	Ferrarese and Merritt (2000)	4.8 ± 0.5	12 elliptical galaxies with known σ
2	Gebhardt *et al.* (2000)	3.75 ± 0.3	26 galaxies with measured $M_\bullet$ and σ
3	Merritt and Ferrarese (2001)	4.72 ± 0.36	27 galaxies with measured $M_\bullet$ and σ
4	Ferrarese (2002)	4.58 ± 0.52	16 spirals and 20 elliptical galaxies
5	Tremaine *et al.* (2002)	4.02 ± 0.32	31 galaxies with measured $M_\bullet$ and σ
6	Ferrarese and Ford (2005)	4.86 ± 0.43	SMBHs which have resolved r_h
7	Gültekin *et al.* (2009)	4.24 ± 0.41	Combination of spiral and elliptical galaxies
8	*ibid*	3.96 ± 0.42	25 Elliptical galaxies
9	Kormendy and Ho (2013)	4.38 ± 0.29	Classical bulges and ellipticals
10	McConnell and Ma (2013)	5.64 ± 0.32	19 late type and 53 early - type galaxies
11	Graham and Scott (2013)	5.53 ± 0.34	51 non - barred galaxies
12	Debattista *et al.* (2013)	4.39 ± 0.42	Sample of Gültekin *et al.* (2009) with newly measured $M_\bullet$ and σ
13	Batiste *et al.* (2017)	4.76 ± 0.60	32 quiescent galaxies
14	*ibid*	3.90 ± 0.93	16 AGN host galaxies
15	Bhattacharyya and Mangalam (2018)	3.81 ± 0.004	12 elliptical galaxies following Nuker intensity profile

TABLE 3.1: A survey of the $M_\bullet - \sigma$ relation giving the historical determinations of the slopes.

3.4 Theoretical models of deriving the $M_\bullet$ - σ relation

3.4.1 Energy driven flow

Soltan (1982) suggested that SMBHs grow mostly by the accretion of gas. The source of the feedback process is probably the outflow driven by the accretion. Due to this feedback, after a certain time, the SMBH would reach a mass that would cause prevention of further accretion because the outflow would drive away the ambient gas required for the accretion to continue (Merritt 2013b).

If η is the accretion efficiency, then the energy released in accretion due to growth of a SMBH of mass $M_\bullet$ is

$$L = \eta \dot{M} c^2, \tag{3.2}$$

where, $\dot{M}$ is the rate of mass accretion and L is the accretion - driven luminosity. The accretion efficiency can be calculated from the comparison of the energy of the accreting material at infinity and the energy at the last stable orbit around the black hole. Taking $\eta = 0.1$, in this case, is a very common assumption. Therefore, the ratio of energy released via accretion and the gravitational binding energy of the bulge is

$$\frac{\eta M_\bullet c^2}{\frac{GM_b^2}{R_b}} \approx \eta \frac{M_\bullet}{M_b} \frac{c^2}{\sigma^2}$$

$$\approx 225 \left(\frac{\eta}{0.1}\right) \left(\frac{\frac{M_\bullet}{M_b}}{10^{-3}}\right) (\sigma_{200})^{-2} >> 1, \tag{3.3}$$

where, M_b is the mass and R_b is the radius of the galactic bulge, $\sigma_{200} = \left(\frac{\sigma}{200\text{km s}^{-1}}\right)$. Therefore, the energy released in the formation of SMBH is enough to unbind the

total mass of a galactic bulge. This energy is coupled to the gas by Thomson scattering process (scattering of the electromagnetic radiation by charged particles). The Eddington luminosity is defined by eqn. (5.4). When $L > L_E$, the net force will be outwards and accretion stops. So from eqns. (5.4, 3.2), we obtain the Eddington accretion rate as

$$\dot{M}_E = \frac{4\pi G M_\bullet m_p}{\eta \sigma_e c} \approx 2.6 \left(\frac{\eta}{0.1}\right)^{-1} \left(\frac{M_\bullet}{10^8 M_\odot}\right) M_\odot \mathrm{yr}^{-1}. \tag{3.4}$$

The SMBHs accrete almost at the Eddington rate during their most luminous phase (quasar); any accretion rate, which is lower than that would not allow black holes to grow to the mass observed in the available time. We show this in case of some quasars in Chapter 6. To calculate the $M_\bullet$, that radiates at Eddington limit and generates energy to unbind the whole mass of galaxy bulge in one crossing time, t_{cross}, we used

$$L_E \cdot t_{cross} \approx L_E \cdot \frac{R_b}{\sigma} \approx \frac{G M_b^2}{R_b}. \tag{3.5}$$

From virial theorem, $GM_b \approx \sigma^2 R_b$. Therefore,

$$M_\bullet \approx \frac{\sigma_e \sigma^5}{4\pi G^2 m_p c} \approx 3 \times 10^5 (\sigma_{200})^5 M_\odot, \tag{3.6}$$

which gives $p = 5$. Throughout this treatment, it was assumed that, all the energy produced by the black hole is available to unbind the mass of the bulge, and hence, it is called "energy driven flow" (Silk and Rees 1998). The main condition for this to operate is the assumption that there are no cooling processes involved here. Haehnelt *et al.* (1998) also derived $p = 5$ in their theoretical model. Here, the relation between the rotational velocity of the self-gravitating disc, v_{rot}, and the virial velocity of the halo, v_{halo} is

$$v_{rot} = j_r^{-1} \left(\frac{\lambda}{0.05}\right)^{-1} \frac{m_r}{0.1} v_{halo}, \tag{3.7}$$

where, $\lambda = JE^{-0.5}G^{-1}M^{-2.5}$ is the angular momentum parameter, m_r is the ratio of disc and halo mass while j_r is the ratio of the specific angular momentum

of the disc and the virialized halo. They have assumed that v_{rot} does not vary with radius and that the accretion rate, $\frac{\beta v_{rot}^2}{G}$, is generated by the gravitational instabilities which is independent of the radius. β is defined as the ratio of the accretion time scale and the dynamical time scale. If $v_{rot} \geq v_{halo}$, then $\beta \sim 0.001$ will be enough for the accretion to occur (Haehnelt *et al.* 1998). For $v_{rot} > 200(\beta/0.001)^{-1/3}\text{km s}^{-1}$, the mass of black hole $\sim 10^6 M_\odot$ will be accumulated in $\leq 10^6$ years and after that collapse occurs due to post-Newtonian gravity. In the initial phase, the accretion will be in Eddington limit and later on the the growth depends on the feedback process. When, the emitted luminosity exceeds the energy required for the process of unbinding the mass of the disc, the accretion stops leading the black hole to a saturated value

$$M_\bullet \sim 10^8 M_\odot (f_{kin}/0/001) j_r^{-5} \left(\frac{\lambda}{0.05}\right)^{-5} \left(\frac{m_r}{0.1}\right)^5 \frac{v_{halo}}{400\text{km s}^{-1}}, \tag{3.8}$$

where, f_{kin} is the same as considered by Silk and Rees (1998), which is the luminosity fraction that has gone to the accretion as kinetic energy. This also follows the $M_\bullet - \sigma$ relation with $p = 5$.

3.4.2 Momentum driven flow

"Momentum - driven flow" is the one where the part of the energy released by the black hole is lost to radiation and the remaining part of it affects the bulge gas and unbinds it. In fact, the flow driven by the accreting black holes are mainly of this type (King 2003), because there are sources of cooling present in the medium. The radiation field generated from the centre can cool the shocked gas out to a distance of kiloparsec by the process of inverse Compton cooling (Ciotti and Ostriker 1997). In this type of flow, if the optical depth is of the order of unity, the momentum of

the outflow is of the order of the photon momentum

$$\dot{M}v \approx \frac{L_E}{c}. \tag{3.9}$$

If the accretion is at Eddington rate, then,

$$\dot{M}_E v \approx \frac{\eta \dot{M}_E c^2}{c}$$

$$\Rightarrow v \approx \eta c \approx 0.1c, \tag{3.10}$$

where, v is the velocity of the gas.

Let us consider a shell of gas with radius $R(t)$, mass $f_g M(R)$ (f_g is the gas fraction, $M(R)$ is the total mass including the stars and gas within the radius R) which has been swept up due to the flow. Its equation of motion can be written as (King 2003)

$$\frac{\mathrm{d}}{\mathrm{d}t}\left[f_g M(R)\dot{R}\right] + \frac{G f_g M(R)[M_\bullet + M(R)]}{R^2} = \frac{L_E}{c}. \tag{3.11}$$

Considering the isothermal sphere model for the galactic bulge we take $M(R) = \frac{2\sigma^2 R}{G}$ so that eqn. (3.11) reduces to the form

$$\frac{\mathrm{d}}{\mathrm{d}t}(R\dot{R}) + \frac{GM_\bullet}{R} = -2\sigma^2\big(1 - \frac{M_\bullet}{M_\sigma}\big), \tag{3.12}$$

where,

$$M_\sigma \equiv \frac{f_g \sigma_e}{\pi G^2 m_p}\sigma^4 \approx 2 \times 10^8 \left(\frac{f_g}{0.1}\right)(\sigma_{200})^4 M_\odot. \tag{3.13}$$

- In eqn. (3.11), if $M_\bullet < M_\sigma$ [given by eqn. (3.13)], then the RHS becomes negative. For large R, the third term on the LHS can be neglected. Therefore, we finally have $\frac{\mathrm{d}}{\mathrm{d}t}(R\dot{R}) < 0$, which in turn implies that force on the shell is not enough to lift it beyond a particular distance. Therefore, there is no solution under this condition (Merritt 2013b).

- If $M_\bullet > M_\sigma$, then the RHS becomes positive implying that $\dot{R}^2 + R\ddot{R} = \sigma^2 \cdot \mathrm{const}$. When the gas stops accelerating, $\dot{R}$ becomes constant leading to

the second term to zero and $\dot{R}^2 \to \sigma^2$. Thus, the shell can get completely expelled. The value for the "cosmic baryon function" (ratio of ordinary matter to the total matter) is approximately 0.16 (Merritt 2013b). Putting $f_g = 0.16$ in the equation a relation close to the observed $M_\bullet$ - σ can be obtained:

$$M_\bullet = 3.2 \times 10^8 (\sigma_{200})^4 M_\odot. \tag{3.14}$$

Therefore, in both the cases, we can see that the $M_\bullet$ - σ relation form comes out naturally. In the second case, the critical mass is larger by a factor of $\sim \frac{c}{\sigma}$. This is because in the first case, the assumption was that, the energy produced by the black hole was totally available for driving the gas, but in the "momentum driven flow" there are sufficient cooling processes which causes a large fraction of that energy to be lost in radiation. These arguments put an upper limit to the SMBH mass. For the active galaxies, which are still undergoing accretion, this implies that $M_\bullet < M_\sigma$. The observations are still unable to rule out that some galaxies may contain underweight SMBHs.

Later on, King (2005) rederived the momentum driven flow while studying the AGN-outburst connection, thus the $M_\bullet - \sigma$ relation including the effect of gravity in the slow down process of the shell moving outwards and finally stalling. The gas that remains in the bubble can form stars and can be again used for the accretion and outflows and in this process the metallicity is enhanced. The expansion of this bubble occurs on dynamical time scale in the beginning that later on happens on the Salpeter timescale which depends on the central black hole mass. After a certain time, when further cooling becomes impossible, the energy driven flow starts, which causes faster removal of gas, saturating the black hole mass. The $M_\bullet - \sigma$ relation was established again, with the constant in front to be twice of the constant given in King (2003). Natarajan and Treister (2009) showed that the upper limit of the mass of black hole can be set by the arguments of [King (2003); King (2005); Silk and Rees (1998); Haehnelt *et al.* (1998)].

Murray *et al.* (2005) used momentum driven formulation using radiation that is generated by continuum absorption and effect of supernovae. They argue that elliptical galaxies reach the Eddington luminosity at $z \gtrsim 1$ and they claim that this is a possible origin of the Faber-Jackson relation. From their analysis, when the luminosity reaches the maximum limit, accretion stops saturating the black hole mass resulting in $M_\bullet \propto \sigma^4$.

3.4.3 Consumption of stars

The SMBHs can also grow by the consumption of stars. This consumption can be in two ways:

- The stars those pass within the event horizon or a relatively capture radius (see Chapter 6) can be directly captured.
- The indirect capture occurs when consumption is done by accreting the gas from tidally disrupted stars.

In some cases, capture occurs at a "full - loss - cone" rate where the assumption is the orbits are somehow repopulated at a rate which is equal to or higher to the rate at which depletion occurs due to capture by the black hole.

Zhao *et al.* (2002) studied the case of a singular isothermal sphere for the calculation of the mass growth rate by stellar capture. From the polytropic equation we can write $P = K\rho^\Gamma$. For the isothermal case, the value of Γ is 1.

In the case of hydrostatic equilibrium, we can write

$$\frac{\mathrm{d}P}{\mathrm{d}r} = \frac{k_B T}{m}\frac{\mathrm{d}\rho}{\mathrm{d}r} = -\rho\frac{\mathrm{d}\Phi}{\mathrm{d}r} = -\rho\frac{GM(r)}{r^2}, \tag{3.15}$$

where, P is the pressure, T is the temperature, ρ is the density of the hydrostatic system where the adiabatic constant is Γ and k_B is the Boltzmann constant. Multiplying both sides by $\frac{r^2 m}{\rho k_B T}$, we find

$$\frac{r^2}{\rho}\frac{\mathrm{d}\rho}{\mathrm{d}r} = -\frac{GMm}{k_B T}, \tag{3.16}$$

and

$$\frac{\mathrm{d}}{\mathrm{d}r}\left(r^2 \frac{\mathrm{d}\ln\rho}{\mathrm{d}r}\right) = -\frac{4\pi r^2 \rho G m}{k_B T}. \tag{3.17}$$

Let, the distribution function be

$$f(\epsilon) = \frac{\rho_1 \exp(\epsilon/\sigma^2)}{(2\pi\sigma^2)^{\frac{3}{2}}}, \tag{3.18}$$

where, $\epsilon = \psi - \frac{1}{2}v^2$. Now, integration over all velocities gives

$$\rho = \int f(\epsilon)\mathrm{d}^3 v = \rho_1 \exp(\epsilon/\sigma^2). \tag{3.19}$$

Therefore, the Poisson's equation in this case of isothermal sphere yields

$$\frac{\mathrm{d}}{\mathrm{d}r}\left(r^2 \frac{\mathrm{d}ln\rho}{\mathrm{d}r}\right) = -\frac{4\pi G r^2 \rho}{\sigma^2}. \tag{3.20}$$

Taking $\rho = Cr^{-b}$ in the Poisson's equation and solving we get

$$-b = \frac{4\pi G C}{\sigma^2} r^{2-b}, \tag{3.21}$$

which implies, $b = 2$ and $C = \frac{\sigma^2}{2\pi G}$. Finally, the density takes the form

$$\rho = \frac{\sigma^2}{2\pi G r^2}. \tag{3.22}$$

The total mass of the system can be calculated to be

$$M(r) = \int \rho(r) 4\pi r^2 \mathrm{d}r = \frac{2\sigma^2 r}{G}. \tag{3.23}$$

Therefore, the stellar potential is given by

$$\Phi(r) = G \int_{r_h}^{r} \frac{M(r)}{r^2} \mathrm{d}r \tag{3.24}$$

$$= \frac{2G\sigma^2}{G} \int_{r_h}^{r} \frac{1}{r} \mathrm{d}r = 2\sigma^2 \ln\left(\frac{r}{r_h}\right), \tag{3.25}$$

where, r_h is the sphere of influence radius of the black hole. Therefore, the expression for stellar potential becomes

$$\psi_*(r) = -2\sigma^2 \ln\left(\frac{r}{r_h}\right). \tag{3.26}$$

For the case of singular isothermal sphere, the rate of mass the stars flowing into a sphere of radius r, when they move along their orbits can be written as

$$\sim 4\pi r^2 \sigma\rho \approx 4\pi r^2 \frac{\sigma^2}{2\pi G R^2} \sigma \approx \frac{2\sigma^3}{G}. \tag{3.27}$$

The fraction, $\frac{r_\ell}{r}$, of stars will go within r_ℓ of the SMBH, where r_ℓ is the loss cone radius of the SMBH. Putting $r = r_h$, the radius of influence and considering r_ℓ to be a multiple of gravitational radius of SMBH, $r_g = \frac{GM_\bullet}{c^2}$, where, $r_g \leq r_\ell \leq 10 r_g$, the capture rate can be written as

$$\dot{M}_\bullet = \frac{2\sigma^3}{G} \frac{r_\ell}{r_h} \approx 10 \frac{\sigma^5}{Gc^2}. \tag{3.28}$$

Therefore, after 10 Gyr, the total mass that is accumulated will be (Zhao *et al.* 2002)

$$M_\bullet = 1 \times 10^8 \left(\frac{\sigma}{200 \mathrm{km\ s^{-1}}}\right)^5 M_\odot, \tag{3.29}$$

which is in agreement with the observed relation of $M_\bullet$ - σ.

3.5 Evolution of the $M_\bullet - \sigma$ relation

The mass evolution equation for black holes (ignoring mergers) can be approximated by

$$M_\bullet(t) = f(t)\mathcal{M} = k_0\sigma^p \simeq M_s + \int \mathrm{d}t(\dot{M}_* + \dot{M}_g) \simeq k_0(t)\sigma^{p(t)} \tag{3.30}$$

where $\dot{M}_* =< m_* > \dot{N} = k_2\sigma^{p_1}$, where $p_1 = 4.3$ for non-relativistic loss cone theory (eg. Mageshwaran & Mangalam 2015), $\dot{M}_g = k_1\sigma^{p_2}$ where $p_2 \simeq 4$ is the gas accretion rate from the momentum-driven flow. The seed black hole mass is derived from BH formation models and is roughly given by $M_s \propto \mathcal{M}$ or $M_s = k_3\sigma^{p_3}$ (Faber-Jackson law by a fiducial argument here gives $p_3 \simeq 5$) although p_3 is quickly irrelevant as $M_\bullet >> M_s$ during the evolution. The similarity of $p_1 \simeq p_2 \simeq p_3$ is why we think that the form of the $M_\bullet - \sigma$ relation approximately holds at all epochs. Shen *et al.* (2015) and Salviander and Shields (2013) have analyzed the evolution of the $M_\bullet - \sigma$ relation from SDSS data for quasars and report no evolution of the relation up to $z \simeq 1$. From the numerical simulations, of the large-scale structure of the universe, done by Sijacki *et al.* (2015) and Taylor and Kobayashi (2016) it is seen that almost up to $z \simeq 4$ this relation holds. Robertson *et al.* (2006) studied the evolution of this relation till $z = 6$, for merging disk galaxies through hydrodynamic simulations and they have taken into account the effects of accretion and supernovae. They found almost no change in $p(z)$ and a very small change of the constant, $k_0(z)$, similarly as suggested by Shankar *et al.* (2009a). From their analysis, $k_0(z) \propto (1+z)^\alpha$, with $\alpha = 0.33$. We study the evolution of $p(z)$ and k, from the formation redshift till today via our evolution model of black holes in Chapter 6. We consider the Faber - Jackson relation to be the initial

condition, which provides $p = 5$ at formation redshift and we see that it reaches near 4 at $z \simeq 0$, due to saturation of the black hole mass. But, throughout the entire redshift range considered, this value of p remains well within 4 - 5, as found observationally whose details are in Chapter 6.

3.6 Resource summary

1. In this chapter, we introduced the $M_\bullet - \sigma$ relation and provided the literature study of this relation [Ferrarese and Merritt (2000), Gebhardt *et al.* (2000)].

2. We discuss the significance of this relation.

3. We presented three theoretical models deriving the $M_\bullet - \sigma$ relation provided by Silk and Rees (1998), King (2003), Zhao *et al.* (2002).

4. We also proposed a basic paradigm of the evolution of the $M_\bullet - \sigma$ relation and presented a literature survey of the evolution of this relation with redshift [Shen *et al.* (2015), Salviander and Shields (2013), Sijacki *et al.* (2015), Taylor and Kobayashi (2016), Robertson *et al.* (2006), Shankar *et al.* (2009a)].

Image: earthsky.org

Chapter 4

$M_\bullet - \sigma$ relation in spherical systems*

4.1 Introduction

There are many theoretical models proposed for explaining the $M_\bullet - \sigma$ relation [discussed in Chapter 4, Silk and Rees (1998), King (2003), Zhao *et al.* (2002)]. The origin of this relation is still a mystery but various models give a range $p = 4 - 5$, which is in rough agreement with observations (see Table 3.1).

From observations, it is seen that bulge mass, $M_\bullet \simeq f M_b$, where, $f = 1.259 \times 10^{-3}$ (Merritt and Ferrarese 2001). Later Marconi and Hunt (2003) and Häring and Rix (2004) found $f = 2 \times 10^{-3}$ and $f = (1.4 \pm 0.4) \times 10^{-3}$ respectively. For higher masses, the relation is said to be nonlinear and given by $M_\bullet \propto M_b^{1.12}$ (Häring and Rix 2004) where the Jeans equation has been applied with zero anisotropy in the

*This chapter is published in Bhattacharyya and Mangalam (2018)

system to determine the velocity dispersion of 30 elliptical galaxies whose bulge masses are sourced from Magorrian *et al.* (1998). Kormendy and Ho (2013) have also found the following relation:

$$\left(\frac{M_\bullet}{10^9 M_\odot}\right) = 0.49^{+0.06}_{-0.05}\left(\frac{M_b}{10^{11} M_\odot}\right)^{1.17\pm0.08}. \tag{4.1}$$

Byun *et al.* (1996) introduced and calculated Nuker profiles for 57 early type galaxies from HST data. This profile is described by two power laws and matches with the observational profiles very well. Instead of conventional structural parameters such as core radius and central surface brightness, new parameters like the break radius r_b, and surface brightness, μ_b, at that radius were used. Another parameter α describes the sharpness of the break and they have calculated these parameters by applying χ^2 minimization technique to the mean surface brightness profiles of the early type galaxies. Faber *et al.* (1997) have analyzed 61 elliptical galaxies and spiral bulges from HST data and derived the parameters like r_b, the intensity at that radius, I_b, σ and L. Wang and Merritt (2004) and Stone and Metzger (2016) used these results in their spherical galaxy model for deriving the distribution function (DF) while we use it to derive the empirical $M - \sigma$ relation.

In this chapter, we describe a theoretical model for calculating line of sight velocity dispersion for spherical systems and thereby derive the $M_\bullet - \sigma$ relation. In §2, we discuss the nexus between the $M_\bullet - \sigma$ relation and the power law mass density index analytically motivating the theoretical models of power law galaxies. In the §3, we have extended the model to the case of Nuker intensity profile, which is much more generalized than the special case of a single power law profile. Using parameters derived from the observational profiles for 12 galaxies we have determined the $M_\bullet - \sigma$ relation and the M_b - $M_\bullet$ relation for the proportionality case from χ^2 analysis. We discuss our results in §5 and present our conclusions in §6.

4.2 Connection of $M_\bullet - \sigma$ relation with power law mass density of galaxies

If $M_\bullet$ is proportional to M_b, then eq. (3.1) can be written as

$$f_b M_b = k\sigma^p. \tag{4.2}$$

The total mass scales as ρr^3, where, ρ is the mass density of the galaxy and r is the distance from the center of the galaxy; similarly σ scales as $\sqrt{\rho r^2}$. Therefore, from the eq. (4.2), it can be seen that

$$\begin{aligned} \rho r^3 &\propto \rho^{\frac{p}{2}} r^p \\ \Rightarrow \rho &\propto r^{\frac{2p-6}{2-p}}. \end{aligned} \tag{4.3}$$

From the above relation it can be infirmed that the density follows a single power law so that

$$\gamma = \frac{2p-6}{2-p};\ \text{or equivalently}\ p = \frac{2\gamma+6}{2+\gamma}, \tag{4.4}$$

where γ is the power law index. Taking typical observational values for p, we find $\gamma = 0.75 - 1.4$ giving p = 3.6 - 5.3. For a single power law profile given by

$$\rho(r) = \rho_0 \left(\frac{r}{r_0}\right)^{-\gamma}, \tag{4.5}$$

we use Poisson's equation to calculate the stellar potential of the system

$$\nabla^2 \Phi = 4\pi G\rho, \tag{4.6}$$

to find a stellar potential of the form

$$\psi_\star(r) = \frac{4\pi G\rho_0 r_0^\gamma r_h^{2-\gamma}}{(2-\gamma)(3-\gamma)} \left[1 - \left(\frac{r}{r_h}\right)^{2-\gamma}\right]. \tag{4.7}$$

The total mass of stars contained within r_h is given by

$$M_\star(r < r_h) = \int_0^{r_h} \rho(r) 4\pi r^2 \mathrm{d}r$$
$$= 4\pi\rho_0 r_0^\gamma \int_0^{r_h} r^{2-\gamma} \mathrm{d}r = 4\pi\rho_0 r_0^\gamma \frac{r_h^{3-\gamma}}{3-\gamma} = 2M_\bullet, \tag{4.8}$$

where, $\rho_0 r_0^\gamma = \frac{(3-\gamma)}{2\pi} M_\bullet r_h^{\gamma-3}$, so that the stellar potential takes the form

$$\psi_\star(r) = \frac{2}{2-\gamma}\frac{GM_\bullet}{r_h}\left[1 - \left(\frac{r}{r_h}\right)^{2-\gamma}\right], \tag{4.9}$$

and the total potential is given by

$$\psi(r) = \psi_\star(r) + \frac{GM_\bullet}{r} + \psi_c, \tag{4.10}$$

where, ψ_c is a constant which ensures that $\psi(r)$ asymptotes to zero. We normalize the total potential in units of $GM_\bullet/r_h$ so that

$$\psi = \frac{1}{r_\star} + \frac{2}{2-\gamma}(1 - (r_\star)^{2-\gamma}) + \psi_0 = x + \frac{2}{2-\gamma}(1 - (x)^{\gamma-2}) + \psi_0, \tag{4.11}$$

where,

$$r_\star = \frac{r}{r_h}, x = \frac{1}{r_\star}, \psi_0 = \frac{\psi_c}{\frac{GM_\bullet}{r_h}}. \tag{4.12}$$

Next, we calculate the DF from Eddington's formula as

$$f(\varepsilon) = \frac{1}{\sqrt{8}\pi^2 m_\star}\frac{\mathrm{d}}{\mathrm{d}\varepsilon}\int_0^\varepsilon \frac{\mathrm{d}\rho}{\mathrm{d}\psi}\frac{\mathrm{d}\psi}{\sqrt{\psi - \varepsilon}}, \tag{4.13}$$

where, $m_\star$ is the stellar mass which results in

$$f(\varepsilon) = \frac{\gamma(3-\gamma)}{4\sqrt{2}\pi^3}\frac{1}{m_\star}\frac{1}{G^3 M_\bullet^2} g(\varepsilon),$$

where,

$$g(\varepsilon) = \frac{\mathrm{d}}{\mathrm{d}\varepsilon} \int_{x_1}^{x_2} \frac{x^{\gamma-1}}{\sqrt{\varepsilon - x - \frac{2}{2-\gamma}(1 - x^{\gamma-2})}} dx, \tag{4.14}$$

and x_1 and x_2 are the roots of the equations $\psi(x) = 0$ and $\psi(x) = \varepsilon$ respectively.

The LOS velocity dispersion is given by (Binney and Tremaine 2008)

$$\sigma_{||}^2 = \frac{\int \mathrm{d}x_{||} \mathrm{d}^3\mathbf{v} v_{||}^2 f(x,v)}{\int \mathrm{d}x_{||} \mathrm{d}^3\mathbf{v} f(x,v)}. \tag{4.15}$$

We use σ in place of $\sigma_{||}$ for the rest of the paper, consider the system to be spherical, and use polar coordinates in velocity space as (see Fig. 2.2),

$$v_r = v\cos\eta, v_\theta = v\sin\eta\cos\psi', v_\phi = v\sin\eta\sin\psi'. \tag{4.16}$$

We take the LOS direction to be an arbitrary direction, $\hat{s}$, which lies in the $r - \theta$ plane making an angle α with $\hat{r}$ axis so that

$$\hat{s} = \cos\alpha\hat{r} + \sin\alpha\hat{\theta}. \tag{4.17}$$

The projected velocity in this plane of LOS is given by

$$\mathbf{v}.\hat{s} = v_{||} = v\cos\eta\cos\alpha + v\sin\eta\cos\psi'\sin\alpha. \tag{4.18}$$

The distance along the LOS is now $x_{||} = r\cos\alpha$ where the perpendicular distance is $x_\perp = \omega = r\sin\alpha$, and

$$x_{||} = \sqrt{r^2 - r^2\sin^2\alpha} = \sqrt{r^2 - \omega^2}, \tag{4.19}$$

where, r^2 varies from ω^2 to ∞. We find the denominator D and the numerator N of the LOS velocity dispersion (eq. (4.15)) separately as

$$D_1 = \int \mathrm{d}x_{||}\mathrm{d}^3\mathbf{v} f(x,v)$$

$$= \frac{1}{2}\int_{r^2=\omega^2}^{\infty} \frac{\mathrm{d}(r^2)}{\sqrt{r^2-\omega^2}} \int_{v=0}^{\sqrt{2\psi}} \int_{\eta=0}^{\pi} \int_{\psi'=0}^{2\pi} v^2 \mathrm{d}v \sin\eta \mathrm{d}\eta \mathrm{d}\psi' f(\varepsilon), \tag{4.20}$$

which after substituting $u = \omega^2/r^2$ and $v^2 = 2(\psi - \varepsilon)$ reduces to

$$D_1 = \pi\omega J_0 \int_0^1 \frac{\mathrm{d}u}{u^2\sqrt{\frac{1}{u}-1}} \int_0^{\psi} \mathrm{d}\varepsilon (2(\psi-\varepsilon))^{\frac{1}{2}} f(\varepsilon), \tag{4.21}$$

where, $J_0 = \int_0^{\pi} \sin\eta \mathrm{d}\eta = 2$. Now,

$$N_1 = \int \mathrm{d}x_{||}\mathrm{d}^3\mathbf{v} v_{||}^2 f(x,v)$$

$$= \frac{1}{2}\int_{r^2=\omega^2}^{\infty} \frac{\mathrm{d}(r^2)}{\sqrt{r^2-\omega^2}} \int_{v=0}^{\sqrt{2\psi}} \int_{\eta=0}^{\pi} \int_{\psi'=0}^{2\pi} v^2 \mathrm{d}v \sin\eta \mathrm{d}\eta \mathrm{d}\psi' v^2 \left(\cos\eta \frac{\sqrt{r^2-\omega^2}}{\sqrt{r^2}} + \sin\eta\cos\psi' \sqrt{\frac{\omega^2}{r^2}} \right)^2 f(\varepsilon) \tag{4.22}$$

Similarly, with the same substitutions, N_1 reduces to

$$N_1 = \omega 2^{\frac{1}{2}} \left[2\pi J_1 \int_0^1 \frac{\mathrm{d}u\sqrt{\frac{1}{u}-1}}{u} \int_0^{\psi} \mathrm{d}\varepsilon (\psi-\varepsilon)^{\frac{3}{2}} f(\varepsilon) + J_2 J_3 \int_0^1 \frac{\mathrm{d}u}{u\sqrt{\frac{1}{u}-1}} \int_0^{\psi} \mathrm{d}\varepsilon (\psi-\varepsilon)^{\frac{3}{2}} f(\varepsilon) \right] \tag{4.23}$$

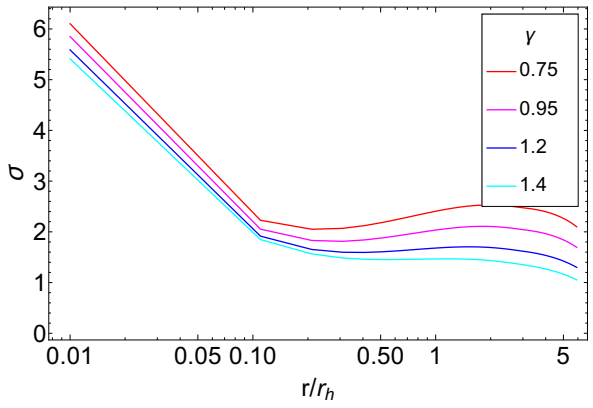

FIGURE 4.1: The dimensionless σ is plotted against projected r/r_h for various power law indices γ.

where,

$$J_1 \int_0^{\pi} \sin\eta \cos^2\eta \mathrm{d}\eta = \frac{2}{3}, J_2 = \int_0^{\pi} \sin^3\eta \mathrm{d}\eta = \frac{4}{3}, J_3 \int_0^{2\pi} \cos^2\psi' \mathrm{d}\psi' = \pi.$$

The dimensionless LOS velocity dispersion given by $\sigma = \sqrt{\frac{N_1}{D_1}}$ for power law galaxies is shown in Fig. 4.1, where we can see that the velocity dispersion is flattening out as we move outwards from the center of the galaxy. Near the center of the galaxy where the SMBH potential dominates $\sigma \propto 1/\sqrt{r}$. Later it flattens out because of the dominance of the stellar potential. By finding σ at any radius one can verify the $M_\bullet - \sigma$ relation if $M_\bullet$ is known.

From the definition, eq. (4.8), r_h for a single power law galaxy can be written as

$$r_h = \left(\rho_0 r_0^{\gamma} \frac{2\pi}{3-\gamma} \frac{1}{M_\bullet}\right)^{\frac{1}{\gamma-3}}. \tag{4.24}$$

The total mass out to the bulge can be calculated to be

$$\int_0^{r_s} \rho_0 \left(\frac{r_0}{r}\right)^{\gamma} 4\pi r^2 \mathrm{d}r = M_s, \tag{4.25}$$

, where, r_s is the radius of the central bulge. Therefore, $\rho_0 r_0^\gamma$ can be written as,

$$\rho_0 r_0^\gamma = \frac{M_s}{\int_0^{r_s} 4\pi r^{2-\gamma} \mathrm{d}r} = \frac{M_s(3-\gamma)}{4\pi r_s^{3-\gamma}}. \tag{4.26}$$

For a range of black hole mass ($M_\bullet = 10^6$ to 10^9 $M_\odot$) our calculated $\sigma(M_s, \gamma)$, $\log k(M_s, \gamma)$ and $p(\gamma)$ (which is observationally within 4 - 5) are shown in Fig. 4.2, where, M_s varies from 10^{10} to 10^{12} $M_\odot$, r_s varies from 1 - 10 kpc and γ varies from 0.75 to 1.5. We can see that for a fixed value of γ, p is independent of the value of M_s. The range of p we find is 3.6 - 5.3, which agrees well with the observations. Fig. 4.2(b) shows a plot of $\log k(M_s, \gamma)$; a change in M_s for a fixed value of γ affects the intercept though the slope is unchanged. To explain the nature of these plots we write eq. (3.1) as

$$M_\bullet = \left(\frac{M_s}{2}\right)^{\frac{1}{\gamma-2}} r_s^{\frac{\gamma-3}{\gamma-2}} (\sigma_h^2 G)^{-\frac{\gamma-3}{\gamma-2}} \sigma^{\frac{2(\gamma-3)}{\gamma-2}}, \tag{4.27}$$

where, σ_h is the value of dimensionless σ at $3r_h$. From the eq. (4.27) we see that the constant k depends on γ, r_s and M_s, but the index, p of the $M_\bullet - \sigma$ relation depends only on γ which clearly explains the nature of the plots in Fig 4.2(a) and 4.2(b).

The contour plot of σ_{200} (see Fig. 4.2) at $3r_h$ for different power laws by varying M_s and $M_\bullet$ for a fixed $r_s = 10^4$ pc is shown in Fig. 4.2. By selecting a physical and observed range for σ, one can obtain the allowed $M_\bullet - M_s$ combinations for those systems.

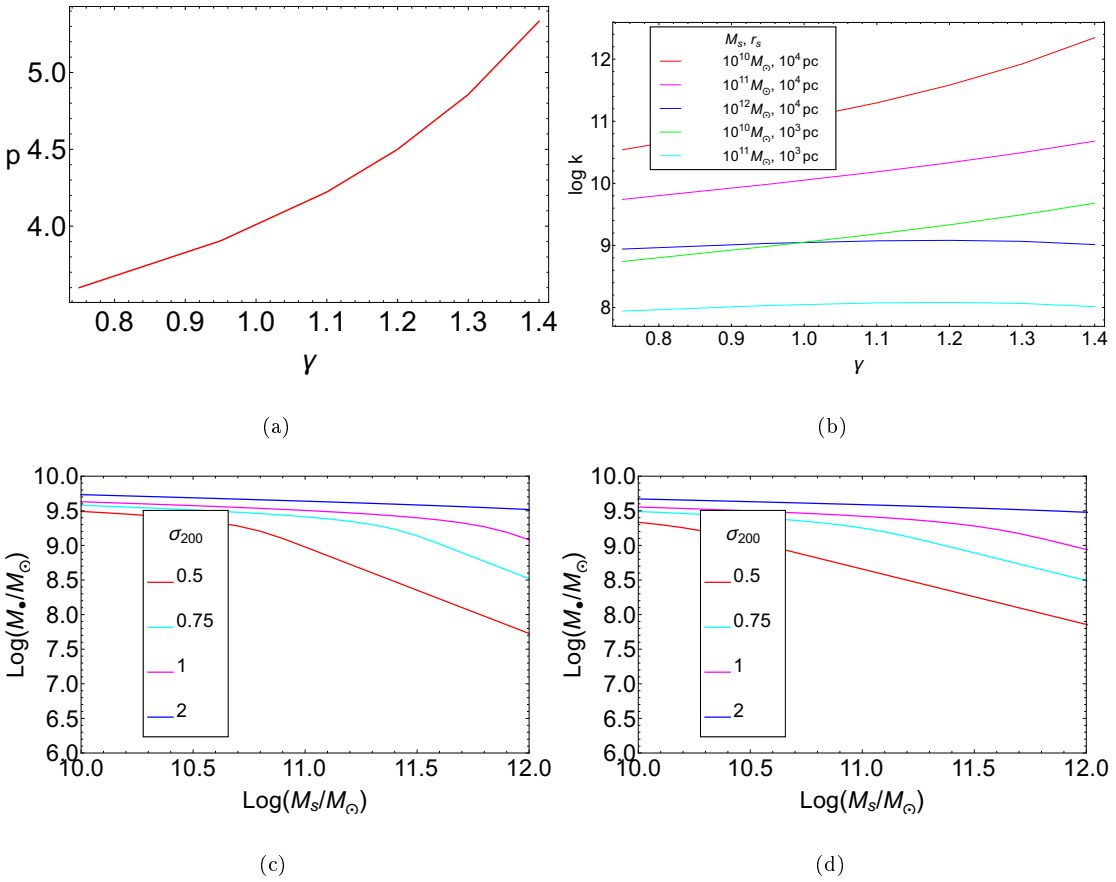

FIGURE 4.2: Plot of $p(\gamma)$ (left) and plot of $\log k(M_s)$ (right) for different values of γ for different $M_s - r_s$ combinations (up). Contour plot of σ_{200} at $3r_h$ for different power laws ($\gamma = 1.2$ (left) and $\gamma = 0.75$ (right)) by varying M_s for different values of $M_\bullet$ for a fixed $r_s = 10^4$ pc (down).

4.3 Spherical galaxies following Nuker profile of intensity

The Nuker profile used to fit the observational luminosity data is given by,

$$I(\xi) = I_b 2^{\frac{(\beta-\Gamma)}{\alpha}} \xi^{-\Gamma} (1 + \xi^\alpha)^{-\frac{(\beta-\Gamma)}{\alpha}}, \tag{4.28}$$

where, $\xi = \frac{R}{r_b}$, r_b is the break radius and I_b is the intensity at the break radius, Γ is the inner slope and the outer slope is β. The visual mass - to - light ratio is denoted by Υ_v (assuming $H_0 = 80$ km s^{-1} Mpc^{-1}) and μ_b is the surface brightness in visual

magnitudes arcsec^{-2} at r_b. The quantity μ represents the apparent magnitude of the equivalent total light observed in a square arcsec at different points in the distribution and it can be related to the physical surface brightness profile through (Binney and Merrifield 1998) :

$$\mu = -2.5 \log I + C, \tag{4.29}$$

where C is a constant. If the intensity is measured in units of $L_\odot \mathrm{pc}^{-2}$, then the constant can be calculated from the distance modulus formula and it is given as

$$C = -5 \log_{10}(\delta\theta) + M_\odot^{abs} - 5, \tag{4.30}$$

where $\delta\theta$ is 1" $= \frac{1}{206265}$ radians and solar absolute magnitude, $M_\odot^{abs}$ is 4.83 so that $I_b(\mu_b)$ can be calculated. The stellar mass density profile was computed via Abel's inversion equation as

$$\rho(r) = \Upsilon_v j(r) = -\frac{\Upsilon_v}{\pi} \int_r^\infty \frac{\mathrm{d}I}{\mathrm{d}R} \frac{\mathrm{d}R}{\sqrt{R^2 - r^2}}, \tag{4.31}$$

where, $j(r)$ is the luminosity density. The stellar potential ψ_* is calculated from the stellar mass density calculated above as shown in Fig. 4.3(a)

$$\psi_*(r) = \frac{4\pi G}{r} \int_0^r \rho(r') r'^2 \mathrm{d}r' + 4\pi G \int_r^\infty \rho(r') r' \mathrm{d}r'. \tag{4.32}$$

As before the gravitational potential $\psi(r) = -\Phi(r)$ is the total potential given by (see Fig. 4.3(b))

$$\psi(r) = \psi_*(r) + \frac{GM_\bullet}{r}. \tag{4.33}$$

The density follows the same profile (double power law) as intensity as shown in

Fig. 4.3(a), where we see the total potential (see Fig. 4.3(b)) is dominated by SMBH potential at the inner radii and is dominated by the stellar potential as we move outwards from the center. Again we use the Eddington's formula, eq.(4.13) to calculate $f(\varepsilon)$ shown in Fig. 4.3(c). The denominator of the LOS velocity dispersion can be written as

$$D_2(\alpha,\beta,\Gamma,\Upsilon,r_b,\mu_b,L,f) = \int \mathrm{d}x_{||}\mathrm{d}^3\mathbf{v}f(x,v)$$

$$= \int_{r=\omega}^{\infty} \frac{r\mathrm{d}r}{\sqrt{r^2-\omega^2}} \int_{v=0}^{\sqrt{2\psi}} \int_{\eta=0}^{\pi} \int_{\psi'=0}^{2\pi} v^2\mathrm{d}v\sin\eta\mathrm{d}\eta\mathrm{d}\psi' f(\varepsilon). \tag{4.34}$$

By replacing the variable r by $1/u$ the denominator can finally be written as

$$D_2(\alpha,\beta,\Gamma,\Upsilon,r_b,\mu_b,L,f) = 2^{\frac{3}{2}}2\pi J_0 \int_{u=0}^{1/\omega} \frac{\mathrm{d}u}{u^2\sqrt{1-\omega^2u^2}} \int_{\varepsilon=0}^{\psi} (\psi(u)-\varepsilon)^{\frac{1}{2}} f(\varepsilon)\mathrm{d}\varepsilon \tag{4.35}$$

The numerator N_2 of the LOS velocity dispersion is

$$\begin{aligned} N_2(\alpha,\beta,\Gamma,\Upsilon,r_b,\mu_b,L,f) &= \int \mathrm{d}x_{||}\mathrm{d}^3\mathbf{v}v_{||}^2 f(x,v) \\ &= \frac{1}{2}\int_{r^2=\omega^2}^{\infty} \frac{\mathrm{d}(r^2)}{\sqrt{r^2-\omega^2}} \int_{v=0}^{\sqrt{2\psi}} \int_{\eta=0}^{\pi} \int_{\psi'=0}^{2\pi} \\ v^2\mathrm{d}v\sin\eta\mathrm{d}\eta\mathrm{d}\psi' v^2 &\left(\cos\eta\frac{\sqrt{r^2-\omega^2}}{\sqrt{r^2}} + \sin\eta\cos\psi'\sqrt{\frac{\omega^2}{r^2}}\right)^2 f(\varepsilon). \end{aligned} \tag{4.36}$$

This finally takes the form

$$\begin{aligned} N_2(\alpha,\beta,\Gamma,\Upsilon,r_b,\mu_b,L,f) = 2^{\frac{5}{2}}\Bigg[& 2\pi J_1 \int_0^{1/\omega} \frac{\sqrt{1-\omega^2u^2}}{u^2} \int_0^{\psi} \mathrm{d}\varepsilon(\psi-\varepsilon)^{\frac{3}{2}} f(\varepsilon) \\ & + J_2 J_3 \int_0^{1/\omega} \frac{\omega^2}{\sqrt{1-\omega^2u^2}} \int_0^{\psi} \mathrm{d}\varepsilon(\psi-\varepsilon)^{\frac{3}{2}} f(\varepsilon)\Bigg]. \end{aligned} \tag{4.37}$$

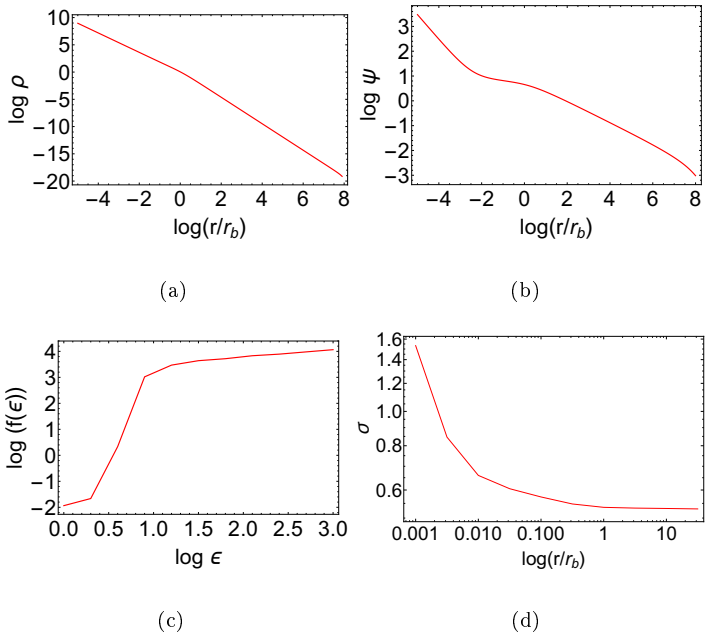

FIGURE 4.3: The density, total potential plots, DF and velocity dispersion plots from left to right for $f = 0.0012$ for NGC 3115.

Using the same procedure as was done in the case of power law galaxies, we compute the LOS velocity dispersion for these galaxies shown in Fig. 4.3(d). The DF (see Fig. 4.3(c)) increases towards the higher side of the energy value implying presence of more high energy stars. Here also the velocity dispersion plot flattens out as we move outwards from the center of the galaxy where the motion of the stars are dominated by the stellar potential.

To simplify our calculation we use the following scales:

$$\rho_s = -\frac{\Upsilon_v}{\pi}\frac{I_b}{r_b}, \quad \psi_s = 4\pi G r_b^2 \rho_s, \quad f_s = \frac{\rho_s}{\sqrt{8}\pi^2 m_* \psi_s^{\frac{3}{2}}}, \tag{4.38}$$

so that σ is in units of $\sqrt{\psi_s}$. In Table 4.1 we tabulate the values of $\sigma(\sqrt{Q})$ at radius $r_e/8$, where, r_e is the effective radius (Ferrarese and Merritt 2000), where,

$Q(\alpha, \beta, \Gamma, r_b, \mu_b) = N_2/D_2$. The value of r_e is obtained from

$$\int_0^{r_e} I(R) 2\pi R dR = \frac{1}{2} L_T. \tag{4.39}$$

#	Galaxy	$\log(\frac{r_b}{\mathrm{pc}})$	μ_b	α	β	Γ	Υ_v $(\frac{M_\odot}{L_\odot})$	$\log(\frac{L_V}{L_\odot})$	$\frac{M_b}{10^{10} M_\odot}$	$\log(\frac{r_e}{\mathrm{pc}})$	σ (km/sec)
1	NGC 3379	1.92	16.10	1.59	1.43	0.18	6.87	10.15	0.90	3.17	230
2	NGC 3377	0.64	12.85	1.92	1.33	0.29	2.88	9.81	1.86	3.15	217
3	NGC 4486	2.75	17.86	2.82	1.39	0.25	17.70	10.88	134.30	3.76	433
4	NGC 4551	2.46	18.83	2.94	1.23	0.80	7.25	9.57	2.69	3.03	218
5	NGC 4472	2.25	16.66	2.08	1.17	0.04	9.20	10.96	83.90	3.75	542
6	NGC 3115	2.07	16.17	1.47	1.43	0.78	7.14	10.23	12.12	3.15	230
7	NGC 4467	2.38	19.98	7.52	2.13	0.98	6.27	8.75	0.35	2.81	108
8	NGC 4365	2.25	16.77	2.06	1.27	0.15	8.40	10.76	48.34	3.68	524
9	NGC 4636	2.38	17.72	1.64	1.33	0.13	10.40	10.60	41.40	3.77	354
10	NGC 4889	2.88	18.01	2.61	1.35	0.05	11.20	11.28	213.4	4.10	469
11	NGC 4464	1.95	17.35	1.64	1.68	0.88	4.82	9.22	0.80	2.70	157
12	NGC 4697	2.12	16.93	24.9	1.04	0.74	6.78	10.34	14.83	3.36	215

TABLE 4.1: The first 10 columns the data used for our calculation are shown (r_b is the break radius, μ_b is the surface brightness, inner slope is Γ and the outer slope is β, sharpness of break is given by α, Υ is the mass - to -light ratio, L is the total luminosity, the bulge mass $M_b = \Upsilon_v L$) and in the last two columns, the output values of r_e and the LOS velocity dispersion are shown (Wang and Merritt 2004).

4.4 $M_\bullet - \sigma$ relation

By using the data given in Wang and Merritt (2004) for elliptical galaxies as shown in Table 4.1, we calculate the bulge mass of those galaxies by multiplying total luminosity by the mass to light ratio as prescribed in Magorrian *et al.* (1998). Using eq. (4.15) we calculate the LOS velocity dispersion to get the $M_\bullet$ - σ relation by fitting a straight line for 12 galaxies as shown in Fig. 4.4(a) for different f_b values. The p and $\log k$ values for different values of f_b are shown in the scatter

plot (see Fig. 4.4(b)). From χ^2 minimization we have determined p and f; the procedure used is shown in a flowchart given in Fig. 6.15.

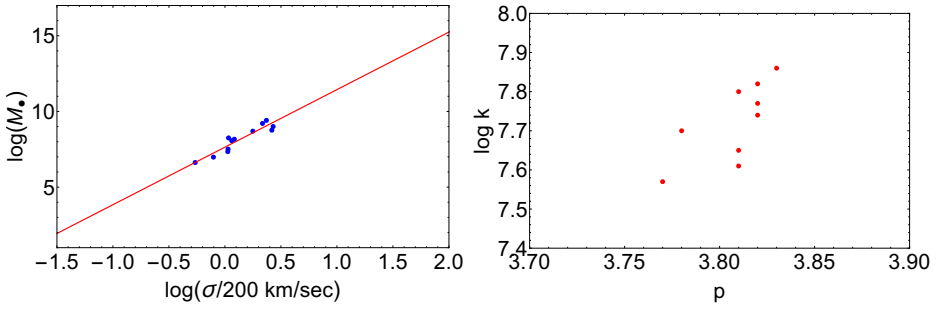

(a) (b)

FIGURE 4.4: The plot of $\log \sigma$ vs $\log M_\bullet$ for 12 galaxies for $f_b = 0.0012$, σ is in units of 200 km/sec (left) and (right) the scatter plot of p and $\log k$, for different values of f, showing a tight range of k and p.

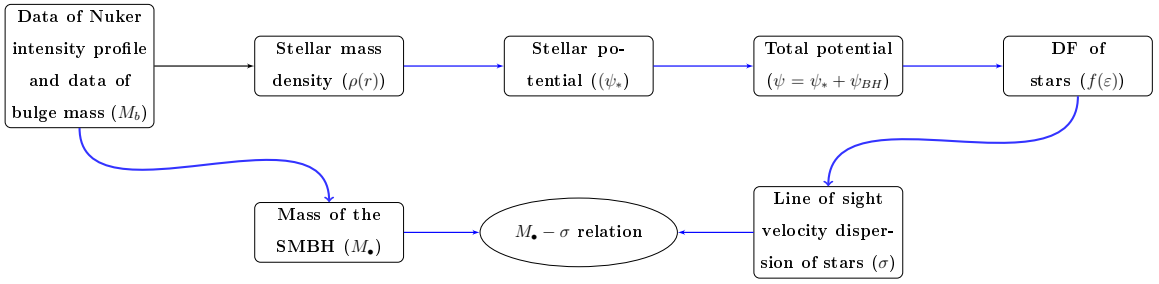

FIGURE 4.5: The flowchart shows the procedure for calculating the $M_\bullet - \sigma$ relation from observational data. For the Nuker profile the stellar mass density is found using Abel inversion and from spherical shell structure the stellar potential is calculated. The SMBH potential is added to get the total potential, Eddington's formula is used to derive DF $f(\varepsilon)$. The SMBH mass is calculated from the proportionality relation of M_b and $M_\bullet$. The path marked by the blue lines only is followed for deriving the $M_\bullet - \sigma$ relation in case of single power law galaxies.

The formula we used for determining χ^2 is (Sivia and Skilling 2006)

$$\chi^2 = \sum_k \left[\frac{(D_k - F_k)^2}{F_k} \right], \tag{4.40}$$

where a uniform prior is used. The observed values, D_k are obtained for $M_\bullet$ and σ from our calculation using the observational data and the expected value, F_k is obtained by the best fit straight line to these points as shown in Fig. 4.4(a).

The range of f_b and p has been taken from previous determinations as well as observational values (f_b = 0.001 - 0.002, p = 3 - 5). The quantity $S(f_b, p) \equiv \left(1 - \frac{\chi^2 - \chi^2_{min}}{\chi^2_{max} - \chi^2_{min}}\right)$ is in the range 0 - 1. The maximum value of $S(f_b, p)$ corresponds to the minimum χ^2 value. In the plot we have shown $S(f_b, p)$ contours where $S(f_b, p) \geq 0.97$ is considered as the allowed range (the red region) for the two parameters and from the plot we determine the value of $p = 3.81 \pm 0.004$ and $f_b = (1.23 \pm 0.09) \times 10^{-3}$.

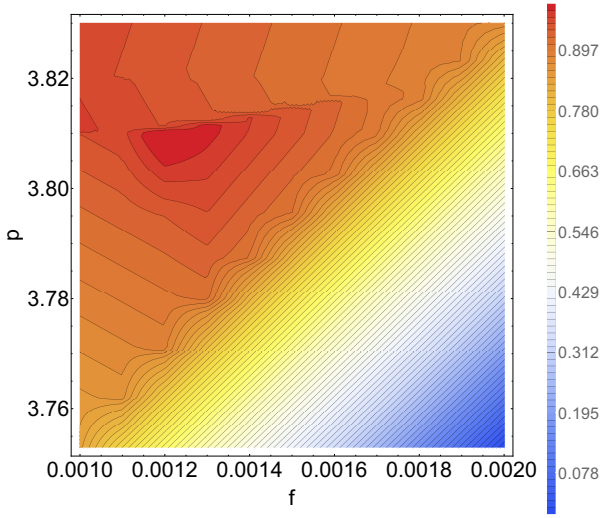

FIGURE 4.6: The $S(f_b, p)$ plot for determination of p and f_b is shown where, the maxima (minima of χ^2) occurs at $p = 3.81 \pm 0.004$ and $f_b = (1.23 \pm 0.09) \times 10^{-3}$.

4.5 Summary of results and discussion

We summarize and discuss our key results below.

1. Assuming the $M_\bullet - \sigma$ relation, $M_\bullet = f_b M_b$ and a single power law profile for the stellar mass density we have analytically shown that $p(\gamma) = (2\gamma + 6)/(2 + \gamma)$ (eq. (4.3)). For a typical a range of γ = 0.75 - 1.4, we find p = 3.6 - 5.3, which is within the observed range.

2. The second analysis shown is for the Nuker profile which is a double power law with two slopes β and Γ. As an approximate analysis, we take an average value of the mean slope to be $(\beta + \Gamma)/2$ for the set of 12 galaxies (tabulated in Table 4.1) resulting $p = 3.86$ from eq. (4.4), where the value of p obtained from χ^2 analysis is 3.81, which is very close. Therefore, our analysis of observational data agrees well with the theoretical expected value.

3. We have described a procedure for determining the $M_\bullet - \sigma$ relation (see Fig. 6.15). Previous models (as discussed in the §4.2) determined the $M_\bullet - \sigma$ relation and also the $M_b - M_\bullet$ relation independently. We have determined those two relations self - consistently in our model from our χ^2 analysis (see eq. (4.40)).

4. For power law galaxies, we started directly from mass density profile, which in the case of Nuker profile was obtained by inverting the intensity profiles. The σ for different power law indices are shown in Fig. 4.1. The variation of p and $\log k$ with different values of γ, r_s and M_s are shown in Fig. 4.2(a) and Fig. 4.2(b). The variation of σ with different $M_\bullet$ and M_s is shown in Fig. 4.2(c) and Fig. 4.2(d). For a fixed value of γ, $\log k$ and σ depend on the value of M_s and r_s. These various diagnostics enable us to interpret the relation by using the observables such as γ and M_s and to predict k and p. From observational Nuker intensity profiles, we have determined the LOS velocity dispersion of the stars in the galaxy through their DF (see Fig. 4.3(c), 4.3(d)). By using a proportionality relation between M_b and $M_\bullet$ we have derived values of p and $\log k$ for different values of f_b by a linear fit (see Fig. 4.4(b) for scatter plot and Fig. 4.4(a) for the linear fit for a fixed f_b) and through χ^2 minimization (see Fig. 4.6) for the Nuker case. From the scatter plot (see Fig. 4.4(b)) it is seen even for a small set of galaxies that the p and $\log k$ values within a specific range of f_b are very close to the observed range; these are consistent with observations. The obtained values are $p = 3.81 \pm 0.004$ and $f_b = (1.23 \pm 0.09) \times 10^{-3}$.

4.6 Conclusions

We have discussed a procedure of deriving the $M_\bullet - \sigma$ relation along with a proportionality relation of M_b and $M_\bullet$ starting from observational data by deriving the DF $f(\varepsilon)$. Using our novel approach we can also determine the index of the nonlinear relation between M_b and $M_\bullet$ (as mentioned earlier) as well as p self consistently. The $M_\bullet - \sigma$ relation is complicated to explain by existing models. The self consistent determination of f, k and p is key for improving the models. The resolution of the problem can come from a DF $f(\varepsilon, L_z)$ built for a central BH and constraining a self - consistent dynamical model from which an explanation of $fM_b = k\sigma^p$ can finally emerge. That needs much more sophisticated analytical and numerical methods applied to both the bulge mass scaling as well as $M_\bullet - \sigma$ determination.

Chapter 5

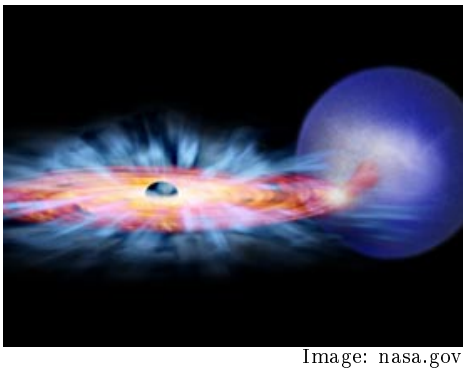

Image: nasa.gov

Physics of the growth of black holes

5.1 Introduction

In this chapter, we introduce the basic physics of the growth of the black holes. The black holes mainly grow their mass and spin by four processes - accretion, stellar capture, mergers, and electromagnetic torque. We will introduce all these processes one by one and discuss how these processes affect the mass and spin growth of the black holes during their evolution from seed masses and spins. Accretion and mergers affect both the mass and the spin of the black hole, while the stellar capture affects the mass and the electromagnetic torque (Blandford-Znajek torque) affects only the spin of the black hole. Our aim in this chapter is to build a foundation for studying the evolution of the black hole (which we discuss in Chapter 6) when all these effects come into play together and contribute to the black hole evolution, which in turn, may be related to the evolution of the galaxy.

5.2 Accretion physics

To investigate the power supply process in many quasars and active galactic nuclei (AGN) and also for some close binary systems, it is now known that the main source of the power of these is the extraction of gravitational potential from material accreting on to a gravitating body. This process is called accretion. Due to the exploitation of the full range of the electromagnetic spectrum, this accretion process has caused an impact in the field of observational astrophysics. For compact objects including black hole, the accretion process is a very powerful source for the production of high - energy radiation.

The potential energy released, mainly in form of electromagnetic radiation, by a gravitating body of radius R with mass M for accretion of mass m on it is

$$\Delta E_{acc} = GMm/R. \tag{5.1}$$

The amount of energy depends on the ratio M/R, the compactness of the body. The energy released by the process of nuclear fusion is

$$\Delta E_{nuc} = 0.007mc^2, \tag{5.2}$$

where the main source of this energy is the burning of Hydrogen and its conversion to Helium. For, black hole and neutron stars, the energy released by accretion is more than nuclear fusion, while in the case of white dwarfs it is opposite. But, there too the accretion is of importance because the timescale of nuclear fusion is quite small compared to the accretion process. For fixed compactness of the object, the luminosity varies as a function of the accretion rate. In the case of high luminosity, some momentum transfer occurs to the accreting material from the outward radiation which in turn can control the accretion rate. As a special case, a maximum luminosity can occur which is termed as the Eddington luminosity.

5.2.1 Eddington limit

In case of spherically symmetric accretion of fully ionized hydrogen the rate of absorption of momentum is given by $\frac{\sigma_T S}{c}$, where σ_T is the Thompson scattering cross section (since electrons and ions are considered to be non-relativistic we can consider Thompson scattering as the scattering process), S is the flux of the radiation energy and c is the speed of light. All these values are in CGS units with $\sigma_T = 6.5 \times 10^{-25}\text{cm}^2$. The radiation pushes out the electrons and protons against their gravitational forces which is given by $\frac{GM(m_p + m_e)}{r^2} \simeq \frac{GMm_p}{r^2}$ (since mass of electron is very small compared to the proton mass). The luminosity L is given by $S = \frac{L}{4\pi r^2}$. Therefore the net force towards the center is

$$\left(GMm_p - \frac{L\sigma_T}{4\pi c}\right)\frac{1}{r^2}$$

For a particular value of the luminosity this expression vanishes which is given by Frank *et al.* (2002)

$$L_E = \frac{4\pi cGMm_p}{\sigma_T} \tag{5.3}$$

$$= 1.3 \times 10^{38}\frac{M}{M_\odot}\text{erg.s}^{-1}, \tag{5.4}$$

is called the Eddington Luminosity.

5.2.2 Gas dynamics

Since all accreting matter is in gaseous form we use gas dynamics for explaining their nature, though this is valid for length scales much greater than the mean free path of the gas. We are considering the gas to be a continuous fluid having velocity v, temperature T and density ρ defined at each point. Therefore, they are

defined as functions of position r and temperature T. We use three conservation laws- mass conservation, momentum conservation, energy conservation.

- For mass conservation we use the continuity equation:

$$\frac{\partial \rho}{\partial t} + \nabla.(\rho \mathbf{v}) = 0. \tag{5.5}$$

The relation among pressure, temperature, density is determined by the perfect gas law

$$P = \frac{\rho k T}{\mu m_H}. \tag{5.6}$$

Here μ is the mean molecular weight measured in units of m_H, the mass of the Hydrogen atom.

- For momentum conservation, the Euler's equation is used:

$$\rho \frac{\partial \mathbf{v}}{\partial t} + \rho \mathbf{v}.\nabla \mathbf{v} = -\nabla P + \mathbf{f}. \tag{5.7}$$

The term $\rho \mathbf{v}.\nabla \mathbf{v}$ represents the convection of momentum by velocity gradients, $\mathbf{f}$ is force acting on the gas per unit volume. $\mathbf{f}$ can be the contributions due to gravity, external magnetic field or viscosity.

- The third conservation is the energy conservation:

$$\frac{\partial}{\partial t}\left(\frac{1}{2}\rho v^2 + \rho \varepsilon_i\right) + \nabla.\left[\left(\frac{1}{2}\rho v^2 + \rho \varepsilon_i + P\right)\mathbf{v}\right] = \mathbf{f}.\mathbf{v} - \nabla.\mathbf{F_{rad}} - \nabla.\mathbf{q}, \tag{5.8}$$

where $\frac{1}{2}\rho v^2$ is the kinetic energy of the gas per unit volume, and ε_i is the temperature dependent internal energy per unit mass,

$$\varepsilon_i = \frac{3kT}{2\mu m_H}. \tag{5.9}$$

The factor of 3 comes for monoatomic gas from the number of degrees of freedom. Thus, $\rho \varepsilon_i$ is the internal energy per unit volume. The term $(\frac{1}{2}\rho v^2 +$

$\rho\varepsilon_i + P$) is the pressure work term. $\nabla.\mathbf{F_{rad}}$ represents the rate of loss of radiation energy per unit volume by emission or gain by absorption. For Bremsstrahlung process, this is approximately given by $\rho^2 T^{\frac{1}{2}}$. The last term, represents the amount of energy produced due to random motion of electrons and this smooths out the temperature differences.

For steady flow with no thermal conduction and no radiation loss,

$$P\rho^{-\Gamma} = K. \tag{5.10}$$

where K is a constant and Γ is the adiabatic constant.

5.2.3 Steady, spherically symmetric accretion

Here, a simple case is studied, where, a star with mass M, is accreting spherically and symmetrically from a gas cloud. In this case, the angular momentum, magnetic field and the motion of the gas in comparison to the star are neglected. Though, for binary systems and active galactic nuclei, this is not a very good approximation, but it gives some insight into some more complicated scenarios. This was worked out by [Hoyle and Lyttleton (1939); Bondi and Hoyle (1944)]. The case of spherical accretion we will be discussing next is based on Bondi (1952). In these models, one can derive the steady accretion rate for a given density, ρ, and temperature, T. Also, the radius up to which the gas is affected due to the presence of the star can be predicted. A relation between the local sound speed and the gas velocity can be obtained which will be useful in more complicated scenarios.

We consider spherical symmetry where the gas velocity will only have a radial component. For inflow of gas to the star, the direction of v_r will be along $-\mathbf{r}$

direction. The continuity equation [eqn. (5.5)] leads to

$$\frac{1}{r^2}\frac{\mathrm{d}}{\mathrm{d}r}(r^2\rho v) = 0. \tag{5.11}$$

We obtain the constant mass accretion rate as

$$4\pi r^2 \rho(-v) = \dot{M} \tag{5.12}$$

For the conservation of momentum, the external force per unit volume can be written as

$$f = \frac{GM\rho}{r^2}. \tag{5.13}$$

Euler's equation [eqn. (5.7)], takes the form

$$v\frac{\mathrm{d}v}{\mathrm{d}r} + \frac{1}{\rho}\frac{\mathrm{d}P}{\mathrm{d}r} + \frac{GM}{r^2} = 0. \tag{5.14}$$

Using the continuity equation, we finally arrive at

$$\frac{1}{\rho}\frac{\mathrm{d}\rho}{\mathrm{d}r} = -\frac{1}{vr^2}\frac{\mathrm{d}}{\mathrm{d}r}(vr^2). \tag{5.15}$$

Using the definition of the sound speed, $c_s = \sqrt{\dfrac{\mathrm{d}P}{\mathrm{d}\rho}}$ in the Euler equation [eqn. (5.7)], we obtain

$$v\frac{\mathrm{d}v}{\mathrm{d}r} + \frac{1}{\rho}\frac{\mathrm{d}P}{\mathrm{d}\rho}\frac{\mathrm{d}\rho}{\mathrm{d}r} + \frac{GM}{r^2} = v\frac{\mathrm{d}v}{\mathrm{d}r} - \frac{c_s^2}{vr^2}\frac{\mathrm{d}}{\mathrm{d}r}(vr^2) + \frac{GM}{r^2} = 0,$$

After rearranging, it takes the form

$$\frac{1}{2}(1 - \frac{c_s^2}{v^2})\frac{\mathrm{d}}{\mathrm{d}r}(v^2) = -\frac{GM}{r^2}\left[1 - \frac{2c_s^2 r}{GM}\right]. \tag{5.16}$$

The temperature can be obtained from $T = \dfrac{\mu m_H P}{\rho k}$, where, k is the Boltzmann constant, P is obtained from the polytropic relation [eqn. (5.10)], $\Gamma = 1$ for isothermal case and $\dfrac{5}{3}$ for the adiabatic case. For a smooth flow the gas goes

through a sonic point. The energy conservation equation [eqn. (5.8)], is replaced by the polytropic equation [eqn. (5.10)]. Therefore, these are the basic conservation equations for the spherical accretion. Next, we discuss the disc accretion, which is a much more general case.

5.2.4 Disc accretion

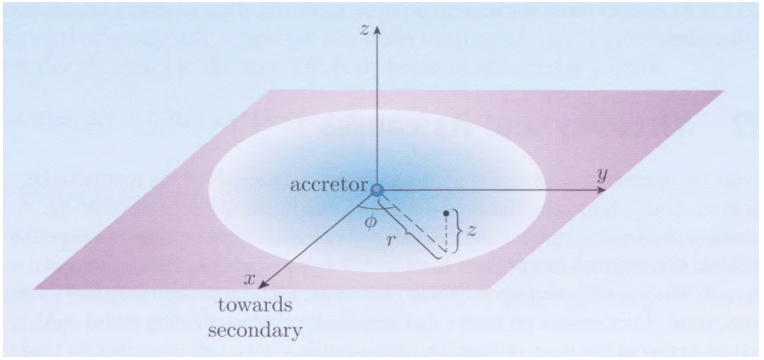

FIGURE 5.1: Geometry of the accretion disc, Image courtesy: Kolb (2010).

Similar to Kolb (2010), the assumption for the study of the accretion disc is that the disc is flat and thus the radial and the vertical structures are possible to be studied separately by decoupling them, the accretion is steady-state, i.e, the accretion flow is explicitly time-independent and also there is no magnetic field to interact with the accretion flow. Fig. 5.1 shows the geometry of the accretion disc. This is basically in cylindrical polar coordinates (R, ϕ, z) and the $z = 0$ plane is the midplane of the disc. The rotation axis is the z - axis and the z coordinates represent the disc height while ϕ coordinates represent the azimuthal angle. The accretion flow, as a first-order approximation, can be considered as a two - dimensional flow if the flow is very closely confined to the orbital plane. This is called the *thin disc approximation* and this approximation is popular and based on this many elaborate models can be made.

Thin disc structure

The surface density of the disc is defined by

$$\Sigma(R) = \int_{-\infty}^{+\infty} \rho(R, z)\mathrm{d}z, \tag{5.17}$$

where, ρ is the density of the disc. Due to the assumption of an axisymmetric system, the term ϕ does not appear here. If ρ is independent of z, then the scale height H of the disc can be related to Σ as

$$\Sigma = H\rho. \tag{5.18}$$

In the case of accretion, particularly for disc accretion, the infalling matter must shed some excess amount of angular momentum to spiral in and fall on the accreting body. The gas particles undergo collisions (it can be distant or close) and thus exchange momentum and energy. Even if the interaction scale is quite small with respect to the radial and vertical extent of the disc, it leads to the transportation of angular or linear momentum by viscosity, as well as energy.

Radial structure

An annulus in the disc lying between R and $R+\Delta R$, will have a mass of $2\pi R\Delta R\Sigma$ and an angular momentum of $2\pi R\Delta R\Sigma R^2\Omega$, where Ω is the angular velocity and it typically has the Keplerian value, $\left(\frac{GM}{R^3}\right)^{1/2}$. The mass evolution of this annulus is given by

$$\begin{aligned}\frac{\partial}{\partial t}(2\pi R\Delta R\Sigma) &= v_R(R,t)2\pi R\Sigma(R,t) - v_R(R+\Delta R,t)2\pi(R+\Delta R)\Sigma(R+\Delta R,t) \\ &\simeq -2\pi\Delta R\frac{\partial}{\partial R}(R\Sigma v_R).\end{aligned} \tag{5.19}$$

The mass conservation in the limit $\Delta R \to 0$ is given by

$$R\frac{\partial \Sigma}{\partial t} + \frac{\partial}{\partial R}(r\Sigma v_R) = 0, \tag{5.20}$$

where v_R is the radial drift velocity in addition to v_ϕ. In the angular momentum conservation equation, the contribution of the viscous torques, G_{vis}, is included (Frank *et al.* 2002) leading to

$$\begin{aligned}\frac{\partial}{\partial t}(2\pi R\Delta R\Sigma R^2\Omega) &= v_R(R,t)2\pi R\Sigma(R,t)R^2\Omega(R) - v_R(R+\Delta R,t)2\pi(R+\Delta R) \\ &\quad \Sigma(R+\Delta R,t)(R+\Delta R)^2\Omega(R+\Delta R) + \frac{\partial G_{vis}}{\partial R}\Delta R \\ &\simeq -2\pi\Delta R\frac{\partial}{\partial R}(R\Sigma v_R R^2\Omega) + \frac{\partial G_{vis}}{\partial R}\Delta R. \end{aligned} \tag{5.21}$$

In the limit $\Delta R \to 0$, this conservation equation yields

$$R\frac{\partial}{\partial t}(\Sigma R^2\Omega) + \frac{\partial}{\partial R}(R\Sigma v_R R^2\Omega) = \frac{1}{2\pi}\frac{\partial G_{vis}}{\partial R}. \tag{5.22}$$

Calculation of the viscous torque

The viscous force exerted between two adjacent annular rings in the accretion disc is given by

$$F_{vis} = 2\pi RH\sigma_s, \tag{5.23}$$

where, $2\pi RH$ is the contact area and σ_s is the shear stress (Kolb 2010). This stress is found to be

$$\sigma_s = -\nu_{vis}\rho R\frac{\partial \Omega}{\partial R}, \tag{5.24}$$

so that

$$G_{vis} = -F_{vis}R = 2\pi R\nu_{vis}\Sigma R^2\frac{\partial \Omega}{\partial R}. \tag{5.25}$$

Using this expression of G_{vis} for the Keplerian case, the surface density conservation equation takes the form

$$\frac{\partial \Sigma}{\partial t} = \frac{3}{R}\frac{\partial}{\partial R}\left[R^{1/2}\frac{\partial}{\partial R}(\nu_{vis}\Sigma R^{1/2})\right]. \tag{5.26}$$

Because of the turbulent motion of the gas particles, a kinematic viscosity is generated. If the characteristic speed of the particle is v_c and the characteristic length is λ_c, then the kinematic viscosity, ν_{vis} is given by,

$$\nu_{vis} \simeq v_c \lambda_c. \tag{5.27}$$

Now, the maximum value of λ_c can be the vertical scale height, H and the local sound speed, c_s is taken to be the maximum value of v_c. Therefore, $\nu_{vis} < Hc_s$. So, ν_{vis} can be written as a fraction, α, of the maximum value as

$$\nu_{vis} = \alpha H c_s. \tag{5.28}$$

This is called the α - viscosity prescription (Shakura and Sunyaev 1973).

The radial momentum conservation equation is written as

$$\frac{\partial(\Sigma v_R)}{\partial t} + \frac{1}{r}\frac{\partial(\Sigma r v_R^2)}{\partial r} + \frac{\partial(\Sigma c_s^2)}{\partial r} - \Sigma\frac{v_\phi^2}{r} = -\Sigma\frac{GM}{r^2}. \tag{5.29}$$

and the angular or tangential momentum conservation equation is given by

$$r\frac{\partial}{\partial t}(\Sigma r^2\Omega) + \frac{\partial}{\partial r}(r\Sigma v_R r^2\Omega) = \frac{\partial}{\partial r}(\Sigma\nu r^3\frac{\mathrm{d}\Omega}{\mathrm{d}r}). \tag{5.30}$$

Since $v_r \ll c_s \ll v_\phi$, in the LHS of eqn. (5.29), we can neglect first three terms with respect to the 4th term and thererby

$$v_\phi^2 = \frac{GM}{r} \tag{5.31}$$

and therefore, $v_\phi = \Omega_K r$ for a Keplerian disc.

If in tangential momentum conservation [eqn. (5.30)], we use the mass conservation equation [eqn. (5.29)], we get the radial drift velocity expression as,

$$v_R = -\frac{3}{\Sigma r^{\frac{1}{2}}}\frac{\partial}{\partial r}(\nu \Sigma r^{\frac{1}{2}}). \tag{5.32}$$

Vertical Structure

Now, we consider the vertical equilibrium structure. The vertical structure is provided by the equation

$$\frac{1}{\rho}\frac{\partial}{\partial z}P + \frac{\partial}{\partial z}\Phi(R,z) = 0. \tag{5.33}$$

For $\Phi(r,\ z) = -GM_\bullet/\sqrt{R^2+z^2}$ in hydrostatic equilibrium, at $z=0$, we can write

$$\frac{1}{\rho}\frac{\partial P}{\partial z} = -\frac{GM\sin\theta}{R^2}. \tag{5.34}$$

For the thin disc, the approximations are

- $\dfrac{\partial P}{\partial z} = \dfrac{P}{H}$,
- $\sin\theta = \dfrac{z}{r} \simeq \dfrac{H}{r}$

Therefore,

$$\frac{1}{\rho}\frac{P}{H} = \frac{GMH}{R^3} \quad \text{or} \quad \frac{c_s^2}{H} = \frac{GMH}{R^3}$$

Finally, we get the height of the disc as

$$H = \left(\frac{c_s^2 R^3}{GM}\right)^{\frac{1}{2}}. \tag{5.35}$$

5.2.5 Growth of black hole mass and spin by accretion

The black hole mainly grows by accretion flow of the gas. In case of an energy-driven flow (Silk and Rees 1998) it is assumed that all the energy from the accretion is used for unbinding the mass of the bulge and the maximum possible mass the SMBH can attain from this accretion process is

$$M_\bullet \simeq 8 \times 10^8 \left(\frac{\sigma}{300\text{km sec}^{-1}} \right)^5 M_\odot. \tag{5.36}$$

King (2003) has proposed that black hole growth occurs by gas flow until it reaches a saturated mass $M_{\bullet t}$, which is a different approach than that of Silk and Rees (1998) who propose an energy-driven flow by assuming that the energy from accretion is completely used in unbinding the mass of the galactic bulge, while there is no loss of energy due to radiation. King (2003) considers Compton cooling for which some energy is lost to radiation and the remaining energy is available for unbinding the mass of the bulge. In the analysis of King (2003), after saturation, the outflow velocity exceeds the escape velocity of the medium and the gas is driven away causing the accretion process to stop. The saturated mass is given as $M_{\bullet t} = 9.375 \times 10^6 \sigma_{100}^4 M_\odot$ derived for a spherical geometry for the ambient gas. However, the infalling matter must possess some amount of angular momentum so that an accretion disc forms and thus there is a small solid angle where only inflow occurs. If most of the gas lies in the plane of the galaxy, the momentum-driven outflow would not halt the inflow; this also implies that accretion from this point adds little mass to the hole. In our model in chapter 6, we ignore accretion after saturation and consider only stellar capture and mergers contribute to the growth of the black hole, at this point the value of p is 4. We take sub - Eddington accretion throughout so that

$$\dot{M}_{\bullet g} = k_1 M_\bullet, \tag{5.37}$$

where, $k_1 = \dfrac{4\pi G m_p \eta}{\sigma_e c}$ and the factor $\eta = \dot{M}_\bullet / \dot{M}_E$, where $\dot{M}_E$ is the Eddington accretion rate. We define $\mu_\bullet = \dfrac{M_\bullet}{M_s}$, where M_s is the seed mass, $\tau = \dfrac{t}{t_0}$, where t_0 = 1 Gyr, so that the gas accretion rate is

$$\dot{\mu}_g = \frac{\dot{M}_{\bullet g} t_0}{M_s}. \tag{5.38}$$

5.2.6 Equations of black hole evolution due to accretion

Mangalam (2015) used a theoretical model for mass and spin evolution of the black hole taking into account the angular momentum torque caused by an electrodynamical jet, where the spin evolution was calculated with the accretion rate taken to be a given fraction of the Eddington rate for different cases such as the thin disc, Bondi accretion and also MHD disc. The mass evolution equation is given by

$$\frac{\mathrm{d}M_\bullet}{\mathrm{d}t} = \epsilon_I(j) \dot{M}_{\bullet g}, \tag{5.39}$$

where $\epsilon_I(j)$ [see eqn. (2) of Mangalam (2015)] is the efficiency of energy conversion with the innermost radius of the disc to be taken typically at ISCO, and $\dot{M}_{\bullet g}$ is the rate of accretion. The spin evolution equation is given by

$$\frac{\mathrm{d}j}{\mathrm{d}t} = \frac{\dot{M}_{\bullet g}}{M_\bullet} \Big(l_I(j) - 2\epsilon_I(j) j \Big), \tag{5.40}$$

where $l_I(j)$ [see eqn. (5) of Mangalam (2015)] is the angular momentum per unit mass at ISCO. The first term is due to the accretion of angular momentum at ISCO, while the second represents the spin-down due to an increase in the black hole inertia; these arguments give

$$J_\bullet = \frac{G M_\bullet^2 j}{c},$$

$$\dot{j} = \frac{c}{G}\frac{\mathrm{d}}{\mathrm{d}t}\left[\frac{J_\bullet}{M_\bullet^2}\right] = \frac{\dot{M}_{\bullet g}}{M_\bullet}\Big(l_I(j) - 2\epsilon_I(j)j\Big). \tag{5.41}$$

5.3 Stellar capture

Calculation of the stellar capture rate

The loss cone is a region in velocity space, where, if a star is within that region, it is captured by the black hole. The capture of stars into the loss cone can occur

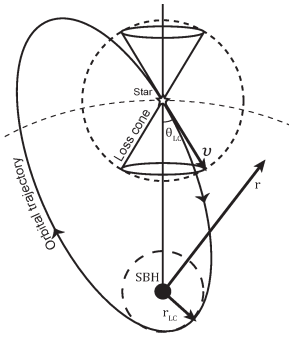

FIGURE 5.2: A schematic of the loss cone. Image courtesy: Merritt (2013a).

in two ways: full loss cone and the steady loss cone. We use the expression of the capture rate for full loss cone theory, $\dot{N}_f$, given by Merritt (2013b) and also derive the steady loss cone theory rate, $\dot{N}_s$. We discuss conditions for which form is more appropriate. To see this, we examine the stellar capture in two situations, one where the loss cone gets filled quickly and another when it is dominated by diffusion. The stars captured populate a loss cone whose angular size is given by (Frank and Rees 1976)

$$\theta_\ell^2(r) = \frac{r_c}{r^2}\frac{GM_\bullet}{\sigma^2}, \tag{5.42}$$

where θ_ℓ is the half angle of the loss cone. The angle scattered in a dynamical time $t_d = r/\sigma$ is approximated by

$$\theta_d = \sqrt{\frac{t_d}{t_R}} \tag{5.43}$$

$$t_d = \begin{cases} \sqrt{\frac{r^3}{GM_\bullet}} & \text{for } r \leq r_h \\ \frac{r}{\sigma} & \text{for } r \geq r_h \end{cases} \tag{5.44}$$

$$t_R = \frac{\sigma^3}{3 \ln \Lambda G^2 m_* n_c}; \tag{5.45}$$

where Λ is the Coulomb logarithm which is obtained from the logarithm of the ratio of maximum and minimum values of the impact parameter and n_c is the cluster mass density with m_* being the stellar mass (Syer and Ulmer 1999). In the diffusive regime, $\theta_d < \theta_\ell$, the loss cone is empty as the star is removed from the loss cone within a dynamical time scale. At other extreme, $\theta_d > \theta_\ell$, the loss cone is always full. Both the regimes are shown in Fig. 5.3 for $m_* = M_\odot$ and $n_c = 10^4 M_\odot \mathrm{pc}^{-3}$, as used by Syer and Ulmer (1999) and for the mass range $M_\bullet = 10^4 - 10^8 M_\odot$, where we have used the $M_\bullet - \sigma$ relation with $p = 4$ to replace σ in terms of $M_\bullet$. From Fig. 5.3, we see that as the mass of the black hole increases,

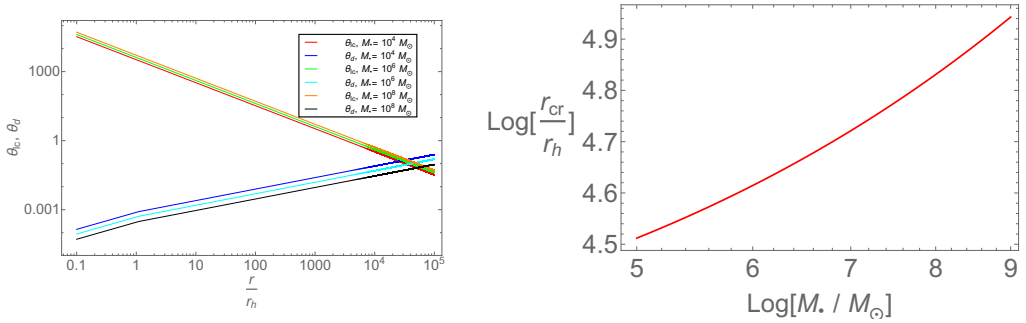

(a) (b)

FIGURE 5.3: The variation of the angular size of loss cone, θ_ℓ and angle scattered in dynamical time, θ_d with r/r_h for $m_* = M_\odot$ and $n_c = 10^4 M_\odot \mathrm{pc}^{-3}$, for the range $M_\bullet = 10^4 - 10^8 M_\odot$ (a) and (b) the variation of the crossing point, $r_{cr}(M_\bullet)$ defined by $\theta_{lc}(r_{cr}) = \theta_d(r_{cr})$, for $m_* = M_\odot$ and $n_c = 10^4 M_\odot \mathrm{pc}^{-3}$ as used by Syer and Ulmer (1999).

the crossing point (r_{cr}/r_h) of the two curves shifts towards the right which implies

that the diffusive region expands with increase in mass. For typical black hole mass under consideration (as $\frac{M_\bullet}{M_\odot}$ evolves from $10^4 \rightarrow 10^8$), the diffusive regime operates and hence it is more appropriate to use the steady loss cone theory.

5.3.1 Full loss cone theory

Here, we consider the case of the full loss cone ($\theta_d >> \theta_\ell$) where the mass density in the galaxy cusp follows a single power law profile and the stars are able to quickly fill the loss cone on dynamical time scales. Therefore

$$\rho = \rho_0 r^{-\gamma}, \tag{5.46}$$

where γ is the power law index. The distribution function of stars in a such a galaxy is given by (Merritt 2013a)

$$f_s(E) = \frac{3-\gamma}{8}\sqrt{\frac{2}{\pi^5}}\frac{\Gamma(\gamma+1)}{\Gamma(\gamma-\frac{1}{2})}\frac{M_\bullet}{m_\star}\frac{\phi_0^{\frac{3}{2}}}{(GM_\bullet)^3}\left(\frac{|E|}{\phi_0}\right)^{\gamma-\frac{3}{2}}, \tag{5.47}$$

where $\phi_0 = \frac{GM_\bullet}{r_m}$, E is the energy, r_m is the gravitational influence radius of the black hole defined as $GM_\bullet/\sigma^2$ and m_* is the stellar mass. The rate of capture of stars within the loss cone is

$$F_f(E) = 4\pi^2 L_\ell^2(E) f_s(E), \tag{5.48}$$

where $L_\ell(E)$ is the angular momentum of the star. An integration of this over all energies gives the total rate of capture in the loss cone,

$$\dot{N}_f = \int_{-\infty}^{\phi_0} F_f(E)\mathrm{d}E, \tag{5.49}$$

so that

$$\begin{aligned}\dot{M}_{\bullet *f} = m_\star \dot{N}_f &= \frac{3-\gamma}{8}\sqrt{\frac{1}{2\pi}}\frac{\Gamma(\gamma+1)}{\Gamma(\gamma-\frac{1}{2})}\frac{l_\ell^2}{GM_\bullet}\frac{1}{r_m}\left(\frac{GM_\bullet}{r_m^3}\right)^{\frac{1}{2}} M_\bullet \\ &= \frac{3-\gamma}{8}\sqrt{\frac{1}{2\pi}}\frac{\Gamma(\gamma+1)}{\Gamma(\gamma-\frac{1}{2})}\frac{l_\ell^2(M_\bullet)}{Gc^2}\sigma^5, \end{aligned} \tag{5.50}$$

where $L_\ell \equiv (GM_\bullet/c)\, l_\ell$. For the non - relativistic case, L_ℓ is given by eqn. (6.22). After simplification, it is seen that this expression for $\dot{M}_{\bullet *} \propto \sigma^5$ for the non-relativistic case does not depend on $M_\bullet$. But, for the relativistic case, $\dot{M}_{\bullet *}$ depends both on σ and $M_\bullet$ through the capture radius. In the full loss cone regime, the depleted orbits are repopulated within orbital periods by the relaxation process; this is a reasonable assumption for $M_\bullet << 10^5 M_\odot$.

5.3.2 Steady loss cone theory

The more practical case is the steady-state theory of Cohn and Kulsrud (1978). By using direct numerical integration of the Fokker - Planck equation in angular momentum and energy space, they derived the stellar distribution in the presence of a black hole in a steady state. The distribution of orbital energies near the black hole can never reach a steady state because no black hole is old enough (Merritt 2013b). This is also expected for the distribution of orbital angular momenta also near l_ℓ because $\tau_{M,*}/t_r << 1$. Therefore a hybrid approach should be used for the calculation of event rates based on the observed distribution of energies where the angular momentum distribution at each energy has reached an approximate steady state under the influence of gravitational encounters. Mageshwaran and Mangalam (2015) have constructed a detailed model of the tidal disruption events using stellar dynamical and gas dynamical inputs like black hole mass, specific orbital energy and also angular momentum, the mass of a single star, its radius and the pericenter of the star orbit. Using the Cohn - Kulsrud boundary layer

theory they calculated the differential rate of number of stars falling in the steady loss cone to be (MM15)

$$\frac{\mathrm{d}^2\dot{N}_s}{\mathrm{d}\bar{e}\mathrm{d}l^2\mathrm{d}m} = 4\pi^2 s_t^{-1}\sigma^2\xi(m)f_*(\bar{e}, M_\bullet, m)L_\ell^2(\bar{e})F(\chi = 1, l), \tag{5.51}$$

where, $s_t = r_t(M_\bullet, j)/r_h$, $\bar{e} = E/(GM_\bullet/r_t)$, E is the energy, f_* is the probability that a star of mass m is tidally captured as a main sequence and $\xi(m)$ is the stellar mass function where $m = m_*/M_\odot$, $F = X(y_{lc})\zeta(q_s)$, and

$$X(y_{lc}) = \frac{f_s(E)}{1 + q_s^{-1}\zeta(q_s)\log(1/R_{lc})}, \tag{5.52}$$

with $q_s = \dfrac{< D(E) >}{R_{lc}}$ and $R_{lc} = \dfrac{L_\ell^2}{J_c^2}$. MM15 have used the $M_\bullet - \sigma$ relation (taking $p = 4.86$) to get the expression for $\dot{N}_s$. By applying steady-state Fokker - Planck equation while using a power-law stellar density profile (having power-law index γ) they obtained the rate of capture of stars $\dot{N} \propto M_\bullet^\beta$, where $\beta = -0.3 \pm 0.01$ for $M_6 > 10$ and the value of $\dot{N}_s$ is $\sim 6.8 \times 10^{-5}$ Yr^{-1} for $\gamma = 0.7$ [see Fig. 5.4]. We also use the same model as provided by MM15, but, we do not apply the

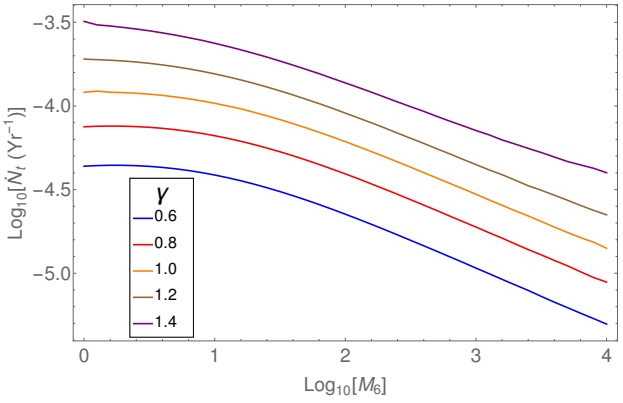

FIGURE 5.4: The capture rate as calculated in MM15. Image: Mageshwaran and Mangalam (2015).

$M_\bullet - \sigma$ relation apriori and also we use relativistic corrections to the tidal radius and loss sone radius, and hence to the loss cone angular momentum, to derive the capture rate in the relativistic framework using the steady loss cone theory (detailed calculation has been shown in Chapter 6).

5.4 Mergers

5.4.1 Effect on mass due to the mergers

When two galaxies collide, the black holes at their centers also merge and this is thought to be one of the major sources of the supermassive black hole growth. Therefore, to calculate the mass growth of SMBH by mergers, one has to take care of the rate of galaxy mergers and thus, in turn, will provide the required mass growth rate, since the black hole mass is related to the dark matter halo mass. We calculate the mass growth rate of mergers in Chapter 6. The rate of mergers assumed is based on the simulations of Stewart *et al.* (2009) where a brief overview is provided of the methods for the construction of merger trees. Stewart *et al.* (2009) give analytic forms for the growth rate that are extremely useful [see also Allgood *et al.* (2006), Wechsler *et al.* (2006), Stewart *et al.* (2008)]. Stewart *et al.* (2008) report high-resolution ΛCDM N-body simulations to investigate the merger histories of $\sim$ 17,000 galaxy dark matter halos with masses $10^{11} - 10^{13}h^{-1}M_{\odot}$ at $z = 0$. They have tracked mergers with masses to the tune of $10^{10}h^{-1}M_{\odot}$, and their goal was to present necessary conditions for the survival of a thin disk. Allgood *et al.* (2006) give six high-resolution dissipationless simulations with a varying box size in a flat ΛCDM universe; we study the mass and redshift dependence of dark matter halo shapes for virial masses $9 \times 10^{11} - 2 \times 10^{14}h^{-1}M_{\odot}$, over the redshift range 0 - 3,and for two values of $\sigma_8 = 0.75$ and 0.9. They also derive the formation scale factor as defined by Wechsler *et al.* (2006) and find that it can be related to the halo shape at $z = 0$ and its evolution over time. We discuss this in detail in Chapter 6.

5.4.2 Effect on spin due to mergers

Gammie *et al.* (2004) considers the collapse of stars, accretion, and major and minor mergers that contribute to the spin of the astrophysical black holes. The major mergers contribute to spinning up the hole whereas minor mergers contribute to spinning it down.

Spin up by the major mergers

The spin of the black hole gets affected because of major merger which is the merging of two black holes of comparable mass. After the binary black holes start to inspiral towards each other due to the gravitational radiation, once they reach the ISCO, they merge together on an orbital timescale. The inspiraling starts initially from circular orbits, because, the gravitational radiation causes a decrease in the eccentricity of the orbit on a timescale shorter than the timescale of the orbital evolution. The exact location of the ISCO is known to a high precession only for the black holes having test particle companion. Fig. 5.5 shows a table listing the available values given in Gammie *et al.* (2004), which they adapted from Baumgarte and Shapiro (2003). To calculate the parameters listed in the table, they consider $M_\bullet = M_{irr}$, where, M_{irr} is the irreducible mass given as

$$M_\bullet = M_{irr} = \left(\frac{A}{16\pi}\right)^{1/2}, \tag{5.53}$$

where, A is the area of the event horizon of the black hole (Christodoulou 1970). The binding energy is written as

$$E_b = M - 2M_\bullet, \tag{5.54}$$

where, M is the total mass measured far from the black hole. The non-dimensional quantities at ISCO are given as

$$\bar{E}_b = E_b/\mu, \quad \bar{\Omega} = m\Omega_a, \quad \bar{J} = J/(\mu m), \tag{5.55}$$

REPRESENTATIVE VALUES FOR NONSPINNING BINARY BLACK HOLES

Reference	$\bar{E}_b$[a]	$\bar{J}$[b]	$\bar{\Omega}$[c]	J/M^2[d]	$(J/M^2)_{max}$[e]
Schwarzschild	−0.0572	3.464	0.068	0.8913	0.9897
Cook 1994	−0.09030	2.976	0.172	0.7788	0.9578
Baumgarte 2000	−0.092	2.95	0.18	0.773	0.955
Grandclément et al. 2002	−0.068	3.36	0.103	0.869	0.985
Damour et al. 2000	−0.0668	3.27	0.0883	0.846	0.980

[a] Binding energy per unit reduced mass at the ISCO.
[b] Angular momentum per unit reduced mass at the ISCO.
[c] Orbital angular velocity at the ISCO.
[d] Estimated spin parameter of final black hole.
[e] Maximum spin parameter of final black hole (see text).

FIGURE 5.5: Spin values for binary black holes [Courtesy: Gammie *et al.* (2004)], adapted from Baumgarte and Shapiro (2003).

where, $\bar{E}_b$ is the non-dimensional binding energy, $\bar{\Omega}$ is the non-dimensional angular velocity and $\bar{J}$ is the non-dimensional angular momentum with angular velocity, Ω_a, reduced mass, $\mu = M_\bullet/2$ and $m = 2M_\bullet$. Assuming that the final black hole will have the mass and angular momentum of the binary system at ISCO, Gammie *et al.* (2004) provide the value of the final spin parameter as

$$\frac{J}{M^2} = \frac{\bar{J}}{4[1 + \frac{E_b}{4}]^2}. \tag{5.56}$$

They also provide, in the last column of the table, the maximum limit of the spin parameter, computed from the area theorem using the equation (Pfeiffer *et al.* 2002)

$$\left(\frac{J}{M^2}\right)_{max} = \frac{2}{x_{max}}\left(1 - \frac{1}{x_{max}^2}\right)^{1/2}, \tag{5.57}$$

where,

$$x_{max}^2 = 1 + \frac{\bar{J}^2}{4[1 + \sqrt{1 - (J/M_\bullet)^2}}. \tag{5.58}$$

To derive this equation, it was also assumed that, the final angular momentum will always be less than that of the total system at the ISCO. Gammie *et al.* (2004)

find that eqn. (5.56) gives a better result because, numerical simulations suggest quite less radiation [Smarr (1979), Anninos *et al.* (1993)] than allowed by the area theorem. Therefore, the final conclusion given by Gammie *et al.* (2004) is that, due to the major mergers, the final spin of the black hole will be $\gtrsim 0.8$.

Since the accretion process is the dominant one for the spinning up of the black hole, we will be considering only the contribution of minor mergers and neglect the major mergers for the spin evolution of the hole in our evolution model (discussed in Chapter 6).

Spin down by the minor mergers

Different models suggest that black holes produced by the collapse of a supermassive star are likely to have $j \sim 0.7$. Though the result of major mergers is not yet known properly, Gammie *et al.* (2004) provide some current estimates and analytic bounds on j for these processes. They apply the formalism of Hughes and Blandford (2003) to minor mergers assuming an isotropic distribution of orbital angular momentum and find that the spin-down occurs with $j \sim M^{7/3}$. They evaluate a power law for spin decay fo the limit of the small value of j, where they expanded the radius and specific energy of ISCO as a function of j. Their simulations for accretion process from fully relativistic magnetohydrodynamic (MHD) flow indicates a spin equilibrium at $j \sim 0.9$, much less than the canonical value 0.998 of Thorne (1974) that was derived excluding the MHD effects. This suggests the possibility that the black holes which grow mainly by the accretion process are not maximally rotating. We use the spin-down term by minor mergers given by Gammie *et al.* (2004) in our evolution model (discussed in Chapter 6) to be valid in the range $z = 4 \rightarrow 0$ (Stewart *et al.* 2009). We see a significant decrease in the final spin value after adding this merger term. Gammie *et al.* (2004) by taking the effect of minor mergers in spin evolution of the black hole find

$$\frac{\mathrm{d}\log j}{\mathrm{d}\log M_\bullet} = -\frac{7}{3} + \frac{9q}{\sqrt{2}j^2}, \tag{5.59}$$

which can be written as

$$\frac{\mathrm{d}j}{\mathrm{d}\tau} = \dot{\mu}_m \cdot \frac{j}{\mu_\bullet}\left(-\frac{7}{3} + \frac{9q}{\sqrt{2}j^2}\right). \tag{5.60}$$

5.5 Blandford - Znajek effect

Blandford and Znajek (1977) shows how the magnetic field drives powerful jets from the black hole from its rotational energy. The magnetic field is frozen to the

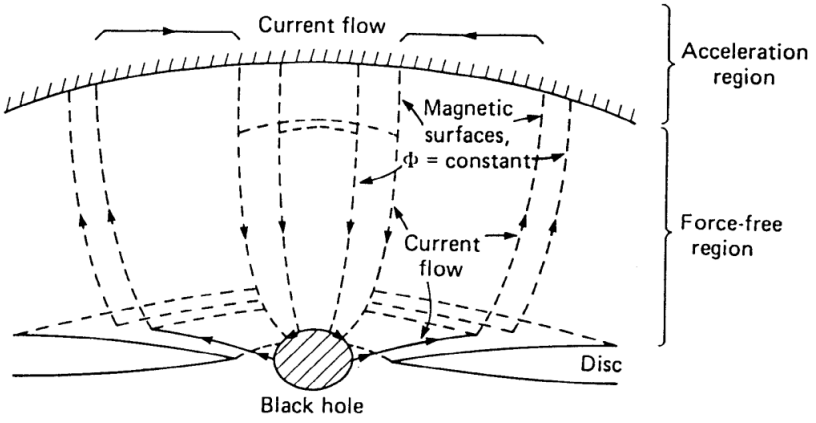

FIGURE 5.6: Magnetic field and the flow of current near the black hole. Image courtesy: MacDonald and Thorne (1982).

disc material approximately because exact freezing will not lead to the presence of toque by the magnetic field and hence, there will be no energy extracted from the hole. According to Ferraro's law, the angular velocity has to be constant on the poloidal field line. Since there is spherical symmetry, the angular velocity will always be independent of the azimuthal angle, ϕ, and therefore, it will be constant along the plane about the symmetry axis $R = 0$. Frank *et al.* (2002) define those surfaces as magnetic surfaces. The flux of the magnetic field, $F_B(R, z)$, at a particular point, is obtained by integrating the magnetic field over a circular surface having the symmetry axis at the center. The obtained flux is constant at

the magnetic surfaces. For the generation of a non-zero magnetic field, B_T, in the magnetic surfaces (with radius R), in a force-free field, a constant current flow, I, has to be present [see Fig. 5.6]. Applying Ampere's law, we find,

$$B_T = \left[\frac{c\mu_0}{4\pi}\right]\frac{2I}{cR}. \tag{5.61}$$

Consider two adjacent surfaces, with radii R and $R + \Delta R$, with interior current flows I and $I + \Delta I$. For avoiding the accumulation of charge, radial current should be present between these two surfaces. In this case, it is not necessary for the current to flow along the magnetic surfaces, because this is not a force-free field. Therefore, in the acceleration region, there will be a dissipation of energy. This region in the accretion disc affects the transmission efficiency, but, because of its radial direction, it has no effect on the overall efficiency. In the intermediate force-free region, there will be no dissipation. The power that flows from the disc (force-free region) to the acceleration region is (Frank *et al.* 2002)

$$\mathbf{S} = \left[\frac{4\pi}{\mu_0 c}\right]\frac{c}{4\pi}\mathbf{E}\times\mathbf{B} = \left[\frac{4\pi}{\mu_0 c}\right]\frac{c}{4\pi}\mathbf{E_P}\times\mathbf{B_T}, \tag{5.62}$$

where, $\mathbf{E_P} - \mathbf{E_T}$ and $\mathbf{B_P} - \mathbf{B_T}$ are the poloidal-toroidal electric and magnetic fields. Now, $\mathbf{E_T} = 0$ and $\mathbf{E_P} = ([c]/c)(\mathbf{R}\times\mathbf{\Omega})\times\mathbf{B_P}$. For black holes, Ω will be equal to the angular velocity of the local fieldlines. Therefore, S is obtained to be

$$S \sim [4\pi/\mu_0]R\Omega B_P B_T/4\pi. \tag{5.63}$$

$\mathbf{B_P}$ and $\mathbf{B_T}$ have to be determined from the condition of non force-free regions. If it is assumed, near the region of acceleration that the particles move up field lines, which are in the parallel direction to $\mathbf{B_P} + \mathbf{B_T}$, the velocity almost approaches c and the circular velocity is $R\Omega$, which is parallel to $\mathbf{B_T}$. From the relative velocity

diagram (Frank *et al.* 2002)

$$B_P/B_T \sim (c^2 - R^2\Omega^2)^{1/2}/r\Omega \sim c/R\Omega. \tag{5.64}$$

The innermost orbits, contribute maximum power and using Ω calculated at the innermost stable orbit, $\leq 3R_s$, the final expression of the luminosity of the disc is found to be

$$L_D \sim 10^{45}(B/10^4\mathrm{G})^2(M_\bullet/10^8 M_\odot)^2 \mathrm{erg\ s^{-1}}. \tag{5.65}$$

This value is quite large to be observationally significant.

In this process, the power extraction from the black hole rotational energy is possible. The magnetic pressure by the magnetic fieldlines is convected to the disc material and the magnetic fieldlines are attached to the hole. The currents are already set up in the disc, though these are fictitious currents acting just as a sink for current flows in the magnetic surfaces for the sake of completion of the circuit [see Fig. 5.6]. Therefore, a net torque acts on the hole due to the difference in the angular velocities of the hole and that of the magnetic field (Frank *et al.* 2002). This is the Blandford-Znajek effect which causes the black hole to spin down. The efficiency of this process is determined from the ratio of the power extraction and the maximum possible power that can be extracted when matter falls onto the black hole.

Mangalam *et al.* (2009) studied the case of rapid loss of cold gas due to AGN feedback which may cause expansion in the effective radii of massive elliptical galaxies from $z \simeq 2 \rightarrow 0$, they quantify the extent of the expansion in terms of the star formation parameters and time of the expulsion of the cold gas and show that cosmological changes are expected to have a major influence on the gas accretion mode, which at high redshifts can be dominantly cold thin disc accretion and at low redshifts could be dominantly hot Bondi fed ADAF accretion. They calculate the

spin down to be $\tau_j \sim M_9^2$ 0.2 Gyr, which explains the cosmological evolution of the luminosity function from powerful to weak radio galaxies. We use the expression of spin evolution caused by BZ torque as implemented in Mangalam *et al.* (2009) in our model. The spin evolution equation by the BZ effect for different initial and final spin values is given by (Mangalam *et al.* 2009)

$$\frac{\mathrm{d}j}{\mathrm{d}t} = x_H^3(j)\frac{\mathcal{G}_0}{\mathcal{J}_0}, \tag{5.66}$$

where, $x_H(j) = 1 + \sqrt{1-j^2}$ and the BZ torque, $\mathcal{G}_0$, is given by

$$\mathcal{G}_0 = \frac{m^3}{8}B_\perp^2 f_{BZ} = 4 \times 10^{46} f_{BZ} B_4 M_8^3(\mathrm{erg}), \tag{5.67}$$

and the angular momentum budget, $\mathcal{J}_0$ is given by

$$\mathcal{J}_0 = cM_\bullet mj = 9 \times 10^{64} M_8^2(\mathrm{g\ cm^2\ s^{-1}}), \tag{5.68}$$

and where $B_4 = B/10^4$Gauss, f_{BZ} is a geometric factor that comes from the averaging of angle over the horizon of magnetic flux and the spin of the magnetic field (Mangalam *et al.* 2009). Therefore in dimensionless form

$$\frac{\mathrm{d}j}{\mathrm{d}\tau} = \frac{4}{9} \times 10^{-5} f_{BZ} B_4 \mu_\bullet M_{s5} x_H^3(j) j, \tag{5.69}$$

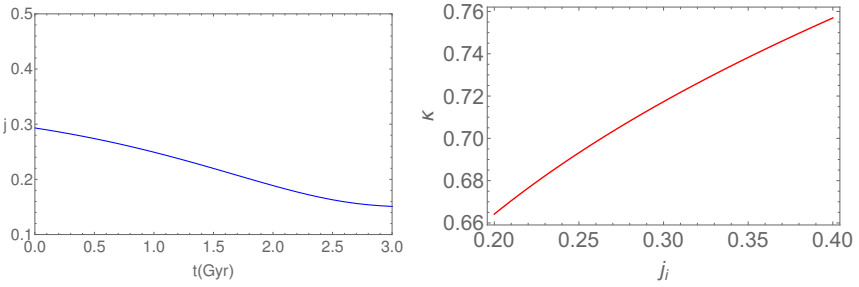

(a) (b)

FIGURE 5.7: The spin down, $j(t)$, due to BZ torque for $B_4 = 5$, $M_\bullet = 10^6 M_\odot$ is shown with an initial spin, $j_i = 0.3$ (a) and (b) the factor of spin down time, $\kappa(j)$, is shown for a fixed $j_f = 0.001$

Mangalam *et al.* (2009) give an analytic solution of spin down time $\tau_{j,BZ}(j)$

$$\tau_{j,BZ} = \frac{\mathcal{J}_0}{\mathcal{G}_0}\int_{j_f}^{j_i}\frac{\mathrm{d}j}{r^3(j)j} = 7.0\times10^8\mathrm{yr}\frac{(\kappa(j_i,j_f)/0.1)}{B_4^2M_9f_{BZ}}, \tag{5.70}$$

where $M_9 = M_\bullet/(10^9M_\odot)$ and

$$\kappa(j_i,j_f) = \left[\left(\frac{1}{16}\right)\log\left(\frac{2-w}{w}\right)+\left(\frac{3w^2+3w-4}{24w^3}\right)\right]_{w_f}^{w_i}, \tag{5.71}$$

with $w_i = x_H(j_i)$, $w_f = x_H(j_f)$. Fig 5.7(a) shows the spin down due to BZ effect for a certain set of parameters. This is equivalent to the study of the spin down for Bondi case with zero accretion in Mangalam (2015).

5.6 Resource summary

1. In this chapter, we discussed all the processes that are responsible for the growth of the black hole and its evolution.

2. In §5.1, we discussed the physics of the accretion process, a simple case of spherical accretion, the thin disc model and the contribution of this process in the evolution of the black holes [Frank *et al.* (2002); Kolb (2010); Mangalam (2015)].

3. §5.2 is dedicated to the growth of the black hole by stellar capture, where, we calculate capture rate in steady (Mageshwaran and Mangalam 2015) and full loss cone theory (Merritt 2013a) to estimate the mass growth rate of the black hole by the stellar capture process and build the platform to present our model (discussed in Chapter 6) where we include relativistic corrections to the tidal, capture and the loss cone radius to derive the relativistic capture rate.

4. In §5.3, we discuss the role of major and minor mergers [Gammie *et al.* (2004); Hughes and Blandford (2003); Stewart *et al.* (2009)], on the mass and spin evolution of the black holes.

5. §5.4 provides the recipe of the electromagnetic spin-down of the black hole, due to the effect of the Blandford - Znajek torque [Blandford and Znajek (1977); Frank *et al.* (2002)] and the process of extraction of energy from rotating black holes for the spin down to occur (Mangalam *et al.* 2009).

Chapter 6

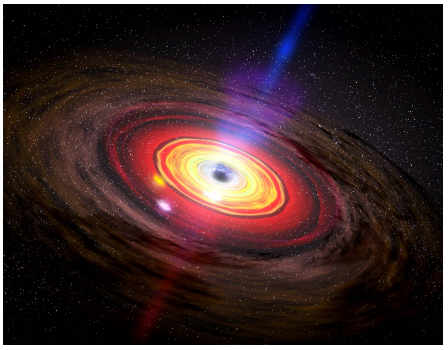

Image: brtannica.com

Evolution of the black holes in ΛCDM cosmology*

6.1 Introduction

From the analysis of Bardeen *et al.* (1972), without thermodynamic effects, the non-rotating black holes can attain maximum spin of ≈ 1 by the accretion of gas from the ISCO. The black hole spin is limited by an upper limit of the spin of 0.998 based on radiation torque due to a difference in cross-section for counter and co-rotating photons near this limit which is responsible for the saturation (Thorne 1974). From Seyfert 1.2 galaxy MCG - 06 - 20 - 15, XXM - Newton observations have analyzed the upper limit to be $0.989^{+0.009}_{-0.002}$ with 90 percent confidence (Brenneman and Reynolds 2006). Later on, Gammie *et al.* (2004) have shown the

*This chapter has been published in ApJ (Bhattacharyya and Mangalam 2020) and part of this has been published in Bhattacharyya and Mangalam (2018b)

maximum value to be around 0.9, less than 0.998 for relativistic MHD disks. This may not be applicable for thin disc cases; this suggests that the black holes which have grown through MHD accretion are not maximally rotating. For the thick disk cases, the saturated value of spin was found to be 0.93. The thin disk analysis by Gammie *et al.* (2004) indicates that only through sub - Eddington accretion, the spin can be very close to the maximal rotation. Volonteri *et al.* (2005) and Volonteri and Rees (2005) have argued that the effect of accretion torque always results in spinning up the black hole. In the former paper, the spin-up process of black holes is assumed to be caused by the accretion and binary coalescence, where the SMBH spins up even if the direction of the spin axis varies with time and accretion dominates over coalescences. But if the accretion disks become self-gravitating their angular momentum per unit mass will be less than that of the black hole. Therefore in such cases, a black hole having sufficient spin will be spun down (King *et al.* 2008). If the black hole is growing by the merger process, the upper limits can be different. After extrapolation of data, Marronetti *et al.* (2008) have suggested that, for merging two similar mass black holes with maximum initial spin and aligned with their orbital angular momentum, the upper value can be 0.951 ± 0.004. Volonteri & Rees (2005) have calculated the growth of black holes as a function of redshift for $z \sim 10 - 20$ of the formation using an accretion rate given by the Bondi - Hoyle formula which is $\propto M_{\bullet}^2$.

Our aim in this chapter to consider all these processes: gas accretion, stellar capture, mergers, and black hole electrodynamical spin down to build a self-consistent model of spin and mass evolution. The main motivation of this study is to construct a detailed evolution model of the black hole, that can be a useful tool to study the co-evolution of the black hole and the galaxy. We take a comprehensive approach by including all the growth channels semi-analytically, with an aim to isolate the important effects. The relativistic treatment is important as all the channels depend on spin and hence would modulate the black hole growth. This

self-consistent evolution model would be handy in comparing results with simulations and in retrodictions of the formation parameters, thus constraining models of black hole formation. In future, detailed demographic studies can be carried out to evolve black hole mass and spin distributions. The three applications that we consider are capture rates of stars applying relativistic corrections to the tidal radius and the capture radius (Rana and Mangalam 2019a) to the loss cone model given by Mageshwaran and Mangalam (2015). Secondly, using the model we predict the evolution of the $M_\bullet - \sigma$ relation. The third application considered is to retrodict the seed mass and spin of the black hole and the formation redshift under various assumptions, given the recent observations at the epoch near $z \simeq 7$ (Campitiello *et al.* 2019).

6.2 Overview of the physics of the growth of the black hole

6.2.1 Growth of black hole mass and spin by accretion

We use the same argument as provided in chapter 5 for spin and mass evolution of black holes in presence of accretion. We list the equations here again, to provide the platform of our evolution model. We take sub - Eddington accretion throughout so that

$$\dot{M}_{\bullet g} = k_1 M_\bullet, \tag{6.1}$$

where, $k_1 = \dfrac{4\pi G m_p \eta}{\sigma_e c}$ and the factor $\eta = \dot{M}_\bullet / \dot{M}_E$, where $\dot{M}_E$ is the Eddington accretion rate.

Therefore in units of $\mu_\bullet = \frac{M_\bullet}{M_s}$, where M_s is the seed mass, $\tau = \frac{t}{t_0}$, where $t_0 = 1$ Gyr

$$\dot{\mu}_g = \frac{\dot{M}_{\bullet g} t_0}{M_s}. \tag{6.2}$$

The mass evolution equation is given by Mangalam (2015), where a theoretical model was used for mass and spin evolution of the black hole taking into account the angular momentum torque caused by the electrodynamical jet (given in chapter 5)

$$\frac{\mathrm{d}M_\bullet}{\mathrm{d}t} = \epsilon_I(j)\dot{M}_{\bullet g}, \tag{6.3}$$

where $\epsilon_I(j)$ [see eqn. (2)] is the efficiency of energy conversion with the innermost radius of the disc to be taken typically at ISCO, and $\dot{M}_{\bullet g}$ is the rate of accretion. The spin evolution equation is given by

$$\frac{\mathrm{d}j}{\mathrm{d}t} = \frac{\dot{M}_{\bullet g}}{M_\bullet}\Big(l_I(j) - 2\epsilon_I(j)j\Big), \tag{6.4}$$

where $l_I(j)$ [see eqn. (5)] is the angular momentum per unit mass at ISCO.

6.2.2 Growth of black holes by stellar consumption

The SMBHs can also grow by the capture of stars in two ways. Those stars that pass within the event horizon can be directly captured and the indirect capture occurs when capture occurs by accreting the gas from tidally disrupted stars. For SMBHs more massive than $10^8 M_\odot$, the direct capture of solar type stars are possible if the angular momentum of the star is smaller than some critical value (Frank and Rees 1976) for the non - relativistic case. We proceed to calculate the limiting value for the relativistic case. For a Kerr black hole, the standard effective potential is written as [Misner *et al.* (1973); Carter (1968); Frolov and Novikov

(1998); Rana and Mangalam (2019a); Rana and Mangalam (2019b); (RM19)]

$$V_{eff}(x,l,j,Q) = -\frac{1}{x} + \frac{l^2+Q}{2x^2} - \frac{[(l-j)^2+Q]}{x^3} + \frac{j^2Q}{2x^4}, \tag{6.5}$$

where L is the angular momentum, $l \equiv L/(GM/c)$, $x = r/r_g$, where $r_g = GM_\bullet/c^2$, j is the spin parameter and Q is the Carter's constant. The solution of $V_{eff}(x_p) = 0$ and $V'_{eff}(x_p) = 0$ gives the equation of separatrix orbit where x_p is the pericenter, as shown in Fig 2(b) of RM19. The condition, $V_{eff}(x_p) = 0$, implies

$$-x_p^3 + \frac{(l^2+Q)x_p^2}{2} - (l-j)^2 x_p + \frac{j^2Q}{2} - Qx_p = 0, \tag{6.6}$$

and $V'_{eff}(x_p) = 0$ gives

$$x_p^3 - x_p^2(l^2+Q) + 3x_p[(l-j)^2+Q] - 2j^2Q = 0. \tag{6.7}$$

From these two conditions, we find the equation for the separatrix $x_p(Q, l_\ell, j)$ to be given by

$$x_p^3 - [(l-j)^2+Q]x_p + j^2Q = 0, \tag{6.8}$$

which represents a turning point condition for an orbit that is just bound or just unbound. This also represents a marginally bound spherical orbit (MBSO). The innermost stable spherical orbit (ISSO) and MBSO are the end points of the separatrix curve fro ($e = 0$, ISSO) to ($e = 1$, MBSO). The star is captured at MBSO (as $r \to \infty$ in Fig. 2(b) of RM19 and r_s is the pericenter. This capture radius (MBSO) $x_c(Q,l,j)$ in units of r_g, is found from eqn. (6.8) to be (see Appendix D of RM19 for details)

$$x_c^8 - 8x_c^7 - 2j^2x_c^6 + 16x_c^6 + 2j^2Qx_c^5 - 8j^2x_c^5 - 6j^2Qx_c^4 + j^4x_c^4 - 2j^4Qx_c^3 + 8j^2Qx_c^3 + j^4Q^2x_c^2 - 2j^4Qx_c^2 - 2j^4Q^2x_c + j^4Q^2 = 0. \tag{6.9}$$

Solving eqn. (6.9) for real roots (numerically for $Q \neq 0$) which are higher than the light radius (?) we find the solution of the capture radius for both prograde

and retrograde cases. If $Q = 0$, the eqn. (6.9) reduces to

$$x_c^4(x_c^2 - 2jx_c + j^2 - 4x_c)(x_c^2 - 4x_c + j^2 + 2jx_c) = 0, \tag{6.10}$$

which leads to the known result (Zhao *et al.* 2002)

$$x_c(j) = \begin{cases} -j + 2(1 + \sqrt{1-j}) & \text{for prograde} \\ j + 2(1 + \sqrt{1+j}) & \text{for retrograde} \end{cases} \tag{6.11}$$

The angular momentum at x_c is given as from eqn. (6.8) is found to be

$$l_c(M_8, j, Q) = j + k\sqrt{x_c^2 - Q + \frac{j^2 Q}{x_c}}. \tag{6.12}$$

The value of l_c will be positive for prograde case ($k = 1$) and negative for retrograde case ($k = -1$) due to the direction of spin of the black hole. The capture of a star by the black hole can occur in two ways, either by tidal disruption of the stars or by direct capture of the black hole. For direct capture, we determine x_c using eqn. (6.9) for $Q \neq 0$ or by using eqn. (6.11) for $Q = 0$. Below a certain critical mass, the stars are tidally disrupted (Merritt 2013a) and above which the stars are swallowed whole. Therefore, r_t is defined as the radius below which the star gets disrupted by the black hole. We calculate the tidal radius in presence of black hole spin applying Poisson's equation

$$\left.\frac{\partial^2 V_{eff}}{\partial r^2}\right|_{r=r_t} = -4\pi G\rho, \tag{6.13}$$

where, ρ is the stellar mass density. Using the generalized form of the effective Kerr potential in natural units [eqn. (6.5)], the tidal radius equation [eqn. (6.13)], finally leads to

$$\left[-\frac{2}{x^3} + \frac{3(l^2+Q)}{x^4} - 12\frac{[(j-l)^2+Q]}{x^5} - \frac{10j^3Q}{x^6}\right]_{x=x_t} = -4\pi\tilde{\rho}, \tag{6.14}$$

where

$$\begin{aligned} \tilde{\rho} &= \frac{\rho}{M_\bullet}\cdot r_g^3 \simeq 0.3 M_8^2\left(\frac{\rho_*}{\rho_\odot}\right), \\ x &= r/r_g, \\ l &= L/\frac{GM_\bullet}{c}. \end{aligned} \tag{6.15}$$

where ρ_* is the density of the star. We solve eqn. (6.14) numerically for $x_t(j, M_8, Q)$ by considering $l = l_c$, the angular momentum of capture taking the above approximation for $\tilde{\rho}$ as 0.3 M_8^2 (assuming the star to be of solar type). An analytic approximation to r_t has been calculated here. Taking $y = 1/x_t$ and $\tilde{y} = y/y_{t0} = 1+\delta$, we find the first order approximation to y defining y_{t0} as the inverse of the dimensionless tidal radius to be

$$y_{t0} = \frac{1}{x_{t0}} = M_8^{-\frac{1}{3}}\left(\frac{\rho_*}{\rho_\odot}\right)^{-\frac{1}{3}} 10^5 \cdot r_g \text{ pc}^{-1}. \tag{6.16}$$

The sixth order equation for δ is

$$2(1+\delta)^3 - 3(l^2+Q)y_{t0}(1+\delta)^4 + 12(1+\delta)^5[(j-l)^2+Q]y_{t0}^2 + 10j^3 Q y_{t0}^3(1+\delta)^6 - 1 = 0. \tag{6.17}$$

Solving eqn. (6.17) numerically we obtain $\delta(j, Q)$ which is shown in Fig. 6.1.

The loss cone radius $x_\ell, \equiv \text{Max}[x_t, x_c]$ is given by

$$x_\ell(M_8, j, Q) = r_\ell/r_g = \text{Max}[r_t(M_8, j, Q), r_c(j, Q)]/r_g. \tag{6.18}$$

The angular momentum at x_ℓ is found by putting $V_{eff}(x, l, j, Q) = 0$ [see eqn. (6.5)] and it is given by

$$l_\ell(M_8, j, Q) = 2j + k\sqrt{\frac{2x_\ell j^2}{(x_\ell - 2)^2} - \frac{Qj^2}{x_\ell(x_\ell - 2)} + \frac{2x_\ell^2}{(x_\ell - 2)} - Q}. \tag{6.19}$$

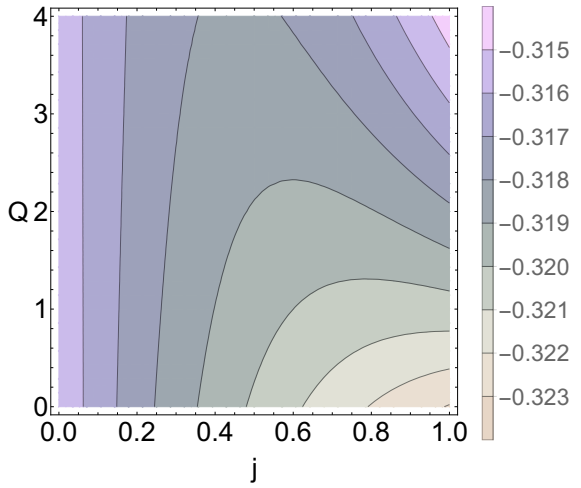

FIGURE 6.1: A contour plot of $\delta(j, Q)$ defined by $y \equiv y_{t0}(1+\delta)$ for $l = l_c$ and $k = -1$ is shown , which lies in the range of 0.32 ± 0.05 for $Q \in [0, 4]$ and $j \in [0, 1]$.

The value of l_ℓ will be positive for prograde case ($k = 1$) and negative for retrograde case ($k = -1$) due to the direction of spin of the black hole. We show both the cases in Fig. 6.7. For $Q = 0$ and $j = 0$ eqn. (6.19) reduces to

$$l_\ell(M_8) = k\sqrt{\frac{2x_\ell^2}{(x_\ell - 2)}}. \tag{6.20}$$

For high values of x_ℓ (in the non - relativistic limit) we can write

$$l_\ell^2 = 2x_\ell, \tag{6.21}$$

which implies

$$L_\ell^2 = \left(\frac{GM_\bullet}{c}\right)^2 l_\ell^2 = 2GM_\bullet r_\ell, \tag{6.22}$$

which is the well known non - relativistic result.

We explore the dependence of $r_t(M_8, j, Q)$ and $r_\ell(M_8, j, Q)$ in Figs. 6.2, 6.3, 6.5 and Fig. 6.6. We observe the following.

- $x_t(M_8, j, Q = 0)$ is shown in Fig. 6.2, where we see that at a fixed j, x_t

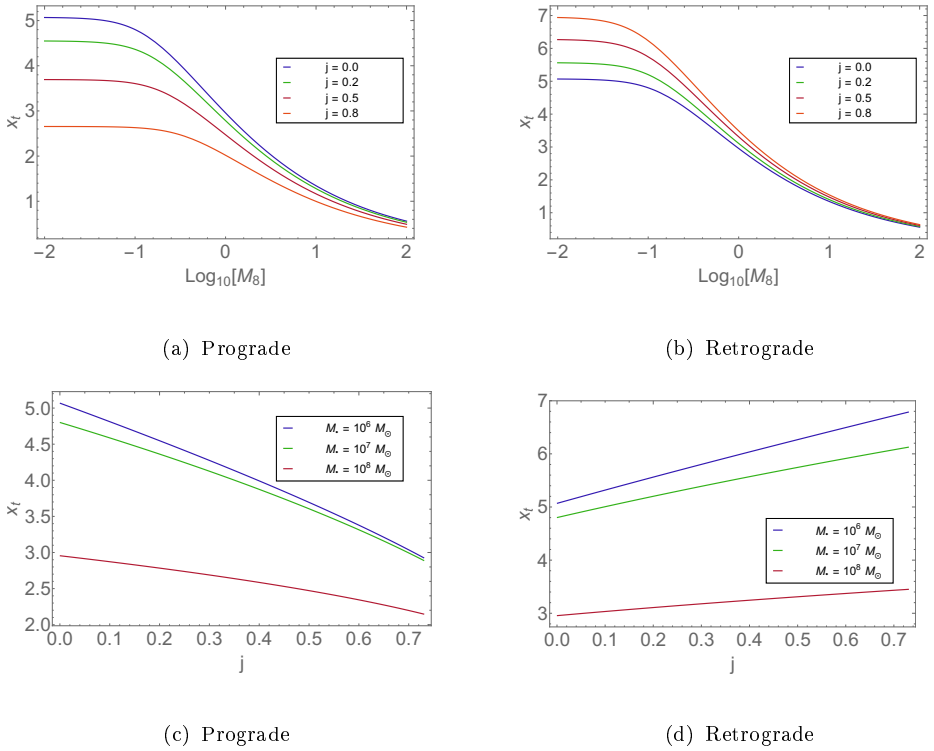

(a) Prograde (b) Retrograde

(c) Prograde (d) Retrograde

FIGURE 6.2: The tidal radius ($x_t(M_8, j, Q) = r_t(M_8, j, Q)/r_g$) given by eqn. (6.14) is shown as a function of M_8 (top) and j (bottom) for $Q = 0$.

decreases with increase of $M_\bullet$. In the high mass regime, the variation of x_t is small with spin but it shows more variation in the low mass regime; this has an impact on the calculation of the stellar capture rate presented later in §6.2.2.

- Fig 6.3 shows the dependence of $x_t(M_8, j, Q)$ on Q. We find that for a fixed value of j, x_t has a small dependence on Q as a function of M_8. But, $x_t(M_8, j, Q)$ decreases as a function of Q for retrograde case for a fixed value of $M_\bullet$. But for the prograde case, $x_t(M_8, j, Q)$ initially decreases for higher Q, but subsequently, it shows an increase with increasing Q.

- Fig. 6.4 shows the ratio of $r_t(M_8, j, Q)/r_c(M_8, j, Q)$ as a function of both j and $M_\bullet$ for $Q = 0$. $M_c(j, Q) = M_\bullet(r_t/r_c = 1)$ is the critical mass which has a dependence on j and matches with the previous simulation results of Kesden (2012) who shows that the mass of the heaviest black hole which is able to

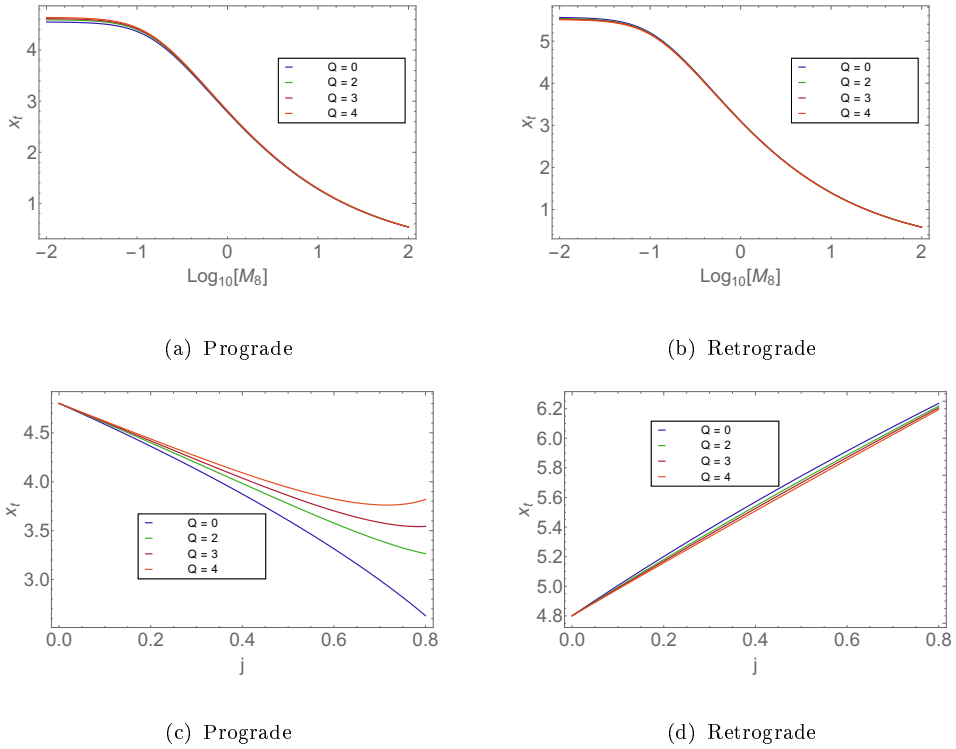

(a) Prograde (b) Retrograde

(c) Prograde (d) Retrograde

FIGURE 6.3: The tidal radius ($x_t(M_8, j, Q) = r_t(M_8, j, Q)/r_g$) given by eqn. (6.14) is shown as a function of M_8 for $j = 0.2$ (top) and j for $M_8 = 0.1$ (bottom).

disrupt a star, changes as a function of j, in the relativistic limit. For black holes more massive than $10^7 M_\odot$, the tidal disruption occurs very close to the horizon and Newtonian treatment of the tidal interactions cannot be applied. Kesden (2012) calculate generically oriented stellar orbits considering the Kerr metric to evaluate the relativistic tidal tensor at the pericenter for the stars which are not directly captured by the black hole and also combine their relativistic treatment with previous calculations of the population of these orbits in order to determine tidal-disruption rates for spinning black holes. They found a strong dependence of tidal-disruption rates on black-hole spin for $M_8 > 1$. Our calculation of r_t shows an increase at high mass end ($M_8 > 1$) as suggested by Kesden (2012). The plots of Fig. 6.4 in the lower panel shows $M_c(j, Q)$ is nearly flat in Q.

- Fig. 6.5 shows $x_\ell(M_8, j, Q)$ for $Q = 0$. When the value of $x_c(j, Q)$ exceeds

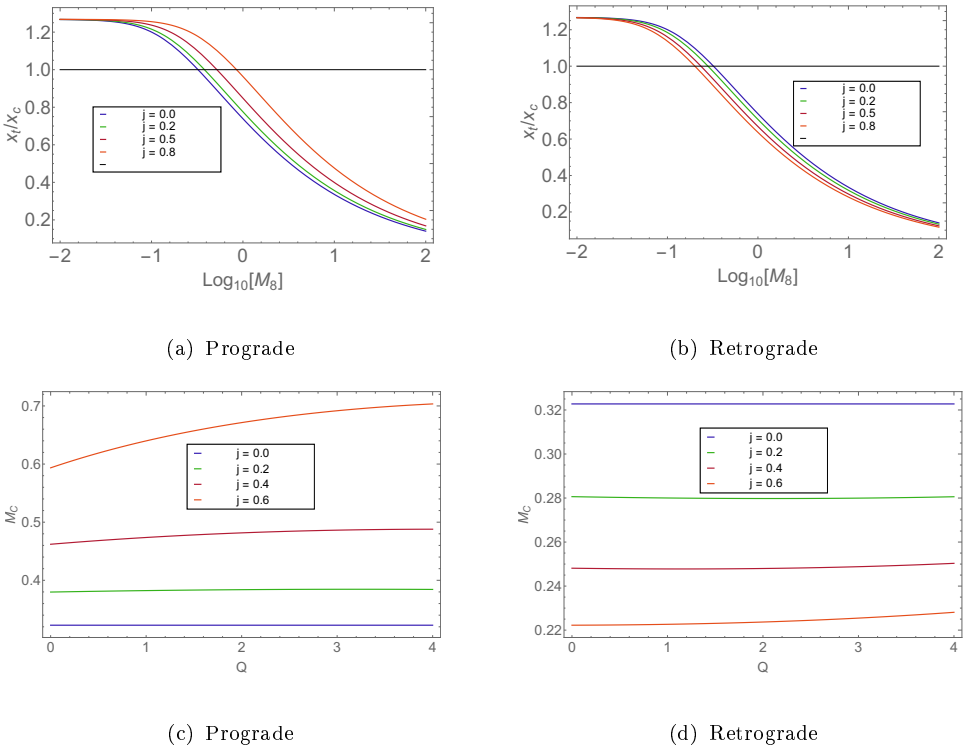

(a) Prograde (b) Retrograde

(c) Prograde (d) Retrograde

FIGURE 6.4: The ratio of tidal radius to the capture radius $(r_t(M_8, j, Q)/r_c(M_8, j, Q) = x_t(M_8, j, Q)/x_c(j, Q))$ is shown as a function of M_8 for $Q = 0$ (top) and the locus of the critical mass, $M_c(j, Q)$ for different j as a function of Q (bottom). The critical mass of the black hole is determined from the plots when $x_t/x_H = 1$; this critical mass is represented by the black line in the plots in the upper panel.

$x_t(M_8, j, Q)$ the stars will be directly captured instead of getting tidally disrupted; hence $x_\ell(M_8, j, Q)$ flattens out after $M_\bullet > M_c$.

- $x_\ell(M_8, j, Q)$ for different Q values are shown in Fig 6.6 for both prograde and retrograde cases. For fixed j, in the retrograde case, we see that $x_\ell(M_\bullet, j, Q)$ increases with Q and decreases with Q for the prograde case. $x_\ell(M_8, j, Q)$ for fixed $M_\bullet$ is nearly the same for different Q. This is true, because as Q increases, $L - L_z$ decreases causing the pericenter to shrink in the prograde case and the opposite holds in the retrograde case.

- The dimensionless angular momentum at $r_\ell(M_8, j, Q)$ defined as $l_\ell(M_8, j, k, Q)$ [eqn. (6.19)] is the loss cone angular momentum in the relativistic regime. Fig 6.7 shows $l_\ell(M_8, j, k, Q)$ for different Q values, where it increases with

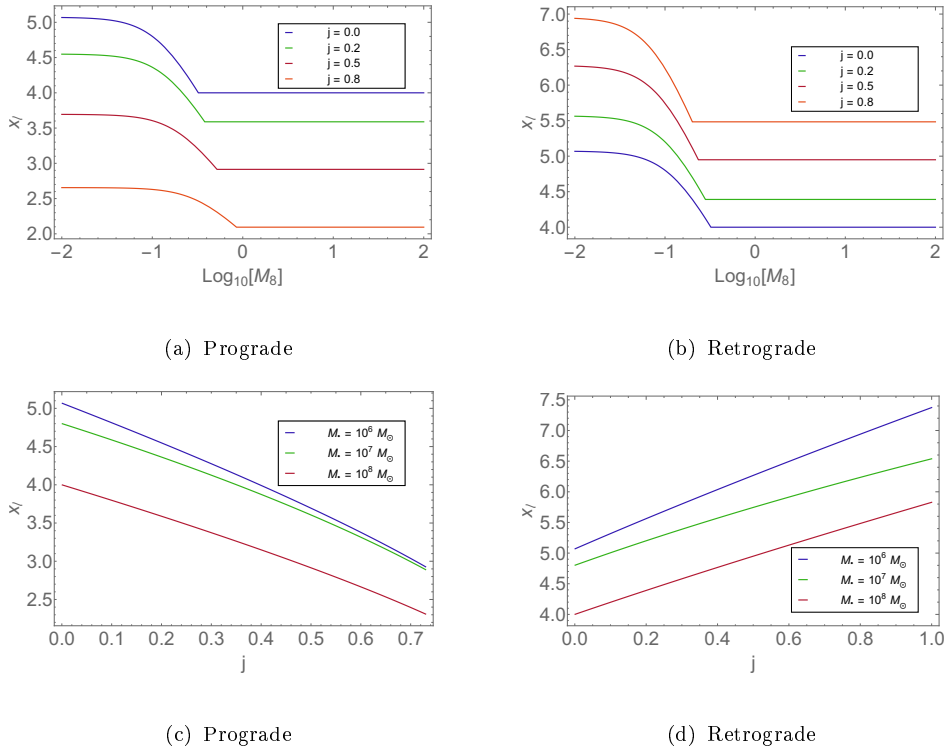

(a) Prograde

(b) Retrograde

(c) Prograde

(d) Retrograde

FIGURE 6.5: The loss cone radius $(x_\ell(M_8, j, Q) \equiv r_\ell(M_8, j, Q)/r_g) = \text{Max}[x_t(M_8, j, Q), x_c(j, Q)]$ is shown as a function of M_8 (top) and j (bottom) for $Q = 0$ is shown.

M_8 for both prograde and retrograde cases for $Q = 0$. For a fixed M_8, $l_\ell(M_8, j, k, Q)$ decreases with increase in Q for the prograde case while it increases for the retrograde case. This can be understood from the fact that Q is a measure of $L - L_z$; so that L_z increases when Q decreases for $L_z > 0$ (prograde) and $|L_z|$ decreases when Q decreases for $L_z < 0$ (retrograde).

Steady loss cone theory

Mageshwaran and Mangalam (2015) have constructed a detailed model of the tidal disruption events using stellar dynamical and gas dynamical inputs like black hole mass, specific orbital energy and also angular momentum, the mass of a single star, its radius and the pericenter of the star orbit. Using the Cohn - Kulsrud boundary layer theory they calculated the differential rate of number of stars falling in the

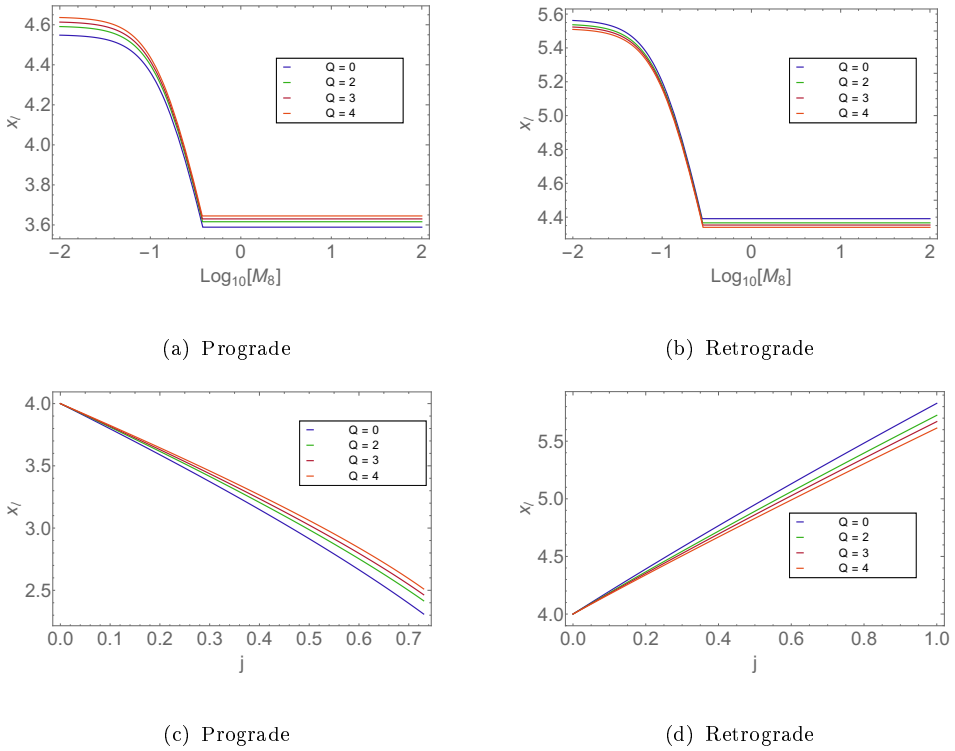

(a) Prograde (b) Retrograde

(c) Prograde (d) Retrograde

FIGURE 6.6: The loss cone radius ($x_\ell(M_8, j, Q) = r_\ell(M_8, j, Q)/r_g = \mathrm{Max}[r_t(M_8, j, Q), r_c(M_8, j, Q)]/r_g$) is shown as a function of M_8 for $j = 0.2$ (top) and j for $M_8 = 1$ (bottom) for different Q values.

steady loss cone to be (MM15)

$$\frac{\mathrm{d}^2\dot{N}_s}{\mathrm{d}\bar{e}\mathrm{d}l^2\mathrm{d}m} = 4\pi^2 s_t^{-1}\sigma^2\xi(m)f_*(\bar{e}, M_\bullet, m)L_\ell^2(\bar{e})F(\chi = 1, l), \tag{6.23}$$

where, $s_t = r_t(M_\bullet, j)/r_h$, $\bar{e} = E/(GM_\bullet/r_t)$, E is the energy, f_* is the probability that a star of mass m is tidally captured as a main sequence and $\xi(m)$ is the stellar mass function where $m = m_*/M_\odot$, $F = X(y_{lc})\zeta(q_s)$, and

$$X(y_{lc}) = \frac{f_s(E)}{1 + q_s^{-1}\zeta(q_s)\log(1/R_{lc})}, \tag{6.24}$$

with $q_s = \dfrac{< D(E) >}{R_{lc}}$ and $R_{lc} = \dfrac{L_\ell^2}{J_c^2}$. MM15 have used the $M_\bullet - \sigma$ relation (taking $p = 4.86$) to get the expression for $\dot{N}_s$. By applying steady-state Fokker - Planck equation while using a power-law stellar density profile (having power-law index γ) they obtained the rate of capture of stars $\dot{N} \propto M_\bullet^\beta$, where $\beta = -0.3 \pm 0.01$

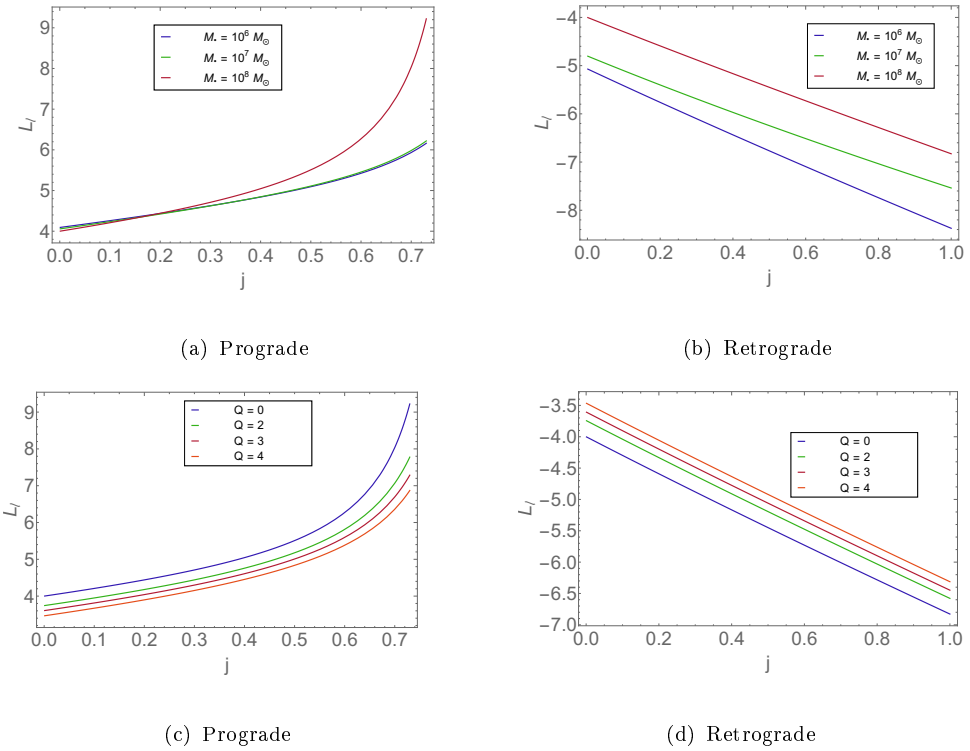

(a) Prograde (b) Retrograde

(c) Prograde (d) Retrograde

FIGURE 6.7: The loss cone angular momentum $l_\ell(M_8, j, k, Q)$ is shown as a function of j for $Q = 0$ (up) and (bottom) different Q values is shown with M_8 =1 for retrograde and prograde cases.

for $M_6 > 10$ and the value of $\dot{N}_s$ is $\sim 6.8 \times 10^{-5}$ Yr^{-1} for $\gamma = 0.7$. We use the same technique to calculate $\dot{N}_s$, but including the relativistic forms of r_t and r_c, but do not assume the $M_\bullet - \sigma$ relation apriori and consider σ as an independent parameter in our model. We start from the basic equation for N_s given by

$$N_s = 4\pi^2 \int P(E)\mathrm{d}E \int f_s(E, J)\mathrm{d}J^2, \tag{6.25}$$

using the same parameters used by MM15 and with the following assumptions

$$\int \xi(m)\mathrm{d}m = 1, \text{ and taking } f_* = 1, \tag{6.26}$$

and where

$$< D(\epsilon_s) >= \frac{32\sqrt{2}}{3}\frac{\pi^2 G^2 < m_f^2 > \log\Lambda}{J_c^2}\frac{M_\bullet}{< m_* >}\frac{1}{\sigma^2}[2h_1(\epsilon_s) + 3h_2(\epsilon_s) - h_3(\epsilon_s)], \tag{6.27}$$

where $\epsilon_s = E/\sigma^2$, h_1, h_2 and h_3 are defined in MM15. Now,

$$J_c^2 = \sigma^2 r_h^2[s_c(\epsilon_s) + 2s_c^{4-\gamma}(\epsilon_s)], \tag{6.28}$$

where s_c is the ratio of radius of circular orbit and horizon radius, ϵ_s dependent part is called as $\beta(\epsilon_s)$, and

$$L_\ell(M_\bullet, j, k, Q) = \frac{GM_\bullet}{c} l_\ell(M_\bullet, j, k, Q). \tag{6.29}$$

Therefore,

$$R_\ell(M_\bullet, j, k, Q, \epsilon_s) = \frac{L_\ell^2}{J_c^2} = \frac{L_\ell^2(M_\bullet, j, k, Q)}{\sigma^2 r_h^2 \beta(\epsilon_s)}, \tag{6.30}$$

where, $\beta(\epsilon) = [s_c(\epsilon_s) + 2s_c^{4-\gamma}(\epsilon_s)]$. From the definition, $q_s(\epsilon_s)$ is written as

$$q_s(\epsilon_s) = \frac{< D(\epsilon_s) >}{R_\ell}, \tag{6.31}$$

which can be simplified to

$$q_s(M_\bullet, j, k, Q, \epsilon_s) = \frac{16\sqrt{2}}{3}\frac{\pi^2 < m_f^2 >}{M_\bullet < m_* >}\frac{r_h^2}{r_c^2(M_\bullet, j, k, Q)}\frac{2h_1(\epsilon_s) + 3h_2(\epsilon_s) - h_3(\epsilon_s)}{r_h/r_c(M_\bullet, j, k, Q) - \epsilon_s}. \tag{6.32}$$

where the expression for $\zeta(q_s)$, as given by MM15 is

$$\zeta(q_s) = \begin{cases} 1 & \text{for } q_s \geq 4 \\ q_s/(0.86q_s^{0.5} + 0.384q_s - 0379q_s^{1.5} + 0.427q_s^2 - 0.095q_s^{2.5}) & \text{otherwise.} \end{cases} \tag{6.33}$$

By integrating eqn. (6.23) assuming $f_* = 1$, we finally arrive at

$$\frac{\mathrm{d}N_s}{\mathrm{d}\epsilon_s}(M_\bullet, j, k, Q, \epsilon_s, \sigma) = \frac{\sqrt{2}\pi^3 L_\ell^2(M_\bullet, j, k, Q)\sigma^2 \epsilon_s^{-\frac{3}{2}}}{G^2 M_\bullet < m_* >} g(\epsilon_s) \frac{\zeta(q_s)}{1 + q_s^{-1}\zeta(q_s)\log(1/R_\ell)}. \tag{6.34}$$

Then dividing eqn. (6.34) by the orbital period $P(\epsilon_s)$ we find an expression of $\frac{\mathrm{d}\dot{N}_s}{\mathrm{d}\epsilon_s}$ as

$$\frac{\mathrm{d}\dot{N}_s}{\mathrm{d}\epsilon_s}(M_\bullet, j, k, Q, \epsilon_s, \sigma) = \frac{4\pi^3 L_\ell^2(M_\bullet, j, k, Q)\sigma^5}{G^3 M_\bullet^2 < m_* >} g(\epsilon_s) \frac{\zeta(q_s)}{1 + q_s^{-1}\zeta(q_s)\log(1/R_\ell)}., \tag{6.35}$$

where we have used relativistic approximation to $r_\ell(M_\bullet, j, k, Q)$ to obtain $\dot{N}(M_\bullet, j, k, Q, \epsilon_s, \sigma)$ in the relativistic limit as a function of the black hole spin. Since the diffusion occurs at very large radius, only the first term of the effective potential dominates. Integrating this expression numerically, we finally find the rate of capture of stars for the case of the steady loss cone and Fig. 6.8 shows the variation of $\dot{N}_s(M_\bullet, j, k, Q, \epsilon_s, \sigma)$ with the $M_\bullet$. This can be explained by the decrease of l_ℓ with M_8 that effectively causes this nature of $\dot{N}_s$. From Fig. 6.8 we see that the trend of $\dot{N}_s(j)$ follows from the dependence of $r_c(M_\bullet, j, k)$ on j (see Fig. 6.2).

From Fig. 6.9, we see that the capture rate, $\dot{N}_s(M_\bullet, j, k, Q, \epsilon_s, \sigma)$ follows the trend of $r_c(M_\bullet, j, Q)$ (see Fig. 6.5) where we used the $M_\bullet - \sigma$ relation with $p = 4.86$. This shows a similar trend as seen in Kesden (2012) (see Figs. 3, 4 in Kesden (2012)), where $\dot{N}_s(j)$ (taking the universal $M_\bullet - \sigma$ relation) has higher $\dot{N}_s$ value for higher j.

In Fig. 6.10, we show $\dot{N}_s(\gamma)$; for higher γ, $\dot{N}_s$ increases for both prograde and retrograde cases, which is similar to the result of in MM15.

From Fig. 6.11, we see that the rate of the number of stars falling into the loss cone is higher in case of full loss cone theory than in the case of steady loss cone by an order of magnitude. Also, the slope is positive at the lower mass end and

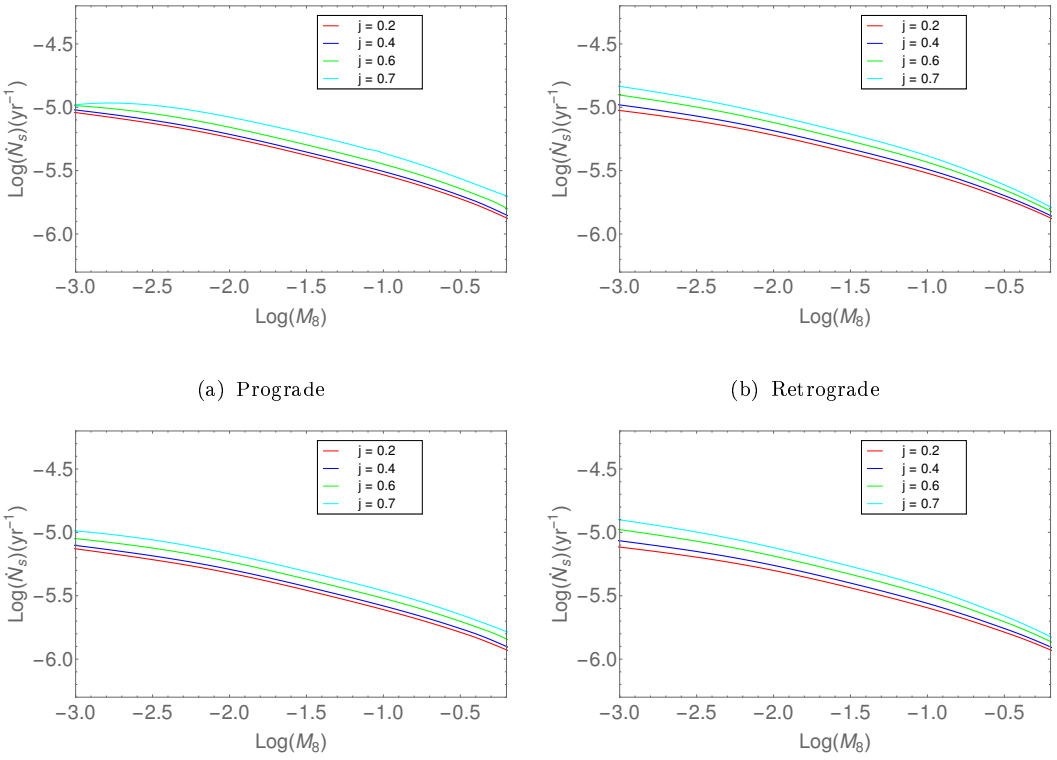

(a) Prograde

(b) Retrograde

(c) Prograde

(d) Retrograde

FIGURE 6.8: The capture rate, $\dot{N}_s(M_\bullet, j, k, Q, \epsilon_s, \sigma)$, is shown which reduces monotonically with M_8 and increases slightly with j when $k = 1$ (left), -1 (right) for $Q = 0$ (top) and (bottom) the same plots for $Q = 4$ where the lower limit of the ϵ_s integration is taken to be ϵ_m = -10, $\gamma = 1.1$ and $\sigma = 200$ km/sec.

it becomes negative as it reaches the higher mass. $\dot{N}_f$ is almost constant and mainly dependent on the σ term, throughout the whole range of masses, because its dependence on mass through l_ℓ^2 is small while the mass dependence of $\dot{N}_s$ is strong. We determine the slope of the curves in case of a steady loss cone for both the curves with and without using the $M_\bullet - \sigma$ relation. In Fig 6.11(a), the slope is -0.3 and in Fig 6.11(b) the slope is -0.6, for the decreasing part. Therefore, we conclude that if we calculate $\dot{N}_s$ using the $M_\bullet - \sigma$ relation, the value drops faster than the case of constant σ. We derive the mass evolution only in the presence of stellar capture and the result obtained is in rough agreement with that of Alexander and Bar-Or (2017b). Fig. 6.12 is similar to the result of Alexander and Bar-Or (2017b) [see Fig. 2] under the same conditions.

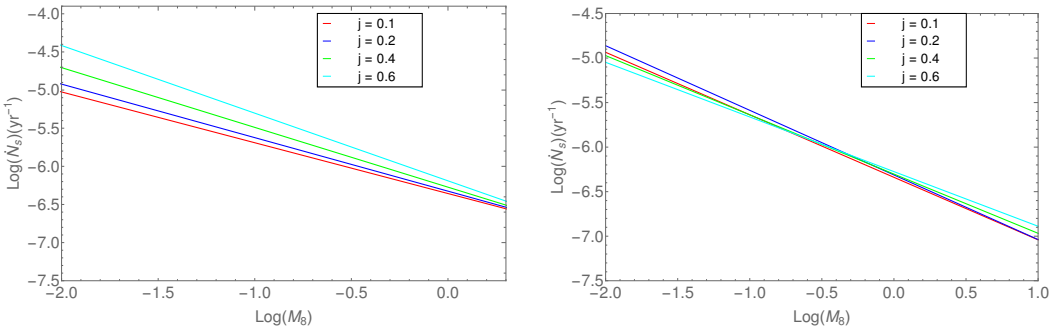

(a) Prograde (b) Retrograde

FIGURE 6.9: The capture rate, $\dot{N}_s(M_\bullet, j, k, Q, \epsilon_s)$, is shown for different values of j using the $M_\bullet - \sigma$ relation ($p = 4.86$) where $k = 1$ (left) for the prograde case, -1 (right) for retrograde case with the lower limit of ϵ_s taken to be ϵ_m = -10, $\gamma = 1.1$.

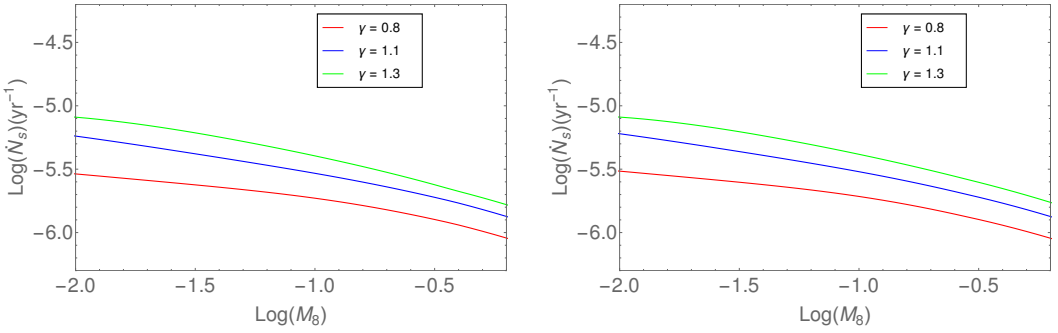

(a) Prograde (b) Retrograde

FIGURE 6.10: Plots of $\dot{N}_s(M_\bullet, j, k, Q, \epsilon_s, \sigma)$ are shown for different values of γ where $k = 1$ (left) for the prograde case, -1 (right) for the retrograde case with the lower limit of ϵ_s taken to be ϵ_m = -10, $j = 0.2$ and σ = 200 km/sec.

6.2.3 Growth of the black hole by mergers

Mass evolution by mergers

The black holes can grow its mass also by the merger process, though the rate is generally much smaller compared to accretion while minor mergers are more probable than the major mergers. When the accretion process stops due to saturation, the dominant contribution to mass growth of the black hole comes from the effect

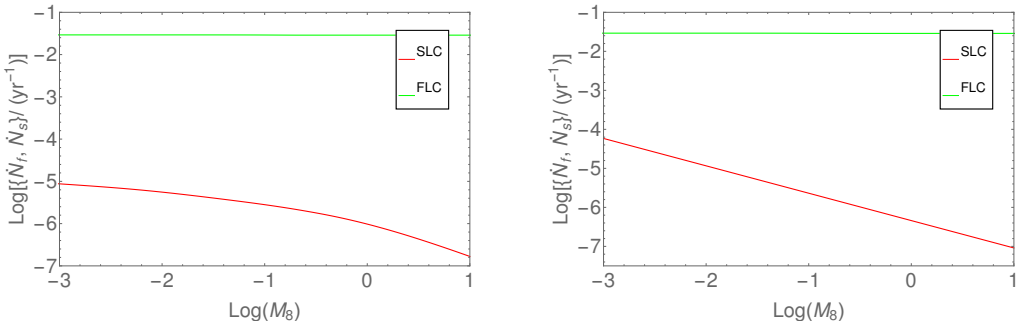

(a) (b)

FIGURE 6.11: $\dot{N}_f$ and $\dot{N}_s(M_\bullet, j, k, Q, \epsilon_s, \sigma)$ are shown for both the steady and the full loss cone theory with $j = 0$, $Q = 0$, $k = -1$, $\gamma = 1.1$, ϵ_m = -10 and σ = 200 km/sec (Left) and (right) using the $M_\bullet - \sigma$ relation with $p = 4.86$, $\gamma = 1.1$, $k = -1$.

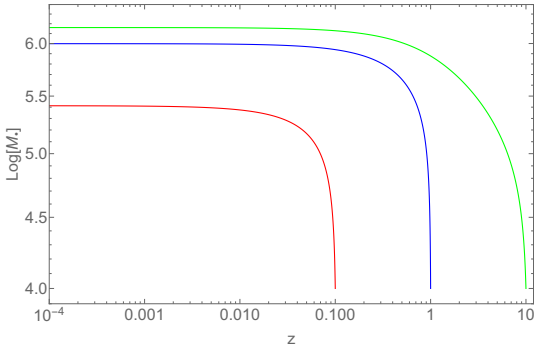

FIGURE 6.12: The mass evolution only in the presence of stellar capture is shown for seed mass of $10^4 M_\odot$, $\gamma = 1.1$ (red is for $z_f = 0.1$, blue is for $z_f = 1$, green is for $z_f = 10$).

of mergers. We compute the mass growth rate by merger activity by integrating the merger rate over the mass of the smaller black hole. Stewart *et al.* (2009) uses high-resolution ΛCDM N-body simulations for predicting merger rates in dark matter halos and investigate the scaling of common merger-related observables with luminosity, stellar mass, merger mass ratio, and redshift $z = 4 \leftarrow 0$. They derive the expression for merger rate (infall) valid for $0 \leq z \lesssim 4$ considering the peak of merger activity; the dependence on different parameters has been determined using simple fitting functions. The developed simulations which contained 512 particles of mass $3.16 \times 10^8 h^{-1} M_\odot$ which was evolved within a comoving volume of $80h^{-1}$ Mpc on a side by the Adaptive Refinement Tree (ART) N - body

code developed by Kravtsov *et al.* (1997, 2004). We use the rate of mergers given in Stewart *et al.* (2009) and integrate it over the mass of the smaller black hole to find $\dot{M}_{\bullet m}$. Following their assumptions, we also consider the merger activity to be valid in the range $z = 4 \rightarrow 0$. In Stewart *et al.* (2009) the empirical expression for merger rate (infall) is

$$\frac{\mathrm{d}N_m}{\mathrm{d}t}(m/M \in (0.1, 0.7)) = A_t(z, M)F(m/M), \tag{6.36}$$

where m and M are the masses of the smaller and larger merging galaxies and N_m is the number of mergers,

$$A_t(z, M) = 0.02\mathrm{Gyr}^{-1}(1+z)^{2.2}M_{12}^b, \tag{6.37}$$

with $b = 0.15$ and $M_{12} = M \ / \ 10^{12}h^{-1}M_\odot$ with $h = 0.7$ that is valid for $0 \leq z \lesssim 4$;

Adopting this, the rate of mass growth due to mergers is given as

$$\frac{\mathrm{d}M}{\mathrm{d}t} = A_t M \int_q^1 F(q)dq = A_t M n(q), \tag{6.38}$$

where $q = m/M$, and $F(q)$ is given as

$$F(q) = q^{-c}(1-q)^d, \tag{6.39}$$

where $c = 0.5$ and $d = 1.3$ and $n(q)$ can be written as a combination of complete and incomplete Beta functions, where the complete and incomplete Beta functions are defined respectively as

$$B(x, y) \equiv \int_0^1 t^{x-1}(1-t)^{y-1}\mathrm{d}t, \tag{6.40}$$

and

$$B_z(x, y) = \int_0^z t^{x-1}(1-t)^{y-1}\mathrm{d}t = \frac{z^x}{x}2F_1(x, 1-y; x+1; z) \tag{6.41}$$

As a result, we can express

$$n(q) = B(1-c, 1+d) - B_q(1-c, 1+d), \tag{6.42}$$

so that the merger mass rate becomes

$$\dot{M}_{\bullet m} = 8.058 \times 10^{-3}(1+z)^{2.2}\left[\frac{M_5}{f_b}\right]^{1.15} n(q) M_5 \ 10^5 M_\odot/\mathrm{Gyr}; \tag{6.43}$$

In units where $\mu_\bullet = \dfrac{M_\bullet}{M_s}$, where, M_s is the seed mass, $\tau = \dfrac{t}{t_0}$, where $t_0 = 1$ Gyr, this can further be expressed as

$$\dot{\mu}_m(q, M_s, z, z_f) = \frac{\dot{M}_{\bullet m} t_0}{M_s} = \frac{8.058 \times 10^{-3}(1+z)^{2.2}\left[\frac{M_5}{f_h}\right]^{1.15} n(q) M_5}{M_{s5}}, \tag{6.44}$$

where $f_h = M_\bullet/M$ and M_5 is mass of the SMBH in units of $10^5 M_\odot$ which simplifies to

$$M_{\bullet 5}(q, M_s, z, z_f) = \left[M_{s5}^{0.15} - 1.21 \times 10^{-3} \int_{z_f}^{z} (1+z)^{2.2} n(q) \frac{\mathrm{d}t}{\mathrm{d}z}(z)\right]^{-\frac{20}{3}}, \tag{6.45}$$

where we have used $f_h = 3 \times 10^{-5}$, $\dfrac{\mathrm{d}t}{\mathrm{d}z}$ is given by eqn. (6.75) and z_f is the formation redshift. For simplicity, we assume a proportionality relation, $M_\bullet = f_h M$, whereas Ferrarese (2002) and Jahnke and Macciò (2011) have assumed the relation to be slightly non-linear, where the index of the relation depends on the choice of the dark matter profile. Furthermore, f_h increases to 2×10^{-4} for halo masses of $\sim 10^{14} M_\odot$ and decreases to 10^{-5} for halo masses $\sim 10^{12} M_\odot$ (Ferrarese 2002). Therefore, as a reasonable approximation, we assume a mean value of f_h in our model. The frequency of major mergers is much less than the frequency of minor ones (Stewart *et al.* 2009).

Fig. 6.13 shows the mass evolution of the black hole in the presence of only merger activities for different z_f. This term dominates after the accretion stops

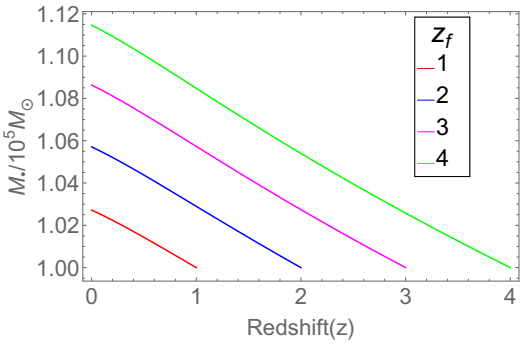

FIGURE 6.13: The evolution of black hole mass due to mergers is shown for different formation redshifts for $q = 0.1$ and $f_h = 3 \times 10^{-5}$.

which happens after the black hole reaches saturation. We have used for $q = 0.1$ and $q > 0.1$ implies major mergers. But the frequency of major mergers is much less than the minor ones and the growth rate by major mergers is almost of the same order for different q values. We see that the mass growth due to mergers is significantly smaller in this case compared to the gas accretion and hence we consider only the minor mergers, as they are more frequent.

Spin evolution by mergers

Gammie *et al.* (2004) considers the collapse of stars, accretion, and major and minor mergers that contribute to the spin of the astrophysical black holes. According to Gammie *et al.* (2004), major mergers contribute to spinning up the hole whereas minor mergers contribute to spinning it down (discussed in chapter 5). Since the accretion process is the dominant one for the spinning up of the black hole, we will be considering only the contribution of minor mergers and neglect the major mergers for the spin evolution of the hole in our evolution model. We use the spin-down term by minor mergers given by Gammie *et al.* (2004) in our evolution model to be valid in the range $z = 4 \rightarrow 0$ (Stewart *et al.* 2009). We see a significant decrease in the final spin value after adding this merger term. Gammie *et al.* (2004) by taking the effect of minor mergers in spin evolution of the black

hole find

$$\frac{\mathrm{d}\log j}{\mathrm{d}\log M_\bullet} = -\frac{7}{3} + \frac{9q}{\sqrt{2}j^2}, \tag{6.46}$$

which can be written as

$$\frac{\mathrm{d}j}{\mathrm{d}\tau} = \dot{\mu}_m \cdot \frac{j}{\mu_\bullet}\left(-\frac{7}{3} + \frac{9q}{\sqrt{2}j^2}\right). \tag{6.47}$$

6.2.4 Effect of the Blandford - Znajek torque on the black hole spin

Blandford and Znajek (1977) shows how the magnetic field drives the powerful jet from the black hole from its rotational energy. We use the expression of spin evolution caused by BZ torque as implemented in Mangalam *et al.* (2009) in our model. We compute the spin evolution equation by the BZ effect for different initial and final spin values (Mangalam *et al.* 2009) (as discussed in chapter 5).

$$\frac{\mathrm{d}j}{\mathrm{d}t} = x_H^3(j)\frac{\mathcal{G}_0}{\mathcal{J}_0}, \tag{6.48}$$

where, $x_H(j) = 1 + \sqrt{1-j^2}$ and the BZ torque, $\mathcal{G}_0$, is given by

$$\mathcal{G}_0 = \frac{m^3}{8}B_\perp^2 f_{BZ} = 4 \times 10^{46} f_{BZ} B_4 M_8^3(\mathrm{erg}), \tag{6.49}$$

and the angular momentum budget, $\mathcal{J}_0$ is

$$\mathcal{J}_0 = cM_\bullet mj = 9 \times 10^{64} M_8^2(\mathrm{g\ cm^2\ s^{-1}}), \tag{6.50}$$

and where $B_4 = B/10^4$Gauss, f_{BZ} is a geometric factor that comes from the averaging of angle over the horizon of magnetic flux and the spin of the magnetic

field (Mangalam *et al.* 2009). Therefore in dimensionless form

$$\frac{\mathrm{d}j}{\mathrm{d}\tau} = \frac{4}{9} \times 10^{-5} f_{BZ} B_4 \mu_\bullet M_{s5} x_H^3(j) j, \tag{6.51}$$

Mangalam *et al.* (2009) give an analytic solution of spin down time $\tau_{j,BZ}(j)$

$$\tau_{j,BZ} = \frac{\mathcal{J}_0}{\mathcal{G}_0} \int_{j_f}^{j_i} \frac{\mathrm{d}j}{r^3(j) j} = 7.0 \times 10^8 \mathrm{yr} \frac{(\kappa(j_i, j_f)/0.1)}{B_4^2 M_9 f_{BZ}}, \tag{6.52}$$

where $M_9 = M_\bullet/(10^9 M_\odot)$ and

$$\kappa(j_i, j_f) = \left[\left(\frac{1}{16} \right) \log \left(\frac{2-w}{w} \right) + \left(\frac{3w^2 + 3w - 4}{24 w^3} \right) \right]_{w_f}^{w_i}, \tag{6.53}$$

with $w_i = x_H(j_i)$, $w_f = x_H(j_f)$.

6.3 BH evolution model in ΛCDM cosmology

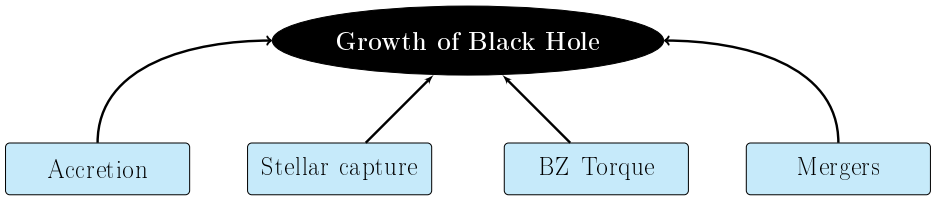

Effects	Region	τ_j	τ_M
Gas accretion	$x_I - r_d$	1 Gyr	1 Gyr
Stellar capture	$r_t - r_h$	-	10 Gyr
Mergers	r_M	10 Gyr	$\sim$ 10 Gyr
BZ Torque	$r_H - r_{ISCO}$	1 Gyr	-

TABLE 6.1: The domain and timescales for different physical effects (shown in Fig. 6.14) contributing to the growth of the black hole.

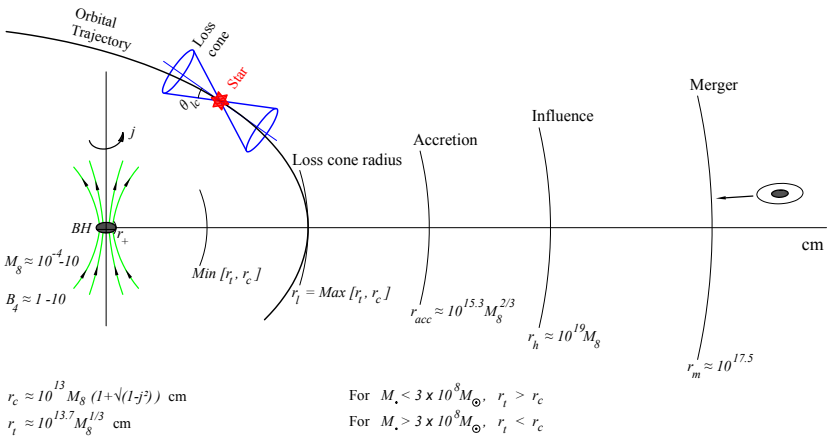

FIGURE 6.14: The important radii corresponding to all the processes contributing to the growth of the black hole is shown for $M_\bullet = 10^4 - 10^6 M_\odot$.

Now we indicate operative time scales in different physical regimes of gas accretion, stellar capture, mergers and electromagnetic torque in Table 6.1, where the evolution timescales for mass τ_M and spin τ_j are calculated as follows.

- Gas accretion: From eqn. (6.70) we see that

$$\tau_{M,g} = \frac{M_\bullet}{\dot{M}_{\bullet g}} = \frac{1}{k_1} \simeq 1 \text{ Gyr}, \tag{6.54}$$

and from eqn. (6.76)

$$\tau_{j,g} = \frac{M_\bullet}{\dot{M}_{\bullet g}} \Big(l_I(j) - 2\epsilon(j) j \Big) \simeq 1 \text{ Gyr} \tag{6.55}$$

- Stellar Capture: We estimate from eqn. (6.70) that

$$\tau_{M,*} = \frac{M_\bullet}{\dot{M}_{\bullet *}} = \frac{M_\bullet}{M_\odot} 10^{5.5} \text{ yr} \simeq 10 \text{ Gyr for } M_\bullet = 10^5 M_\odot \tag{6.56}$$

- Merger: Also from eqn. (6.44) we find

$$\tau_{M,m} = \frac{M_\bullet}{\dot{M}_{\bullet m}} = \frac{M_\bullet}{M_5^{1.15} \cdot 8.058 \cdot 10^{-3} \cdot (1+z)^{2.2} 10^5 M_\odot} \text{ Gyr} \simeq 10 \text{ Gyr for } M_\bullet = 10^5 M_\odot, z \simeq 3, \tag{6.57}$$

and from eqn. (6.47)

$$\tau_{j,m} = \frac{M_\bullet}{\dot{M}_{\bullet m}} \left(-\frac{7}{3} + \frac{9q}{\sqrt{2} j^2} \right) \simeq 10 \text{ Gyr} \tag{6.58}$$

- BZ Torque: We see from eqn. (6.51)

$$\tau_{j,BZ} = \frac{\mathcal{J}_0}{\mathcal{G}_0} \int_{j_f}^{j_i} \frac{\mathrm{d}j}{r^3(j) j} = 7.0 \times 10^8 yr \frac{(\kappa(j_i, j_f)/0.1)}{B_4^2 M_9 f_{BZ}} \simeq 1 \text{ Gyr}, \tag{6.59}$$

where M_9 is $M_\bullet$ in units of $10^9 M_\odot$ and

$$\kappa(j_i, j_f) = \left[\left(\frac{1}{16} \right) \log \left(\frac{2-w}{w} \right) + \left(\frac{3w^2 + 3w - 4}{24 w^3} \right) \right]_{w_f}^{w_i}, \tag{6.60}$$

with $w_i = x_H(j_i)$, $w_f = x_H(j_f)$.

It is clear that the evolution timescales of both mass and spin are of order 1-10 Gyr. This motivates us to use $t_0 = 1$ Gyr as the unit of time in our model. Next we examine the details of the loss cone theory that is an important input to determine M_*.

The black hole growth can occur by both gas flow as well as by capture of stars and mergers till it reaches a saturated mass $M_{\bullet t}$ at a time $t = t_s$ when the gas flow stops and it grows only by the capture of stars and mergers. This happens because the outflow velocity exceeds the escape velocity of the medium and the gas is driven away causing the accretion process to stop. The saturated mass is given by King (2003) as

$$M_{\bullet t} = 9.375 \times 10^6 \sigma_{100}^4 M_\odot. \tag{6.61}$$

For the rate of growth of mass by mergers, we use eqn. (6.38), which is valid from $z = 4$ to present time; given that the merger activity peaks at $z = 5 - 0.5$ (Wetzel *et al.* 2009). We perform five experiments which we discuss in this section. For the mass evolution, we consider the contribution from both major mergers as well as the minor ones and for the spin evolution, we consider the contribution from the minor mergers in spinning down the black hole (Gammie *et al.* 2004) as the contribution of accretion process in spinning up the black hole is much higher than the contributions from major mergers. But due to a smaller frequency of the major mergers, the final mass attained by the merger process does not vary significantly with the value of q. For merger case, we have dealt with two scenarios: (i) for $z_f \lesssim 4$ the contribution of the merger will be present throughout and (ii) for $z_f \gtrsim 4$, initially, there will be only accretion and stellar capture and mergers will come into play after $z = 4$; from then on until t_s all of three terms will contribute after which the accretion stops.

To summarize, our model is based on some assumptions and conditions:

1. Black hole seeds are formed at a lookback time which of the order of the Hubble time.

2. At the saturation time when the mass reaches $M_{\bullet t} = 9.375 \times 10^6 \sigma_{100}^4 M_\odot$, $p \to 4$.

3. The merger activity exists only for $z \lesssim 4$ (Stewart *et al.* 2009).

As before, we have normalized mass by $\mu_\bullet = \dfrac{M_\bullet}{M_s}$, where, M_s is the seed mass, and time by $\tau = \dfrac{t}{t_0}$, where $t_0 = 1$ Gyr. The mass evolution equation is given by

$$\frac{\mathrm{d}M_\bullet}{\mathrm{d}t} = \epsilon_I(j)\dot{M}_{\bullet g} + \epsilon(j)\dot{M}_{\bullet *} + \dot{M}_{\bullet m}, \tag{6.62}$$

where $\epsilon(j)$ is the mass accretion efficiency given by

$$\epsilon(j) = \begin{cases} \epsilon_I(j) & \text{for } M_\bullet < M_c \\ 1 & \text{for } M_\bullet \geq M_c, \end{cases} \tag{6.63}$$

where (Bardeen *et al.* 1972)

$$\epsilon_I(j) = \frac{z_m^2(j) - 2z_m(j) + j\sqrt{z_m(j)}}{z_m(j)(z_m^2(j) - 3z_m(j) + 2j\sqrt{z_m(j)})^{1/2}}, \tag{6.64}$$

and

$$z_m(j) = \frac{r_{ms}}{M_\bullet} = 3 + Z_2 - \sqrt{(3 - Z_1)(3 + Z_1 + 2Z_2)}, \tag{6.65}$$

with $Z_1 = 1 + (1 - j^2)^{1/3}((1 + j)^{1/3} + (1 - j)^{1/3})$ and $Z_2 = (3j^2 + Z_1^2)^{1/2}$ (Bardeen *et al.* 1972). The dimensionless equation becomes

$$\frac{\mathrm{d}\mu_\bullet}{\mathrm{d}\tau} = \epsilon_I(j)\dot{\mu}_g + \epsilon(j)\dot{\mu}_* + \dot{\mu}_m. \tag{6.66}$$

The first term in the RHS of eqn. (6.66) represents the gas accretion and comes from eqn. (6.3), the second term due to the stellar capture is calculated from eqn. (6.35) and represented below by eqn. (6.70), and the third term comes from the contribution of mergers provided by eqn. (6.44). In eqn. (6.63), we see that $\epsilon(j)$ is given by efficiency at ISCO for $M_\bullet < M_c$ and 1 for $M_\bullet > M_c$. This is because, beyond the critical mass, the stars are directly captured leading to the efficiency of 1, while for lesser masses, the gas has to come through ISCO (by accretion of tidally disrupted stars). The disc accretion always comes through ISCO, but, the stars can come through ISCO as well as direct capture.

The spin evolution equation of black hole taking into account gas accretion, stellar capture, mergers and BZ torque is given by (see §6.2 for the various terms)

$$\frac{\mathrm{d}j}{\mathrm{d}t} = \frac{\dot{M}_{\bullet g}}{M_\bullet}\left(l_I(j) - 2\epsilon_I(j)j\right) + \frac{\dot{M}_{\bullet *}}{M_\bullet}\left(l_*(j) - 2\epsilon(j)j\right) + \dot{M}_{\bullet m}\cdot\frac{j}{M_\bullet}\left(-\frac{7}{3} + \frac{9q}{\sqrt{2}j^2}\right) + x_H^3(j)\frac{\mathcal{G}_0}{\mathcal{J}_0}. \tag{6.67}$$

The dimensionless version of eqn. (6.67) is

$$\frac{\mathrm{d}j}{\mathrm{d}\tau} = \frac{\dot{\mu}_g}{\mu_\bullet}\left(l_I(j) - 2\epsilon_I(j)j\right) + \frac{\dot{\mu}_*}{\mu_\bullet}\left(l_*(j) - 2\epsilon(j)j\right) + \dot{\mu}_m\cdot\frac{j}{\mu_\bullet}\left(-\frac{7}{3} + \frac{9q}{\sqrt{2}j^2}\right) + \frac{4}{9}\times 10^{-5} f_{BZ} B_4 \mu_\bullet M_{s5} x_H^3(\tag{6.68}$$

where

$$\dot{\mu}_g = \begin{cases} \dfrac{\dot{M}_{\bullet g} t_0}{M_s} = \dfrac{k_1 M_\bullet t_0}{M_s} & \text{for } M_\bullet \le M_{\bullet t} \\ 0 & \text{for } M_\bullet > M_{\bullet t}, \end{cases}, \tag{6.69}$$

$$\dot{\mu}_* = \frac{\dot{M}_{\bullet *} t_0}{M_s} = \begin{cases} m_\star \dot{N}_f t_0 / M_s & \text{for full loss cone} \\ m_\star \dot{N}_s t_0 / M_s & \text{for steady loss cone} \end{cases}, \tag{6.70}$$

where $\dot{N}_f$ and $\dot{N}_s$ are the stellar capture rates derived for full or steady loss cone theories.

$$\dot{\mu}_m = \begin{cases} \dfrac{\dot{M}_{\bullet m} t_0}{M_s} & \text{for } z \le 4 \\ 0 & \text{for } z > 4 \end{cases}, \tag{6.71}$$

where M_{s5} is the mas of seed black hole in units of $10^5 M_\odot$; for our calculations we have used $f_{BZ} = 1$. The first term in the RHS of eqn. (6.68) for gas accretion stems from eqn. (6.4) [which shuts off after saturation, as implemented in eqn. (6.69)], the second term represents the stellar capture which can happen in two ways; by tidal disruption (for $M_\bullet < M_c$) when the gas has to pass through ISCO with an angular momentum and efficiency at ISCO, or by a direct capture (for $M_\bullet > M_c$), then it will retain its original angular momentum and efficiency, $\epsilon(j) = 1$ as given by eqns. (6.63, 6.72). The third term represents mergers and stems from eqn. (6.47) [effective during $z = 4 \to 0$, see (4) in our assumptions as implemented in eqn. (6.71)] and the last term represents the contribution of BZ torque [see eqn.

(6.51)]. The angular momentum of the stellar component is given by

$$l_* = \begin{cases} l_I(j) = \dfrac{z_m^2(j) - 2j\sqrt{z_m(j)} + j^2}{z_m^{1/2}(j)[z_m^2(j) + 2j\sqrt{z_m(j)} - 3z_m(j)]^{1/2}} & \text{for } M_\bullet < M_c(j) \\ l_\ell(M_\bullet, j, k, Q) = 2j + k\sqrt{\dfrac{2x_\ell j^2}{(x_\ell - 2)^2} - \dfrac{Qj^2}{x_\ell(x_\ell - 2)} + \dfrac{2x_\ell^2}{(x_\ell - 2)} - Q} & \text{for } M_\bullet \geq M_c(j), \end{cases} \tag{6.72}$$

where, $l_I(j)$ is given by eqn. (6.80) (Bardeen *et al.* 1972) and $l_\ell(M_\bullet, j, k, Q)$ is given by eqn. (6.19). Also, $L_\ell = l_\ell \dfrac{GM_\bullet}{c}$ is given by

$$L_\ell(M_\bullet, j, k, Q) = \begin{cases} \sqrt{2GM_\bullet r_{lc}} & \text{non - relativistic case} \\ \dfrac{GM_\bullet}{c}\left(2j + k\sqrt{\dfrac{2x_\ell j^2}{(x_\ell - 2)^2} - \dfrac{Qj^2}{x_\ell(x_\ell - 2)} + \dfrac{2x_\ell^2}{(x_\ell - 2)} - Q}\right) & \\ k = 1 \text{ (prograde)}, \; k = \text{-1 (retrograde)} & \end{cases} \tag{6.73}$$

where j is the spin parameter of the black hole, r_{lc} is the loss cone radius for non - relativistic case and x_ℓ is the loss cone radius in units of r_g which is taken as Max[x_t, x_c]. If we take $j = 0, Q = 0$ we obtain the non - relativistic result from the expression of $L_\ell(M_\bullet, j, k, Q)$ as shown in eqn. (6.22). For ΛCDM cosmology, taking [$\Omega_r \simeq 10^{-5}$, taken to be 0, $\Omega_m = 0.3$, $\Omega_\Lambda = 0.7$] the time as a function of redshift can be written as,

$$t(z) = \frac{1}{H_0}\int_{1/(1+z_f)}^{1/(1+z)} da \frac{1}{\sqrt{\Omega_m a^{-1} + \Omega_\Lambda a^2}} = t_z(z) - t_z(z_f), \tag{6.74}$$

where, z_f is the formation redshift and H_0 is the present day Hubble constant (H_0 = 70 km s^{-1} Mpc^{-1}) and where we find by integration that

$$t_z(z) = \frac{1}{H_0}\frac{2}{3}\frac{1}{\sqrt{1-\Omega_m}} \log\left[\sqrt{1-\Omega_m}\sqrt{\Omega_m + \frac{1-\Omega_m}{(1+z)^3}} + (1-\Omega_m)\left(\frac{1}{1+z}\right)^{\frac{3}{2}}\right]. \tag{6.75}$$

which matches with the result of Mo *et al.* (2010) for $z_f = \infty$. The boundary conditions are

- At $t = 0$, $M_\bullet = M_s$, $z = z_f$ and $j = j_0$.

- At $t = t_s$, $M_\bullet = M_{\bullet t}$, $z = z_s$.

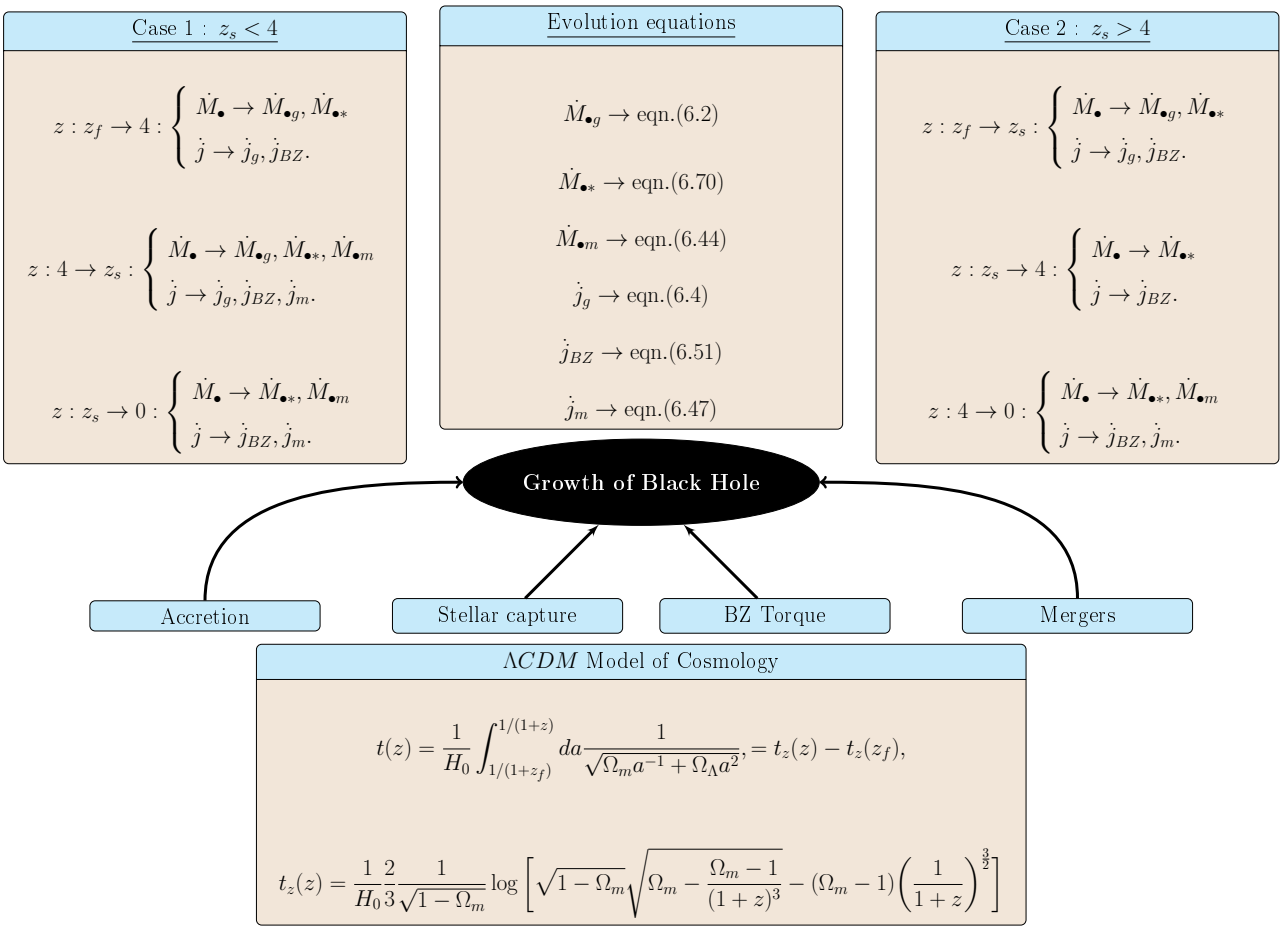

FIGURE 6.15: A schematic for our model of evolution of the mass and the spin of black hole in ΛCDM cosmology.

We perform the following experiments which we tabulate in Table 6.2. Next, we discuss the parameter range.

Models	Accretion	BZ Torque	Stellar capture	Mergers	Parameter sets
Expt 1	$\surd$				M_s, η, j_0, z_f
Expt 2	$\surd$		(FLC)$\surd$		$M_s, \eta, j_0, z_f, \sigma_{100}$
Expt 3	$\surd$	$\surd$			M_s, η, j_0, z_f, B_4
Expt 4	$\surd$	$\surd$	(SLC)$\surd$		$M_s, \eta, j_0, z_f, \sigma_{100}$
Complete model	$\surd$	$\surd$	(SLC)$\surd$	$\surd$	$M_s, \eta, j_0, z_f, \sigma_{100}, q$

TABLE 6.2: The five different experiments performed

Justification of the chosen parameter ranges: We have used a certain set of parameters to perform the experiments mentioned above. Here we provide the justification for choosing those parameter sets based on literature and observational values. The minimum σ measured till date is around 30 - 40 km sec^{-1} (Xiao *et al.* 2011). For this low σ, the saturated mass is of the order of around $10^5 M_\odot$. Therefore the seed masses considered should be $\lesssim 10^5 M_\odot$. The ranges we consider for seed mass, formation redshift are consistent with the values considered in Alexander and Bar-Or (2017a). The values of z_f is taken to be in the range z_f = 5 - 8. Average observed values of σ are within the range of 100 - 200 km sec^{-1}. Values of $\gamma \simeq 1.1$ - 1.5 are consistent with the observed values (Merritt 2013a). The B_4 values are taken to be in the typical range 1 -10 (Blandford *et al.* 1990), for the black hole of mass $10^8 - 10^{10} M_\odot$, Blandford and Znajek (1977) show that the field strength should be more than 10^5 Gauss for supplying electromagnetic power equal to or more than Eddington power. The η typically are taken to be sub - Eddington accretion ($\eta \gtrsim 0.07$) and below that it will not be possible to attain the high mass of the present-day black holes. We have used η in the range [0.07, 0.09] as given in Shankar *et al.* (2009b) considering the effect of duty cycles. We have also illustrated the case of $\eta = 0.01$ which clearly indicates a very slow

mass growth.

Parameter sets used

Parameters	Ranges	References
$M_{\bullet s}$	$10^3 - 10^5\ M_\odot$	Alexander and Bar-Or (2017a)
j_0	0.001 - 0.4	Mangalam (2015)
z_f	5 - 8	Alexander and Bar-Or (2017a)
η	0.07 - 0.09	Shankar *et al.* (2009b)
σ_{100}	1 - 2.5	(Xiao *et al.* 2011), Bhattacharyya and Mangalam (2018)
γ	1.1 - 1.5	(Merritt 2013a)
B_4	1 - 10	Blandford *et al.* (1990)

TABLE 6.3: Ranges of the parameters used.

Table of the parameter sets for runs

6.3.1 Experiment 1: Only gas accretion is present

In presence of only accretion the spin and mass evolution equations (eqns. 6.68, 6.66) take the form

$$\frac{\mathrm{d}j}{\mathrm{d}\tau} = \frac{\dot{\mu}_g}{\mu_\bullet}\Big(l_I(j) - 2\epsilon_I(j)j\Big), \tag{6.76}$$

$$\frac{\mathrm{d}\mu_\bullet}{\mathrm{d}\tau} = \epsilon_I(j)\dot{\mu}_g. \tag{6.77}$$

where, $e_I = \left(1 - \frac{2}{3x}\right)^{\frac{1}{2}}$, $l_I = \frac{2}{3\sqrt{3}} r_g(1 + 2(3x_H - 2)^{\frac{1}{2}})$ (Bardeen 1970). The solution of j as a function of black hole mass when there is only accretion present

Run #	$M_s(10^5 M_\odot)$	B_4	σ_{100}	z_f	η	j_0	Varying parameter	Comments
1.1	1	5		4	0.09	0.001	$j_0 = 0$	Expt 1
1.2	1	10		4	0.09	0.2		
2.1.	0.1		1	10	0.09		M_s	Expt 2
2.2	0.5		1	10	0.09			
2.3	1		1	10	0.09			
3.1.1	1	1		4	0.09	0.2	B_4	Expt 3.1
3.1.2	1	5		4	0.09	0.2		
3.1.3	1	10		4	0.09	0.2		
3.2.1	1	5		4	0.01	0.2	Lower limit of η	Expt 3.2
3.2.2	1	5		4	0.05	0.2		
4.1.1	0.5	5	1	6	0.07	0.2	M_s	Expt 4.1
4.1.2	0.6	5	1	6	0.07	0.2		/Expt 5.1*
4.1.3	0.7	5	1	6	0.07	0.2		
4.1.4	1	5	1	6	0.07	0.2		
4.2.1	1	5	1	6	0.07	0.2	B_4	Expt 4.2
4.2.2	1	6	1	6	0.07	0.2		/Expt 5.2*
4.2.3	1	8	1	6	0.07	0.2		
4.2.4	1	10	1	6	0.07	0.2		
4.3.1	1	5	1	6	0.07	0.2	σ_{100}	Expt 4.3
4.3.2	1	5	1.5	6	0.07	0.2		/Expt 5.3*
4.3.3	1	5	2	6	0.07	0.2		
4.3.4	1	5	2.5	6	0.07	0.2		
4.4.1	1	5	1	5	0.07	0.2	z_f	Expt 4.4
4.4.2	1	5	1	6	0.07	0.2		/Expt 5.4*
4.4.3	1	5	1	7	0.07	0.2		
4.4.4	1	5	1	8	0.07	0.2		
4.5.1	1	5	1	6	0.07	0.2	η	Expt 4.5
4.5.2	1	5	1	6	0.075	0.2		/Expt 5.5*
4.5.3	1	5	1	6	0.08	0.2		
4.5.4	1	5	1	6	0.09	0.2		
4.6.1	1	5	1	6	0.07	0.0	j_0	Expt 4.6
4.6.2	1	5	1	6	0.07	0.2		/Expt 5.6*
4.6.3	1	5	1	6	0.07	0.3		
4.6.4	1	5	1	6	0.07	0.4		

TABLE 6.4: Sets of the parameters used for the runs with $k = 0$, $\gamma = 1.1$ used for the experiments we perform. For each experiment we specify the parameter sets used. * indicates that along with the same parameters used for Expt 4 we have one more parameter $q = 0.1$ for Expt 5 which prescribes the complete model.

was derived by Bardeen (1970) using the solution of the geodesic equation for the Kerr metric found by Felice (1968) and Carter (1968) to be

$$j = \frac{1}{3}x_H^{\frac{1}{2}}(4 - (3x_H - 2)^{\frac{1}{2}}), \tag{6.78}$$

where, $x_I = x_I/r_g$, $x_H = r_H/r_g$, where r_H is the horizon, e_I is the energy per unit mass and l_I is the angular momentum per unit mass for the innermost stable circular orbit. The value of x varies from 6 to 1 for j varying from 0 to 1. The derivation of these equations are as follows (Bardeen *et al.* 1972)

$$l_I - je_I = \pm\frac{1}{\sqrt{3}}x_I, \tag{6.79}$$

Using the expressions of l_I and e_I, i.e,

$$l_I = \frac{\sqrt{x_I}(x_I^2 + j^2 - 2j\sqrt{x_I})}{x_I(x_I^2 - 3x_I + 2j\sqrt{x_I})^{1/2}},\ e_I = \frac{(x_I^2 - 2x_I + j\sqrt{x_I})}{x_I(x_I^2 - 3x_I + 2j\sqrt{x_I})}, \tag{6.80}$$

and after squaring both the sides we finally arrive at a quadratic equation of j given as,

$$3j^2 + 6x_I - 8j\sqrt{x_I} - x_I^2 = 0. \tag{6.81}$$

The solution to this equation is

$$j = \frac{x_I}{3}(4 \pm \sqrt{3x_I - 2}). \tag{6.82}$$

Since $j < 1$, the negative sign is the correct choice, so that

$$j(x_H) = \frac{1}{3}x_H^{\frac{1}{2}}(4 - (3x_H - 2)^{\frac{1}{2}}). \tag{6.83}$$

Now,

$$l_I = je \pm \frac{x_I}{\sqrt{3}}. \tag{6.84}$$

The final expression for l_I becomes (Bardeen *et al.* 1972),

$$l_I = \frac{2}{3\sqrt{3}}[2(3x_I - 2)^{1/2} + 1] + \frac{x_I}{\sqrt{3}}(-1 \pm 1). \tag{6.85}$$

Here positive sign is the correct choice since for $a = 1$, $l_I = 0$. Therefore, final expression of l_I is

$$l_I(x_I, m_d) = \frac{2}{3\sqrt{3}} m_d (1 + 2(3x_I - 2)^{\frac{1}{2}}), \tag{6.86}$$

where, m_d is the mass of the disk consumed by the hole. The analytic relation between x_H and r_g (Bardeen 1970) is

$$\left(\frac{x_H}{x_1}\right) = \left(\frac{r_{g1}}{r_g}\right)^2, \tag{6.87}$$

where x_1 and r_{g1} are the initial values when $j = 0$. Using this solution it is found that (Bardeen 1970),

$$\frac{r_g}{r_{g1}} = \left(\frac{3x_1}{2} - 1\right)^{\frac{1}{2}} \sin\left[\left(\frac{2}{3x_1}\right)^{\frac{1}{2}} \frac{\Delta m_0}{r_{g1}}\right] + \cos\left[\left(\frac{2}{3x_1}\right)^{\frac{1}{2}} \frac{\Delta m_0}{r_{g1}}\right], \tag{6.88}$$

where, Δm_0 is the accreted rest mass when the change in mass is from r_g to r_{g1}. Fig. 6.16 shows $j(\mu_\bullet)$ for Bardeen (1970) solution using eqns. (6.68, 6.66) where

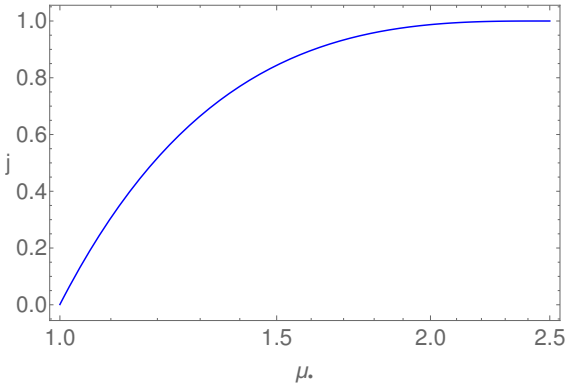

FIGURE 6.16: The Bardeen (1970) solution, $j(\mu_\bullet)$ of the spin is shown when there is only accretion (run #1.1).

there is only accretion. After the black hole spin saturates, only the mass increases leaving the spin parameter unchanged at the saturated value of 1.

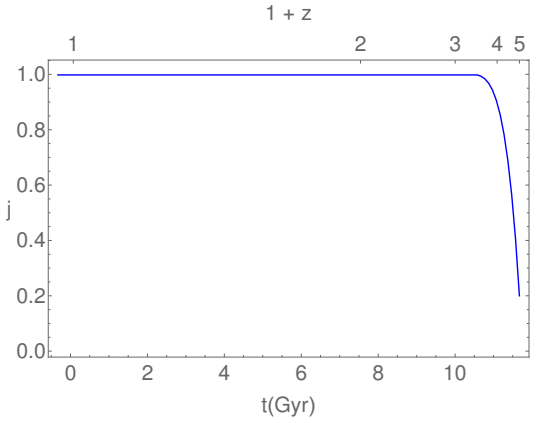

(a)

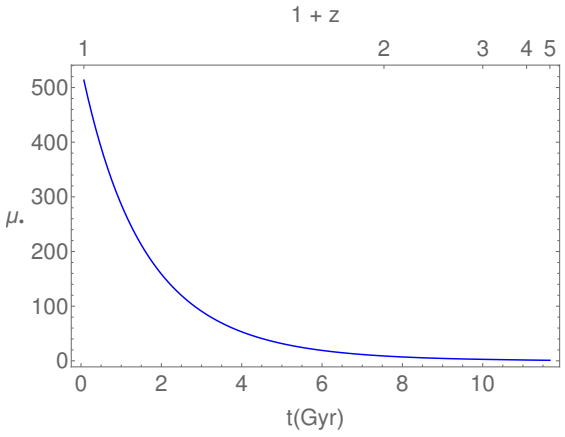

(b)

FIGURE 6.17: (a) The spin evolution, $j(t)$, and (b) the mass evolution, $\mu_\bullet(t)$, for $B_4 = 5$, $z_f = 4$, $\eta = 0.09$, $M_s = 10^5 M_\odot$ are shown when only accretion is present (run # 1.2).

Fig. 6.17 shows $j(t)$ and $\mu_\bullet(t)$ when there is only accretion. The mass continues to grow and the spin reaches a saturated value and afterwards it remains the same.

6.3.2 Experiment 2: Non - relativistic accretion with feedback and full loss cone theory

Full loss cone theory: Here we consider the case of the full loss cone ($\theta_d >> \theta_\ell$) where the mass density in the galaxy cusp follows a single power law profile and the stars are able to quickly fill the loss cone on dynamical time scales. Therefore

$$\rho = \rho_0 r^{-\gamma}, \tag{6.89}$$

where γ is the power law index. The distribution function of stars in a such a galaxy is given by (Merritt 2013a)

$$f_s(E) = \frac{3-\gamma}{8}\sqrt{\frac{2}{\pi^5}}\frac{\Gamma(\gamma+1)}{\Gamma(\gamma-\frac{1}{2})}\frac{M_\bullet}{m_\star}\frac{\phi_0^{\frac{3}{2}}}{(GM_\bullet)^3}\left(\frac{|E|}{\phi_0}\right)^{\gamma-\frac{3}{2}}, \tag{6.90}$$

where $\phi_0 = \dfrac{GM_\bullet}{r_m}$, E is the energy, r_m is the gravitational influence radius of the black hole defined as $GM_\bullet/\sigma^2$ and m_* is the stellar mass. The rate of capture of stars within the loss cone is

$$F_f(E) = 4\pi^2 L_\ell^2(E) f_s(E), \tag{6.91}$$

where $L_\ell(E)$ is the angular momentum of the star. An integration of this over all energies gives the total rate of capture in the loss cone,

$$\dot{N}_f = \int_{-\infty}^{\phi_0} F_f(E)\mathrm{d}E, \tag{6.92}$$

so that

$$\dot{M}_{\bullet * f} = m_\star \dot{N}_f = \frac{3-\gamma}{8}\sqrt{\frac{1}{2\pi}}\frac{\Gamma(\gamma+1)}{\Gamma(\gamma-\frac{1}{2})}\frac{l_\ell^2}{GM_\bullet}\frac{1}{r_m}\left(\frac{GM_\bullet}{r_m^3}\right)^{\frac{1}{2}} M_\bullet = \frac{3-\gamma}{8}\sqrt{\frac{1}{2\pi}}\frac{\Gamma(\gamma+1)}{\Gamma(\gamma-\frac{1}{2})}\frac{l_\ell^2(M_\bullet)}{Gc^2}\sigma^5, \tag{6.93}$$

where $L_\ell \equiv (GM_\bullet/c)\, l_\ell$. For the non - relativistic case, L_ℓ is given by eqn. (6.22).

After simplification, it is seen that this expression for $\dot{M}_{\bullet *} \propto \sigma^5$ for the non - relativistic case does not depend on $M_\bullet$. But, for the relativistic case, $\dot{M}_{\bullet *}$ depends both on σ and $M_\bullet$ through the capture radius. In the full loss cone regime, the depleted orbits are repopulated within orbital periods by the relaxation process; this is a reasonable assumption for $M_\bullet << 10^5 M_\odot$.

Here, we study the non-relativistic case with no spin and full loss cone theory applied to stellar capture for which a fully analytic solution can be obtained. We solve the mass evolution equation [eqn. (6.62] to find that

$$t(M_\bullet) = \begin{cases} \int_{M_s}^{M_\bullet} \frac{dM_\bullet}{\dot{M}g + \dot{M}_*} & \text{for } t > t_s \\ \\ t_s + \int_{M_{\bullet t}}^{M_\bullet} \frac{dM_\bullet}{\dot{M}_*}. & \text{for } t \leq t_s, \end{cases} \tag{6.94}$$

where t_s is time at which feedback has stopped accretion. Solving eqn. (6.94) using eqn. (6.3) for $\dot{M}g$ and eqn. (6.93) for $\dot{M}_*$ for $t \leq t_s$, we find $\tau_s = k_1 t_s$ where

$$\tau_s = \log\left[\frac{k_1 M_{\bullet t} + k_2\sigma^5}{k_1 M_s + k_2\sigma^5}\right] = k_1 t_z(z_s) - k_1 t_z(z_f), \tag{6.95}$$

where, $M_* = k_2\sigma^5$ for the non relativistic full loss cone theory and k_1 is defined by eqn. (6.1). Using eqn. (6.74) it can be written as

$$\left(\tau_s + k_1 t_z(z_f) - k_1 \frac{2}{3}\frac{1}{\sqrt{1-\Omega_m}} \log\sqrt{1-\Omega_m}\right)\frac{3\sqrt{1-\Omega_m}}{2k_1} = \log(\alpha_1 + \sqrt{\Omega_m + \alpha_1^2}), \tag{6.96}$$

where

$$\alpha_1^2 = \frac{1-\Omega_m}{(1+z_s)^3}.$$

Writing LHS of eqn. (6.96) as $\log\beta_1$, we derive

$$z_s = \left[\frac{2\beta_1\sqrt{1-\Omega_m}}{\beta_1^2 - \Omega_m}\right]^{\frac{2}{3}} - 1. \tag{6.97}$$

After solving eqn. (6.94) for $t > t_s$, the final equation for $M_\bullet$ as a function of redshift is given by

$$M_\bullet(\tau, M_s, \sigma_{100}) = \begin{cases} \mu_M(\tau)M_s + M_s = M_s + (e^\tau + C\sigma_{100}^5(e^\tau - 1))M_s & \text{for } z < z_s \\ M_{\bullet t} + [\mu_s + (\tau - \tau_s)C\sigma_{100}^5]M_s. & \text{for } z \geq z_s, \end{cases} \tag{6.98}$$

where, $C = k_2(100 \text{ km sec}^{-1})^5/(k_1 M_s)$ and

$$\mu_M = \frac{M_\bullet - M_s}{M_s} = \mu_\bullet - 1, \tag{6.99}$$

where $M_s = f_b M_b \sigma^5$.

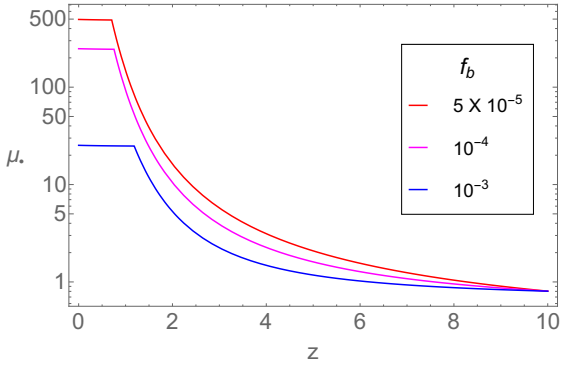

FIGURE 6.18: The mass evolution, $\mu_\bullet(z)$, is shown for different f_b for $\sigma_{100} = 1$ (run #2.1, #2.2, #2.3) with $j_0 = 0$, $B_4 = 0$.

In Fig. 6.18, the late part represents the black hole mass growth only by capture of stars and the growth rate of black hole mass by accretion of gas dominates much earlier.

- In the later experiments, we have scaled eqn. (6.68) by eqn. (6.66) to obtain an equation for $\frac{\mathrm{d}j}{\mathrm{d}M_\bullet}$ which is solved to find $j(M_\bullet)$ and fed into eqn. (6.66) to obtain $M_\bullet(t)$.
- We derive $j(t)$ similarly, using the solution of $j(M_\bullet)$ in eqn. (6.68).
- All the solutions are dependent on the value of σ which we have considered to be constant throughout for a particular galaxy.

Taking into account the saturation, we will now present the results for the more realistic evolution experiments (3 and 4) in Table 6.2 where we include the effects one at a time.

6.3.3 Experiment 3: Gas accretion and BZ torque are present

Here, the spin and mass evolution equations (eqns. 6.68, 6.66) take the form

$$\frac{\mathrm{d}j}{\mathrm{d}\tau} = \frac{\dot{\mu}_g}{\mu_\bullet}\left(l_I(j) - 2\epsilon_I(j)j\right) + \frac{4}{9}\times 10^{-5} f_{BZ} B_4 \mu_\bullet M_{s5} x_H^3(j) j. \tag{6.100}$$

$$\frac{\mathrm{d}\mu_\bullet}{\mathrm{d}\tau} = \epsilon_I(j)\dot{\mu}_g. \tag{6.101}$$

First we study a canonical case (run # 2.1) of this experiment (see Fig. 6.19(a)), and then we change the parameters one by one keeping others constant.

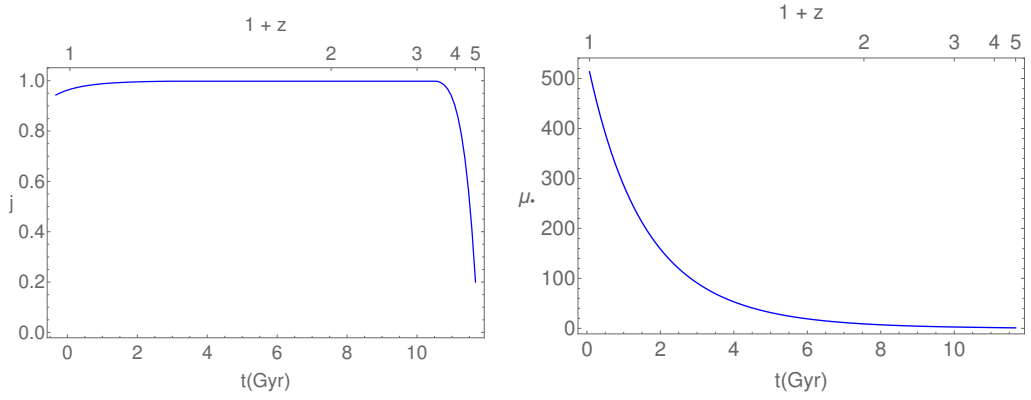

(a) (b)

FIGURE 6.19: The spin evolution, $j(t)$, (Fig. 6.19(a)) and the mass evolution $\mu_\bullet(t)$, (Fig. 6.19(b)) are shown for $B_4 = 5$, $z_f = 4$, $\eta = 0.09$, $M_s = 10^5 M_\odot$ when there is only accretion and BZ torque present and accretion continues to occur (canonical case, run # 3.1.1).

We now present the results for different runs listed in Table 6.4.

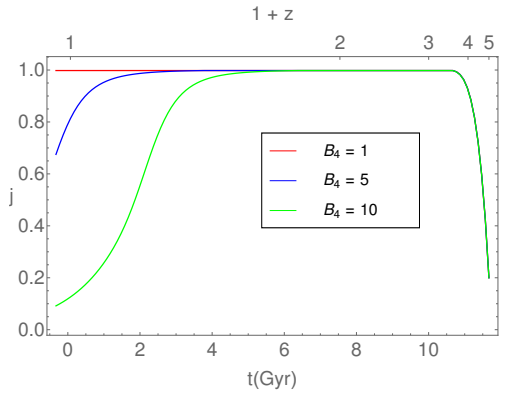

(a)

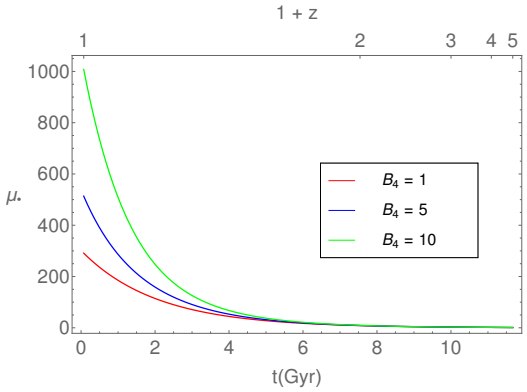

(b)

FIGURE 6.20: The spin evolution, $j(t)$, (Fig. 6.20(a)) and the mass evolution, $\mu_\bullet(t)$, (Fig. 6.20(b)) are shown for run# 3.1.1 and run # 3.1.2 when there is only accretion and BZ torque present.

- From Figs. 6.19(b) and 6.19(a), we see that the saturates without feedback and the mass continues to grow while the spin saturates.

- It can be seen from Figs. 6.19(a) and 6.20(a) that the BZ torque causes the spin down of black hole reducing it from the highest saturated spin value. As the B_4 value is increased, the spin down is more effective while the accretion is enhanced.

- From the plots (see Figs. 6.21) it can be seen that mass growth by accretion with an efficiency of ($\eta = 0.01$ or 0.05) is very small which can not generate

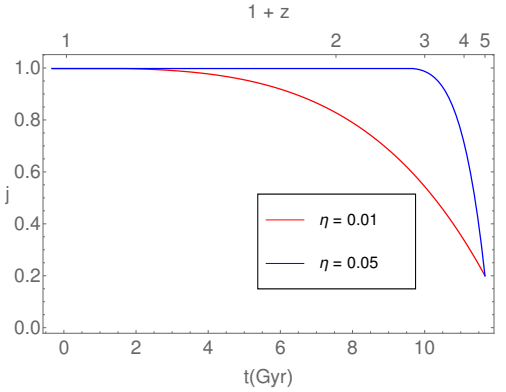

(a)

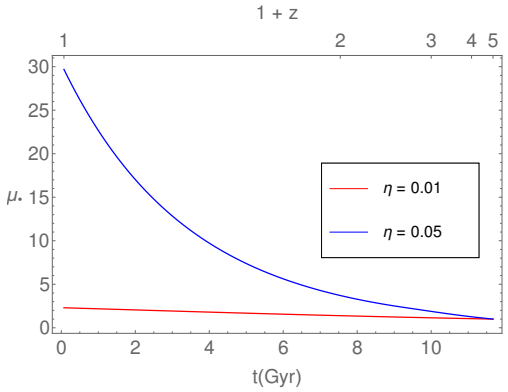

(b)

FIGURE 6.21: The spin evolution, $j(t)$, and the mass evolution, $\mu_\bullet(t)$, are shown for run # 3.2.1 and # 3.2.2 when there is only accretion and BZ torque present.

high mass black holes in the universe. Therefore $\eta \geq 0.05$.

6.3.4 Experiment 4: Gas accretion, stellar capture and BZ torque are present

In this experiment, the spin and mass evolution equations (eqns. 6.68, 6.66) take the form

$$\frac{\mathrm{d}j}{\mathrm{d}\tau} = \frac{\dot{\mu}_g}{\mu_\bullet}\Big(l_I(j) - 2\epsilon_I(j)j\Big) + \frac{\dot{\mu}_*}{\mu_\bullet}\Big(l_*(j) - 2\epsilon(j)j\Big) + \frac{4}{9}\times 10^{-5} f_{BZ} B_4 \mu_\bullet M_{s5} x_H^3(j) j. \tag{6.102}$$

$$\frac{\mathrm{d}\mu_\bullet}{\mathrm{d}\tau} = \epsilon_I(j)\dot{\mu}_g + \epsilon(j)\dot{\mu}_*. \tag{6.103}$$

where accretion, BZ torque and the stellar capture with steady loss cone theory are taken into account (Fig. 6.22).

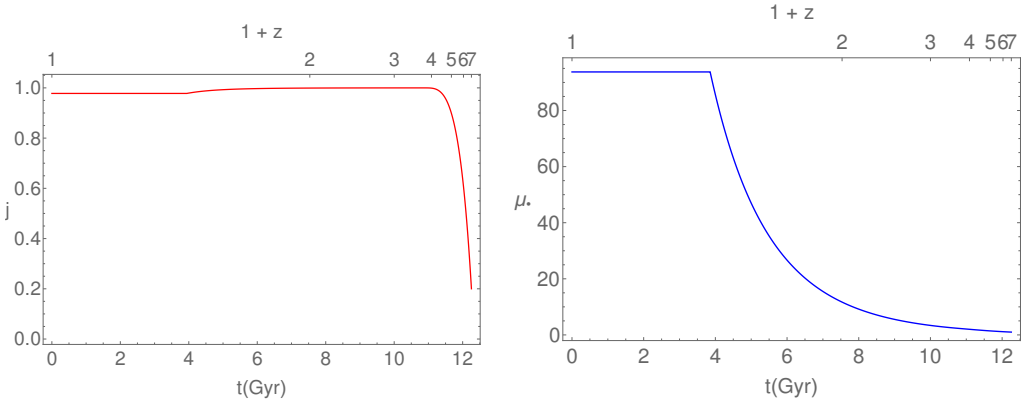

FIGURE 6.22: (a) Plots of $j(t)$ and (b) $\mu_\bullet(t)$ for $B_4 = 5$, $z_f = 6$, $\eta = 0.07$, $\gamma = 1.1$, $M_s = 10^5 M_\odot$ when there is accretion, stellar capture and BZ torque present for the canonical case (run # 4.5.4).

- By studying canonical case (run # 2.1), we find that the mass evolution does not show any significant variation with changes in parameters (k, γ, j_0) and the spin evolution does not show variation for changes in (k, γ). This is because the accretion is a dominant process in the evolution not compared to

the stellar capture. Therefore, the factors which control the stellar capture do not make a significant impact for the range of parameters considered.

We present the results and discuss the runs (# 4.1 to # 4.6) given in Table 6.4.

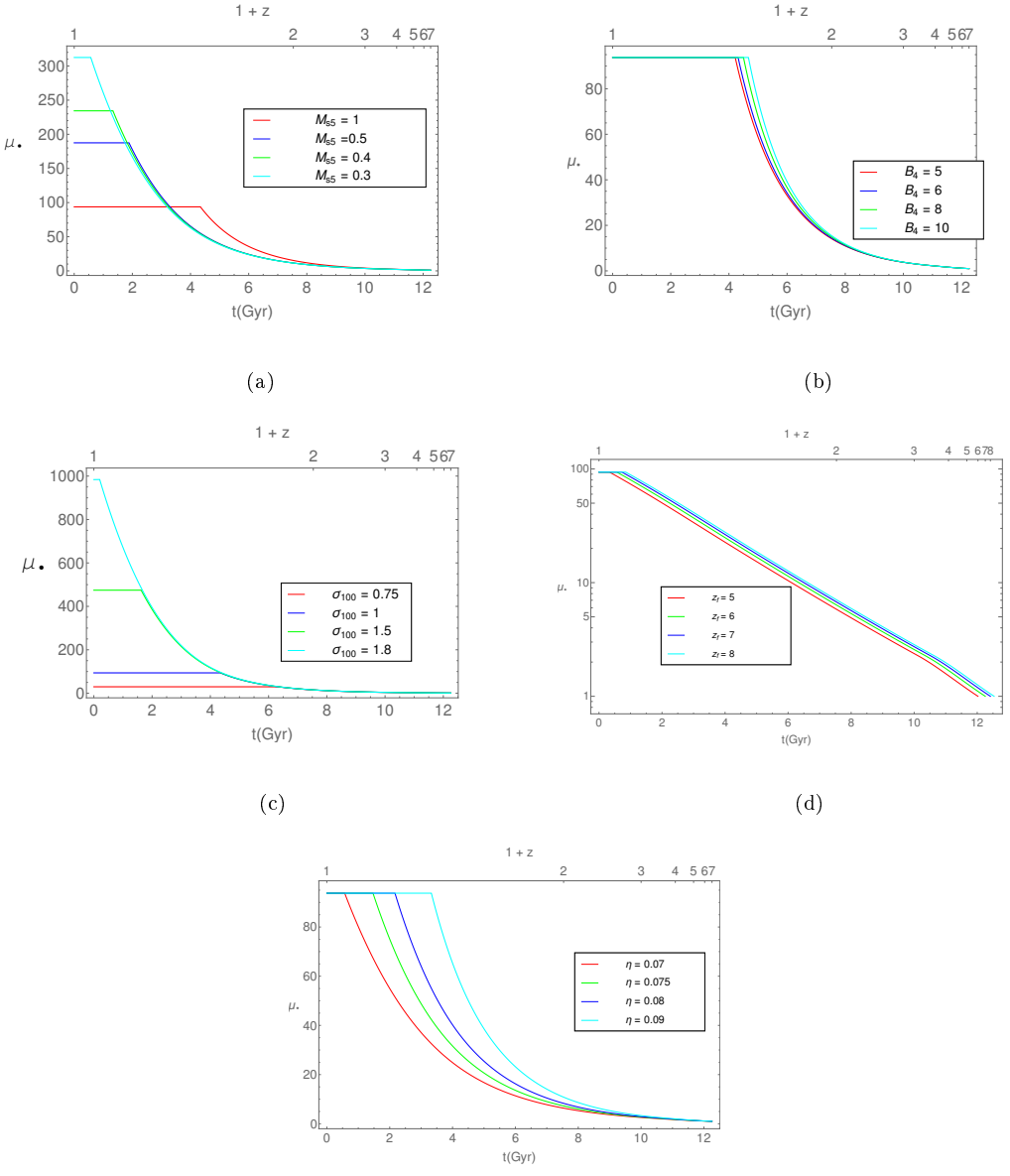

(a) (b) (c) (d) (e)

FIGURE 6.23: Plots of $\mu_\bullet(t)$ for k = -1 for run # 4.1 to run # 4.5 [(a) - (e)], for the case when there is accretion, stellar capture and BZ torque present.

- Figs [Fig. 6.23(a)) - (Fig. 6.23(e)] show the evolution of black hole mass for run # 4.1 to run # 4.5 given in Table 6.4. We see that the evolution has a small dependence on the parameters $\{k,\ \gamma,\ j_0\}$ by studying its deviation from the canonical set; so we do not show those cases here.

- If the σ is same then the final mass will be almost the same, irrespective of their initial masses [see Fig. 6.23(a)].

- Changes in B_4 and z_f (run # 4.2 and # 4.4 respectively) make little impact on the evolution and does not affect the final mass much [see Figs. 6.23(b), 6.23(d)].

- Variation of σ (run # 4.3) shifts the saturation point because of the dependence of the saturation mass on σ [see eqn. (6.61)]. Higher the σ, higher the saturation mass and larger the time taken to reach the saturation point [Fig. 6.23(c)].

- Increase of η (run # 4.5) increases the accretion rate which is the main source of mass growth. Hence for higher η, the system reaches the saturation point earlier [see Fig. 6.23(e)].

- The spin parameter j has a small dependence on the parameters $\{M_s,\ z_f,\ \eta,\ j_0\}$ (run # 4.1, # 4.4, # 4.5, # 4.6 respectively) [See Figs. (a), (d), (e), (f)] which show variation at the starting points because of different initial values of the mentioned parameters., but the final values attained are nearly the same. This result is different from that of experiment 4, where only accretion is present, this is because, we incorporate the concept of saturated mass here which causes the accretion to stop, thereby reducing the final mass attained.

- Since the decrease in j occurs at the high mass end because of the BZ effect, the decrease is small compared to the run # 3.1.1 [see Fig 6.24(b)].

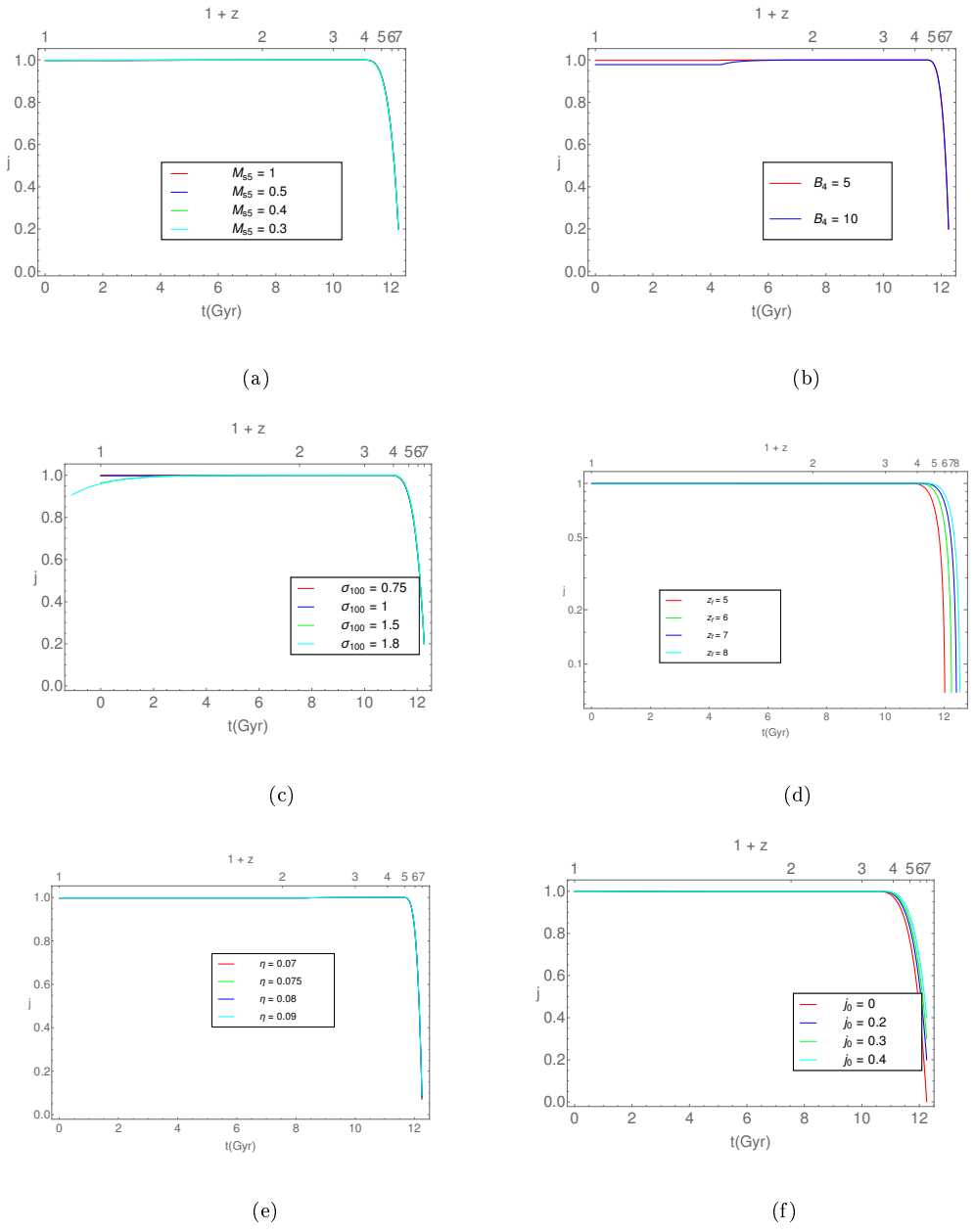

FIGURE 6.24: Plots of $j(t)$ for k = -1 for run # 4.1 to run # 4.6 [Fig. 6.24(a)) - (Fig. 6.24(f)], for the cases when there is accretion, stellar capture and BZ torque present.

- Fig. 6.24(b) shows that an increase in B_4 value (run # 4.2), decreases the final spin, as expected.

- A higher σ (run # 4.3) implies a higher final mass of the black hole; hence, the final spin value decreases with increase in σ, (Fig. 6.24(c)) keeping M_s

constant.

6.3.5 Complete model: Accretion, stellar capture, merger and BZ torque are present

Here we add the contribution of mergers to the spin and mass evolution and retain all the terms in eqn. (6.68) and eqn. (6.66) for our calculations (see Fig. 6.25).

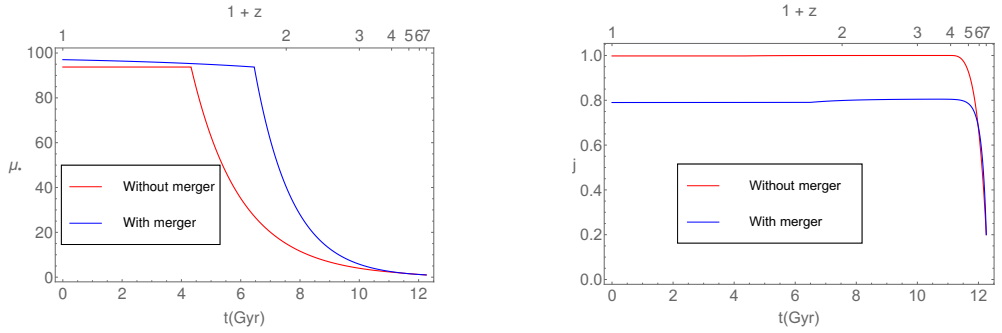

(a) Mass (b) Spin

FIGURE 6.25: Evolution of $\mu_\bullet(t)$ (a) and (b) $j(t)$ of the black hole are shown without and without the effect of mergers for the canonical case (run # 4.5.4).

Our results are the following.

- From Fig. 6.25 (run # 4.5.4) we observe the difference in evolution plots in the presence and absence of mergers. It is clearly seen from mass evolution that in presence of the mergers, the black hole reaches the saturation mass earlier due to the higher mass growth rate and that the final mass attained is higher because of the contribution of mergers.
- As we consider the merger activity to be effective from $z \lesssim 4$, we see that the two curves start deviating from each other after $z \gtrsim 4$.
- We observe from the spin evolution [see Fig. 6.25, right], that the saturated or the final spins are different for the two cases. This is due to the minor

mergers which cause the spin down of the black holes; again the evolution changes after $z \simeq 4$.

Now, we discuss the evolution in presence of all the effects and its dependence on the parameters used. Fig. 6.25 represents the evolution for the canonical case (run # 5.1.4). For the runs (run # 5.1 to # 5.6 in Table 6.4), we discuss our results obtained in Figs. [6.26(a) - 6.26(e)] for the mass evolution and Figs. [6.27(a) - 6.27(f)] for the spin evolution.

- We found that the evolution has small dependence on the parameters $\{k, \gamma, j_0\}$ in the input range.
- The difference between the complete model with (Expt 4) is that the mass evolution is faster after saturation because of the presence of the merger term as this also contributes along with the stellar capture when the gas accretion stops.

- Again, we observe from (run # 5.1 to # 5.5) [see Fig. 6.27(a)) - (Fig. 6.27(f)], that there is little variation of j for changes in parameters $\{k, \gamma, M_0\}$.
- The difference of the complete model with the experiments (Expts 3, 4) is due to the presence of the mergers; the highest value of spin acquired is lesser since the minor merger contributes in spinning down the hole.

By calculating $M_\bullet(\sigma, z)$, we obtain the evolution of the $M_\bullet - \sigma$ relation. We present a schematic of our evolution model in a flowchart (Fig. 6.15). The motivation is to isolate the contribution of different effects to the evolution of the black hole individually, and also together from $z = z_f \rightarrow 0$. This, in turn, can give us

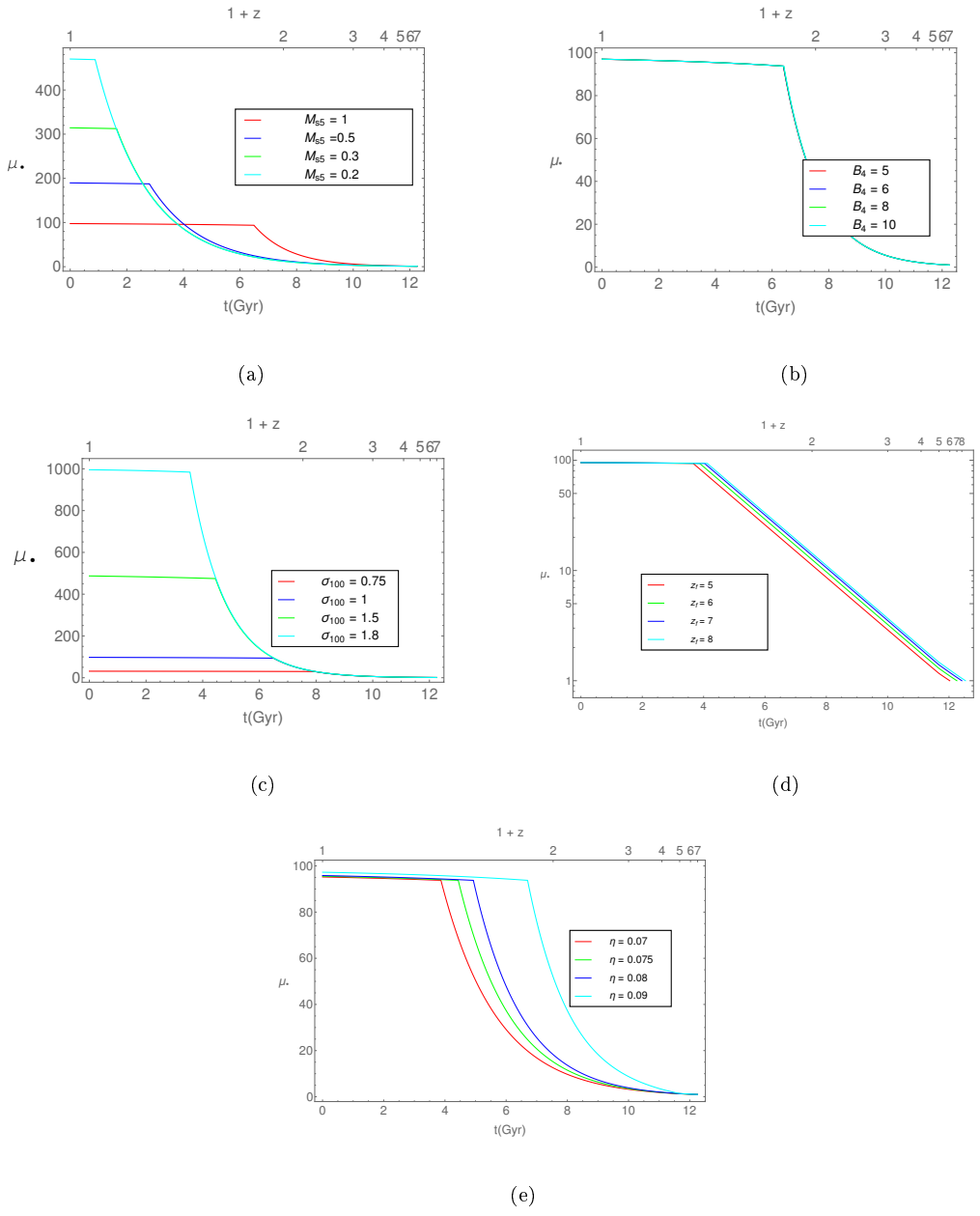

FIGURE 6.26: The mass evolution, $\mu_\bullet(t)$, for k = -1 for run # 5.1 to run # 5.5 [(a) - (e)] are shown, when there is accretion, stellar capture, merger and BZ torque present for deviation of various parameters from their values in the canonical set.

information about for the co-evolution of the black hole and the galaxy.

Next, we discuss some applications of our model.

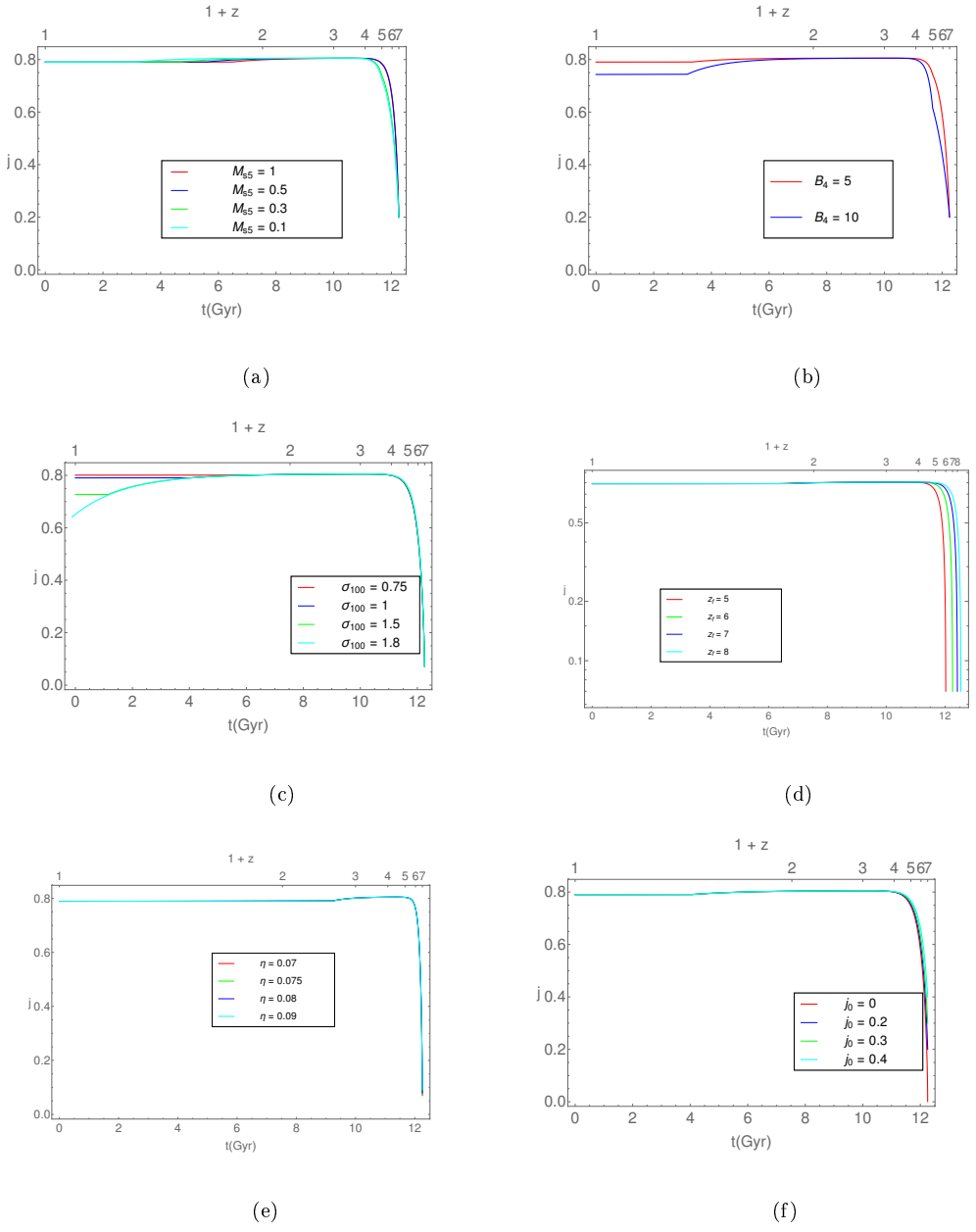

FIGURE 6.27: The spin evolution, $j(t)$, for k = -1 for run # 5.1 to run # 5.6 [(a) - (f)] are shown, when there is accretion, stellar capture, merger and BZ torque present for deviation of various parameters from their values in the canonical set.

6.4 Applications of our model

6.4.1 Impact on the $M_\bullet - \sigma$ relation

All the solutions of $M(z)$ are dependent on the value of σ, which fixes the value of t_s and z_s for different galaxies given the same M_s. We have assumed the value σ is constant from formation redshift till present time since its variation is relatively small and reduces over Hubble time by a factor $\sim 15\%$ (Shankar *et al.* (2009a), Fig. 8). We have discussed this in §6. In the future, we can include the time variation of σ using an empirical form motivated by (Shankar *et al.* 2009a) which assumes a small variation $\sigma(z) = \sigma_0(1+z)^{-\gamma}$, where σ_0 is the present-day value of σ. But for now, the focus is to isolate all the other effects first. We have calculated $M_\bullet(\sigma, z)$ and derived $p(z)$, the index of the $M_\bullet - \sigma$ relation [see Fig 6.28]. In deriving $p(z)$, we have considered the observed range of $\sigma(z)$, to derive the corresponding range of $M_\bullet(z)$ using our evolution model. To start with, we assumed that at the formation redshift, the index $p = 5$, which is provided by the Faber - Jackson relation. It is a reasonable assumption, given that BH formation models produce masses proportional to the bulge mass (Mangalam 2001). Even if this were not true for the small initial seed mass, the power-law index $p(z)$ would eventually be dominated by the gas and star accretion that inflates the final mass by a factor $M_\bullet \simeq (10^3 - 10^4)M_s$. This is just an initial condition to derive the evolution which clearly does not change the long term or near term value of p; it is an initial fiducial value. At the saturation time, the value of $p = 4$, as predicted by the King (2003) model. Thereafter, the black holes grow by stellar capture and mergers alone. Since the growth rate reduces, the slope almost remains near 4 after the saturation.

Now, we discuss the dependence of $p(z)$ on the parameters $\{B_4, z_f, j_0\}$. First figure in the upper panel of Fig. 6.28 shows $p(z)$ for the canonical case and the other

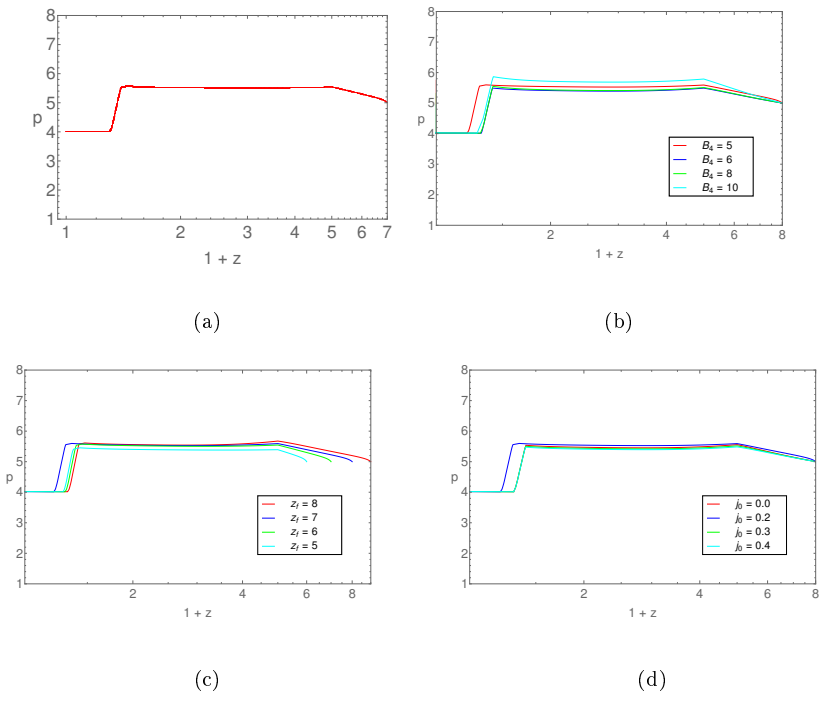

FIGURE 6.28: The evolution of $p(z)$ for $\gamma = 1.1$, $M_s = 10^4 M_\odot$ is presented above [the top left figure shows the canonical case, the variation with B_4 is seen in the top right figure for $\{z_f = 7, j_0 = 0.2\}$, the variation with z_f in the bottom left for $\{B_4 = 5, j_0 = 0.2\}$, and the variation with j_0 in the bottom right with $\{z_f = 7, B_4 = 5\}$].

plots of Fig. 6.28 shows its deviation in the parameter space of $\{(B_4,\ z_f,\ j_0)\}$ in Figs. 6.28. We see a change of slope to $p = 4$ near the saturation point as expected, following the dependence for momentum driven flow [see eqn. (6.61)]. Before z_s, the the p value is almost constant which agrees with the previous work that find little evolution of the $M_\bullet - \sigma$ relation. A more accurate evolution can be carried out by considering the mass and redshift distribution function of the black holes to carry out a population synthesis to derive $p(z)$ (Sijacki *et al.* 2015). In the Fig. 6.28, we observe for all the cases that there is little variation with changes in $\{B_4, z_f, j_0\}$ in the considered range. Thus, we conclude that this relation is expected to be within the observed range of 4 - 5 as $z_f \to 0$. Next, we compare our results with data obtained in Bhattacharyya and Mangalam (2018) from the observed intensity profiles of these galaxies listed in Wang and Merritt (2004). These galaxies are within redshift range 0.004 - 0.002 (see Table 6.5).

#	Galaxy	$M_\bullet$ (in $10^7 M_\odot$)	σ (km/sec)	z
1	NGC 3379	13.6	230	0.00304 ± 0.00001
2	NGC 3377	2.60	217	0.00222 ± 0.00001
3	NGC 4486	188	433	0.00428 ± 0.00002
4	NGC 4551	3.77	218	0.00392 ± 0.00002
5	NGC 4472	117	542	0.00327 ± 0.00002
6	NGC 3115	17.0	230	0.00221 ± 0.00001
7	NGC 4467	0.493	77	0.00475 ± 0.00004
8	NGC 4365	67.7	453	0.00415 ± 0.00002
9	NGC 4636	58.0	251	0.00313 ± 0.00001
10	NGC 4889	299	467	0.02167 ± 0.00004
11	NGC 4464	1.12	112	0.00415 ± 0.00001
12	NGC 4697	20.76	215	0.00414 ± 0.00001

TABLE 6.5: Data from BM18 (based on Wang and Merritt (2004) for 12 galaxies used for matching our results with observations are given above.

In Fig. 6.29, the red curve corresponds to $z = 0.003$ and the green curve corresponds to $z = 0.23$. We see that the red curve gives the better fit to the data presented in Table 6.5, which is similar to observed values as the range of redshifts of these galaxies are in the range 0.001 - 0.004.

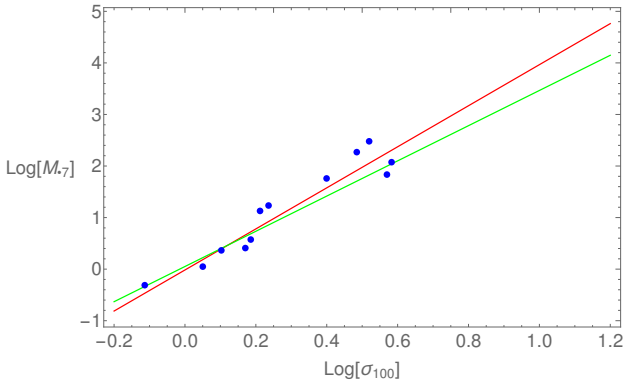

FIGURE 6.29: A plot of $\log(M_{\bullet 7})$ vs $\log(\sigma_{100})$ for two different redshifts [$z = 0.003$, (red) and $z = 0.23$, (green)] is shown, calculated from our evolution model and compared with the data obtained from our model in BM18 for the 12 elliptical galaxies (whose) redshift lies in the range 0.004 - 0.002).

Shankar *et al.* (2009a), analyzed the data of over 40000 early-type galaxies from Sloan Digital Sky Survey (SDSS) and they determined $k_0(z) \propto (1+z)^{0.33}$ [see

eqn. (3.1)]. According to their analysis, this relation almost holds throughout the age of the Universe. Our model also predicts an almost a constant p throughout the entire redshift range as expected from eqn. (3.30). We have also shown $k_0(z)$ starting from an approximate value (considering the Faber Jackson relation with the seed mass within the considered range and σ). Since we have considered a constant σ, $k_0(z)$ is predicted to decrease.

According to Shankar *et al.* (2009a), the $M_\bullet - \sigma$ relation is given by

$$\log[M_\bullet/M_\odot] = 8.21 + 3.83\log[\sigma_{200}] + \alpha\log[1+z]. \tag{6.104}$$

If we consider the definition above using $\alpha = 0.33$ and assume the empirical relation $\sigma(z) = \sigma_0(1+z)^{-0.25}$, where σ_0 is the present day velocity dispersion to calculate $M_\bullet(t)$ we find that the final $M_\bullet$ is similar to the prediction from our evolution model; see Fig. 6.30(b) which compares $M_{\bullet 5}(t)$ from eqn. (6.104) with our model prediction for ($M_s = 10^5 M_\odot$, $\sigma_{100} = 1$). We see that if the σ stays constant, the final mass attained is also nearly same which was also concluded by Alexander and Bar-Or (2017b).

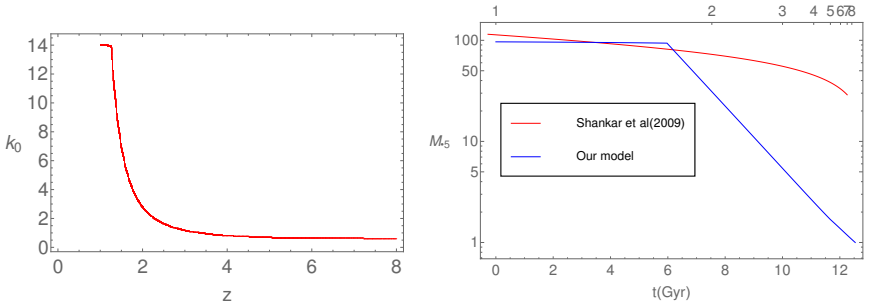

(a) (b)

FIGURE 6.30: The evolution of the index $k_0(z)$ for $\gamma = 1.1$, $M_s = 10^4 M_\odot$ is shown for the canonical case (left) and (right) $M_{\bullet 5}(t)$ from prescription of Shankar *et al.* (2009a) and our model for $M_s = 10^5 M_\odot$.

6.4.2 Black hole archaeology

If we use the final mass and spin as boundary conditions of the mass evolution, we can evolve our model backward in time, a process which we coin as *black hole archaeology*. Campitiello *et al.* (2019) studied the Optical-UV emission of distant quasars ULASJ134208.10+092838.61 (z=7.54), ULASJ112001.48+064124.3 (z=7.08) and DELSJ003836.10-152723.6 (z=7.02) to study their properties and found the presence of an accretion disk. They used relativistic disk models KERRBB and SLIMBH to model the emission with approximations to describe the emission as a function of $M_\bullet$, η, j and the viewing angle, θ_ν. They found that the accretion rate for all sources is sub - Eddington. They find out if the seed black holes with masses in the range $10^2 - 10^4 M_\odot$, grow during $z_f = 20 - 10$ in these sources, at Eddington accretion rate, it will reach the present-day mass within 0.7 Gyr.

	Input parameters		Combinations of$\{M_{\bullet s}$ (in $10^9 M_\odot$), $j_0\}$		
#	η	j_f	$z = 10$	$z = 15$	$z = 20$
1	1	0.7	{0.12, 0.76}	{0.06, 0.8}	{0.02, 0.5}
2	0.1	0.7	{0.75, 0.65}	{0.63, 0.55}	{0.6, 0.27}
3	1	0.45	{0.1, 0.7}	{0.05, 0.75}	{0.02, 0.5}
4	0.1	0.45	{0.75, 0.45}	{0.63, 0.38}	{0.6, 0.25}

TABLE 6.6: Combinations of seed mass and spin, $\{M_{\bullet s}, j_0\}$, at $z_f = \{10, 15, 20\}$ for quasars with mass $\simeq 10^9 M_\odot$ at $z \simeq 7$ for different sets of input parameters, $\{\eta, j_f\}$, where, j_f is the final spin at $z = 7$.

We observe from the mass and spin values for the quasars listed in Table 1 of Campitiello *et al.* (2019), (as determined through KERRBB and SLIMBH models), that the following input sets of $\{\eta, j_f\} = \{\{1, 0.7\}, \{0.1, 0.7\}, \{1, 0.45\}, \{0.1, 0.45\}\}$ are suggested. They have also calculated $M_\bullet$ for $j_f = \{0, 1\}$, the extreme ends of the spin values. We have taken the final mass to be $M_\bullet \simeq 10^9 M_\odot$ at $z \simeq 7$ (as suggested by their models) and evolved our model backwards the for different sets

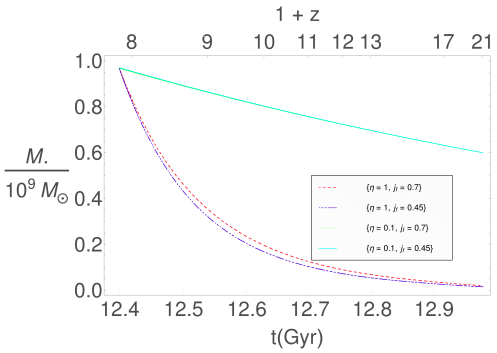

(a)

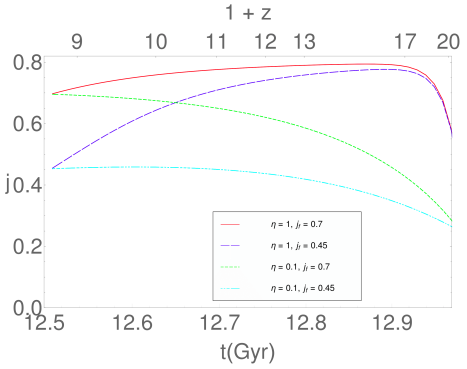

(b)

FIGURE 6.31: $M_\bullet(t)$ and $j(t)$ evolution for different combinations of η and final spin at $z \simeq 7$, j_f for $z_f = 20$ are shown for final mass at $z \simeq 7$, $M_f \simeq 10^9 M_\odot$.

of $\{\eta, j_f\}$ given above to find the initial seed masses at $z_f = 20$. We see that when $\eta = 1$, the seed mass is also quite lower as compared with the case of $\eta = 0.1$ (see Table 6.6); this is expected due to the difference in accretion rate [see Fig. 6.31(a)]. The j_f values does not make much difference to $M_\bullet(t)$ when η is fixed. For the case of spin evolution, when $\eta = 1$, the j increases and then decreases, but for $\eta = 0.1$, it continues to decrease [see Fig. 6.31(b)] as we see from Table 6.6. The reason is that for high accretion rate, the spin reaches maximum value rapidly and then it reduces due to the presence of BZ torque and minor mergers to j_f; but, when $\eta = 0.1$, the mass growth is slower, so it does not reach the maximum spin within the short time of less than a Gyr, as both BZ and merger terms are mass dependent and hence not as effective. It seems that a heavy seed of nearly

$M_s = 10^7 M_\odot$ is required at $z = 20$ even if $\eta = 1$ (see Table 6.6). This poses difficulties for black hole formation models (eg. Pandey and Mangalam (2018)) or for the mass suggested by Campitiello *et al.* (2019).

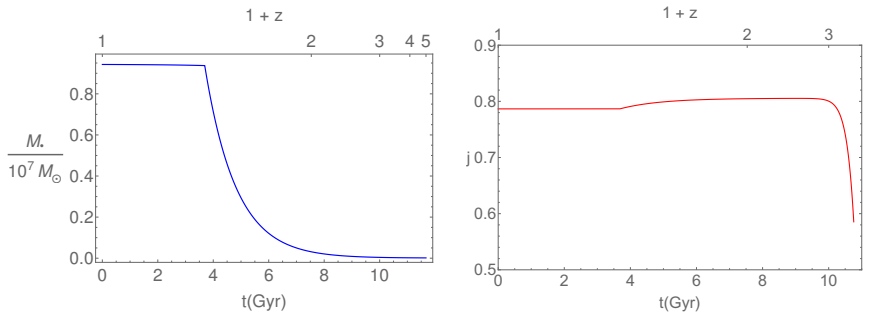

(a) (b)

FIGURE 6.32: (a) $M_\bullet(t)$ and (b) $j(t)$ evolution for the complete model, are shown, starting from final mass $\mu_{\bullet 5} = 94.3$ with other parameters the same as that of run # 5.1.4.

For comparison, we also evolve the final configuration, $\{M_\bullet = 10^7 M_\odot, j_f = 0.8, z_f = 0\}$, that is shown in Fig. 6.32. We see from Fig 6.32(a) that the mass reaches a seed value of $3.5 \times 10^4 M_\odot$, which is typical and Fig. 6.32(b), indicates a seed spin of $j_s = 0.58$. With these illustrations, it is clear that our model is a useful tool for black hole archaeology.

We summarize our results in the next section.

6.5 Summary of the results and caveats

The key novel aspects of the paper are the relativistic inputs of the capture radius and tidal radius to the loss cone formalism, determining the applicable range of steady loss cone theory, and including all known contributions of gas, stellar, electromagnetic torque and mergers through detailed formulae as recipes for calculating the joint spin and mass evolution relativistically while taking into account

the effects of saturation, merger regimes, and the mode of stellar ingestion. We have applied this elaborate model to make predictions for the capture rate of stars, $\dot{N}_s$, for the evolution of the $M_\bullet - \sigma$ relation and in retrodicting the initial black hole configurations from their more recent inferred ones. The detailed findings are summarized as follows.

1. We calculate r_t using the effective Kerr potential to include the effect of the spin parameter and find $x_t(M_8, j, Q)$ (see Figs. 6.2, 6.3 for both prograde and retrograde case). We see from Fig. 6.2, that a higher j reduces x_t due to the relativistic potential. From Fig. 6.3, we see that $x_t(Q)$ is important in deriving r_t and $l_\ell(Q)$, which has an impact on $\dot{N}$. Even a small change in $x_t(Q)$ has an impact on l_ℓ.

2. We calculate the loss cone radius $x_\ell = \mathrm{Max}[x_t, x_c]$ (Fig. 6.5). For higher mass black holes, the prograde capture radius, x_c goes down dramatically, so it reduces the capture rate. x_ℓ (see Fig. 6.6) has an impact on $\dot{N}_s(M_\bullet, j, k, Q, \epsilon_s, \sigma)$ which reduces with mass but increases with spin for both the prograde and the retrograde cases. This can be further explored with axisymmetric distributions $f(E, L_z)$ as as it is known that the Carter's constant represents $L^2 - L_z^2$. A critical mass value of $M_c(j, Q) \simeq 3 \times 10^8 M_\odot$ is found; for higher masses r_ℓ is set by r_c instead of the tidal radius (Fig. 6.4); $M_c(j, Q)$ changes significantly with spin and this has implications for cosmic evolution and its impact on $\dot{N}$ and black hole growth that needs to be explored (see Fig. 6.4).

3. We also calculate an relativistic correction to the tidal radius shown in eqn. (6.14).

4. We calculate the effects of stellar capture for both full and steady loss cone theory. For practical purposes, we find that the steady loss cone model is more appropriate. We have calculated the $\dot{N}_s$ using the prescription given by MM15 (but by not assuming an $M_\bullet - \sigma$ relation) while adding the relativistic

corrections to r_ℓ, as shown in Fig. 6.8 to obtain $\dot{N}_s(M_\bullet, j, k, Q, \epsilon_s, \sigma)$. This is smaller typically by a factor of 10 than the non - relativistic model of MM15. Our predicted capture rates (see Fig. 6.8) of 10^{-5} – 10^{-6} yr^{-1} can explain the observed (Komossa 2015; Donley *et al.* 2002; Gezari *et al.* 2009) of around 10^{-5} yr^{-1} (dominated by black holes of $M_8 \lesssim 0.01$) and is a key result.

5. We calculate the impact of the evolution on the spin, mass of the SMBH [Fig. 6.27, 6.26] and $M_\bullet - \sigma$ relation (Fig. 6.28) as a function of redshift in a ΛCDM cosmology. We performed five experiments by adding the contributions of gas accretion, stellar capture, BZ effect, and mergers one by one and showed how it impacts the evolution and are useful illustrations of the individual effects.

6. In §6.3.2, we derive the mass evolution in non - relativistic case assuming full loss cone theory by analytical expressions considering only accretion and stellar capture. We present the evolution of $M_\bullet(z)$ for different cases in Fig. 6.18. We have also considered the BZ torque which contributes to spinning down the black hole with a strong poloidal magnetic field that extracts the spin energy, causing a spin down of the black hole. Next, we studied the evolution of the spin and mass including all the effects one at a time. Fig. 6.20 shows the evolution in the presence of only accretion and BZ torque. while Figs. 6.24 and 6.23 show the evolution in presence of accretion, stellar capture and BZ torque. All the effects of accretion, stellar capture, mergers, and BZ torque have been included for different parameter sets in Figs. 6.26 and 6.27. The merger activity drops off after $z \gtrsim 4$.

7. We compare our results of $p(z)$ with available observations (Fig. 6.29) given in Bhattacharyya and Mangalam (2018), where σ was calculated from observed intensity profiles for a set of galaxies given in Wang and Merritt (2004).

8. Our model for $p(z)$ in the range $z = z_f \to 0$ is with a constant σ, assuming that minor mergers do not change it substantially. This is seemingly consistent with observed p in the nearby redshift range. But our predictions need to be tested by simulations and data available from future missions like Thirty Meter Telescope (TMT), Very Large Telescope (VLT) and Extremely Large Telescope (ELT).

9. We have assumed that the seed mass, $M_s \propto \sigma^5$, as suggested by the Faber Jackson relation for deriving the evolution of the $M_\bullet - \sigma$ relation, as an application of our evolution model. Subsequently, the black hole grows impacting $p(z)$.

10. We conclude that $p(z)$ changes gradually with redshift. Therefore we expect that the late-type galaxies will have a higher p compared to the early types as suggested by McConnell and Ma (2013).

11. Our model is useful for carrying out black hole archaeology. Fig. 6.32 shows the evolution obtained when we run our model backward using the present day $\{M_\bullet, j\}$ as the initial conditions and we found the seed mass to be $\simeq 3.5 \times 10^4 M_\odot$, which is within the range of seed masses considered.

We discuss these results in the next section.

6.6 Discussion

Stellar capture rate of black holes: The rates of tidal disruption events for a single black hole in steady-state have been derived by different authors as already mentioned in chapter 1, with various physical effects included such as the Nuker profiles (Syer and Ulmer 1999), non-spherical galaxies, (Magorrian and Tremaine

1999), resonant relaxation (Rauch and Tremaine 1996) and its quenching by relativistic precession (Rauch and Ingalls 1998), and black hole spin (Kesden 2012). The theoretical estimates range from $10^{-6} - 10^{-4}$ yr^{-1} for the most part, while the observational results of Komossa (2015); Donley *et al.* (2002) (ROSAT surveys), Gezari *et al.* (2009) (in UV band) have provided rates of TDEs for different wavelength bands to be about $\lesssim 10^{-5}$yr^{-1}. MM15 model the non-relativistic steady-state loss cone regime, taking into account the angular momentum dependence. We have expanded the theory to include relativistic effects in a Kerr potential to calculate the tidal and capture radius which in turn, is an input to the loss cone theory that determines the rate of stellar capture. MM15 considered non-relativistic theory and used $L_\ell(\sigma, r_t) = \sqrt{2r_t^2\phi_(r_t) - E}$. But in our relativistic model, $L_\ell(j, k, x_\ell, Q)$ is given by eqn. (6.19) where the loss cone radius, x_ℓ is used instead of x_t as was done in MM15; this causes a decrease in the value of $\dot{N}_s$ by a factor of a few, due to the decrease of the loss cone radius, bring it more in line with observed estimates.

Alexander and Bar-Or (2017b) determined the minimal mass of the present-day black holes by including the stellar capture process. They conclude irrespective of the seed masses that, if σ of the galaxies are nearly equal, then all the black holes reach almost the same mass, assuming that the $M_\bullet - \sigma$ relation holds throughout. All the black holes grow over the age of the Universe to the present-day mass scale of $M_6 \gtrsim 0.2$ (5% lower confidence level), independent of their initial seed mass and the formation process. They conclude that the present-day $M_\bullet$ is nearly independent of the uncertainties in the black hole formation time, and provide a universal minimal mass estimate for the black holes that grow by gas accretion or mergers. This can explain the reason for not finding any intermediate-mass BHs with $M_6 \lesssim 0.2$, and which in turn implies that present-day galaxies which have $\sigma \lesssim 35$ km s^{-1} (5% lower confidence level) do not contain a central BH. We derive the evolution without any apriori assumption of $M_\bullet - \sigma$ relation throughout and also take into account all known effects causing the growth of the black hole

and with relativistic effects in case of stellar capture including the spin evolution which is not included by Alexander and Bar-Or (2017b). Our result agrees with their finding that the final mass attained by the hole is nearly independent of the formation time. Fig. 6.12 shows the mass evolution in the presence of only stellar capture which matches the result of Alexander and Bar-Or (2017b) [see Fig. 6.12]. The black holes with higher seed masses will reach the saturation point earlier as they will grow their masses lesser by accretion and more by mergers and stellar capture as compared to the smaller mass seed black holes.

Mass and spin evolution of the black hole: The spin and the mass evolution of a supermassive black hole (SMBH) is mainly dependent on three processes, gas accretion, the capture of stars and mergers. We built a formation for relativistic loss cone theory and included it in the mass and spin evolution of black holes. For accretion, we have used a constant sub - Eddington accretion efficiency throughout the process, taking into account duty cycles. In the case of gas accretion with cooling sources, the flow is momentum-driven (King 2003). The stellar capture rate has been carried out in both full and steady loss cone theory framework. We have incorporated the prescription of saturated mass by King (2003), which causes a halt in accretion leaving the stellar capture and mergers only to contribute to the growth of the black hole. For the mass growth of SMBH by mergers, we have considered both the contributions of major and minor mergers (Stewart *et al.* 2009). The rate of minor mergers is more frequent compared to the major ones. Major mergers contribute to spinning up the black hole while minor mergers spin it down (Gammie *et al.* 2004). We neglect the contribution of the major merger in spinning up the hole and consider only the effect of the minor merger in spinning down the hole. We have considered the mergers to be effective from $z \lesssim 4$.

We now compare our results with previous studies. Mangalam (2015) used a theoretical model for mass and spin evolution of the accreting black hole taking into account the spin-down torque caused by the electrodynamical jet. The evolution

in the presence and absence of accretion was studied for different cases such as the thin disk, Bondi accretion, and the MHD disk. When accretion stops, the jet power shows an increase before a gradual decrease if the initial spin, $j > \sqrt{3}/2$, because of the increase in the size of the black hole. The results indicate that the black hole achieves the maximum spin value in the absence of a jet. We use the evolution equations given there and add to it terms representing stellar capture and mergers. Dubois *et al.* (2014) has derived the mass evolution through simulations caused by accretion and mergers and used semi-analytic methods for spin evolution for the same. Our results agree with their result that the low mass black holes grow their mass mainly by the accretion process whereas high mass black holes ($> 10^8 M_\odot$) grow their mass mostly by mergers. This is because accretion halts due to saturation beyond $M_\bullet > M_{\bullet t}$ and the low mass grows slowly by stellar capture. We have considered a constant rate of Eddington accretion while they have considered to be reducing over time due to gas rarefaction in galaxies. The justification for considering our parameter ranges is given in §6.3. From the mass evolution plot (Fig. 6.25) we see a change in the slope near the saturation time. This is expected that the accretion of gas stops and stellar capture and merger activity take over for subsequent growth. The rate of growth for mass accretion is much greater than the other two; so the halt of accretion causes the slope change. Zhang and Lu (2019) have studied the spin evolution via two-phase accretion and have found that higher mass black holes have intermediate spin (~ 0.5), while the low mass black holes have higher spin ($\gtrsim 0.8$). In our paper, we have studied accretion only in the the thin disc mode. The low value of spin for higher masses can be explained: as and when the BZ effect dominates, it causes the spin-down of the black hole. It is possible that the low mass black holes are a result of gas accretion alone and without mergers; hence the spins are higher. Zhang and Lu (2019) have also assumed a power-law dependence of the radiative efficiency with the black hole mass where it decreases with an increase in mass, though they have found the dependence to be weak. This is in contradiction with the model of Davis and Laor (2011), who claims an increase with mass with power-law index

0.5. Here, we aim to capture a complete picture of black hole growth using all the factors contributing to it. For simplicity, we consider the radiative efficiency to be constant with a goal to study and compare all the other contributing factors. We intend to include the mass variation of radiative efficiency in the future. Since the dependence is weak, it is not likely to make a significant difference in our results.

From Fig. 6.25, we see that the spin of the black hole initially increases because of accretion, after which there is a spin down due to the BZ torque. Since we have considered a thin disc accretion, the spin value very quickly reaches the maximum spin as mentioned by Li (2012). Gammie *et al.* (2004) showed how accretion, major and minor mergers contribute to the spin evolution of the black hole. Using the prescription given by Gammie *et al.* (2004) for minor mergers, we see that the value of the maximum spin attained is much less than those where the contribution of mergers is considered. We have included minor mergers only to the spin-down of the hole as the spin-up process is already dominated by the accretion process.

Our model is useful for retrodicting the initial black hole configuration when we run our model backward from the observed $\{M_\bullet, j\}$ as the initial conditions as shown in §6.4.2. More observations and models that provide the final spin state will provide useful clues for such exercises in black hole demographics.

Evolution of the $M_\bullet - \sigma$ relation: We have combined all the known effects contributing to the mass and spin evolution of the black hole and thus derived the evolution of the $M_\bullet = k_0(z)\sigma^{p(z)}$ relation by semi-analytic methods; some preliminary results were shown in Bhattacharyya and Mangalam (2018b). Shen *et al.* (2015) and Salviander and Shields (2013) have studied the evolution of the relation from SDSS data for quasars and have found no evolution of the $M_\bullet - \sigma$ relation up to $z \simeq 1$. Numerical simulations of the large-scale structure of the universe as done by Sijacki *et al.* (2015) and Taylor and Kobayashi (2016) show that this relation holds almost up to $z \simeq 4$. Robertson *et al.* (2006) have studied the evolution of

this relation till $z = 6$ for merging disk galaxies through hydrodynamic simulations taking into account the effects of accretion and supernovae. They have found almost no change in $p(z)$ and a very small change of $k_0(z)$ similarly as suggested by Shankar *et al.* (2009a). From their analysis, $k_0(z) \propto (1+z)^{\alpha}$, with $\alpha = 0.33$. In our analysis, since we consider σ to be a constant throughout so that the value of k_0 is expected to decrease at higher redshift as we show in Fig 6.30(a). At the saturation point, the value of p is $\simeq 4$ from our model as per the prescription by King (2003). We have considered a range of values of $\sigma_{100} = \{1-2\}$, which is the average observed range of σ for different galaxies and assumed $M_{\bullet}(z = z_f) \propto \sigma^5$ as set by the Faber Jackson relation. From Fig. 6.28, we see that $p(z)$ remains in the range $4-5$ throughout the entire time, which roughly agrees with the empirical result of Shankar *et al.* (2009a). Fig. 6.28 shows higher value of $p(z)$ at higher redshifts. Therefore, we conclude that $p(z)$ will be higher for late-type galaxies as suggested by McConnell and Ma (2013). One possibility is that the σ varies with redshift due to major mergers, but this is outside the scope of this paper. For minor mergers, σ = constant is a reasonable assumption that is based on the work of several authors [Oser *et al.* (2012), Hopkins *et al.* (2009), Bezanson *et al.* (2009), and the dissipative model described by Shankar *et al.* (2009a)], where they have stated that σ changes little with redshift [σ reduces over Hubble time by a factor $\sim 15\%$, Shankar *et al.* (2009a)]. The elliptical galaxies which obey the $M_{\bullet} - \sigma$ relation is within this specified redshift. We conclude from our simulations that although $p(z)$ varies with $\{j_0,\ B_4,\ z_f\}$, it stays within the predicted range of $4-5$.

6.7 Conclusions

Our model of deriving the joint evolution of black hole mass, spin as well as the $M_{\bullet} - \sigma$ relation throws light on the co-evolution of the black hole and its

environment from the time of formation. We have incorporated all the factors contributing to the growth of the black hole to build a comprehensive evolution model of the black hole.

1. We have included relativistic effects in the process of tidal and direct capture. A key consequence is that the capture rate reduces to the range $10^5 - 10^6$ yr^{-1}, which is more in line with observations.

2. We have built a semi-analytic self-consistent evolution model of the black hole.

3. We have explored the role and phases of importance of each of the growth channels. We find that accretion is dominant before saturation.

4. We illustrated the effect of saturation on the evolution of the $M_\bullet(z) = k(z)\sigma^{p(z)}$ relation.

5. By running the models backward in time, we retrodict the formation parameters of seed black holes. This will enable us to discriminate among models of black hole formation.

6. We expect our transparent and detailed formulation in a fully relativistic framework to be useful for future simulational studies.

This model can be improved by incorporating a model for time variation of η which is an uncertain input. The data from future surveys at high redshift, for example from TMT, VLT and ELT along with measurements of σ from SKA, can be used to probe the $M_\bullet - \sigma$ evolution to test our model. We also plan to work on the demographics of the black hole, based on a model for the prior of seed mass and spin distribution functions..

Chapter 7

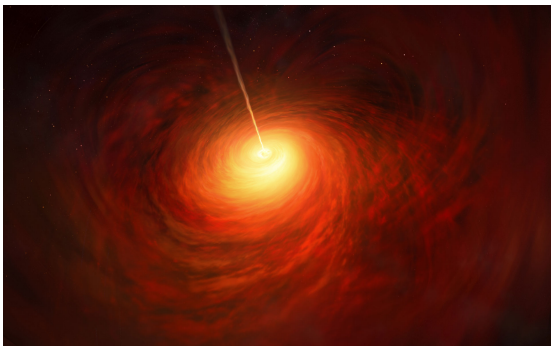

Image: scitechdaily.com

Unfulfilled agenda: $M_\bullet - \sigma$ relation in axisymmetric systems and the initial seed mass and spin function*

In this chapter, we will discuss two ongoing projects: $M_\bullet - \sigma$ relation in axisymmetric systems and derivation of initial seed mass and spin functions. We will also present some preliminary results for these two problems and discuss the future plans of these two projects.

*This chapter contains material from papers in preparation

7.1 $M_\bullet - \sigma$ relation in axisymmetric systems

We extend the formulation for spherical systems (Bhattacharyya and Mangalam 2018) for prescribing the $M_\bullet - \sigma$ relation and the $M_\bullet - M_b$ relation simultaneously to axisymmetric systems. Unlike the spherical case, finding the axisymmetric distribution function is much more challenging and it involves complex analysis (Hunter and Qian 1993). But, in their analysis, they used only the stellar potential for deriving the distribution function (DF) while we need to include the black hole potential to obtain the distribution function in presence of the black hole. This is to be used for determining the LOS velocity dispersion, σ, which in turn gives the $M_\bullet - \sigma$ relation. Later on, Qian *et al.* (1995) added the black hole potential and derived the distribution function separately for large and small radii using the Hunter and Qian (1993) algorithm. Here, we also use the same DFs derived by Qian *et al.* (1995) and using the continuity of the DF to be a boundary condition, to obtain a joint DF to derive σ. The geometry of the system used here is the same, as the one discussed in Chapter 2 [see Fig. 2.4].

7.1.1 The model of Qian *et al.* (1995)

A density of the form $\rho(m^2)$ is assumed, which is a well known form of the density previously used by Perek (1962), de Zeeuw and Pfenniger (1988). Qian *et al.* (1995) uses the mass density given by

$$\rho(m^2) = \rho_0 \left(\frac{m}{b}\right)^{\alpha} \left(1 + \frac{m^2}{b^2}\right)^{\beta}, \tag{7.1}$$

where, $m^2 = R^2 + z^2/\bar{q}^2$, $\bar{q}$ is the axis ratio axis ratio, ρ_0 is a reference density, b is the reference length , $-3 < \alpha \leq 0$, and $\beta \leq 0$. For, $\alpha = 0$, the central density is ρ_0, which is finite and for $\alpha < 0$, the central density shows a cusp profile. Far from the center, the density varies as $r^{\alpha+2\beta}$. The surface density of these spheroidal

models can be written as

$$\Sigma(m'^2) = \frac{\bar{q}}{\bar{q}'} \int_{m'^2}^{\infty} \frac{\rho(m^2) dm^2}{\sqrt{m^2 - m'^2}}, \tag{7.2}$$

where, $q'^2 = x'^2 + \dfrac{y'^2}{q'^2}$, and $\bar{q}'$ is the axial ratio observed, which is given by

$$\bar{q}'^2 = \cos^2 i + \bar{q}^2 \sin^2 i, \tag{7.3}$$

where, i is the inclination. For ellipsoidal bodies, the gravitational potential can be written as

$$\psi_*(R^2, z^2) = \pi G \bar{q} \int_0^{\infty} \frac{\mathrm{d}u}{\Delta u} \int_U^{\infty} \rho(m^2) \mathrm{d}m^2, \tag{7.4a}$$

$$= \psi_*^0 - \pi G \bar{q} \int_0^{\infty} \frac{\mathrm{d}u}{\Delta u} \int_0^{U} \rho(m^2) \mathrm{d}m^2, \tag{7.4b}$$

where, Δu and U are given as

$$\begin{aligned} \Delta u &= (1+u)\sqrt{\bar{q}^2 + u}, \\ U &= \frac{R^2}{1+u} + \frac{z^2}{\bar{q}^2 + u}, \end{aligned} \tag{7.5}$$

and the central potential, ψ_*^0, can be written as

$$\psi_*^0 = \frac{2\pi G \bar{q} \sin^{-1} e}{e} \int_0^{\infty} \rho(m^2) \mathrm{d}m^2. \tag{7.6}$$

For $\alpha > -2$ and $\alpha + 2\beta < -2$, the potential is given by eqn. (7.4) with the central value

$$\psi_*^0 = \frac{2\pi G \bar{q} \rho_0 b^2 \sin^{-1} e}{e} B\left(\frac{\alpha}{2} + 1, -\frac{\alpha}{2} - \beta - 1\right), \tag{7.7}$$

where, B is the beta function. For the region, $\alpha \leq -2$, the potential is provided by eqn. (7.4a) and for the other region, $\alpha + 2\beta \geq 2$, it is represented by eqn. (7.4b). In the region, bounded by the lines $\alpha = -3$ and $\alpha + 2\beta = -3$, the total

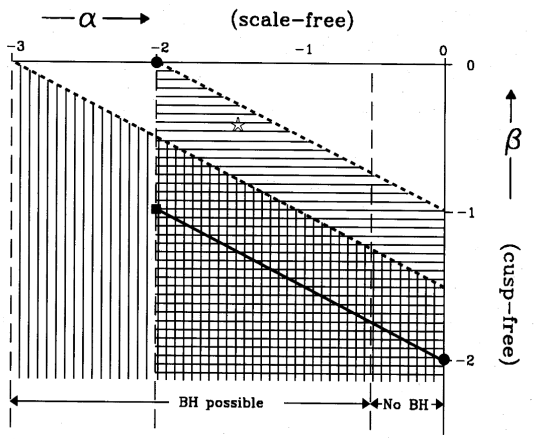

FIGURE 7.1: A region plot of (α, β), showing different regions mentioned. Image courtesy: Qian *et al.* (1995).

mass is finite and is given by

$$M = 2\pi\bar{q}\rho_0 b^3 B\left(\frac{\alpha}{2}+\frac{3}{2}, -\frac{\alpha}{2}-\beta-\frac{3}{2}\right). \tag{7.8}$$

The DF obtained by this two integral model, with a central black hole, is positive, therefore, physical, only when $\alpha \leq -\frac{1}{2}$. The regions mentioned are shown in Fig. 7.1.

Small radii

At the small radii, eqn. (7.1) takes the form

$$\rho(m^2) = \rho_0\left(\frac{m}{b}\right)^{\alpha}. \tag{7.9}$$

In the absence of the black hole at the center, the stellar potential will be provided by the potential of scale free spheroids [discussed in §3.2 of Qian *et al.* (1995)]. In presence of the central black hole, for the region of finite mass, the potential can

be written as

$$\psi(R^2, z^2) = \frac{GM_\bullet}{\sqrt{R^2 + z^2}} + \psi_0^*. \tag{7.10}$$

The first term, representing the black hole potential dominates near the center for the small radii; but, adding the stellar potential, gives a more accurate result. After solving for z^2 from eqn. (7.10) and plugging it into the density profile [eqn. (7.9), it can be seen that

$$\tilde{\rho}(\psi, \bar{R}^2) = \frac{\rho_0}{\bar{q}^\alpha}\left(\frac{\psi - \psi_0^*}{B}\right)^{-\alpha}\left[1 - e^2\bar{R}^2\left(\frac{\psi - \psi_0^*}{B}\right)^2\right], \tag{7.11}$$

where, the reference potential, $B = \dfrac{GM_\bullet}{b}$ and $e^2 = 1 - \bar{q}^2$. This is a modified expression of the component given by Dejonghe (1986). The DF in this case, for the density given by eqn. (7.11), is derived using the Hunter and Qian (1993) algorithm and given by

$$f(E, L_z) = \frac{\rho_0 q^{-\alpha}}{B_S^{3/2}}\left(\frac{E - \psi_0^*}{B_S}\right)^{-\alpha-3/2} f_\alpha(e^2\eta^2), \tag{7.12}$$

where,

$$f_\alpha(e^2\eta^2) = \frac{1}{(2\pi)^{3/2}}\frac{\Gamma(1-\alpha)}{\Gamma(-\alpha - \frac{1}{2})} 3F_2\left(\frac{1-\alpha}{2}, 1 - \frac{\alpha}{2}, -\frac{\alpha}{2}; -\alpha - \frac{1}{2}, -\frac{1}{2}; e^2\eta^2\right), \tag{7.13}$$

given by Dejonghe (1986), with $e^2\eta^2 = e^2\dfrac{L_z^2}{L_c^2(E)}$ and $L_c^2(E) = \dfrac{(GM_\bullet)^2}{2(E - \psi_0^*)}$.

Large radii

At large radii, eqn. (7.1) can be written as

$$\rho(m^2) = \rho_0\left(\frac{m}{b}\right)^{\alpha+2\beta}. \tag{7.14}$$

Here, the DF is given by eqn. (7.12) where α is replaced by $\alpha+2\beta$, in the definition of B; the stellar mass M is added to $M_\bullet$ and ψ_0^* is zero. In this case, the DF is found to be

$$f(E, L_z) = \frac{\rho_0 q^{-\alpha-2\beta}}{B_L^{3/2}} \left(\frac{E}{B_L}\right)^{-\alpha-2\beta-3/2} f_{\alpha+2\beta}(e^2\eta^2), \tag{7.15}$$

and the total potential can be written as

$$\psi(R^2, z^2) = \frac{G(M_\bullet + M_*)}{\sqrt{R^2+z^2}}. \tag{7.16}$$

Solution to the joint DF

The equations from Chapter 2, used for deriving the LOS σ are

$$\sigma_{||} = \sqrt{\bar{v_{||}^2} - (\bar{v_{||}}^2)} \tag{7.17}$$

where,

$$v_{||} = v_R \sin\theta + v_\phi \cos\theta. \tag{7.18}$$

Therefore, $\bar{v_{||}}$ can be written as

$$\bar{v_{||}} = \frac{\int \mathrm{d}x_{||}\mathrm{d}^3\mathbf{v} v_{||} f(\mathbf{x}, \mathbf{v})}{\Sigma} = \frac{2pb}{\Sigma} \int_p^\infty \frac{\rho \bar{v_\phi}}{\sqrt{t^2-p^2}} \mathrm{d}t, \tag{7.19}$$

with $\dfrac{R}{b} = t$, $\dfrac{R'}{b} = p$. Now, v_ϕ is given by

$$\bar{v_\phi} = \frac{4\pi}{\rho R^2} \int_0^\psi \mathrm{d}\varepsilon \int_0^{R\sqrt{2(\psi-\varepsilon)}} \mathrm{d}L_z L_z f(\varepsilon, L_z). \tag{7.20}$$

The surface density is given by the expression as

$$\Sigma(p) = 2b \int_p^\infty \frac{t\mathrm{d}t}{\sqrt{t^2-p^2}} \rho(t). \tag{7.21}$$

and $\bar{v_{||}^2}$ is expressed as

$$\bar{v_{||}^2} = \frac{2}{\Sigma}\int_{R'}^{\infty} \mathrm{d}R \frac{\sqrt{R^2 - R'^2}}{R}\rho\bar{v_R^2} + \frac{2R'^2}{\Sigma}\int_{R'}^{\infty} \mathrm{d}R \frac{1}{R\sqrt{R^2 - R'^2}}\rho\bar{v_\phi^2}, \tag{7.22}$$

where,

$$\bar{v_R^2} = \frac{4\pi}{\rho R}\int_0^{\psi} \mathrm{d}\varepsilon \int_0^{R\sqrt{2(\psi-\varepsilon)}} \mathrm{d}L_z f(\varepsilon, L_z)\left(\psi - \varepsilon - \frac{L_z^2}{2R^2}\right), \tag{7.23}$$

and

$$\bar{v_\phi^2} = \frac{4\pi}{\rho R^3}\int_0^{\psi} \mathrm{d}\varepsilon \int_0^{R\sqrt{2(\psi-\varepsilon)}} \mathrm{d}L_z f(\varepsilon, L_z) L_z^2. \tag{7.24}$$

Using eqns. (7.19, 7.22), we derive σ, numerically, which we plot in Fig. 7.2 along with the complete distribution function (obtained numerically by joining two distribution functions using the continuity of the distribution function). We are attempting to build a complete DF directly without using the limiting cases.

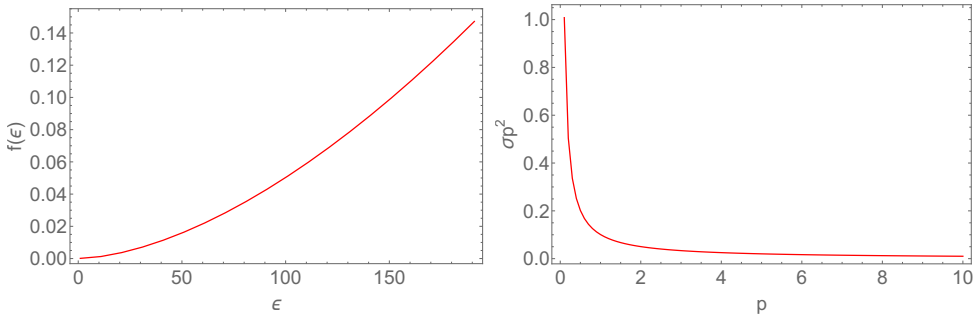

(a) (b)

FIGURE 7.2: The general distribution function, $f(\epsilon)$ in arbitrary units (a) and (b) square of the velocity dispersion, $\sigma_{||}^2$, normalized with respect to the maximum value are plotted.

7.2 Initial seed mass and spin distributions

Schechter initial mass function of halos is given by

$$\phi(\mathcal{M}) = \phi_* \left(\frac{\mathcal{M}}{M_{*s}} \right)^{\beta} e^{-(\mathcal{M}/M_*)^{4/5}}, \tag{7.25}$$

where $\mathcal{M}$ is the mass of the halo, ϕ_*, M_{*s} and β are the Schechter parameters.

The probability distribution of the spin parameter of the halo λ (which in turn gives the angular momentum of the halo) can be obtained by cosmological N - body simulations and is given by log normal distribution as [Lodato and Natarajan (2007), Warren *et al.* (1992)]

$$p(\lambda)\mathrm{d}\lambda = \frac{1}{\sqrt{2\pi}\sigma_\lambda} \frac{1}{\lambda} \exp\left[- \frac{\ln^2(\lambda/\bar{\lambda})}{2\sigma_\lambda} \right] \mathrm{d}\lambda, \tag{7.26}$$

where, $\bar{\lambda} = 0.05$ and $\sigma_\lambda = 0.5$.

From Mangalam (2001)

$$\lambda = \frac{L|E|^{\frac{1}{2}}}{GM^{\frac{5}{2}}}, \quad \frac{\lambda_d}{\lambda_v} = \left(\frac{E_d}{\mathcal{E}} \right)^{\frac{1}{2}} \left(\frac{\mathcal{M}}{M_d} \right)^{\frac{1}{2}}, \tag{7.27}$$

where M_d and $\mathcal{M}$ are the masses of the disk and the halo respectively, E_d and $\mathcal{E}$ are the energies of the disc and the halo, and λ_d and λ_v are the spin parameters of the disc and the virialized halo respectively.

Again, Mangalam (2001) has shown

$$\frac{E_d}{\mathcal{E}} = C_1 \frac{M_d^2}{\mathcal{M}^2} \frac{r_v}{r_d}, \tag{7.28}$$

where r_d and r_v are the extents of the disk and the virialized halo, $C_1 \simeq \frac{2}{3}$. This factor of $\frac{2}{3}$ comes for a constant density halo, where, $k_1 = 0.3$ and k_2 can be

calculated as $\frac{\pi\theta}{\sqrt{k_1}} \simeq 0.2$ for $\theta = 1/8$ and $C_1 = \frac{k_2}{k_1}$. The binding energies of the disc and the halo are given as $E_d = -k_2\frac{GM_d^2}{r_d}$ and $\mathcal{E} = -k_1\frac{G\mathcal{M}^2}{r_v}$ respectively. Again

$$\frac{r_v}{r_d} = \frac{C_2}{\lambda_v}, \tag{7.29}$$

where λ_v is the spin parameter of the virialized halo (which we write as λ), $C_2 \simeq 1$ (for an exponential disc). It is calculated as $s\sqrt{k_1}$, where $s = 2$ for an exponential disc. Using these two relations we finally arrive at

$$\lambda = C_3 j^2 \frac{M_\bullet}{\mathcal{M}}, \tag{7.30}$$

where, $C_3 \simeq 1.37$ (calculated using the values of C_1 and C_2) and we have replaced M_d by black hole mass and spin parameter of the disk, λ_d by black hole spin parameter j. To derive the seed spin and mass distribution, we need to integrate over λ in the range 0.01 - 0.1. Now,

$$\frac{J}{\mathcal{M}} = \frac{J_d}{M_d}, \quad j = \frac{c}{G}\frac{J_d}{M_d^2} = \frac{c\mathcal{M}^3\lambda_v}{M_d}, \tag{7.31}$$

where, we used $J = G\mathcal{M}^{\frac{5}{2}}\lambda_v$.

The joint seed mass and spin function of the black hole is then given by

$$F_s(M_{\bullet s}, j) = \int_{\lambda=0.01}^{\lambda=0.1} p(\lambda)\frac{\mathrm{d}\lambda}{\mathrm{d}M_{\bullet s}}\phi[\mathcal{M}(\lambda, M_{\bullet s}, j)]\mathrm{d}\mathcal{M} \tag{7.32}$$

To obtain the seed mass and spin functions separately we integrate $F_s(M_{\bullet s}, j)$ over the spin and the mass ranges respectively; they are shown in Fig. 7.3.

We plan to combine the seed functions in our evolution model (chapter 6). To derive black hole demographics we can use the continuity equation of the black hole population as a function of spin and mass [Small and Blandford (1992), Shankar

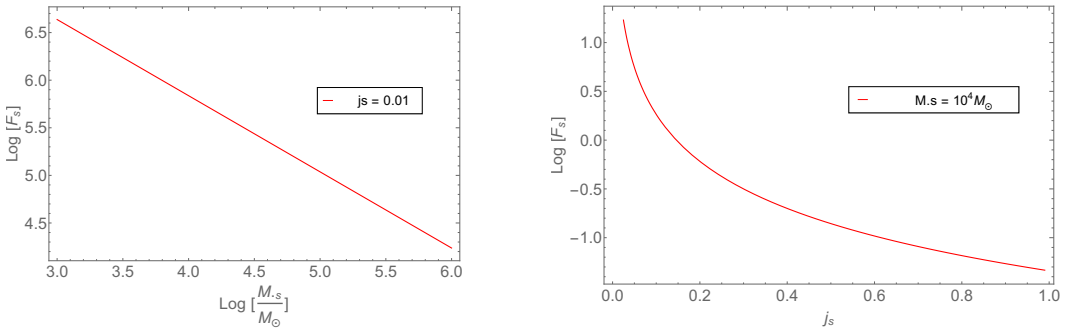

(a) (b)

FIGURE 7.3: (a) The initial seed mass function of seed black hole for a fixed z_f = 6. (b) The initial spin function of seed black hole for $M_{\bullet s} = 10^6 M_\odot$.

(2013)].

7.3 Summary

1. We have discussed the two integral model to find the DF in axisymmetric galaxies given by Hunter and Qian (1993) and its application provided by Qian *et al.* (1995). We discuss our extension of this model of Qian *et al.* (1995), by using the continuity condition of the distribution function and to derive σ for the axisymmetric systems. We plan to derive the $M_\bullet - \sigma$ relation and the $M_\bullet - M_b$ relation from this model in the near future.

2. We discussed our preliminary result of deriving the initial seed mass and spin function of the black holes. We took inputs from Lodato and Natarajan (2007), Warren *et al.* (1992), and Mangalam (2001) and derived a joint distribution function of seed black hole mass and spin. We plan to study this in detail and use this distribution in our evolution model (discussed in Chapter 6), to get better estimates for the evolution of the $M_\bullet - \sigma$ relation and to build black hole demographics using population synthesis.

Chapter 8

Summary, conclusions, and caveats

So Einstein was wrong when he said, "God does not play dice". Consideration of black holes suggests, not only that God does play dice, but that he sometimes confuses us by throwing them where they can't be seen.

Stephen Hawking

This thesis is devoted to a study of the evolution of black holes and the $M_\bullet - \sigma$ relation. We proposed a model for deriving the $M_\bullet - \sigma$ relation in spherical systems, and a model for black hole mass and spin evolution with all the contributing factors whose applications include the evolution of the $M_\bullet - \sigma$ relation and black hole archaeology. Then, we also discuss two ongoing projects: $M_\bullet - \sigma$ relation in axisymmetric systems and derivation of the initial seed and mass function of black holes. In this chapter, we summarize the thesis, discuss the novel aspects and its impact. We will then discuss the implications for future theoretical work.

8.1 Highlights

Below, we summarize the highlights of each chapter in sequence:

- *Chapter 1:* We discuss the basic physics of black holes and the motivation of our work. We present the importance of studying the mass and spin evolution of the black holes and present a brief introduction of all the factors that contribute to the growth and evolution of them. Then, we introduce the $M_\bullet - \sigma$ relation and discuss its possible origin and its evolution story. We provide a resource summary.

- *Chapter 2:* Chapter 2 gives an introduction to the stellar dynamics where, we derive the basic equations connecting the distribution function (DF) of the stars and the observable quantities in spherical and axisymmetric systems, which we use later in our models. We also derive the DF for some known potential-density pairs: Hernquist, Jaffe, and isochrone models. Jeans equations in spherical and axisymmetric systems are also discussed, which can be used to derive the $M_\bullet - \sigma$ relation.

- *Chapter 3:* We present the introduction of the $M_\bullet - \sigma$ relation followed by a literature survey of this relation. Then, we discuss some well known theoretical models to derive the $M_\bullet - \sigma$ relation and after that, we present a literature study of the evolution of the $M_\bullet - \sigma$ relation. Finally, we provide a resource summary.

- *Chapter 4:* This chapter presents our model of deriving the $M_\bullet - \sigma$ relation and $M_\bullet - M_b$ relation simultaneously for spherical systems. For single power law systems, we derive σ from the mass density profiles and the $M_\bullet - \sigma$ relation. For 12 elliptical galaxies, following Nuker intensity profile, we derive the DF and σ. Assuming the $M_\bullet - \sigma$ relation, $M_\bullet = fM_b$ and a single power law profile for the stellar mass density we have analytically shown

that $p(\gamma) = (2\gamma+6)/(2+\gamma)$. For a typical a range of $\gamma = 0.75$ - 1.4, we find $p = 3.6$ - 5.3, which is within the observed range. For the 12 Nuker profile cases, we derive the $M_\bullet - \sigma$ relation and $M_\bullet - M_b$ relation simultaneously by using a χ^2 analysis. The obtained values are $p = 3.81 \pm 0.004$ and $f_b = (1.23 \pm 0.09) \times 10^{-3}$.

- *Chapter 5:* In this chapter, we discuss the basic physics of all the factors that contribute to the growth of black hole mass and spin - accretion, stellar capture, mergers, and the Blandford-Znajek effect. We present different well-cited models from literature and discuss its modifications in our formalism for deriving the evolution of black hole mass and spin.

- *Chapter 6:* This chapter presents the relativistic treatment of tidal, capture and loss cone radius and using that we calculate the stellar capture rate. The predicted capture rates of $10^{-5} - 10^{-6}$ yr^{-1} are closer to the observed range. Then, we present our model for studying the black hole evolution in ΛCDM cosmology including all the effects - accretion, stellar capture, mergers, and Blandford-Znajek torque. In the case of gas accretion in the presence of cooling sources, the flow is momentum-driven and after a certain time, the black hole reaches a saturated mass. Subsequently, it grows only by stellar capture and mergers. We have considered the merger activity to be effective for $z \lesssim 4$. We studied the spin and mass evolution with all the effects individually, by switching on the effects one by one and in the final case, the complete model. Then, we discuss two applications of our model - the evolution of the $M_\bullet - \sigma$ relation and black hole archaeology. We model some specific cases of the quasars ULASJ134208.10+092838.61 (z=7.54), ULASJ112001.48+064124.3 (z=7.08) and DELSJ003836.10-152723.6 (z=7.02) and run our model backward to find their formation parameters at $z = \{10, 15, 20\}$ and show that heavy seeds of $10^7 M_\odot$ are required.

- *Chapter 7:* In this chapter, we present two ongoing projects with some preliminary results. Firstly, we discuss the derivation of the $M_\bullet - \sigma$ relation in axisymmetric systems, where we use the DF derived using the Hunter-Qian algorithm for large and small radii; then we obtain the σ, in presence of the black hole, by using the condition of continuity of the distribution function. We have obtained the behaviour of the complete distribution function and the velocity dispersion. Secondly, we formulate the joint initial seed spin and mass function of black holes and present the distributions. At the end, we discuss future directions to be explored in these projects.

8.2 The novel aspects and their impact

1. We presented a model of deriving the $M_\bullet - \sigma$ relation and $M_\bullet - M_b$ relation simultaneously. Previously, there were models of deriving these two relations independently, but by our model, we self-consistently determined both of them using the χ^2 analysis.

2. We incorporated the relativistic effects in the calculation of tidal, capture and loss cone radius and we employed these results to calculate the relativistic stellar capture rate.

3. We constructed a complete semi-analytic and self-consistent evolution model, with all the contributing factors to the evolution of black hole mass and spin.

4. We illustrated the effect of saturation on the evolution of the $M_\bullet(z) = k(z)\sigma^{p(z)}$ relation.

5. We deduce the evolution of the $M_\bullet - \sigma$ relation and black hole archaeology as two applications of our evolution model. The first application has important implications for the galaxy-black hole co-evolution paradigm while the

second application, we retrodict the initial mass and spin of seed black holes at earlier redshifts.

6. We show preliminary results on deriving the $M_\bullet - \sigma$ relation and $M_\bullet - M_b$ relation in axisymmetric systems jointly in presence of the black hole at the center of the galaxy.

7. We show some preliminary results of the seed mass and spin function of the black hole, which is still an unsolved topic.

We have demonstrated the basic physics of the evolution of the black hole and the $M_\bullet - \sigma$ relation. This relation is a an important tool to probe the co-evolution of the galaxy and the black hole from future observations from TMT. Also, black hole archaeology can determine the possible seed mass and spin of black holes given their present values, which can be helpful in testing the formation scenarios.

8.3 Caveats

We list some of the caveats below:

1. For deriving the self-consistent model of the $M_\bullet - \sigma$ relation and $M_\bullet - M_b$ relation, we assumed a linear proportionality relation, between $M_\bullet$ and M_b. But, in practice the relation could be slightly non linear. We can incorporate that in future.

2. While considering the accretion process for the growth of the black hole, we assumed a constant sub-Eddington accretion rate and a constant radiative efficiency. But, the accretion rate and the radiative efficiency can vary as a function of redshift and time. Incorporation of these variations will expand

our model, though the results are not supposed to change much, as the average over cosmic time is likely to be the same.

3. In case of deriving the mass growth rate by mergers, we assumed a proportionality relation between the halo mass and the black hole mass. Inclusion of non-linearity can broaden our models.

4. While deriving the evolution of the $M_\bullet - \sigma$ relation, we assumed σ to be a constant throughout, though it has a slight variation with redshift. In the future, we plan to include this variation to improve our model.

8.4 Future directions

1. We plan to extend our model of deriving the $M_\bullet - \sigma$ relation and $M_\bullet - M_b$ relation in more general axisymmetric systems with observed non-linear relationship of $M_\bullet - M_b$.

2. We plan to include the time variation of σ for the derivation of the evolution of the $M_\bullet - \sigma$ relation.

3. We are working on the initial seed mass and spin function, which can be built into the evolution to improve the model and also for better estimation of the evolution of the $M_\bullet - \sigma$ relation.

4. The data from future surveys at high redshift, for example from TMT, VLT and ELT along with measurements of σ from SKA, can be used to test the predictions of $M_\bullet - \sigma$ evolution from our model.

5. We also plan to work on the demographics of the black hole by population synthesis, based on a model for seed mass and spin distribution functions.

Our model in the new relativistic framework can be used for future simulational studies and can be probed through observations at high redshift.

THE END!

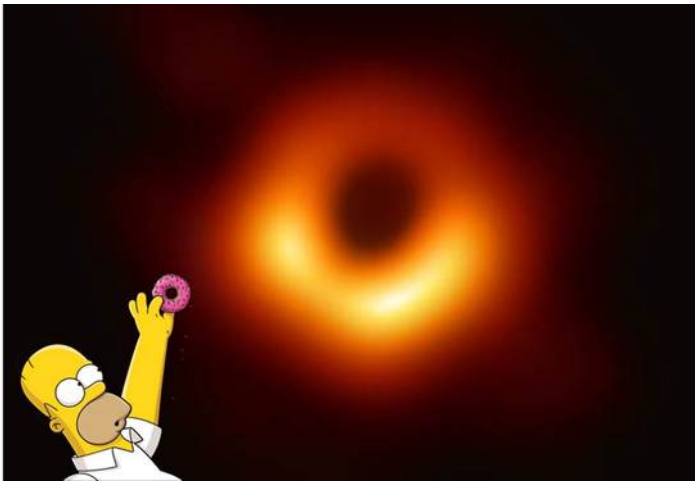

Bibliography

Alexander, T. and Bar-Or, B., 2017a, "A universal minimal mass scale for present-day central black holes", *ArXiv e-prints*. [ADS], [arXiv:1701.00415]

Alexander, Tal, 2015, "Relativistic Stellar Dynamics Around a Massive Black Hole in Steady State", *arXiv e-prints*, arXiv:1505.04823. [ADS], [arXiv:1505.04823 [astro-ph.GA]]

Alexander, Tal and Bar-Or, Ben, 2017b, "A universal minimal mass scale for present-day central black holes", *Nature Astronomy*, **1**, 0147. [DOI], [ADS], [arXiv:1701.00415 [astro-ph.GA]]

Allgood, Brandon, Flores, Ricardo A., Primack, Joel R., Kravtsov, Andrey V., Wechsler, Risa H., Faltenbacher, Andreas and Bullock, James S., 2006, "The shape of dark matter haloes: dependence on mass, redshift, radius and formation", *Mon. Not. Roy. Astron. Soc.*, **367**(4), 1781–1796. [DOI], [ADS], [arXiv:astro-ph/0508497 [astro-ph]]

Anninos, Peter, Hobill, David, Seidel, Edward, Smarr, Larry and Suen, Wai-Mo, 1993, "Collision of two black holes", *Physical Review L*, **71**(18), 2851–2854. [DOI], [ADS], [arXiv:gr-qc/9309016 [gr-qc]]

Bardeen, J. M., 1970, "Kerr Metric Black Holes", *Nature*, **226**, 64–65. [DOI], [ADS]

Bardeen, J. M., Press, W. H. and Teukolsky, S. A., 1972, "Rotating Black Holes: Locally Nonrotating Frames, Energy Extraction, and Scalar Synchrotron Radiation", *Astrophys. J.*, **178**, 347–370. [DOI], [ADS]

Batiste, M., Bentz, M. C., Raimundo, S. I., Vestergaard, M. and Onken, C. A., 2017, "Recalibration of the M $_{BH}$-σ Relation for AGN", *Astrophys. J. Lett.*, **838**, L10. [DOI], [ADS], [arXiv:1612.02815]

Baumgarte, Thomas W. and Shapiro, Stuart L., 2003, "Numerical relativity and compact binaries", *Phys. Rep*, **376**(2), 41–131. [DOI], [ADS], [arXiv:gr-qc/0211028 [gr-qc]]

Bezanson, R., van Dokkum, P. G., Tal, T., Marchesini, D., Kriek, M., Franx, M. and Coppi, P., 2009, "The Relation Between Compact, Quiescent High-redshift Galaxies and Massive Nearby Elliptical Galaxies: Evidence for Hierarchical, Inside-Out Growth", *Astrophys. J.*, **697**, 1290–1298. [DOI], [ADS], [arXiv:0903.2044 [astro-ph.CO]]

Bhattacharyya, D. and Mangalam, A., 2018, "M_{\bullet } - σ relation in spherical systems", *Journal of Astrophysics and Astronomy*. [arXiv:1710.05672]

Bhattacharyya, D. and Mangalam, A., 2018b, "Evolution of the $M_\bullet - \sigma$ relation", *Proceedings of the International Astronomical Union*, **14**(S342), 254âĂŞ256. [DOI]

Bhattacharyya, Dipanweeta and Mangalam, A., 2020, "Cosmic spin and mass evolution of black holes and its impact", *arXiv e-prints*, arXiv:2004.05000. [ADS], [arXiv:2004.05000 [astro-ph.HE]]

Binney, J. and Merrifield, M., 1998, *Galactic Astronomy*. [ADS]

Binney, J. and Tremaine, S., 2008, *Galactic Dynamics: Second Edition*, Princeton University Press. [ADS]

Blandford, R. D. and Znajek, R. L., 1977, "Electromagnetic extraction of energy from Kerr black holes", *Mon. Not. Roy. Astron. Soc.*, **179**, 433–456. [DOI], [ADS]

Blandford, R. D., Netzer, H., Woltjer, L., Courvoisier, T. J.-L. and Mayor, M. (Eds.), 1990, *Active Galactic Nuclei*. [ADS]

Bondi, H., 1952, "On spherically symmetrical accretion", *Mon. Not. Roy. Astron. Soc.*, **112**, 195. [DOI], [ADS]

Bondi, H. and Hoyle, F., 1944, "On the mechanism of accretion by stars", *Mon. Not. Roy. Astron. Soc.*, **104**, 273. [DOI], [ADS]

Brenneman, Laura W. and Reynolds, Christopher S., 2006, "Constraining Black Hole Spin via X-Ray Spectroscopy", *Astrophys. J.*, **652**(2), 1028–1043. [DOI], [ADS], [arXiv:astro-ph/0608502 [astro-ph]]

Brockamp, M., Baumgardt, H. and Kroupa, P., 2011, "Tidal disruption rate of stars by supermassive black holes obtained by direct N-body simulations", *Mon. Not. Roy. Astron. Soc.*, **418**(2), 1308–1324. [DOI], [ADS], [arXiv:1108.2270 [astro-ph.GA]]

Byun, Y.-I., Grillmair, C. J., Faber, S. M., Ajhar, E. A., Dressler, A., Kormendy, J., Lauer, T. R., Richstone, D. and Tremaine, S., 1996, "The Centers of Early-Type Galaxies With HST. II. Empirical Models and Structural Parameters", *Astron. J.*, **111**, 1889. [DOI], [ADS], [astro-ph/9602117]

Campitiello, Samuele, Celotti, Annalisa, Ghisellini, Gabriele and Sbarrato, Tullia, 2019, "Black hole mass and spin estimates of the most distant quasars", *Astron. Astrophys.*, **625**, A23. [DOI], [ADS], [arXiv:1809.00010 [astro-ph.HE]]

Carter, B., 1968, "Global Structure of the Kerr Family of Gravitational Fields", *Physical Review*, **174**, 1559–1571. [DOI], [ADS]

Carter, Brandon, 1968, "Global Structure of the Kerr Family of Gravitational Fields", *Phys. Rev.*, **174**, 1559–1571. [DOI]URL: `https://link.aps.org/doi/10.1103/PhysRev.174.1559`

Christodoulou, Demetrios, 1970, "Reversible and Irreversible Transformations in Black-Hole Physics", *Physical Review L*, **25**(22), 1596–1597. [DOI], [ADS]

Ciotti, Luca and Ostriker, Jeremiah P., 1997, "Cooling Flows and Quasars: Different Aspects of the Same Phenomenon? I. Concepts", *Astrophys. J. Lett.*, **487**(2), L105–L108. [DOI], [ADS], [arXiv:astro-ph/9706281 [astro-ph]]

Cohn, H. and Kulsrud, R. M., 1978, "The stellar distribution around a black hole - Numerical integration of the Fokker-Planck equation", *Astrophys. J.*, **226**, 1087–1108. [DOI], [ADS]

Davis, Shane W. and Laor, Ari, 2011, "The Radiative Efficiency of Accretion Flows in Individual Active Galactic Nuclei", *Astrophys. J.*, **728**(2), 98. [DOI], [ADS], [arXiv:1012.3213 [astro-ph.CO]]

de Zeeuw, Tim and Pfenniger, Daniel, 1988, "Potential-density pairs for galaxies.", *Mon. Not. Roy. Astron. Soc.*, **235**, 949–995. [DOI], [ADS]

Debattista, V. P., Kazantzidis, S. and van den Bosch, F. C., 2013, "Disk Assembly and the M $_{BH}$-σ_e Relation of Supermassive Black Holes", *Astrophys. J.*, **765**, 23. [DOI], [ADS], [arXiv:1301.2669]

Dejonghe, H., 1986, "Stellar dynamics and the description of stellar systems.", *Phys. Rep*, **133**(3), 217–313. [DOI], [ADS]

Donley, J. L., Brandt, W. N., Eracleous, M. and Boller, T., 2002, "Large-Amplitude X-Ray Outbursts from Galactic Nuclei: A Systematic Survey using ROSAT Archival Data", *Astron. J.*, **124**, 1308–1321. [DOI], [ADS], [astro-ph/0206291]

Dubois, Y., Volonteri, M. and Silk, J., 2014, "Black hole evolution - III. Statistical properties of mass growth and spin evolution using large-scale hydrodynamical cosmological simulations", *Mon. Not. Roy. Astron. Soc.*, **440**, 1590–1606. [DOI], [ADS], [arXiv:1304.4583]

Evans, N. W., 1993, "Simple galaxy models with massive haloes", *Mon. Not. Roy. Astron. Soc.*, **260**(1), 191–201. [DOI], [ADS]

Faber, S. M., Tremaine, S., Ajhar, E. A., Byun, Y.-I., Dressler, A., Gebhardt, K., Grillmair, C., Kormendy, J., Lauer, T. R. and Richstone, D., 1997, "The Centers of Early-Type Galaxies with HST. IV. Central Parameter Relations.", *Astron. J.*, **114**, 1771. [DOI], [ADS], [astro-ph/9610055]

Felice, F., 1968, "Equatorial geodesic motion in the gravitational field of a rotating source", *Nuovo Cimento B Serie*, **57**, 351–388. [DOI], [ADS]

Ferrarese, L., 2002, "Beyond the Bulge: A Fundamental Relation between Supermassive Black Holes and Dark Matter Halos", *Astrophys. J.*, **578**, 90–97. [DOI], [ADS], [astro-ph/0203469]

Ferrarese, L. and Ford, H., 2005, "Supermassive Black Holes in Galactic Nuclei: Past, Present and Future Research", *Space Sci. Rev.*, **116**, 523–624. [DOI], [ADS], [astro-ph/0411247]

Ferrarese, Laura and Merritt, David, 2000, "A Fundamental Relation between Supermassive Black Holes and Their Host Galaxies", *Astrophys. J. Lett.*, **539**(1), L9–L12. [DOI], [ADS], [arXiv:astro-ph/0006053 [astro-ph]]

Frank, J. and Rees, M. J., 1976, "Effects of massive central black holes on dense stellar systems", *Mon. Not. Roy. Astron. Soc.*, **176**, 633–647. [DOI], [ADS]

Frank, Juhan, King, Andrew and Raine, Derek J., 2002, *Accretion Power in Astrophysics: Third Edition*. [ADS]

Frolov, Valeri P. and Novikov, Igor D., 1998, *Black hole physics : basic concepts and new developments*. [ADS]

Gammie, C. F., Shapiro, S. L. and McKinney, J. C., 2004, "Black Hole Spin Evolution", *Astrophys. J.*, **602**, 312–319. [DOI], [ADS], [astro-ph/0310886]

Gebhardt, K., Bender, R., Bower, G., Dressler, A., Faber, S. M., Filippenko, A. V., Green, R., Grillmair, C., Ho, L. C., Kormendy, J., Lauer, T. R., Magorrian, J., Pinkney, J., Richstone, D. and Tremaine, S., 2000, "A Relationship between

Nuclear Black Hole Mass and Galaxy Velocity Dispersion", *Astrophys. J. Lett.*, **539**, L13–L16. [DOI], [ADS], [astro-ph/0006289]

Gezari, S., Heckman, T., Cenko, S. B., Eracleous, M., Forster, K., Gonçalves, T. S., Martin, D. C., Morrissey, P., Neff, S. G., Seibert, M., Schiminovich, D. and Wyder, T. K., 2009, "Luminous Thermal Flares from Quiescent Supermassive Black Holes", *Astrophys. J.*, **698**, 1367–1379. [DOI], [ADS], [arXiv:0904.1596 [astro-ph.CO]]

Graham, A. W. and Scott, N., 2013, "The M $_{BH}$-L $_{spheroid}$ Relation at High and Low Masses, the Quadratic Growth of Black Holes, and Intermediate-mass Black Hole Candidates", *Astrophys. J.*, **764**, 151. [DOI], [ADS], [arXiv:1211.3199]

Gültekin, K., Richstone, D. O., Gebhardt, K., Lauer, T. R., Tremaine, S., Aller, M. C., Bender, R., Dressler, A., Faber, S. M., Filippenko, A. V., Green, R., Ho, L. C., Kormendy, J., Magorrian, J., Pinkney, J. and Siopis, C., 2009, "The M-σ and M-L Relations in Galactic Bulges, and Determinations of Their Intrinsic Scatter", *Astrophys. J.*, **698**, 198–221. [DOI], [ADS], [arXiv:0903.4897 [astro-ph.GA]]

Haehnelt, Martin G., Natarajan, Priyamvada and Rees, Martin J., 1998, "High-redshift galaxies, their active nuclei and central black holes", *Mon. Not. Roy. Astron. Soc.*, **300**(3), 817–827. [DOI], [ADS], [arXiv:astro-ph/9712259 [astro-ph]]

Häring, N. and Rix, H.-W., 2004, "On the Black Hole Mass-Bulge Mass Relation", *Astrophys. J. Lett.*, **604**, L89–L92. [DOI], [ADS], [astro-ph/0402376]

Hénon, M., 1960, "L'amas isochrone. - III. Fonction de distribution", *Annales d'Astrophysique*, **23**, 474. [ADS]

Hernquist, Lars, 1990, "An Analytical Model for Spherical Galaxies and Bulges", *Astrophys. J.*, **356**, 359. [DOI], [ADS]

Hopkins, P. F., Bundy, K., Murray, N., Quataert, E., Lauer, T. R. and Ma, C.-P., 2009, "Compact high-redshift galaxies are the cores of the most massive present-day spheroids", *Mon. Not. Roy. Astron. Soc.*, **398**, 898–910. [DOI], [ADS], [arXiv:0903.2479]

Hoyle, F. and Lyttleton, R. A., 1939, "The effect of interstellar matter on climatic variation", *Proceedings of the Cambridge Philosophical Society*, **35**(3), 405. [DOI], [ADS]

Hughes, S. A. and Blandford, R. D., 2003, "Black Hole Mass and Spin Coevolution by Mergers", *Astrophys. J. Lett.*, **585**, L101–L104. [DOI], [ADS], [astro-ph/0208484]

Hunter, C. and Qian, Edward, 1993, "Two-integral distribution functions for axisymmetric galaxies.", *Mon. Not. Roy. Astron. Soc.*, **262**, 401–428. [DOI], [ADS]

Jaffe, W., 1983, "A simple model for the distribution of light in spherical galaxies.", *Mon. Not. Roy. Astron. Soc.*, **202**, 995–999. [DOI], [ADS]

Jahnke, Knud and Macciò, Andrea V., 2011, "The Non-causal Origin of the Black-hole-galaxy Scaling Relations", *Astrophys. J.*, **734**(2), 92. [DOI], [ADS], [arXiv:1006.0482 [astro-ph.CO]]

Kesden, M., 2012, "Tidal-disruption rate of stars by spinning supermassive black holes", *Physical Review D*, **85**(2), 024037. [DOI], [ADS], [arXiv:1109.6329 [astro-ph.CO]]

King, A., 2003, "Black Holes, Galaxy Formation, and the M_{BH}-σ Relation", *Astrophys. J. Lett.*, **596**, L27–L29. [DOI], [ADS], [astro-ph/0308342]

King, A. R., Pringle, J. E. and Hofmann, J. A., 2008, "The evolution of black hole mass and spin in active galactic nuclei", *Mon. Not. Roy. Astron. Soc.*, **385**, 1621–1627. [DOI], [ADS], [arXiv:0801.1564]

King, Andrew, 2005, "The AGN-Starburst Connection, Galactic Superwinds, and M_{BH}-σ", *Astrophys. J. Lett.*, **635**(2), L121–L123. [DOI], [ADS], [arXiv:astro-ph/0511034 [astro-ph]]

King, Andrew and Pounds, Ken, 2015, "Powerful Outflows and Feedback from Active Galactic Nuclei", *Ann. Rev. Astron. Astrophys.*, **53**, 115–154. [DOI], [ADS], [arXiv:1503.05206 [astro-ph.GA]]

Kolb, Ulrich, 2010, *Extreme Environment Astrophysics*. [ADS]

Komossa, S., 2015, "Tidal disruption of stars by supermassive black holes: Status of observations", *Journal of High Energy Astrophysics*, **7**, 148–157. [DOI], [ADS], [arXiv:1505.01093 [astro-ph.HE]]

Kormendy, J. and Ho, L. C., 2013, "Coevolution (Or Not) of Supermassive Black Holes and Host Galaxies", *Ann. Rev. Astron. Astrophys.*, **51**, 511–653. [DOI], [ADS], [arXiv:1304.7762]

Kravtsov, A. V., Klypin, A. A. and Khokhlov, A. M., 1997, "Adaptive Refinement Tree: A New High-Resolution N-Body Code for Cosmological Simulations", *Astrophys. J. Suppl.*, **111**, 73–94. [DOI], [ADS], [astro-ph/9701195]

Kravtsov, A. V., Berlind, A. A., Wechsler, R. H., Klypin, A. A., Gottlöber, S., Allgood, B. and Primack, J. R., 2004, "The Dark Side of the Halo Occupation Distribution", *Astrophys. J.*, **609**, 35–49. [DOI], [ADS], [astro-ph/0308519]

Li, L.-X., 2012, "Accretion, growth of supermassive black holes, and feedback in galaxy mergers", *Mon. Not. Roy. Astron. Soc.*, **424**, 1461–1470. [DOI], [ADS], [arXiv:1205.0363]

Lodato, Giuseppe and Natarajan, Priyamvada, 2007, "The mass function of high-redshift seed black holes", *Mon. Not. Roy. Astron. Soc.*, **377**(1), L64–L68. [DOI], [ADS], [arXiv:astro-ph/0702340 [astro-ph]]

MacDonald, D. and Thorne, K. S., 1982, "Black-hole electrodynamics - an absolute-space/universal-time formulation", *Mon. Not. Roy. Astron. Soc.*, **198**, 345–382. [DOI], [ADS]

Mageshwaran, T. and Mangalam, A., 2015, "Stellar and Gas Dynamical Model for Tidal Disruption Events in a Quiescent Galaxy", *Astrophys. J.*, **814**, 141. [DOI], [ADS], [arXiv:1510.07828]

Magorrian, J. and Tremaine, S., 1999, "Rates of tidal disruption of stars by massive central black holes", *Mon. Not. Roy. Astron. Soc.*, **309**, 447–460. [DOI], [ADS], [astro-ph/9902032]

Magorrian, J., Tremaine, S., Richstone, D., Bender, R., Bower, G., Dressler, A., Faber, S. M., Gebhardt, K., Green, R., Grillmair, C., Kormendy, J. and Lauer, T., 1998, "The Demography of Massive Dark Objects in Galaxy Centers", *Astron. J.*, **115**, 2285–2305. [DOI], [ADS], [astro-ph/9708072]

Magorrian, John and Binney, James, 1994, "Predicting line-of-sight velocity distributions of elliptical galaxies", *Mon. Not. Roy. Astron. Soc.*, **271**, 949. [DOI], [ADS]

Mangalam, A., 2001, "Formation of a proto-quasar from accretion flows in a halo.", *Astron. Astrophys.*, **379**, 1138–1152. [DOI], [ADS], [astro-ph/0110591]

Mangalam, A., 2015, "Cosmic evolution of AGN using self-consistent black hole energetics", in *Astronomical Society of India Conference Series*, Astronomical Society of India Conference Series, [ADS]

Mangalam, A., Gopal-Krishna and Wiita, P. J., 2009, "The changing interstellar medium of massive elliptical galaxies and cosmic evolution of radio galaxies and quasars", *Mon. Not. Roy. Astron. Soc.*, **397**, 2216–2224. [DOI], [ADS], [arXiv:0904.0712]

Marconi, A. and Hunt, L. K., 2003, "The Relation between Black Hole Mass, Bulge Mass, and Near-Infrared Luminosity", *Astrophys. J. Lett.*, **589**, L21–L24. [DOI], [ADS], [astro-ph/0304274]

Marronetti, P., Tichy, W., Brügmann, B., González, J. and Sperhake, U., 2008, "High-spin binary black hole mergers", *Physical Review D*, **77**(6), 064010. [DOI], [ADS], [arXiv:0709.2160 [gr-qc]]

McConnell, N. J. and Ma, C.-P., 2013, "Revisiting the Scaling Relations of Black Hole Masses and Host Galaxy Properties", *Astrophys. J.*, **764**, 184. [DOI], [ADS], [arXiv:1211.2816]

Merritt, D., 2013a, "Loss-cone dynamics", *Classical and Quantum Gravity*, **30**(24), 244005. [DOI], [ADS], [arXiv:1307.3268]

Merritt, D., 2013b, *Dynamics and Evolution of Galactic Nuclei*. [ADS]

Merritt, D. and Ferrarese, L., 2001, "The M-σ Relation for Supermassive Black Holes", *Astrophys. J.*, **547**, 140–145. [DOI], [ADS], [astro-ph/0008310]

Misner, C. W., Thorne, K. S. and Wheeler, J. A., 1973, *Gravitation*. [ADS]

Mo, H., van den Bosch, F. C. and White, S., 2010, *Galaxy Formation and Evolution*. [ADS]

Murray, Norman, Quataert, Eliot and Thompson, Todd A., 2005, "On the Maximum Luminosity of Galaxies and Their Central Black Holes: Feedback from Momentum-driven Winds", *Astrophys. J.*, **618**(2), 569–585. [DOI], [ADS], [arXiv:astro-ph/0406070 [astro-ph]]

Natarajan, Priyamvada and Treister, Ezequiel, 2009, "Is there an upper limit to black hole masses?", *Mon. Not. Roy. Astron. Soc.*, **393**(3), 838–845. [DOI], [ADS], [arXiv:0808.2813 [astro-ph]]

Oser, L., Naab, T., Ostriker, J. P. and Johansson, P. H., 2012, "The Cosmological Size and Velocity Dispersion Evolution of Massive Early-type Galaxies", *Astrophys. J.*, **744**, 63. [DOI], [ADS], [arXiv:1106.5490]

Pandey, Kanhaiya L. and Mangalam, A., 2018, "Role of primordial black holes in the direct collapse scenario of supermassive black hole formation at high redshifts", *Journal of Astrophysics and Astronomy*, **39**(1), 9. [DOI], [ADS], [arXiv:1801.06649 [astro-ph.GA]]

Perek, L., 1962, "Distribution of Mass in Oblate Stellar Systems", *Advances in Astronomy and Astrophysics*, **1**, 165–287. [DOI], [ADS]

Pfeiffer, Harald P., Cook, Gregory B. and Teukolsky, Saul A., 2002, "Comparing initial-data sets for binary black holes", *Physical Review D*, **66**(2), 024047. [DOI], [ADS], [arXiv:gr-qc/0203085 [gr-qc]]

Qian, E. E., de Zeeuw, P. T., van der Marel, R. P. and Hunter, C., 1995, "Axisymmetric galaxy models with central black holes, with an application to M32", *Mon. Not. Roy. Astron. Soc.*, **274**(2), 602–622. [DOI], [ADS], [arXiv:astro-ph/9412067 [astro-ph]]

Rana, P. and Mangalam, A., 2019a, "Astrophysically relevant bound trajectories around a Kerr black hole", *Classical and Quantum Gravity*, **36**(4), 045009. [DOI], [ADS], [arXiv:1901.02730 [gr-qc]]

Rana, Prerna and Mangalam, A., 2019b, "Astrophysically relevant bound trajectories around a Kerr black hole", *arXiv e-prints*, arXiv:1901.02730. [ADS], [arXiv:1901.02730 [gr-qc]]

Rauch, K. P. and Tremaine, S., 1996, "Resonant relaxation in stellar systems", *New Astronomy*, **1**, 149–170. [DOI], [ADS], [astro-ph/9603018]

Rauch, Kevin P. and Ingalls, Brian, 1998, "Resonant tidal disruption in galactic nuclei", *Mon. Not. Roy. Astron. Soc.*, **299**(4), 1231–1241. [DOI], [ADS], [arXiv:astro-ph/9710288 [astro-ph]]

Robertson, B., Hernquist, L., Cox, T. J., Di Matteo, T., Hopkins, P. F., Martini, P. and Springel, V., 2006, "The Evolution of the M_{BH}-σ Relation", *Astrophys. J.*, **641**, 90–102. [DOI], [ADS], [astro-ph/0506038]

Saglia, R. P., Colless, Matthew, Baggley, G., Bertschinger, Edmund, Burstein, David, Davies, Roger L., McMahan, Robert K. and Wegner, Gary, 1997, "The EFAR Fundamental Plane", in *The Nature of Elliptical Galaxies; 2nd Stromlo Symposium. ASP Conference Series; Vol. 116; 1997; ed. M. Arnaboldi; G. S. Da Costa; and P. Saha (1997), p.180*, (Eds.) Arnaboldi, M., Da Costa, G. S., Saha, P., Astronomical Society of the Pacific Conference Series, 116, [ADS]

Salviander, S. and Shields, G. A., 2013, "The Black Hole Mass-Stellar Velocity Dispersion Relationship for Quasars in the Sloan Digital Sky Survey Data Release 7", *Astrophys. J.*, **764**, 80. [DOI], [ADS], [arXiv:1210.7263]

Shakura, N. I. and Sunyaev, R. A., 1973, "Reprint of 1973A&A....24..337S. Black holes in binary systems. Observational appearance.", *Astron. Astrophys.*, **500**, 33–51. [ADS]

Shankar, F., Bernardi, M. and Haiman, Z., 2009a, "The Evolution of the M_{BH}-σ Relation Inferred from the Age Distribution of Local Early-Type Galaxies and Active Galactic Nuclei Evolution", *Astrophys. J.*, **694**, 867–878. [DOI], [ADS], [arXiv:0806.3459]

Shankar, F., Weinberg, D. H. and Miralda-Escudé, J., 2009b, "Self-Consistent Models of the AGN and Black Hole Populations: Duty Cycles, Accretion Rates, and the Mean Radiative Efficiency", *Astrophys. J.*, **690**, 20–41. [DOI], [ADS], [arXiv:0710.4488]

Shankar, Francesco, 2013, "Black hole demography: from scaling relations to models", *Classical and Quantum Gravity*, **30**(24), 244001. [DOI], [ADS], [arXiv:1307.3289 [astro-ph.CO]]

Shen, Yue, Greene, Jenny E., Ho, Luis C., Brand t, W. N., Denney, Kelly D., Horne, Keith, Jiang, Linhua, Kochanek, Christopher S., McGreer, Ian D., Merloni, Andrea, Peterson, Bradley M., Petitjean, Patrick, Schneider, Donald P., Schulze, Andreas, Strauss, Michael A., Tao, Charling, Trump, Jonathan R., Pan, Kaike and Bizyaev, Dmitry, 2015, "The Sloan Digital Sky Survey Reverberation Mapping Project: No Evidence for Evolution in the M• -σ_* Relation to zÌČ 1", *Astrophys. J.*, **805**(2), 96. [DOI], [ADS], [arXiv:1502.01034 [astro-ph.GA]]

Sheth, Ravi K. and Lemson, Gerard, 1999, "The forest of merger history trees associated with the formation of dark matter haloes", *Mon. Not. Roy. Astron. Soc.*, **305**(4), 946–956. [DOI], [ADS], [arXiv:astro-ph/9805322 [astro-ph]]

Sijacki, D., Vogelsberger, M., Genel, S., Springel, V., Torrey, P., Snyder, G. F., Nelson, D. and Hernquist, L., 2015, "The Illustris simulation: the evolving population of black holes across cosmic time", *Mon. Not. Roy. Astron. Soc.*, **452**, 575–596. [DOI], [ADS], [arXiv:1408.6842]

Silk, J. and Rees, M. J., 1998, "Quasars and galaxy formation", *Astron. Astrophys.*, **331**, L1–L4. [ADS], [astro-ph/9801013]

Sivia, D. S. and Skilling, J., 2006, *Data Analysis: A Bayesian Tutorial*, Oxford University Press

Small, Todd A. and Blandford, Roger D., 1992, "Quasar evolution and the growth of black holes.", *Mon. Not. Roy. Astron. Soc.*, **259**, 725–737. [DOI], [ADS]

Smarr, L., 1979, "Basic concepts in finite differencing of partial differential equations", in *Sources of Gravitational Radiation*, (Ed.) Smarr, L. L., [ADS]

Soltan, A., 1982, "Masses of quasars", *Mon. Not. Roy. Astron. Soc.*, **200**, 115–122. [DOI], [ADS]

Somerville, Rachel S. and Kolatt, Tsafrir S., 1999, "How to plant a merger tree", *Mon. Not. Roy. Astron. Soc.*, **305**(1), 1–14. [DOI], [ADS], [arXiv:astro-ph/9711080 [astro-ph]]

Stewart, K. R., Bullock, J. S., Barton, E. J. and Wechsler, R. H., 2009, "Galaxy Mergers and Dark Matter Halo Mergers in ΛCDM: Mass, Redshift, and Mass-Ratio Dependence", *Astrophys. J.*, **702**, 1005–1015. [DOI], [ADS], [arXiv:0811.1218]

Stewart, Kyle R., Bullock, James S., Wechsler, Risa H., Maller, Ariyeh H. and Zentner, Andrew R., 2008, "Merger Histories of Galaxy Halos and Implications for Disk Survival", *Astrophys. J.*, **683**(2), 597–610. [DOI], [ADS], [arXiv:0711.5027 [astro-ph]]

Stone, N. C. and Metzger, B. D., 2016, "Rates of stellar tidal disruption as probes of the supermassive black hole mass function", *Mon. Not. Roy. Astron. Soc.*, **455**, 859–883. [DOI], [ADS], [arXiv:1410.7772 [astro-ph.HE]]

Syer, D. and Ulmer, A., 1999, "Tidal disruption rates of stars in observed galaxies", *Mon. Not. Roy. Astron. Soc.*, **306**, 35–42. [DOI], [ADS], [astro-ph/9812389]

Taylor, P. and Kobayashi, C., 2016, "Time evolution of galaxy scaling relations in cosmological simulations", *Mon. Not. Roy. Astron. Soc.*, **463**, 2465–2479. [DOI], [ADS], [arXiv:1608.06685]

Thorne, K. S., 1974, "Disk-Accretion onto a Black Hole. II. Evolution of the Hole", *Astrophys. J.*, **191**, 507–520. [DOI], [ADS]

Tremaine, S., Gebhardt, K., Bender, R., Bower, G., Dressler, A., Faber, S. M., Filippenko, A. V., Green, R., Grillmair, C., Ho, L. C., Kormendy, J., Lauer, T. R., Magorrian, J., Pinkney, J. and Richstone, D., 2002, "The Slope of the Black Hole Mass versus Velocity Dispersion Correlation", *Astrophys. J.*, **574**, 740–753. [DOI], [ADS], [astro-ph/0203468]

Volonteri, M. and Rees, M. J., 2005, "Rapid Growth of High-Redshift Black Holes", *Astrophys. J.*, **633**, 624–629. [DOI], [ADS], [astro-ph/0506040]

Volonteri, M., Madau, P., Quataert, E. and Rees, M. J., 2005, "The Distribution and Cosmic Evolution of Massive Black Hole Spins", *Astrophys. J.*, **620**, 69–77. [DOI], [ADS], [astro-ph/0410342]

Wang, Jianxiang and Merritt, David, 2004, "Revised Rates of Stellar Disruption in Galactic Nuclei", *Astrophys. J.*, **600**(1), 149–161. [DOI], [ADS], [arXiv:astro-ph/0305493 [astro-ph]]

Warren, Michael S., Quinn, Peter J., Salmon, John K. and Zurek, Wojciech H., 1992, "Dark Halos Formed via Dissipationless Collapse. I. Shapes and Alignment of Angular Momentum", *Astrophys. J.*, **399**, 405. [DOI], [ADS]

Wechsler, Risa H., Zentner, Andrew R., Bullock, James S., Kravtsov, Andrey V. and Allgood, Brandon, 2006, "The Dependence of Halo Clustering on Halo Formation History, Concentration, and Occupation", *Astrophys. J.*, **652**(1), 71–84. [DOI], [ADS], [arXiv:astro-ph/0512416 [astro-ph]]

Wegner, G., Colless, M., Saglia, R. P., McMahan, R. K. Jr, Davies, R. L., Burstein, D. and Baggley, G., 1999, "VizieR Online Data Catalog: EFAR galaxies redshifts & velocity dispersions (Wegner+, 1999)", *VizieR Online Data Catalog*, J/MNRAS/305/259. [ADS]

Wetzel, A. R., Cohn, J. D. and White, M., 2009, "Simulating subhaloes at high redshift: merger rates, counts and types", *Mon. Not. Roy. Astron. Soc.*, **395**, 1376–1390. [DOI], [ADS], [arXiv:0810.2537]

Xiao, T., Barth, A. J., Greene, J. E., Ho, L. C., Bentz, M. C., Ludwig, R. R. and Jiang, Y., 2011, "Exploring the Low-mass End of the M $_{BH}$-σ_* Relation with Active Galaxies", *Astrophys. J.*, **739**, 28. [DOI], [ADS], [arXiv:1106.6232 [astro-ph.CO]]

Zhang, Xiaoxia and Lu, Youjun, 2019, "On Constraining the Growth History of Massive Black Holes via Their Distribution on the Spin-Mass Plane", *Astrophys. J.*, **873**(2), 101. [DOI], [ADS], [arXiv:1902.07056 [astro-ph.HE]]

Zhao, H., Haehnelt, M. G. and Rees, M. J., 2002, "Feeding black holes at galactic centres by capture from isothermal cusps", *New Astronomy*, **7**, 385–394. [DOI], [ADS], [astro-ph/0112096]